# Investigation into the cell biological roles of class II PI3K-C2β

Charis Kampyli

Supervisor:

Prof. Bart Vanhaesebroeck

UCL Cancer Institute

Doctor of Philosophy

2019

# Declaration

I, Charis Kampyli confirm that the work presented in this thesis is my own. Where information has been derived from other sources, I confirm that this has been indicated in the thesis.

# Abstract

The family of PI3Ks generate PI3P, $PI(3,4)P_2$ or $PI(3,4,5)P_3$. These lipids control the function and the localisation of several downstream effectors which regulate many intracellular processes including signalling and membrane traffic (Vanhaesebroeck et al., 2010; Falasca and Maffucci, 2012; Vanhaesebroeck et al., 2012; Maffucci and Falasca, 2014; Bilanges et al., 2019).

In mammals, there are eight PI3K isoforms which are classified into class I, II and III PI3Ks (Vanhaesebroeck et al., 2010; Banfic et al., 2009; Maffucci and Falasca, 2014; Falasca and Maffucci, 2012; Bilanges et al., 2019). Among them, class I PI3Ks have been most broadly studied and are often mutated in cancer. Class II and III PI3Ks produce PI3P in intracellular membranes and, in the case of class II PI3Ks, also $PI(3,4)P_2$. These PI3Ks have emerged as regulators of intracellular vesicular traffic (Posor et al., 2013; Marat and Haucke, 2016; Franco et al., 2014; Yoshioka et al., 2012). However, the understanding of their roles *in vivo* is still limited.

The aim of this study was to increase the currently incomplete knowledge on the biological roles and molecular mechanisms of action of the class II PI3K-C2β isoform. For this purpose, siRNA-mediated depletion of PI3K-C2β in HeLa cells and MEFs derived from a PI3K-C2β kinase-dead knock-in (KI) mouse model engineered by the host laboratory prior to this study were used. The latter strategy allows the assessment of the kinase-dependent functions rather than possible scaffolding functions of the targeted PI3K, without affecting the expression levels of the targeted or non-targeted PI3K isoforms (Alliouachene et al., 2015).

Here I show that PI3K-C2β regulates focal adhesion (FA) dynamics and cell migration. PI3K-C2β depletion or inactivation leads to an increased number of FAs, delayed FA disassembly and impaired cell migration. Additionally, in live cells PI3K-C2β accumulates at disassembling FAs upon blebbistatin treatment, a tool to induce FA dismantling. Moreover, a yeast-two hybrid screen identified DEPBC1B, a promoter of FA disassembly (Marchesi et al., 2014) as a potential PI3K-C2β interactor. Immunoprecipitation assays confirmed this interaction. I also provide evidence that PI3K-C2β interacts with talin, a well-characterised FA component. The mechanistic characterisation of a potential interplay between PI3K-C2β, talin and DEPDC1B in the regulation of FA dynamics requires further investigation.

# Impact statement

The lipid kinase family of phosphoinositide 3-kinases (PI3Ks) regulate many intracellular processes, such as cell proliferation, growth, survival, migration, glucose homeostasis and intracellular transport, through PI3P, $PI(3,4)P_2$ or $PI(3,4,5)P_3$ production, which act as second messengers (Vanhaesebroeck et al., 2010; Falasca and Maffucci, 2012; Vanhaesebroeck et al., 2012; Maffucci and Falasca, 2014; Bilanges et al., 2019).

The present work is focused on the class II PI3K isoform PI3K-C2β, one of the eight members of PI3Ks. The understanding of the biological roles and mechanisms of action of this PI3K isoform is still very limited. PI3K-C2β has been implicated in attenuation of mTORC1 signalling and lysosomal positioning (Marat et al., 2017) and the regulation of cell migration (Blajecka et al., 2012; Maffucci et al., 2005; Domin et al., 2005; Katso et al., 2006). Nonetheless, at the outset of this study the mechanism of action of PI3K-C2β in regulation of cell migration remained obscure. Therefore, I aimed to elucidate the cell biological aspect underlying cell migration which is affected by PI3K-C2β.

Cell migration is a multi-step process which requires finely-coordinated orchestration between continuous focal adhesion (FA) assembly, maturation and disassembly, and actin cytoskeleton remodelling (Webb et al., 2002; Ridley et al., 2003; Lauffenburger and Horwitz, 1996; Ridley, 2015; Le Clainche and Carlier, 2008; Huttenlocher and Horwitz, 2011). My study has revealed a previously unappreciated positive regulatory role of PI3K-C2β in FA disassembly, providing the first mechanistic insight on how this PI3K isoform regulates cell migration. Therefore, this study significantly advances our understanding of the mechanism of action of PI3K-C2β, thus contributing to progress in the field of class II PI3Ks. Based on the data generated by this study a manuscript will be prepared over the course of next year.

Additionally, this study has sparked collaboration between the laboratories of Professor Bart Vanhaesebroeck (UCL Cancer Institute, London, UK) and Professor Volker Haucke (Leibniz-Forschungsinstitut für Molekulare Pharmakologie, Berlin, Germany). These two laboratories are world-leading in the PI3K field, and during the course of this study have established a fruitful exchange of expertise and reagents. This will foster future collaborative efforts between these groups, with the potential to promote science and progress in class II PI3Ks and phosphoinositide research in general.

My PhD thesis received funding from a PhD Training Programme funded from European Union's Horizon 2020 research and Innovation programme under the Marie Sklodowska-Curie grant agreement No 675392, which has allowed me and my host laboratory to engage and develop an EU-wide network of scientists, which has worked extremely well and will form network of contacts for future engagement in research, development and research communication.

# Acknowledgements

I am extremely grateful to my supervisor Bart Vanhaesebroeck for his excellent guidance, supervision and mentorship throughout the time of my PhD studies. My PhD training in his lab was a great adventure in the world of science and broadened my perspectives both academically and personally.

I would also like to express my deep gratitude to York Posor for always being very supportive and investing significant amount of his time to help start with my project and always being willing to share his knowledge with me and answer every question that I had. You helped me overcome every difficulty that I faced in the lab and I cannot thank you enough for that!

Special thanks go to all the past and current members of the Cell Signalling group who made my PhD an enjoyable and unforgettable experience! Samira Alliouachene for getting me started in the lab and for always being very kind, patient and encouraging with me! Sandra D. Castillo for helping with all the mouse retina related lab work and for always being so smiley! Benoit Bilanges for his scientific guidance and for his great sense of humour which made the lab life delightful! Elena Rebollo, Elena Lopez Guadamillas, Evelyn Keet Wai Lau, Veronica Dominguez, Georgia Constantinou, PriyankaTibarewal and Emily Colbeck for always being there for me and for all the happy and also the more serious moments we spent together. Daniele Morellifor being the best technician ever! Grace Gong, Victoria Rathbone, Lizzie Foxall, Sarah Conduit, Wayne Pearce and Alex Sullivan for the nice moments we shared together! Romain Galmes for his scientific imput and guidance! I am really lucky and happy for meeting you all guys!!

I am also very grateful for the fruitful collaboration we set up with Volker Haucke and his group at the Leibniz-Forschungsinstitut für Molekulare Pharmakologie (FMP) in Berlin. I had a really pleasant experience during my two secondments in his lab.

My PhD thesis received funding from a PhD Training Programme funded from European Union’s Horizon 2020 research and Innovation programme under the Marie Sklodowska-Curie grant agreement No 675392. The experience of being part of this network was amazing! I owe sincere thanks to all the group leaders: Mariona Graupera, Julie Guillerment-Guibert, Volker Haucke, Phillip Hawkins, Emilio Hirsch, Jocelyn Laporte, Klaus Okkenhaug, Violeta Serra, Len Stephens, Bart Vanhaesebroeck, Matthias Wymman, Christian Gotze, Jordi Rodon, for always being very supportive and providing very useful advice! A huge thank you also to all the

fellows: Silvia Arucci, Paula Samso, Christina Courreges, Abhishek Derle, Piotr Jung, Erhan Keles, Piotr Kobialka, Albert Mackintosh, Vasugi Nattarayan, Fernanda Ramos, Elena Rebollo, Monica Sanchez-Guixe, Iosif Serafeimidis and Jasmina Zanoncello. You guys are amazing and I enjoyed every moment I spent with you!

Lastly but most importantly, I would like to express my deepest gratitude to my parents and my sister, the best parents and sister in the world, for their unconditional love and their endless support. Your continuous encouragement gave me strength to accomplish my PhD. I also owe an honest thank you to Panos Athanasopoulos for believing in me and supporting me during the four years of my PhD. Furthrermore, I would also like to deeply thank Panos Papadopoulos for his support during the end of my PhD.

# Table of Contents

# List of Figures

# List of Tables

# Abbreviations

| | |
|---|---|
| AMPK | 5' adenosine monophosphate-activated protein kinase |
| APPL1 | Adaptor protein, phosphotyrosine interacting with PH domain and leucine zipper 1 |
| ATP | Adenosine triphosphate |
| BAR | Bin1 / amphiphysin / Rvs |
| bp | Base pair |
| BSA | Bovine serum albumin |
| CCPs | Clathrin- coated pits |
| CME | Clathrin-mediated endocytosis |
| CHC | Clathrin heavy chain |
| DAPI | 4′,6-diamidino-2-phenylindole |
| DMEM | Dulbecco's Modified Eagle Medium |
| DMSO | Dimethylsulfoxide |
| DNA | Deoxyribonucleic acid |
| dNTP | Deoxynucleotide triphosphate |
| DTT | Dithiothreitol |
| ECL | Enhanced chemiluminescence |
| ECM | Extracellular matrix |
| EDTA | Ethylenediamine tetra-acetic acid |
| EEA1 | Early endosome antigen 1 |
| EGF | Epidermal growth factor |
| eGFP | Enhanced green fluorescent protein |
| eIF4E | Eukaryotic translation initiation factor 4E |
| ER | Endoplasmic reticulum |
| ERK | Extracellular signal-related kinase |
| 4EBPs | Eukaryotic translation initiation factor 4E binding proteins |
| FA | Focal adhesion |
| FAK | Focal adhesion kinase |
| FBS | Fetal bovine serum |
| FYVE | Fab1, YOTB, Vac1, EEA1 (FYVE) zinc finger domain |
| GAP | GTPase-activating protein |
| GDP | Guanosine diphosphate |
| GEF | Guanine nucleotide exchange factor |
| GF | Growth facors |
| GPCR | G protein-coupled receptor |
| Grb2 | Growth factor receptor bound protein 2 |
| GST | Glutathione-*S*-transferase |
| GTP | Guanosine triphosphate |
| HEK293 | Human embryonic kidney cell line |
| HeLa | Cervical cancer cell line |
| HEPES | 4-(2-hydroxyethyl)-1-piperazineethanesulfonic acid |
| HGF | Hepatocyte growth factor |
| IF | Immunofluorescence |
| HRP | Horseradish peroxidase |
| INPP4B | Type II inositol 3,4-bisphosphate 4-phosphatase |
| ITSN | Intersectin |
| KD | Kinase-dead |
| kDa | kilo Dalton |
| KI | Knock in |
| KO | Knockout |
| LPA | Lysophosphatidic acid |
| MAPK | Mitogen-activated protein kinase |
| MEF | Mouse embryonic fibroblast |
| MEK | Mitogentic effector kinase |

| | |
|---|---|
| mRNA | Messenger RNA |
| MTM1 | Myotubularin 1 |
| mTOR | Mammalian target of rapamycin |
| mTORC | Mammalian target of rapamycin complex |
| myc | Myelocytomatosis viral oncogene |
| NaOH | Sodium hydroxide |
| PAGE | Polyacrylamide gel electrophoresis |
| PBS | Phosphate-buffered saline |
| PCR | Polymerase chain reaction |
| PDGF | Platelet-derived growth factor |
| PDK | 3-phosphoinositide-dependent protein kinase |
| PH | Pleckstrin-homology |
| PI | Phosphoinositide |
| PI(3)P | Phosphatidylinositol-3-phosphate |
| $PI(3,4)P_2$ | Phosphatidylinositol-3,4-bisphosphate |
| $PI(3,4,5)P_3$ | Phosphatidylinositol-3,4,5-trisphosphate |
| $PI(3,5)P_2$ | Phosphatidylinositol-3,5-bisphosphate |
| PI(4)P | Phosphatidylinositol-4-phosphate |
| $PI(4,5)P_2$ | Phosphatidylinositol-4,5-bisphosphate |
| PI3K | Phosphoinositide-3-kinase |
| PKD1 | Protein Kinase D1 |
| PTEN | Phosphatase and tensin homologue deleted on chromosome 10 |
| PX | Phox homology |
| RT-PCR | Real-time polymerase chain reaction |
| REN | Restriction endonuclease |
| RTK | Receptor tyrosine kinase |
| SDS | Sodium dodecyl sulphate |
| SH2 | Src homology 2 |
| SH3 | Src homology 3 |
| SHIP | SH2 domain-containing inositol 5-phosphatase |
| shRNA | Small or short hairpin RNA |
| siRNA | Small or short interfering RNA |
| S6K | Ribosomal S6 kinase |
| SNP | Single nucleotide polymorphism |
| SNX | Sorting nexin |
| SNX9 | Sorting nexin 9 |
| TGN | *trans*-Golgi network |
| TBS | Tris-buffered saline |
| TBS-T | Tris-buffered saline with 0.1% Tween-20 solution |
| TIRF | Total internal reflection fluorescence |
| TRIM27 | Tripartite motif containing protein 27 |
| Vps15 | Vacuolar protein sorting 15 |
| Vps34 | Vacuolar protein sorting 34 |
| UVRAG | UV radiation resistance-associated gene protein |
| WAVE | WASP family verprolin homologous protein |
| WT | Wild- type |
| YFP | Yellow fluorescent protein |

# 1. Introduction

## 1.1 Cellular membranes

Cellular membranes are of fundamental importance for the integrity and architecture of cells. The plasma membrane is not only a barrier between the inner space and the surrounding environment, but also serves as a platform for induction of intracellular signals and mediates cell-cell interactions. Additionally, within one cell distinctive compartments are formed by other membranes, giving rise to the cell's organelles. Cellular membranes are fluid lipid bilayers consisting of amphipathic lipids whose hydrophobic portions form an internal core which is kept away from aqueous environments, while their hydrophilic head groups face the aqueous surroundings. The main components of eukaryotic membranes are glycerophospholipids, sphingolipids, cholesterol, and membrane-integral proteins. Membranes also associate with the cytoskeleton to preserve their structure (Casares et al., 2019; van Meer et al., 2008).

Lipid synthesis occurs primarily in the endoplasmic reticulum (ER). All organelles acquire by transport at least some lipids that have been produced in different organelles, with plasma membrane, endosomes and lysosomes relying completely on this process since they have limited or no capability to generate their own lipids (Casares et al., 2019). Membranes are not static and during a process called membrane trafficking, membrane proteins and lumenal content are transported and exchanged between different compartments using membrane-bound vesicles (Casares et al., 2019; Di Paolo and De Camilli, 2006). With the multitude of processes taking place on the surfaces of intracellular membranes, it is of crucial importance that the different membranes within the cell remain distinguishable for proteins that interact with them (Casares et al., 2019; Di Paolo and De Camilli, 2006). A very efficient way to encode such organelle identity within the cytoplasmic leaflet of membranes is the distinct composition of phosphoinositides, which can be quickly interconverted from one species to another through reversible phosphorylation and dephosphorylation (Casares et al., 2019; Di Paolo and De Camilli, 2006).

## 1.2 Phosphoinositides

Phosphoinositides (PIs) are lipid signalling molecules with fundamental roles in many aspects of cell physiology. Phosphoinositides derive from phosphatidylinositol which is produced in ER or in mobile ER-derived structures and is then delivered to other membranes via phosphatidylinositol transfer proteins and vesicular trafficking

(Balla, 2013; Di Paolo and De Camilli, 2006). Phosphatidylinositol consists of two fatty acid tails, which are linked to the *myo*-inositol head group via a glycerol backbone (Figure 1-1) (Balla, 2013; Di Paolo and De Camilli, 2006; De Craene et al., 2017). The majority of PIs contain a stearoyl residue at position 1 and an arachidonyl residue at position 2 of their glycerol backbone (Figure 1-1). Five out of six hydroxyl groups of the *myo*-inositol ring are equatorial and only the hydroxyl group at position 2 is axial (Figure 1-1) (Balla, 2013). The *myo*-inositol ring can be reversibly phosphorylated at positions 3, 4 and 5, resulting in the generation of seven known phosphoinositide species: phosphatidylinositol-3-phosphate (PI3P), phosphatidylinositol-4-phosphate (PI4P), phosphatidylinositol-5-phosphate (PI5P), phosphatidylinositol-3,4-bisphosphate [$PI(3,4)P_2$], phosphatidylinositol-4,5-bisphosphate [$PI(4,5)P_2$], phosphatidylinositol-3,5-bisphosphate [$PI(3,5)P_2$], and phosphatidylinositol-3,4,5-trisphosphate [$PI(3,4,5)P_3$] (Balla, 2013; Di Paolo and De Camilli, 2006; Burke, 2018). Despite their low abundance, with PI4P and $PI(4,5)P_2$ corresponding to around 0.2-1% of total cellular lipids and the rest to even smaller quantities, these short-lived PIs are key regulators of a broad spectrum of cellular functions, such as signal transduction, membrane traffic, endocytosis, exocytosis, autophagy, cell migration, cell division and ion channel regulation (Balla, 2013; Di Paolo and De Camilli, 2006; Hawkins and Stephens, 2016; Schink et al., 2016). PIs are able to mediate all these processes through recruitment of cytosolic proteins or cytosolic domains of membrane proteins which can specifically bind them and also through regulation of the activity of proteins that associate with them (Balla, 2013; Di Paolo and De Camilli, 2006; Hawkins and Stephens, 2016; Posor et al., 2013; Schink et al., 2016).

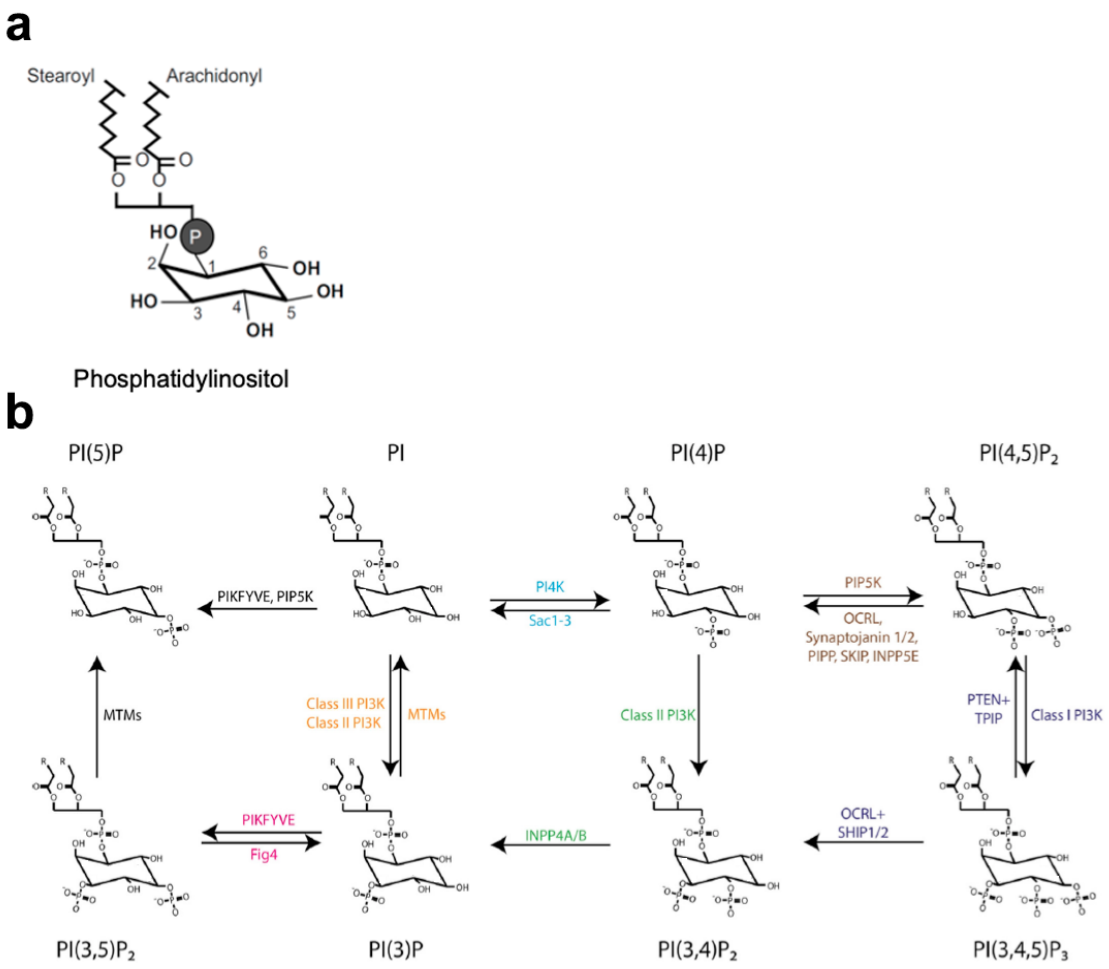


**Figure 1-1: Phosphoinositides. a) Chemical structure of phosphatidylinositol. a)** Chemical structure of phosphatidylinositol which is composed of two fatty acids connected to the inositol head group via glycerol [Adapted from (Di Paolo and De Camilli, 2006). Copyright obtained by Springer Nature]. **b) Schematic representation of phosphoinositide metabolism.** PI3P is generated by the class III PI3K, called Vps34, and class II PI3Ks. PI3P can be converted to $PI(3,5)P_2$ by PIKFYVE (a FYVE finger-containing phosphoinositide kinase) which can also produce PI5P from PI. PI4P is synthesised by PI 4-kinase (PI4K). PI4P is the substrate for PIP5K (type I PI 4-phosphate 5-kinase) which produces $PI(4,5)P_2$. .Class I PI3Ks catalyses the phosphorylation of $PI(4,5)P_2$ at position 3-OH and generates $PI(3,4,5)P_3$. $PI(3,4)P_2$ is generated by class II PI3Ks after catalysing the phosphorylation of PI4P at position 3-OH. $PI(3,4,5)P_3$ can be converted to $PI(4,5)P_2$ by the 3-phosphatases PTEN and TPIP or to $PI(3,4)P_2$ by the 5-phosphatases OCRL and SHIP1/2, which can be further dephosphorylated to PI3P by the 4-phosphatasesINPP4A/B. MTMs are 3-phosphatases which produce PI5P and PI from $PI(3,5)P_2$ and PI3P respectively. $PI(3,5)P_2$ can be converted to PI3P by Fig4 which is a 5-phosphatase. Sac1-3, which are 4-phosphatases, produce PI from PI4P.
PI3K: phosphoinositide 3-kinase, PTEN: phosphatase and tensin homologue deleted on chromosome 10, TPIP: TPTE (transmembrane phosphatase with tensin homology) and PTEN homologous inositol lipid phosphatase, OCRL: oculocerebrorenal syndrome of Lowe protein, SHIP1/2: Src-homology 2 domain-containing inositol 5-phosphatase 1/2, INPP4A/B: inositol polyphosphate 4-phosphatase A/B, MTMs: myotubularins, Fig4: Factor Induced gene. [Adapted from (Wallroth and Haucke, 2018).This research was originally published in the Journal of Biological Chemistry. Wallroth, A. and Haucke, V. Phosphoinositide conversion in endocytosis and the endolysosomal system. J. Biol. Chem. 2017; Vol: 293, Issue: 5, Pages: 1526-1535. © the American Society for Biochemistry and Molecular Biology *or* © the Author(s). Copyright permission also obtained by Professor Volker Haucke].

The synthesis and degradation of phosphoinositides is subject to tight spatial and temporal regulation. The interconversion of the different phosphorylated phosphatidylinositol species is mediated by PI kinases and phosphatases through rapid cycles of phosphorylation and dephosphorylation (Figure 1-1b) (Wallroth and Haucke,

2018; De Matteis and Godi, 2004; Krauss and Haucke, 2007; Burke, 2018). Each PI species displays a specific subcellular distribution and the distinct pattern of enrichment of different PIs contributes to define the identity of distinctive membrane compartments. Each subcellular compartment is characterised by a well-defined composition of PI-metabolising enzymes and this contributes greatly to the distinctive PI profile displayed by each organelle (De Matteis and Godi, 2004; Krauss and Haucke, 2007; Marat and Haucke, 2016; Wallroth and Haucke, 2018). The PI profile of the exocytic pathway is enriched in 4'-phosphorylated PI species, differing markedly from the endocytic pathway, which is enriched in 3'-phosphorylated PI species (Di Paolo and De Camilli, 2006; Marat and Haucke, 2016; Wallroth and Haucke, 2018) (Figure 1-2). PI4P is principally found at the Golgi complex and at the plasma membrane, $PI(4,5)P_2$ and its derivative $PI(3,4,5)P_3$ are concentrated at the plasma membrane, while PI3P and $PI(3,5)P_2$, are enriched at early and late endosomes/lysosomes, respectively (Figure 1-2) (Wallroth and Haucke, 2018; Marat and Haucke, 2016; Di Paolo and De Camilli, 2006; Schink et al., 2016).

The recruitment of PI kinases and phosphatases to specific subdomains and their activation are often mediated by small GTPases of the Rab and Arf families, resulting in the local generation or degradation of a specific PI (Behnia and Munro, 2005; De Matteis and Godi, 2004; Di Paolo and De Camilli, 2006; Krauss and Haucke, 2007; Marat and Haucke, 2016; Wallroth and Haucke, 2018).

Another interesting aspect of the finely orchestrated activity of PIs is the ability of the same PI to promote opposite effects depending on its localisation. At the plasma membrane, $PI(3,4)P_2$ production indirectly [mediated by the 5-phosphatases OCRL (oculocerebrorenal syndrome of Lowe protein) and SHIP1/2 (Src-homology 2 domain-containing inositol 5-phosphatase 1/2)] upon class I phosphoinositide 3-kinases (PI3Ks) activation is associated with mTORC1 activation, whereas its synthesis at late endosomes/lysosomes by the class II isoform PI3K-C2β in the absence of growth factors causes mTORC1 inhibition (Burke, 2018; Marat et al., 2017).

Additionally, PIs together with GTPases can promote the anchoring of effectors to distinct membranes and also PIs are able to mediate the activation of both GEFs (guanine nucleotide exchange factors) and GAPs (GTPase-activating proteins) after associating with their PI-binding sites (Di Paolo and De Camilli, 2006).

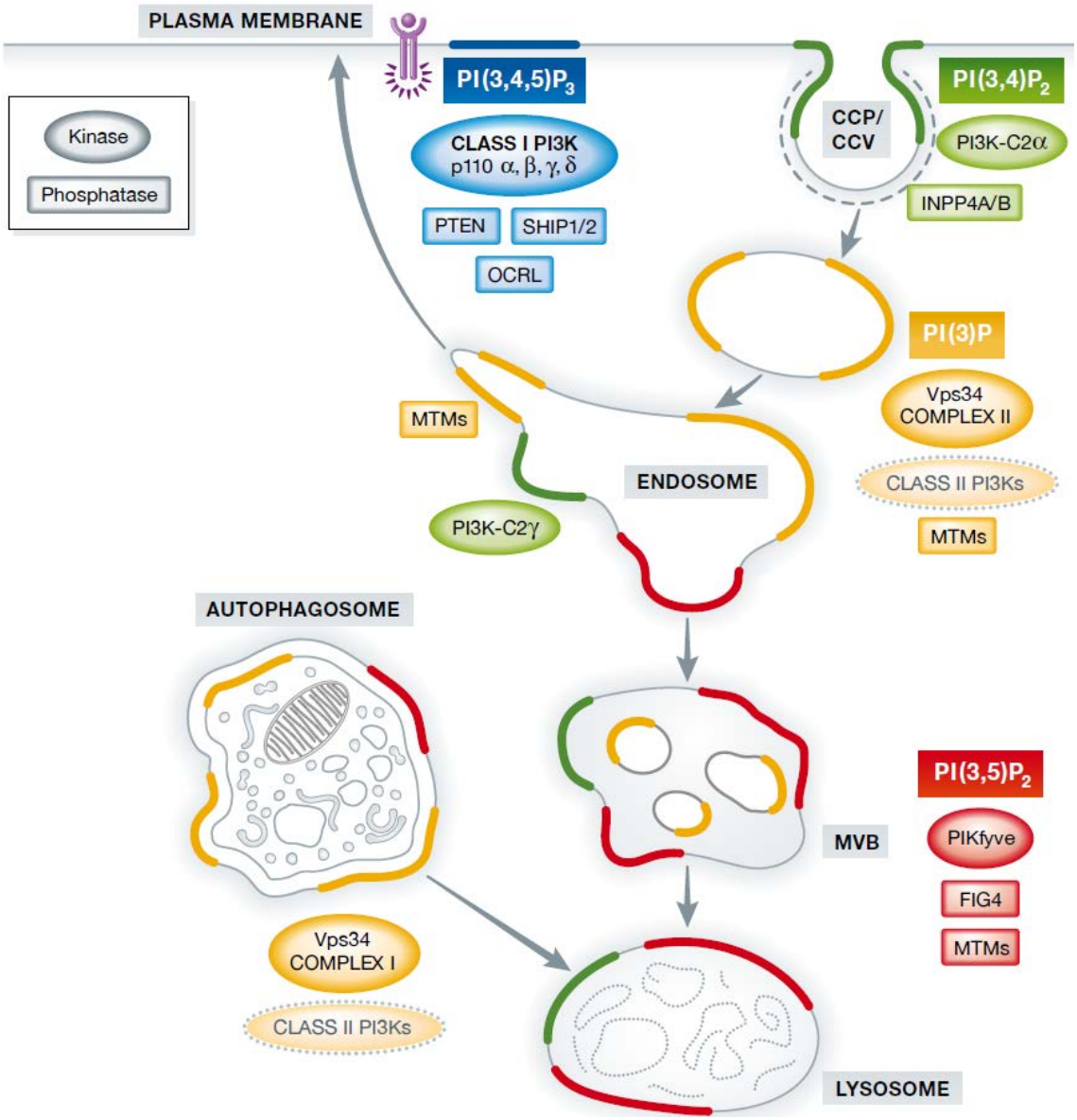


**Figure 1-2: Lipid products of PI3Ks and their localisation.** $PI(3,4,5)P_3$ is produced by class I PI3Ks (with four catalytic subunits -p110α, p110β, p110γ or p110δ-) at plasma membrane upon their activation mediated by activated receptor tyrosine kinases. $PI(3,4,5)P_3$ can be converted to $PI(4,5)P_2$ by the 3-phosphatase PTEN or to $PI(3,4)P_2$ by the 5-phosphatases OCRL and SHIP1/2. At plasma membrane, during endocytosis, class II PI3K-C2α is responsible for the generation of a local $PI(3,4)P_2$ pool which is required for the maturation of clathrin-coated pits (CCP) and synthesis of of free clathrin-coated vesicles (CCV). At early endosomes, PI3P is principally produced by the class III PI3K Vps34 complex II. Class II PI3Ks may also contribute to this PI3P pool either directly or indirectly through $PI(3,4)P_2$ production which in turn is converted to PI3P by the 4-phosphatases INPP4A/B. PI3P to $PI(3,5)P_2$ conversion mediated by PIKFYVE is observed during the process of maturation of endosomes to late endosomes/multivesicular bodies (MVBs). A pool of $PI(3,4)P_2$ is also found at endosomes and lysosomes. Class II PI3K-C2γ is responsible for the production of this pool in liver. Class II PI3K-C2β also generates $PI(3,4)P_2$ at late endosomes/lysosomes. Class III PI3K Vps34 complex I generates PI3P at autophagosomes with a potential contribution of class II PI3Ks to this pool. The PI3P and $PI(3,5)P_2$ 3-phosphatases myotubularins (MTMs) catalyse the dephosphorylation of PI3P and $PI(3,5)P_2$ and the $PI(3,5)P_2$ 5-phosphatase Fig4 catalyse the hydrolysis of $PI(3,5)P_2$.
PI3K: phosphoinositide 3-kinase, PTEN: phosphatase and tensin homologue deleted on chromosome 10, OCRL: oculocerebrorenal syndrome of Lowe protein, SHIP1/2: Src-homology 2 domain-containing inositol 5-phosphatase 1/2, INPP4A/B: inositol polyphosphate 4-phosphatase A/B, MTMs: myotubularins, Fig4: Factor Induced gene. [Adapted from (Marat and Haucke, 2016), Copyright permission obtained by the EMBO journal and also by ProfessorVolker Haucke].

## 1.3 Phosphoinositide 3-kinases (PI3Ks)

The lipid kinase family of phosphoinositide 3-kinases (PI3Ks) catalyse the synthesis of PI 3'-phosphates, namely PI3P, PI(3,4)$P_2$ and PI(3,4,5)$P_3$, by phosphorylating the 3'-hydroxyl group of the inositol ring of specific phosphatidylinositol lipids that reside at both plasma and intracellular membranes (Vanhaesebroeck et al., 2012; Vanhaesebroeck et al., 2010; Falasca and Maffucci, 2012; Marat and Haucke, 2016; Maffucci and Falasca, 2014). These 3'-phosporylated PI species bind to various downstream effector proteins via distinct lipid-binding domains and control their localisation and activity. These downstream effectors regulate in turn multiple cellular processes, like cell growth, proliferation, survival, metabolism and intracellular vesicular traffic (Vanhaesebroeck et al., 2012; Vanhaesebroeck et al., 2010; Maffucci and Falasca, 2014; Falasca and Maffucci, 2012). FYVE and Phox-homology (PX) domains mostly bind to PI3P, whereas the specific recognition of PI(3,4,5)$P_3$ and PI(3,4)$P_2$ is in many cases mediated by Pleckstrin homology (PH) domains (Lemmon, 2008; Vanhaesebroeck et al., 2010).

PI(3,5)$P_2$ is not directly produced by PI3Ks, but its synthesis is catalysed by the PI 5-kinase, PIKfyve, through phosphorylation of PI3P (Wallroth and Haucke, 2018; Marat and Haucke, 2016; Balla, 2013).

Mammals have eight isoforms of PI3Ks which are divided into three classes (class I, II and III) according to their structure, their lipid substrate specificity and their association with regulatory subunits. All PI3K isoforms consist of a PI3K signature motif, the PI3K core, which contains the catalytic domain, a helical domain and a C2 membrane-binding domain (Vanhaesebroeck et al., 2010; Marat and Haucke, 2016; Falasca and Maffucci, 2012; Bilanges et al., 2019). The main *in vivo* lipid product of class I PI3K isoforms is PI(3,4,5)$P_3$ whose synthesis is triggered upon their activation by cell surface receptors. Class II PI3Ks via PI3P and PI(3,4)$P_2$ production have emerged as regulators of intracellular vesicular traffic and membrane dynamics (Bilanges et al., 2019; Margaria et al., 2019). Vps34, the sole class III PI3K, produces PI3P to regulate endosomal maturation and autophagy (Bilanges et al., 2019). In contrast to class I PI3Ks, the class II and III PI3Ks have a mostly indirect impact on cell signalling (Figure 1-2) (Bilanges et al., 2019). However, the understanding of their roles *in vivo* is still limited.

### 1.3.1 Class I PI3Ks

Class I PI3Ks have been the most broadly investigated among the three PI3K classes. In normal physiological conditions, class I PI3K isoforms are implicated in

immunity, metabolism, cardiac function and angiogenesis. They are often upregulated in cancer and they are the main target of drug development (Vanhaesebroeck et al., 2016; Denley et al., 2008; Fruman and Rommel, 2014; Thorpe et al., 2015; Ciraolo et al., 2011; Courtney et al., 2010; Liu et al., 2009; Janku et al., 2018; Burke, 2018; Fruman et al., 2017; Vanhaesebroeck et al., 2012).

Class I PI3Ks function as heterodimers, which consist of one of the four catalytic subunits (p110α, p110β, p110γ or p110δ) and a regulatory subunit (Figure 1-3). Further classification of class I PI3Ks into two subclasses (class IA and class IB) depends on the regulatory subunit that binds the catalytic subunit. The class IA PI3K isoforms p110α, β, and δ associate with one of the five p85 regulatory subunits (p85α, p55α, p50α, p85β and p55γ), while the class IB PI3Ks consists of the single catalytic subunit p110γ that forms a complex with the regulatory subunits p101 or p84 (also known as p87) (Figure 1-3) (Vanhaesebroeck et al., 2010; Vanhaesebroeck et al., 2012; Marat and Haucke, 2016; Burke, 2018; Liu et al., 2009; Thorpe et al., 2015; Fruman et al., 2017; Bilanges et al., 2019). Although p110α and p110β are ubiquitously expressed, p110γ and p110δ expression is mainly enriched in leukocytes (Vanhaesebroeck et al., 2010; Thorpe et al., 2015; Liu et al., 2009; Ciraolo et al., 2011) (Ciraolo et al., 2011). Each class IA p110 isoform contains an adaptor-binding domain (ABD) which is responsible for the interaction with the p85 regulatory subunit (Figure 1-3) (Vanhaesebroeck et al., 2010; Dornan and Burke, 2018; Burke, 2018; Bilanges et al., 2019) but is absent from the class IB p110γ isoform (Burke, 2018; Bilanges et al., 2019).

The p85 regulatory subunits of class IA PI3Ks are responsible for at least three major functions: p110 stabilisation, inhibition of p110 catalytic activity in absence of activating stimuli and, in presence of activating stimuli, p110 recruitment to activated receptor tyrosine kinases (RTKs). The latter depends on phosphorylated tyrosine residues in the cytoplasmic tails of RTKs or adaptor proteins associated with the RTKs such as IRS1 (insulin receptor substrate 1) through the Src homology 2 (SH2) domains of the p85 subunits (Vanhaesebroeck et al., 2010; Burke, 2018; Thorpe et al., 2015).

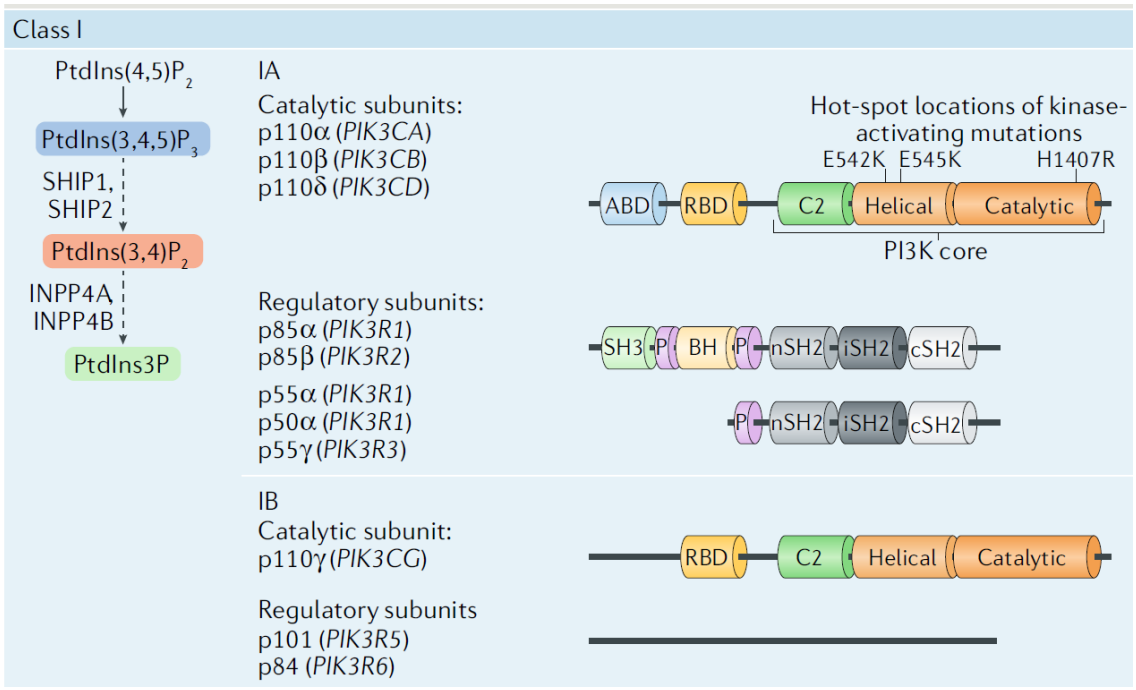


**Figure 1-3: Structure and substrate specificity of class I PI3Ks.** Class I PI3Ks catalyses the phosphorylation of PI(4,5)$P_2$ at position 3-OH and generates PI(3,4,5)$P_3$, which can in turn be converted to PI(3,4)$P_2$ by SHIP1/2, which can further be converted to PI3P by INPP4A/B. Class I PI3Ks form heterodimers, which consist of one of the four catalytic subunits (p110α, p110β, p110γ or p110δ) and a regulatory subunit. Class I PI3Ks are classified further into class IA and IB, depending on the regulatory subunit which associates with each catalytic subunit. The class IA isoforms p110α, β and δ associate with one of the five p85 regulatory subunits (p85α, p55α, p50α, p85β and p55γ), while the class IB isoform p110γ interacts with the regulatory subunits p101 or p84. The catalytic subunits contain the PI3K core - consisting of the catalytic domain, a helical domain and a C2 membrane-binding domain -, a Ras binding domain (RBD) and an adaptor-binding domain (ABD) which is responsible for the interaction with a regulatory subunit, but this domain is absent from the class IB p110γ isoform. All p85 subunits contain SH2 (Src homology 2) domains and a proline-rich domain in their N-termianl region. The variability among p85 subunits is found in their N-terminal regions. p85α and p85β also have a second proline-rich domain, a SH3 (Src homology 3) domain and a BCR (breakpoint cluster region) homology (BH) domain. The symbol of the genes that encode each PI3K subunit appear in parentheses. Interestingly, p85α, p55α and p50α are encoded by PIK3R1 via differential usage of promoter. Class IB regulatory subunits do not contain any particular domain. In *PIK3CA,''* three hot spot'' mutations- E542K, E545K, H1407R-related with cancer are also indicated in this figure.
PI3K: phosphoinositide 3-kinase, SHIP1/2: Src-homology 2 domain-containing inositol 5-phosphatase 1/2, INPP4A/B: inositol polyphosphate 4-phosphatase A/B, C2: protein kinase C conserved region 2, SH2: Src homology 2 domain, nSH2: N- terminal SH2, iSH2: inter- SH2 domain, P: proline- rich region, PtdIns3P/PI3P: phosphatidylinositol 3-phosphate, PtdIns(3,4)$P_2$/PI(3,4)$P_2$: phosphatidylinositol 3,4-bisphosphate, PtdIns(4,5)$P_2$/PI(4,5)$P_2$: phosphatidylinositol 4,5-bisphosphate, PtdIns(3,4,5)$P_3$/PI(3,4,5)$P_3$: phosphatidylinositol 3,4,5-trisphosphate. [Adapted from (Bilanges et al., 2019). Copyright permission obtained by Springer Nature (Nature Reviews Molecular Cell Biology) and also by the authors: Dr Benoit Bilanges, Dr York Posor and Professor Bart Vanhaesebroeck].

Growth factor or insulin stimulation triggers class I PI3K recruitment to activated RTKs (Figure 1-4). The p85-SH2 interaction with phosphotyrosines leads to the release of the p85-mediated inhibition of p110 and to localisation of PI3K at the plasma membrane, where it catalyses the production of PI(3,4,5)$P_3$ from PI(4,5)$P_2$. The class IB p110γ isoform, but also p110β, are activated downstream of G protein-coupled receptors (GPCRs) by association with the βγ-subunits of heterotrimeric G proteins (Figure 1-4) (Vanhaesebroeck et al., 2012; Vanhaesebroeck et al., 2010; Marat and

Haucke, 2016; Thorpe et al., 2015; Liu et al., 2009; Courtney et al., 2010; Ciraolo et al., 2011; Burke, 2018; Fruman et al., 2017).

Every class I PI3K isoform possesses a Ras binding domain (RBD). Thus, it is not surprising that members of the Ras superfamily of small GTPases can also promote the activation of these enzymes. Each class I PI3K isoform is characterised by a different capability of being activated by distinct small GTPases. More specifically, class IA p110α, γ and δ isoforms bind to activated Ras GTPases, while p110β can bind Rho GTPases and Rab5 instead (Figure 1-4) (Vanhaesebroeck et al., 2010; Marat and Haucke, 2016; Fruman et al., 2017; Burke, 2018; Bilanges et al., 2019).

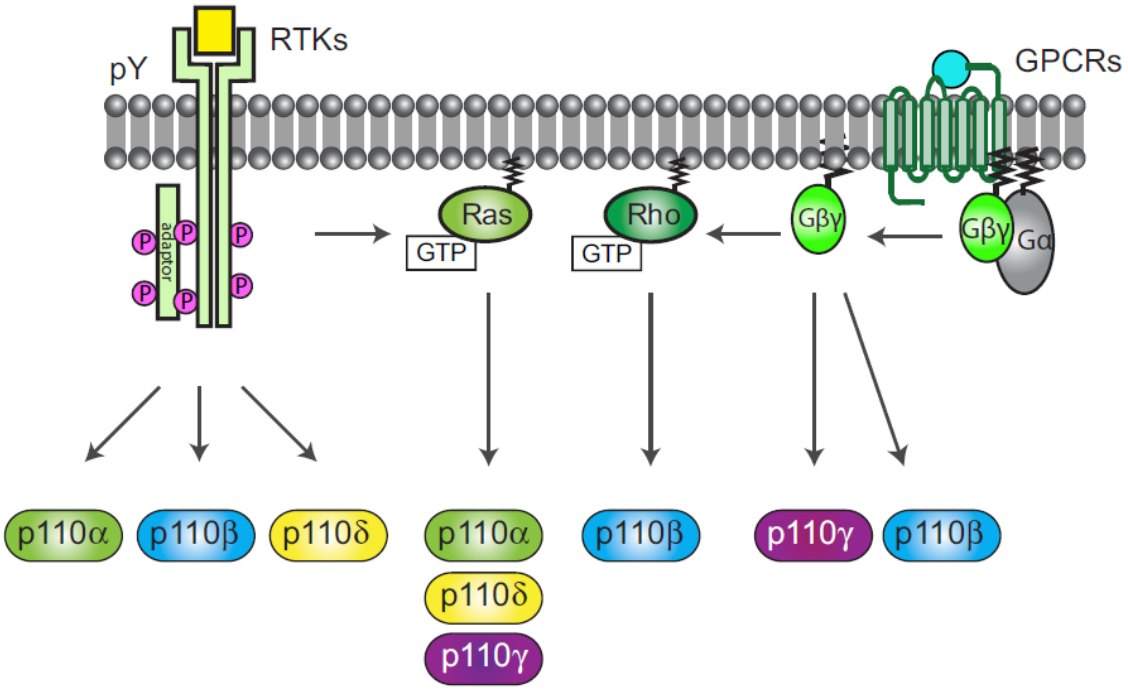


**Figure 1-4: Activation of class I PI3Ks.** Activated RTKs (receptor tyrosine kinases), members of the Ras superfamily of small GTPases in their active GTP-bound, like Ras-GTP and Rho-GTP and also G protein-coupled receptors (GPCRs) represent activating stimuli for p110 isofroms. [Adapted from (Burke, 2018). Copyright obtained by Elsevier (Molecular Cell) and also by Professor John Burke].

Activation of class I PI3K isoforms results in local conversion of $PI(4,5)P_2$ to $PI(3,4,5)P_3$ and also in indirect $PI(3,4)P_2$ production mediated by SH2-domain-containing inositol 5-phosphatase 1 (SHIP1) and 2 (SHIP2) at the plasma membrane (Vanhaesebroeck et al., 2012; Marat and Haucke, 2016). $PI(3,4,5)P_3$ promotes the recruitment and activation of various PH domain-containing effector proteins to the plasma membrane (Vanhaesebroeck et al., 2010; Marat and Haucke, 2016; Vanhaesebroeck et al., 2012; Bilanges et al., 2019).

*Akt*

The most well investigated downstream PI3K effector is the protein kinase Akt (also known as PKB), which translocates to the plasma membrane and is

phosphorylated at Thr308 by phospoinositide-dependent kinase 1 (PDK1) and is fully activated after a second phosphorylation at Ser473 mediated by mammalian target of rapamycin complex 2 (mTORC2) (Figure 1-5). Activated Akt, in turn, phosphorylates multiple downstream targets which control a wide range of cellular functions, including cell survival (suppression of BAD, a pro-apoptotic Bcl-2 antagonist of cell death), proliferation (cytosolic accumulation and inhibition of p21 (Zhou et al., 2001) and p27 (Viglietto et al., 2002; Shin et al., 2002; Liang et al., 2002)), growth and glucose metabolism (inhibition of glycogen synthase kinase 3 (GSK3)) (Figure 1-5) (Cross et al., 1995; Vanhaesebroeck et al., 2012; Courtney et al., 2010; Liu et al., 2009; Thorpe et al., 2015; Fruman et al., 2017; Hemmings and Restuccia, 2012).

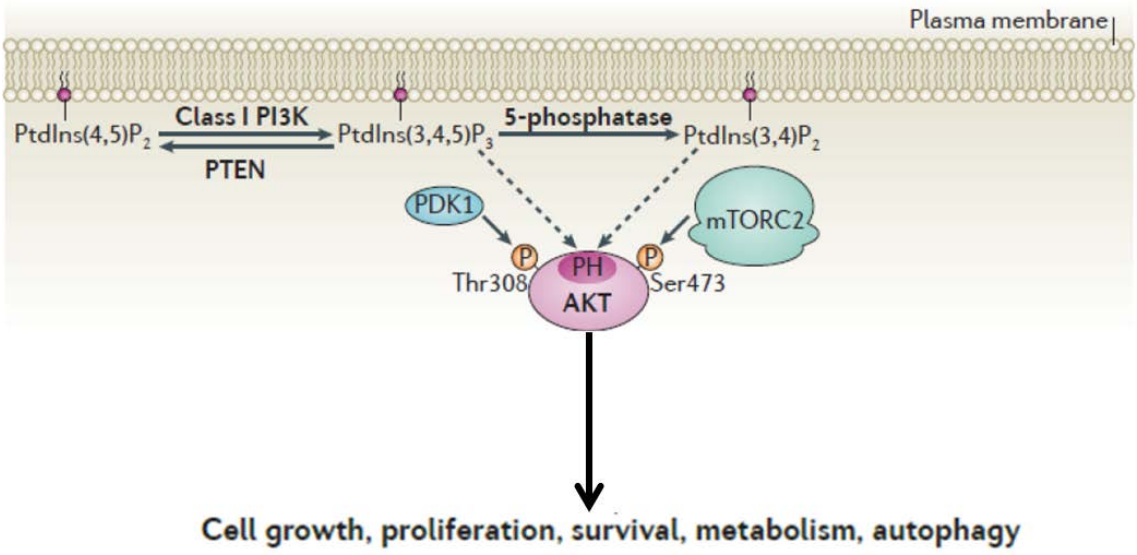


**Figure 1-5: Akt is the most well-investigated downstream effector of PI3Ks.** After being activated, class I PI3Ks produce PI(3,4,5)$P_3$ and indirectly, PI(3,4)$P_2$-through the action of Src-homology 2 domain-containing inositol 5-phosphatase 1/2 (SHIP1/2) -, which in turn interact with the PH-domain (pleckstrin homology)-containing Akt triggering its recruitment to the plasma membrane. Phosphorylation of Akt at Thr308 by phospoinositide-dependent kinase 1 (PDK1) and a second phosphorylation at Ser473 mediated by mTORC2 (mammalian target of rapamycin complex 2) results to its complete activation. Phosphorylation of multiple downstream targets is then mediated by activated Akt, leading to the regulation of various cellular functions, like cell growth, proliferation, survival, metabolism and autophagy. PI3K: phosphoinositide 3-kinase, PtdIns(3,4)$P_2$/PI(3,4)$P_2$: phosphatidylinositol 3,4-bisphosphate, PtdIns(3,4,5)$P_3$/PI(3,4,5)$P_3$: phosphatidylinositol 3,4,5-trisphosphate. [Adapted from (Vanhaesebroeck et al., 2012), Copyright permission obtained by Springer Nature (Nature Reviews Molecular Cell Biology) and also by Professor Bart Vanhaesebroeck].

*mTORC1*

Activated Akt promotes cell growth and proliferation through activation of mechanistic target of rapamycin complex 1 (mTORC1), which is a fundamental regulator of these processes, by inhibiting the tuberous sclerosis proteins 1/2 (TSC1/2), thereby allowing the small GTPase Rheb to bind and activate mTORC1 (Saxton and Sabatini, 2017; Fruman et al., 2017; Ciraolo et al., 2011; Courtney et al., 2010; Bilanges et al., 2019). mTORC1 senses the nutrient abundance (glucose and amino acids) on lysosomes. In low nutrient abundance, it shuts down, leading to

decreased cell growth and autophagy. In high nutrient abundance, it stimulates anabolic processes (such as protein, lipid and nucleotide synthesis and metabolism) and suppresses catabolic processes (such as autophagy). Other regulators of mTORC1 include oxygen and energy status, inflammation and DNA damage (Laplante and Sabatini, 2009; Saxton and Sabatini, 2017; Sabatini, 2017; Bilanges et al., 2019). The positioning of lysosomes, which function as the platform of mTORC1 activation, plays a critical regulatory role in mTORC1 activity. Under nutrient-low conditions, lysosomes are found in the perinuclear region, while in presence of nutrients they localise close to the plasma membrane. mTORC1 is thereby positioned in close proximity to signals from cell surface receptors. Consequently, peripheral lysosomal dispersion correlates with high activity of mTORC1, whereas perinuclear clustering correlates with inhibition of mTORC1 activity (Bilanges et al., 2019; Korolchuk et al., 2011; Wallroth and Haucke, 2018). The availability of intra-lysosomal and cytoplasmic amino acids regulates translocation of mTORC1 to the lysosomes, which is mediated by the small GTPases RagA and RagC (Laplante and Sabatini, 2009; Saxton and Sabatini, 2017; Sabatini, 2017; Bilanges et al., 2019).

Key downstream effectors of Akt/mTORC1 pathway are the ribosomal p70S6 kinase 1 (S6K1), which promotes glycolysis and biosynthesis of proteins, lipids and nucleotides, and the eukaryotic translation initiation factor 4E binding proteins (4EBPs), whose phosphorylation prevents their association with eukaryotic translation initiation factor 4E (eIF4E) and permits the initiation of the cap-dependent translation (Saxton and Sabatini, 2017; Fruman et al., 2017; Ciraolo et al., 2011; Courtney et al., 2010). Many cancer types are characterised by a deregulated and abnormally activated PI3K/Akt/mTOR signalling pathway, and anticancer drug development aims to target this signalling pathway (Fruman et al., 2017; Fruman and Rommel, 2014; Ciraolo et al., 2011; Asati et al., 2016; Janku et al., 2018; Courtney et al., 2010; Liu et al., 2009).

*PTEN*

PI3K activity is counteracted by phosphatase and tensin homologue located on chromosome 10 (PTEN), which catalyses the dephosphorylation of $PI(3,4,5)P_3$ to $PI(4,5)P_2$, thus counterbalancing Akt activation. PTEN is also capable of mediating the dephosphorylation of $PI(3,4)P_2$ both *in vitro* and *in vivo* (Malek et al., 2017). PTEN is a tumour suppressor and is frequently mutated in many cancers (Lee et al., 2018). On the contrary, SHIP1/2- mediated $PI(3,4)P_2$ generation from $PI(3,4,5)P_3$ sustains the PI3K/Akt signalling pathway, since the plasma membrane recruitment and activation of the fundamental PH domain-containing PI3K downstream effectors, Akt and PDK1, is mediated by both $PI(3,4,5)P_3$ and $PI(3,4)P_2$ (Marat and Haucke, 2016; Vanhaesebroeck

et al., 2012; Vanhaesebroeck et al., 2010; Ciraolo et al., 2011; Hemmings and Restuccia, 2012).

### 1.3.2 Class III PI3K Vps34

The sole class III PI3K Vps34 (vacuolar protein sorting 34) is the PI3K conserved from yeast to human and exists as a heterodimer with the myristoylated Vps15 (a pseudokinase), tethering the Vps34/Vps15 dimer to intracellular membranes (Figure 1-6). Vps34 produces only PI3P and can be found in distinct multiprotein complexes at different sites within the cell. It is thereby involved in the regulation of various cellular processes, like autophagy, endosomal trafficking and phagocytosis (Backer, 2016; Ktistakis and Tooze, 2016b; Vanhaesebroeck et al., 2010).

The main domains of Vps34 are an N-terminal C2 domain, a helical domain and a C-terminal kinase domain, i.e. the PI3K core (Figure 1-6). Vps34 forms at least two major tetrameric complexes, namely complex I with a role in autophagy and complex II with a role in endocytic sorting and endosomal maturation (Figure 1-6). The core complex is composed of Vps34, beclin-1/Atg6 and Vps15, which in turn associates with either ATG14 (autophagy-related protein 14) to form complex I or with UVRAG (UV radiation resistance-associated gene) to form complex II in a mutually exclusive way (Figure 1-6) (Backer, 2016; Stjepanovic et al., 2017; Bilanges et al., 2019). Lysosomal positioning and activation of mTORC1 are regulated by PI3P production on lysosomes via Vps34 complexes, however its remains elusive which complex is implicated in this process (Bilanges et al., 2019).

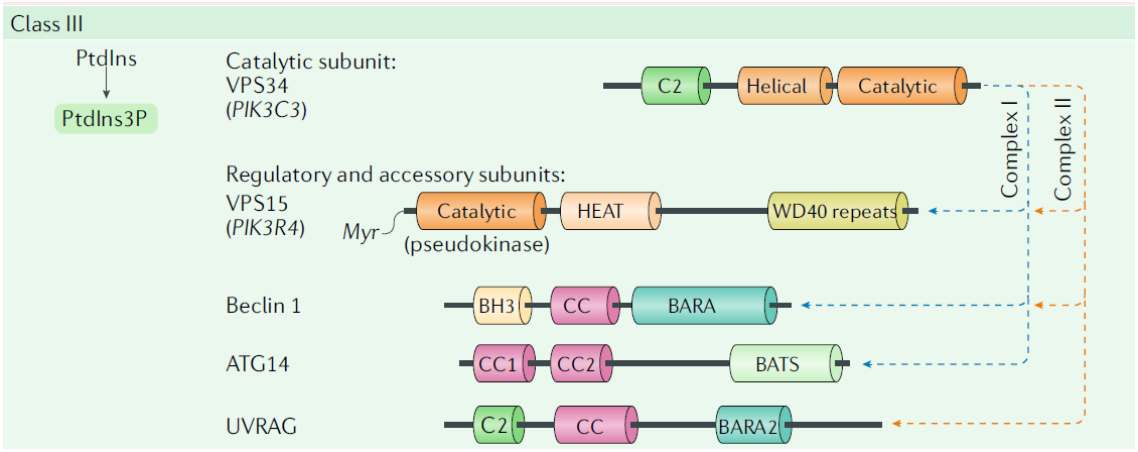


**Figure 1-6: Structure and substrate specificity of class III PI3K.** PI serves as a substrate for class III Vps34. Vps34 (vacuolar protein sorting 34) is the sole catalytic member of class III PI3K and it consists of an N-terminal C2 domain, a helical domain and a C-terminal kinase domain. Vps34 exists in two major tetrameric complexes, namely complex I, which is composed of Vps34, beclin-1/Atg6, Vps15 and ATG14 (autophagy-related protein 14), and complex II which is composed of Vps34, beclin-1/Atg6, Vps15 and UVRAG (UV radiation resistance-associated gene). Vps15 contains a catalytic domain, HEAT domains and WD40 repeats.
PtdIns/PI: phosphatidylinositol, PtdIns3P/PI3P: phosphatidylinositol 3-phosphate, C2: protein kinase C conserved region 2, CC1: coiled- coil domain 1, CC2: coiled- coil domain 2, HEAT: huntingtin, Myr: N-

terminal myristoylation of Vps15, BH3: Bcl-2 homology 3 domain, WD40 repeat: Trp–Asp (W–D), BARA: β/α- repeated,autophagy- related domain, BATS: Barkor/Atg14(L) autophagosome targeting sequence. [Adapted from (Bilanges et al., 2019). Copyright permission obtained by Springer Nature (Nature Reviews Molecular Cell Biology) and also by the authors: Dr Benoit Bilanges, Dr York Posor and Professor Bart Vanhaesebroeck].

*Complex I Vps34*

Vps34 promotes autophagy initiation. Under low nutrient abundance, the autophagy-initiating kinase ULK1 mediates ATG14 and Vps34 phosphorylation resulting in recruitment and activation of Vps34 complex I to the endoplasmic reticulum. Subsequent local PI3P synthesis by Vps34 leads to WIPI2 and DFCP1 recruitment and autophagosome nucleation. Lipidation of LC3 protein follows and in its lipidated state, LC3 serves as an autophagic cargo receptor and promotes autophagosome expansion and closure. Following maturation, autophagosome fusion with either late endosomes or lysosomes generates autolysosomes, where the digestion of cytoplasmic material occurs. Vps34 complex II is implicated in this process but its mechanism of action is unclear (Bilanges et al., 2019).

*Complex II Vps34*

Vps34 complex II anchoring to early endosomes through association of Vps15 with Rab5-GTP leads to PI3P synthesis, which in turn results in recruitment of PX domain- or FYVE-domain-containing effectors. Such effectors include EEA1, which promotes endosomal fusion, and glucocorticoid-regulated kinase 3 (SGK3), which is capable of signal transmission from endosomes. Additionally, this complex mediates the maturation of Rab5-positive early endosomes into Rab7-positive late endosomes by mediating the Rab shift. Moreover, interaction between the complex II subunit UVRAG and homotypic fusion and vacuole protein sorting (HOPS) complex enables late endosome/lysosome fusion. Furthermore, during phagocytosis this Vps34 complex is anchored to the nascent phagosome via association with Rab5. Then, maturation to late endosomes followed by fusion with lysosomes takes place, where degradation of sequestered material occurs (Bilanges et al., 2019).

Vps34 has a crucial role in embryonic development. Homozygous global knockout of Vps34 leads to early embryonic lethality between E7.5 and E8.5 with severely decreased cell proliferation. Heterozygous mice did not display any overt phenotype (Zhou et al., 2011). Additionally, the host laboratory in order to assess the catalytic-dependent functions of Vps34, generated the Vps34 kinase-dead knockin mouse model in which Vps34 kinase activity is constitutively inactive by introducing a D761A point mutation in the conserved DFG sequence in the ATP-binding site. Interestingly, while homozygous $Vps34^{D761A/D761A}$ mice were embryonically lethal

between E6.5 and E8.5, heterozygous mice were viable and fertile but displayed increased insulin sensitivity and glucose tolerance and were partially protected against high-fat-diet induced liver steatosis through AMPK pathway activation in liver and muscle without affecting insulin-induced Akt/mTORC1 pathway. These phenotypes were mimicked by Vps34 pharmacological inactivation, suggesting that Vps34 may represent a drug target for treating insulin resistance (Bilanges et al., 2017).

### 1.3.3 Class II PI3Ks

Among the three classes of PI3Ks, class II is still the least well understood class. In *D. melanogaster* and *C. elegans,* only a sole class II PI3K isoform has been identified, namely PI3K_68D (MacDougall et al., 1995) and PIKI-1 (Lu et al., 2012) (Zou et al., 2009), respectively, while class II PI3Ks are absent from yeast (Vanhaesebroeck et al., 2010). In mammals, three class II PI3K isoforms are present, namely PI3K-C2α, PI3K-C2β and PI3K-C2γ (Figure 1-7). Class II PI3K-C2α and PI3K-C2β are broadly expressed across tissues, while PI3K-C2γ is mainly enriched in the liver (Domin et al., 1997; Ho et al., 1997; Braccini et al., 2015; Misawa et al., 1998).

All class II PI3K isoforms share the conserved PI3K catalytic core, consisting of a helical domain, a kinase domain and a central C2 domain (Figure 1-7). They also contain a so-called Ras binding domain (RBD) (Figure 1-7) (Vanhaesebroeck et al., 2010; Falasca and Maffucci, 2012; Gulluni et al., 2019; Falasca et al., 2017), which most likely does not have the capability of binding Ras yet may interact with other small GTPases. For example, it has been reported that upon insulin stimulation, PI3K-C2γ is capable of binding to active Rab5 on early endosomes and through production of an endosomal pool of $PI(3,4)P_2$ maintains long-term Akt2 activation (Braccini et al., 2015). Additionally, in case of PI3K-C2β it has been speculated that its RBD is capable of binding the nucleotide-free form of Ras and this association leads not only to prevention of GTP loading of Ras, but also to suppression of PI3K-C2β lipid kinase activity *in vitro*, thus this interaction results in mutual inhibition of both partners involved (Wong et al., 2012). However, no proof of physiological significance of this speculation has been provided.

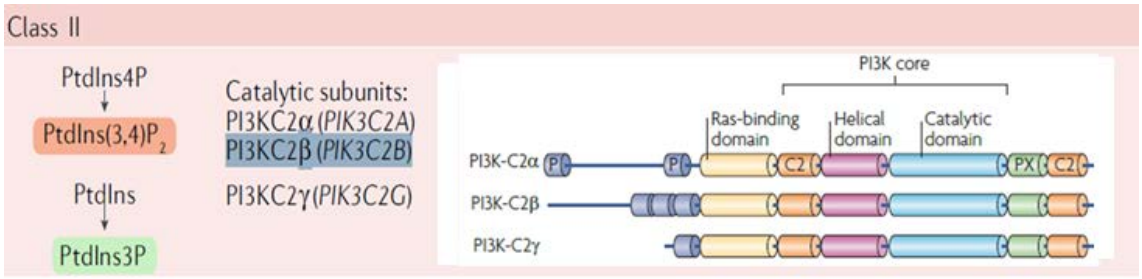


**Figure 1-7: Structure and substrate specificity of class II PI3Ks.** Class II PI3Ks generate both PI3P and PI(3,4)$P_2$. All class II PI3K isoforms contain the conserved PI3K catalytic core - consisting of a helical domain, a kinase domain and a C2 domain -, a Ras binding domain (RBD) and a C-terminal region composed of a PI-binding PX domain and a second C2 domain. The N-terminal region is distinguishable among the three class II PI3K isoforms, with PI3K-C2α containing a clathrin-binding motif and PI3K-C2β a proline-rich region. [Adapted from (Bilanges et al., 2019) and (Vanhaesebroeck et al., 2010). Copyright permission obtained by Springer Nature (Nature Reviews Molecular Cell Biology) and also by Dr Benoit Bilanges, Dr York Posor and Professor Bart Vanhaesebroeck.].

In contrast to class I PI3Ks, class II PI3Ks are large monomers lacking regulatory subunits (Figure 1-7) (MacDougall et al., 1995). They feature an extended N-terminal region which is distinct among the different isoenzymes, with PI3K-C2α containing a clathrin-binding motif and PI3K-C2β a proline-rich region (Figure 1-7). The class II PI3Ks also feature a C-terminal region composed of a PI-binding PX domain and a second C2 domain, from which the name ‘’PI3K-C2’’ is derived (Figure 1-7) (Vanhaesebroeck et al., 2010; Falasca and Maffucci, 2012; Gulluni et al., 2019; Falasca et al., 2017). The regulation of the activity of these isoenzymes is likely mediated by these N- and C-terminal regions (Falasca et al., 2017; Falasca and Maffucci, 2012; Gulluni et al., 2019; Wang et al., 2018b). A recent study showed that the PI-binding PX-C2 module in PI3K-C2α exhibits a distinct mode of kinase activity regulation (Figure 1-8) (Wang et al., 2018b). More specifically, when PI3K-C2α is found in the cytosol, it is maintained in an inactive state since its C-terminal PX-C2 module folds back onto the kinase domain, thus preventing its membrane recruitment and catalytic activity (Figure 1-8). Plasma membrane anchoring of PI3K-C2α via the interaction between its N-terminal region and clathrin results in binding of its C-terminal PX-C2 region to PI(4,5)$P_2$ and is required for PI3K-C2α full catalytic activation, thus enabling PI3K-C2α-mediated PI(3,4)$P_2$ synthesis (Figure 1-8) (Wang et al., 2018b). Interestingly, the critical residues in the kinase domain that mediate the inhibitory interaction with the PX-domain are conserved in PI3K-C2β, indicating that PI3K-C2β catalytic activity is potentially controlled by this mode of auto-inhibition (Wang et al., 2018b). A previous study also suggested that the catalytic activity of PI3K-C2β is negatively regulated by its C-terminal C2 domain, since the deletion of this domain resulted in enhanced PI3K-C2β lipid kinase activity towards PI in presence of $Mg^{2+}$ (Arcaro et al., 1998).

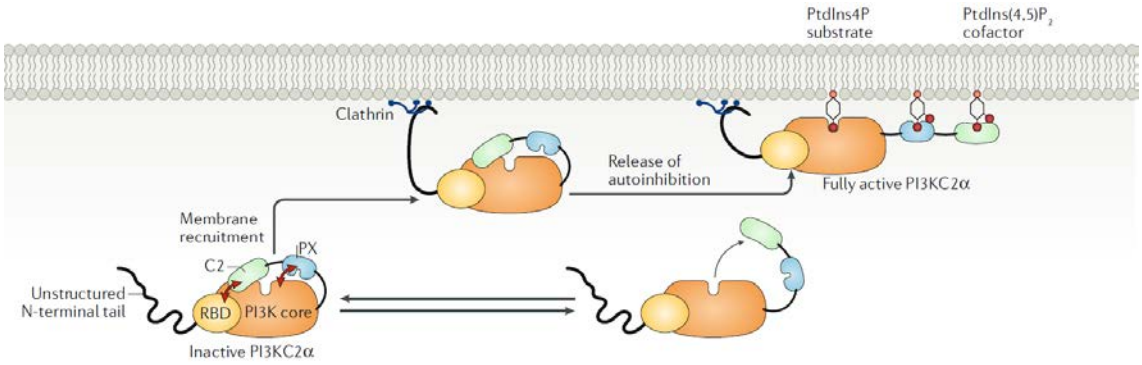


**Figure 1-8: Mechanism of activation of PI3K-C2α.** When PI3K-C2βα is cytosolic, it is maintained in an inactive state by its C-terminal PX-C2 module which folds back onto the kinase domain, resulting in the inhibition of its membrane recruitment and catalytic activity. Association between the unstructured N-terminal region of PI3K-C2α and the clathrin terminal domain leads to PI3K-C2α plasma membrane anchoring allowing the binding of its C-terrminal PX-C2 region to $PI(4,5)P_2$ resulting in their displacement from the kinase domain and PI3K-C2α full activation. In this membrane-tethering open state, PI3K-C2α kinase domain is accessible to PI4P.
PI3K: phosphoinositide 3-kinase, PtdIns4P/PI4P: phosphatidylinositol 4-phosphate, $PtdIns(4,5)P_2$/ $PI(4,5)P_2$: phosphatidylinositol 4,5-bisphosphate, [Adapted from (Bilanges et al., 2019). Copyright permission obtained by Springer Nature (Nature Reviews Molecular Cell Biology) and Dr Benoit Bilanges, Dr York Posor and Professor Bart Vanhaesebroeck.].

## 1.3.4 PI3K-C2α and PI3K-C2γ

*PI3K-C2α: Involvement in endocytic pathway*

PI3K-C2α through production of both PI3P and $PI(3,4)P_2$ has emerged as a regulator of vesicular trafficking (Bilanges et al., 2019).

During clathrin-mediated endocytosis (CME), cargo from the cell surface is transported into cells assisted by vesicles, namely clathrin-coated vesicles, thereby regulating cell surface membrane proteins (Figure 1-9). This process plays key roles in various cell biological processes such as neurotransmission, signal transmission and plasma membrane activity regulation (McMahon and Boucrot, 2011). For the different steps of clathrin-mediated endocytosis and for membrane exchange between compartments to occur, the PI-defined membrane identity is required to change. Therefore, spatiotemporal regulation of PI-metabolising enzymes plays a key role in this process (Posor et al., 2015). It is therefore not surprising that PI3K-C2α plays a role in this process. Early studies reported the presence of PI3K-C2α at clathrin-coated pits (Prior and Clague, 1999; Domin et al., 2000) as well as at the trans-Golgi network (TGN) (Domin et al., 2000). PI3K-C2α binds directly through its clathrin-box motif within its N-terminal domain to clathrin (Gaidarov et al., 2001) and produces a plasma membrane pool of $PI(3,4)P_2$ which is required for the maturation of clathrin-coated pits. $PI(3,4)P_2$ or PI3K-C2α depletion leads to defective maturation of late stage clathrin coated pits and failure to reach a fission-competent state (Posor et al., 2013). $PI(3,4)P_2$ synthesis promotes the recruitment of the PX-BAR domain protein sorting

nexin 9 (SNX9) which triggers the constriction of the membrane at the neck of the nascent vesicle, thereby promoting dynamin-mediated scission (Posor et al., 2013; Schoneberg et al., 2017).

Interestingly, PI3K-C2α by producing PI3P is also involved in cargo recycling from early and recycling endosomes to the plasma membrane (Figure 1-9) (Campa et al., 2018; Franco et al., 2014; Franco et al., 2016). PI3P synthesis by PI3K-C2α at the recycling endosomal compartment at the primary cilium base is required for Rab11 localisation and activation (Figure 1-9). Genetic loss of PI3K-C2α results in impaired Rab11 activation and primary cilia. Additionally, PI3K-C2α$^{-/-}$ embryos displayed defective delivery of the sonic hedgehog (Shh) receptor, Smoothened, to primary cilia (Franco et al., 2014). A FRET biosensor for assessing the Rab11 activity further revealed that PI3K-C2α-mediated PI3P production at early endosomes regulates Rab11 activation. Rab11-GTP in turn promotes PI 3'-phosphatase MTM1 recruitment, leading to PI3P removal and release of recycling cargo (Figure 1-9) (Campa et al., 2018).

Interestingly, PI3K-C2α has been reported to play a key regulatory role in vesicular trafficking in endothelial cells (Yoshioka et al., 2012; Biswas et al., 2013; Aki et al., 2015). There, PI3K-C2α induces angiogenic signalling pathways upon vascular endothelial growth factor (VEGF) (Yoshioka et al., 2012), sphingosine-1-phosphate (S1P1) (Biswas et al., 2013) or transforming growth factor-β (TGF-β) (Aki et al., 2015) stimulation and deficient signalling is a consequence of impaired receptor internalisation due to PI3K-C2α depletion (Yoshioka et al., 2012; Biswas et al., 2013; Aki et al., 2015). Thereby, defective endothelial cell migration, proliferation, tube formation and barrier integrity were noticed due to PI3K-C2α depletion (Yoshioka et al., 2012; Biswas et al., 2013; Aki et al., 2015).

*PI3K-C2α: Scaffolding roles*

PI3K-C2α displays not only kinase-dependent but also kinase-independent scaffold-dependent functions, as it has been demonstrated by its regulatory role in enhancing mitotic spindle stabilisation during metaphase (Figure 1-9). PI3K-C2α associates with both clathrin and Transforming Acidic Coiled-coil-Containing protein 3 (TACC3), promoting complex stability and thus acting as a crosslinker of kinetochore fibres. Loss of PI3K-C2α results in delayed mitosis and impaired cell proliferation (Gulluni et al., 2017).

*PI3K-C2α: Organismal roles*

Homozygous global PI3K-C2α knockout (Yoshioka et al., 2012; Franco et al., 2014) or constitutive PI3K-C2α kinase inactivation by a point mutation in the conserved

ATP-binding DFG site (kinase-dead knockin mouse model) (Alliouachene et al., 2016) leads to lethality between embryonic day E10.5-11.5 as a consequence of defective vascular formation (Yoshioka et al., 2012) and impaired primary cilia as well as deficient Sonic Hedgehog (Shh) signalling (Franco et al., 2014). Endothelial cell-specific loss of PI3K-C2α leads to lethality only at E16.5-E18.5 indicating that different factors from impaired angiogenesis cause embryonic lethality in PI3K-C2α knockout mice (Yoshioka et al., 2012; Bilanges et al., 2019). PI3K-C2α$^{+/-}$ mice display disrupted vascular barrier function (Yoshioka et al., 2012). Moreover, mice heterozygous for the germline kinase-inactive knock-in D1268A mutation in *PIK3C2A* (in this PI3K-C2α kinase-dead knock-in (KI) mouse model, the kinase activity of PI3K-C2α is constitutively inactivated using a gene targeting approach that introduces a D1268A point mutation in the conserved DFG motif of the ATP binding site, thereby converting it to AFG), PI3K-C2α$^{D1268A/WT}$, are characterised by abnormal platelet morphology and function (Valet et al., 2015), which leads to aberrant thrombus formation both *in vitro* and *in vivo* (Mountford et al., 2015). Additionally, PI3K-C2α$^{D1268A/WT}$ male mice display a metabolic phenotype characterised by leptin resistance and mild, late onset obesity, insulin resistance and glucose intolerance (Alliouachene et al., 2016).

Furthermore, a small percentage of patients displaying short stature, cataracts, secondary glaucoma and skeletal abnormalities amongst other symptoms, have been reported to be characterised by homozygous PI3K-C2α loss. Intriguingly, fibroblasts derived from these patients presented notably elevated PI3K-C2β expression, indicating that a potential compensatory mechanism may occur in humans (Tiosano et al., 2019).

*PI3K-C2γ*

PI3K-C2γ is the least studied amongst class II PI3Ks and is primarily expressed in the liver (Bilanges et al., 2019).

PI3K-C2γ homozygous null mice are viable and reach adulthood without displaying any apparent phenotype (Braccini et al., 2015). Nonetheless, these mice display a metabolic phenotype characterised by decreased glycogen storage in the liver, increased triglyceride levels and insulin resistance development with age or after a high-fat diet. The molecular basis for this is that PI3K-C2γ promotes Akt2 activation downstream of insulin stimulation, which specifically activates GSK3β without affecting Akt1-mediated phosphorylation of FoxO1-3 or S6K (Figure 1-9) (Braccini et al., 2015).

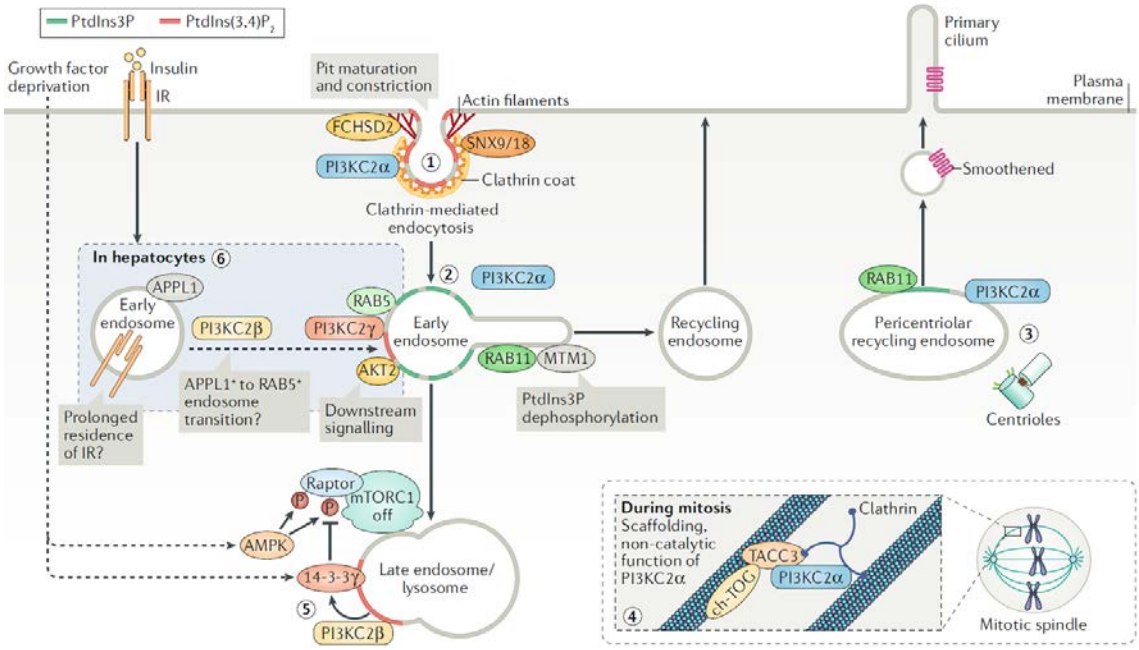


**Figure 1-9: Cell biological functions of class II PI3Ks. 1)** Class II PI3K-C2α has a well-characterised role in clathrin-mediated endocytosis. PI3K-C2α generates a - necessary for the maturation and constriction of clathrin-coated pits - plasma membrane pool of $PI(3,4)P_2$ after its direct binding through its clathrin-box motif within its N-terminal domain to clathrin. $PI(3,4)P_2$ synthesis promotes the recruitment of the PX-BAR domain proteins sorting nexin 9 (SNX9) and 18 (SNX18) which trigger the constriction of the membrane at the neck of the nascent vesicle. F- BAR domain- containing protein FCHSD2 is also activated by $PI(3,4)P_2$, enhancing further constriction. **2)** PI3K-C2α is also implicated in cargo recycling from early and recycling endosomes to the plasma membrane, through production of a PI3P pool at early endosomes, which is necessary for the RAB11 activation which in turn leads to MTM1 recruitment and PI3P reduction from the vesicles which are directed for recycling. **3)** PI3P generation mediated by PI3K-C2α in the pericentriolar recycling compartment results in RAB11 activation which is necessary for cargo delivery to the primary cilium, like the sonic hedgehog (Shh) receptor, Smoothened. **4)** PI3K-C2α also displays a kinase-independent scaffold-dependent function during mitosis by promoting mitotic spindle stabilisation during metaphase. It associates with both clathrin and Transforming Acidic Coiled-coil-Containing protein 3 (TACC3), promoting clathrin–ch- TOG–TACC3 complex stability and thus acting as a crosslinker of kinetochore fibres. **5)** In absence of growth factors, PI3K-C2β is recruited to lysosomes/late endosomes via association with the mTORC1 subunit Raptor to produce a local pool of $PI(3,4)P_2$ which promotes recruitment of 14-3-3 proteins contributing to mTORC1 repression. In response to energy stress, AMPK phosphorylates Raptor which in turn associates with 14-3-3 proteins leading to mTORC1 suppression. **6)** In hepatocytes, PI3K-C2β has emerged as a negative regulator of insulin receptor signalling without the precise mechanism for this function being characterised, APPL1 positive endosomal compartment expansion has been reported upon PI3K-C2β inactivation though. Therefore, this may result in deficient insulin receptor turnover, correlated with augmented Akt signalling upon insulin stimulation. Interestingly, PI3K-C2γ role in insulin signalling is opposed to the one of PI3K-C2β and through generation of an edosomal $PI(3,4)P_2$ pool, PI3K-C2γ maintains extended AKT2 activation.
PI3K: phosphoinositide 3-kinase, PtdIns3P/PI3P: phosphatidylinositol 3-phosphate, $PtdIns(3,4)P_2$/ $PI(3,4)P_2$: phosphatidylinositol 3,4-bisphosphate, AMPK: AMP- activated protein kinase, ch- TOG: colonic and hepatic tumor overexpressed gene. [Adapted from (Bilanges et al., 2019). Copyright permission obtained by Springer Nature (Nature Reviews Molecular Cell Biology) and Dr Benoit Bilanges, Dr York Posor and Professor Bart Vanhaesebroeck].

## 1.3.5 Activation and regulation of class II PI3K-C2β

In humans, the *PIK3C2B* gene encoding the class II PI3K-C2β isoenzyme is located on chromosome 1 at locus 1q32 (Brown et al., 1997).

The mechanisms of regulation and activation of PI3K-C2β remain largely unknown.

Early studies reported that PI3K-C2β can be activated downstream of both RTKs upon stimulation with EGF (Wheeler and Domin, 2001; Katso et al., 2006; Arcaro et al., 2000; Wheeler and Domin, 2006), PDGF (Arcaro et al., 2000) or stem cell factor (SCF) (Arcaro et al., 2002) and GPCRs following lysophosphatidic acid (LPA) (Maffucci et al., 2005) or sphingosine 1-phosphate (S1P) stimulation (Tibolla et al., 2013). Interestingly, another early study claimed that in platelets PI3K-C2β can be activated downstream of the integrin $\alpha_{IIb}\beta_3$ (Zhang et al., 1998). However, a well described physiological function of these findings is still missing. Nonetheless, PI3K-C2β has been reported to be implicated in the regulation of cell migration upon EGF (Katso et al., 2006), PDGF (Blajecka et al., 2012) or LPA (Maffucci et al., 2005) stimulation, thus the significance of these early findings can probably be seen in the context of cell migration.

Interestingly, a recent study (Marat et al., 2017) showed that PI3K-C2β is capable of regulating mTORC1 signalling and lysosomal positioning in absence of growth factors, a seemingly unrelated process to its activation upon growth factor stimulation. The N-terminal region of PI3K-C2β contains two sites (residues 80-130 and 200-280) that can associate with the Raptor subunit of mTORC1 (Marat et al., 2017). Furthermore, a following study from the same laboratory (Wallroth et al., 2019) showed that growth factor signalling suppresses PI3K-C2β through its phosphorylation at T279 mediated by protein kinase N 2 (PKN2) whose activation is induced by mTORC2. PI3K-C2β phosphorylation generates a docking site for 14-3-3 proteins that leads to PI3K-C2β cytoplasmic retention (Wallroth et al., 2019).

Similarly to PI3K-C2α, clathrin has been reported to interact with the N-terminal region (residues 1-130) of PI3K-C2β (Wheeler and Domin, 2006) and GFP-PI3K-C2β localisation at clathrin–coated pits (CCPs) has also been shown (Nakatsu et al., 2010). However, no function during endocytosis has been identified for this class II PI3K isoform, thus the biological significance of these findings needs to be investigated further. Additionally, based on yeast two-hybrid screening (Y2H), PI3K-C2β was identified as an interaction partner of intersectin (ITSN) (Das et al., 2007), a scaffold protein which is involved in the regulation of endocytosis and signal transduction (Das et al., 2007; Hunter et al., 2013), and this interaction was further confirmed by GST-pull down assays. The first out of five C-terminal SH3 domains of ITSN binds within the PI3K-C2β N-terminal region (Das et al., 2007).

Another function of PI3K-C2β has been reported to be in the activation of T cells (Srivastava et al., 2009; Cai et al., 2011) and mast cells (Srivastava et al., 2012; Srivastava et al., 2017) through regulation of the intermediate-conductance calcium-activated potassium channel KCa3.1. PI3K-C2β is activated downstream of the T cell

receptor (TCR) to promote the opening of KCa3.1 channel which through $K^+$ efflux sustains a negative membrane potential required for $Ca^{2+}$ influx and production of cytokines (Srivastava et al., 2009). PI3K-C2β polyubiquitination at lysine 49 mediated by tripartite motif containing protein 27 (TRIM27), an E3 ubiquitin ligase, results in its catalytic inactivation, thus negatively regulating KCa3.1 channel activity (Cai et al., 2011). Similarly, in mast cells PI3K-C2β functions as a positive regulator of their activation and TRIM27 antagonises this function (Srivastava et al., 2012; Srivastava et al., 2017). Therefore, further investigation needs to be performed in order to explore a potential pharmacological significance of these findings, for example in allergy.

Consistent with a potential inhibitory role of the C-terminal C2 domain of PI3K-C2β, several studies reported that calcium-dependent proteases, namely calpains, mediate PI3K-C2β activation. This effect is thought to be achieved by proteolytic cleavage of the C-terminal C2 domain and can be prevented by calpeptin, a pharmacological inhibitor of calpains. This mode of PI3K-C2β activity regulation has been reported to happen upon hepatocyte growth factor (HGF) stimulation of kidney cortical slices (Crljen et al., 2002), in platelet aggregation (Zhang et al., 1998) and also in nuclei during liver regeneration (Sindic et al., 2001; Sindic et al., 2006) and during G2/M phase (Visnjic et al., 2003). Another study claimed that nuclear PI3K-C2β activation can be mediated by its phosphorylation in ATRA (all-*trans*-retinoic acid)-induced cell differentiation (Visnjic et al., 2002).

### 1.3.6 Cell biological functions of PI3K-C2β

Despite the increasing attention PI3K-C2β is receiving, its precise biological functions and mechanisms of action have not been fully characterised yet. The majority of studies attempting to uncover the biological roles of this PI3K isoform are cell-based studies using either siRNA- or shRNA-mediated depletion of PI3K-C2β or overexpression approaches and hence do not allow the discrimination between kinase-dependent and scaffolding roles. Two seemingly unconnected processes have been reported to be influenced by PI3K-C2β: cell migration and regulation of mTORC1.

*Cell migration*

Several lines of evidence implicate PI3K-C2β in regulation of cell migration and actin cytoskeleton remodelling (Maffucci et al., 2005; Domin et al., 2005; Katso et al., 2006; Kitatani et al., 2015; Blajecka et al., 2012). siRNA mediated depletion of PI3K-C2β led to reduced cell migration (Kitatani et al., 2015) upon LPA (Maffucci et al., 2005), sphingosine 1-phosphate (S1P) or high density lipoprotein ($HDL_3$) (Tibolla et al., 2013) stimulation and also to decreased lamellipodium formation (Kitatani et al., 2015).

Consistent with these observations, overexpression approaches also reported a regulatory role of PI3K-C2β in cell migration (Katso et al., 2006; Domin et al., 2005).

Additionally, PI3K-C2β has been linked to Ras-related C3 botulinum toxin substrate (Rac), which is a member of the Rho GTPase family with a key role in cell migration by promoting actin polymerisation and lamellipodium formation (Ridley, 2015). PI3K-C2β has been reported to regulate cell migration in a Rac-dependent manner (Katso et al., 2006; Blajecka et al., 2012), with PI3P being its supposed lipid product (Domin et al., 2005; Maffucci et al., 2005). The implication of this PI3K isoform in the regulation of Rac activity has been proposed to be mediated by its association with the Eps8/Abi1/Sos1 complex (Katso et al., 2006), which exhibits Rac-specific GEF (guanine nucleotide exchange factor) activity (Scita et al., 1999; Katso et al., 2006). Therefore, upon EGF stimulation the PI3K-C2β-Grb2-Abi1-Eps8-Sos1 complex can be generated and recruited to the activated EGFR directly or indirectly via Shc (Katso et al., 2006). PI3K-C2β has also been suggested to be involved in the regulation of Rac activity upon PDGF stimulation (Blajecka et al., 2012), further indicating a potential role of this isoform in the regulation of Rac activity. PI3K-C2β has also been reported to be involved in the regulation of RhoA activity, which is another member of Rho GTPase family and plays a crucial regulatory role in cell migration by promoting assembly of bigger and mature integrin-based cell-matrix adhesions and stress fibres and also actomyosin contraction (Ridley, 2015), upon LPA stimulation and in presence of serum (Blajecka et al., 2012). This is consistent with the suggested role of PI3K-C2β in the regulation of cell migration upon LPA stimulation (Maffucci et al., 2005) and in presence of serum (Kitatani et al., 2015; Domin et al., 2005). The potential role of PI3K-C2β in the regulation of RhoA or Rac activity has also been suggested to be mediated by its association with the RhoGEF, Dbl (Blajecka et al., 2012).

Cell migration plays a crucial role in progression of cancer. Cancer is one of the most severe health problems around the world. More than 90% of deaths caused by cancer are due to metastasis formation, i.e. the capability of cancer cells to migrate to distant organs where they proliferate and generate secondary tumours (Spano et al., 2012). The involvement of PI3K-C2β in cancer cell migration has recently started being identified in breast cancer (Chikh et al., 2016) and in prostate cancer (Mavrommati et al., 2016). More specifically, increased PI3K-C2β expression levels have been reported in several human breast cancer cell lines and in human breast cancer biopsies (Chikh et al., 2016) and inhibition of breast cancer cell invasion *in vitro* and of breast cancer metastasis generation *in vivo* is observed upon its shRNA mediated-depletion (Chikh et al., 2016). Similarly, downregulation of PI3K-C2β in prostate cancer cells reduces cell migration and invasion *in vitro* (Mavrommati et al., 2016). Furthermore, miR-362-5p, a

microRNA (miRNA) which acts as tumour suppressor and shows decreased expression in metastatic neuroblastoma, has been suggested to prevent neuroblastoma cell growth, migration and invasion at least in part through direct downregulation of PI3K-C2β (Wu et al., 2015b). Additionally, it has also been hypothesised that PI3K-C2β promotes cell invasion through downregulation of miR-449a, microRNA with potentially tumour suppressing properties (Chikh et al., 2016). Further investigation is required to define the potential link between PI3K-C2β and microRNAs and its involvement in the regulation of cell invasion. Furthermore, it has been reported that PI3K-C2β depletion in ovarian cancer cells leads to inhibition of lamellipodium formation and decreased metastasis in a xenograft model of human ovarian cancer (Kitatani et al., 2015).

Overall, a bulk of studies implicates PI3K-C2β in the regulation of cell migration and invasion. However, it is relatively little known about how PI3K-C2β affects the process of cell migration. Thus, further investigation to uncover the precise molecular mechanism of PI3K-C2β in cell migration is required considering the high organismal importance of this process, for example in cancer metastasis.

*mTORC1 regulation*

Another biological process that PI3K-C2β has been shown to regulate is mTORC1 signalling and lysosomal positioning in response to growth factors (Figure 1-9) (Marat et al., 2017). More specifically, in absence of growth factors, PI3K-C2β is recruited to lysosomes/late endosomes through its N-terminal region (residues 80–130 and 200–280) by binding to the mTORC1 subunit Raptor (Figure 1-9). Local synthesis of $PI(3,4)P_2$ mediates mTORC1 suppression by facilitating the recruitment of 14-3-3 proteins (Figure 1-9) (Marat et al., 2017). This is in agreement with an earlier study showing that in response to energy stress, Raptor phosphorylation by AMPK results in its association with 14-3-3 proteins and mTORC1 repression/inhibition (Gwinn et al., 2008). Of note, mTORC1 signalling in PI3K-C2β-depleted breast cancer cell lines seems not to be affected (Chikh et al., 2016), indicating that in a tumour context mTORC1 signalling is possibly regulated independently of PI3K-C2β.

mTORC1 activity is also regulated by the positioning of lysosomes, the obligate platform of mTORC1 activation within the cell. In the absence of nutrients, lysosomes are clustered in the perinuclear area, while in nutrient abundance, they localise close to the plasma membrane, and thus mTORC1 is found in close proximity to signals form cell surface receptors. Therefore, peripheral lysosomal dispersion correlates with mTORC1 high activity, whereas perinuclear clustering correlates with mTORC1 activity suppression (Bilanges et al., 2019; Korolchuk et al., 2011; Wallroth and Haucke, 2018).

Consistently, depletion of PI3K-C2β leads to peripheral lysosomal dispersion and elevated mTORC1 activity (Marat et al., 2017). However, further investigation is required in order to define the upstream part of this signalling pathway, i.e. how this association between PI3K-C2β and Raptor is induced upon growth factor deprivation and also how increased PI3K-C2β activation is correlated with absence of growth factors. Furthermore, it is remains unknown whether the regulation of lysosomal positioning is a cause or consequence of PI3K-C2β mediated mTORC1 regulation.

### 1.3.7 Organismal functions of PI3K-C2β

PI3K-C2β knockout (KO) mice are viable without any overt phenotype (Harada et al., 2005). Additionally, the host laboratory in order to assess the catalytic-dependent functions of PI3K-C2β, generated the kinase-dead knockin (KI) mouse model in which PI3K-C2β kinase activity is constitutively inactive by introducing a D1212A point mutation in the conserved DFG motif of the ATP binding site (Alliouachene et al., 2015). Similarly to PI3K-C2β KO mice (Harada et al., 2005), the PI3K-C2β kinase-dead KI mice are viable without any overt phenotype but are characterised by augmented insulin sensitivity and glucose tolerance and are also protected against high-fat-diet-induced liver steatosis (Alliouachene et al., 2015). Furthermore, upon insulin stimulation, PI3K-C2β catalytic inactivation leads to enhanced class I PI3K-dependent Akt signalling specifically in metabolic tissues (liver, muscle and white adipose) (Alliouachene et al., 2015). Interestingly, Akt activation downstream of PI3K-C2β activation has also been reported by an earlier study in neurons upon EGF stimulation (Das et al., 2007). Additionally, PI3K-C2β inactivation in hepatocytes results in decreased PI3P synthesis and this in turn causes APPL1 positive endosomal compartment expansion. This potentially leads to defective insulin receptor turnover, corresponding to enhanced Akt signalling in response to insulin (Figure 1-9) (Alliouachene et al., 2015). This hypothesis is consistent with an earlier study showing that accumulation of APPL1 positive endosomes caused by decreased levels of PI3P leads to increased EGFR signalling (Zoncu et al., 2009).

Intriguingly, this metabolic phenotype displayed by PI3K-C2β kinase dead KI mice (Alliouachene et al., 2015) is quite different from the one demonstrated by PI3K-C2γ homozygous null mice (Braccini et al., 2015) (see section 1.3.3), indicating that these two class II isoforms in hepatocytes mediate quite different functions in insulin signalling. Therefore, the distinctive roles of PI3K-C2β and PI3K-C2γ in the liver indicate that different class II PI3K isoforms are not redundant but display specific functions.

A surprising physiological role of PI3K-C2β has been described in the context of X-linked myotubular myopathy, a severe paediatric neuromuscular disease caused by loss-of-functions mutations in the PI 3'-phosphatase myotubularin 1 (MTM1). This results in elevated PI3P levels which are correlated with the pathogenesis of this disorder (Sabha et al., 2016). Interestingly, muscle specific PI3K-C2β KO in MTM1 KO mice brings PI3P levels back to normal and restores muscle morphology. Moreover, the survival of these mice is similar to WT mice (Sabha et al., 2016). Overall PI3K-C2β deletion is capable of preventing and reversing the phenotype caused by *MTM1* loss even at the late stages of this disorder (Sabha et al., 2016), highlighting the therapeutic potential of pharmacological PI3K-C2β kinase inhibitors in this human disorder.

### 1.3.8 PI3K-C2β and cancer

The majority of available studies involving PI3K-C2β in cancer indicate a positive role for this PI3K isoform in promoting tumorigenesis.

Overexpression of PI3K-C2β has been reported to occur in many human cancers (Arcaro et al., 2002; Boller et al., 2012; Zhang et al., 2007; Chikh et al., 2016; Liu et al., 2011; Knobbe and Reifenberger, 2003; Russo and O'Bryan, 2012; Russo et al., 2015; Sato et al., 2004). Interestingly, *PIK3C2B* shares its locus (1q32) with *MDM4* (which encodes a negative p53 tumour suppressor protein regulator), thus the amplification of *PIK3C2B* potentially happens subsequently form amplification of *MDM4* (Rao et al., 2010; Riemenschneider et al., 2003; Nobusawa et al., 2010), but it is unclear whether PI3K-C2β amplification itself actually promotes tumour growth. Moreover, whole exome sequencing has revealed *PIK3C2B* to be highly mutated in non-small cell lung cancer (Liu et al., 2012). More specifically, this study aimed to analyse common and unique mutations as well as activation of related to lung cancer pathwaysin both lung adenocarcinomas (ADC) and squamous cell carcinomas (SCC) (Liu et al., 2012). Interestingly, *PIK3C2B* was detected to harbour missense mutations with prediction to alter protein function and it was mutated in both ADC and SCC, without being identifying which regulatory process or pathway related to lung cancer was affected though (Liu et al., 2012). It has also been reported that the correlation between SNPs in the *PIK3C2B* promoter region and the prostate cancer risk is important (Koutros et al., 2010). The implication of PI3K-C2β in resistance to anti-cancer drugs has also been claimed (Diouf et al., 2011; Liu et al., 2011; Low et al., 2008). Furthermore, it has been reported that PI3K-C2β depletion reduces neuroblastoma tumour growth (Russo et al., 2015) as well as breast cancer growth (Chikh et al., 2016) *in vivo*.

Nonetheless, it is relatively little known about how PI3K-C2β affects the process of tumorigenesis, thus further investigation needs to be performed to elucidate its mechanism of action in this process. It will be also interesting to investigate whether the effect of PI3K-C2β in cancer is through its regulatory role in cell migration.

## 1.4 Cell adhesions

Integrin-dependent cell-matrix adhesions are dynamic, bidirectional structures connecting the actin cytoskeleton and intermediate filaments with the extracellular matrix (ECM) or other cells. They play crucial roles in multiple processes, such as morphogenesis, cell migration, cell growth and proliferation, cell differentiation, signal transmission across the cell membrane and also inflammatory responses (Kanchanawong et al., 2010; Geiger et al., 2001; Walker and Assoian, 2005; Assoian and Klein, 2008; Schwartz and Assoian, 2001; Barone and Heisenberg, 2012; Brown et al., 2000; Bergmeier and Hynes, 2012). It is therefore not surprising that abnormal regulation of cell adhesions is implicated in pathological conditions, such as cancer (Playford and Schaller, 2004; Sulzmaier et al., 2014; Kanteti et al., 2016).

### 1.4.1 Integrins

The family of integrins are the most well-characterised cell surface adhesion receptors. They connect the intracellular with the extracellular environment by linking the ECM with the actin cytoskeleton and intermediate filaments. Integrins are transmembrane heterodimers composed of α and β subunits, which are paired via non-covalent interactions. Eighteen α and eight β subunits exist and through different combinations generate at least twenty-four distinctive integrin heterodimers. The large extracellular domain of integrins specifies the ECM components (or cell), such as fibronectin, laminins, collagens and vitronectin that are recognised by them; thereby the ECM substrates that a cell can bind are defined by the repertoire of expressed and active integrins on its plasma membrane. The majority of integrins can associate with more than one ligand and also the same ligands can be recognised by different integrins. The short cytoplasmic tail of integrins lacks enzymatic activity and mediates the linkage to the actin cytoskeleton through multiprotein complexes (Manakan Betsy Srichai, 2010; Askari et al., 2009; Legate et al., 2009; Bridgewater et al., 2012; Hohenester, 2014; Takagi et al., 2002; Moreno-Layseca et al., 2019; De Franceschi et al., 2015).

Integrins are able to switch between conformations with low- and high-affinity for extracellular ligands. They can be found in either i.) a bent conformation with low ligand affinity, ii.) a ‘’primed’’, extended conformation with low ligand affinity or iii.) an active,

extended conformation with high ligand affinity and they are capable of transmitting signals bi-directionally (Figure 1-10). Therefore, they are able not only to induce intracellular responses upon ligand binding (classical ‘’outside-in’’ signalling) but also to alter their affinity for extracellular ligands in response to intracellular stimuli (‘’inside-out’’ signalling or integrin activation) (Figure 1-10). In ‘’inside-out’’ signalling, intracellular signals induce the association of proteins, like talin and kindlins, with the β integrin cytoplasmic tail. This in turn controls the activation state of integrins by promoting a conformational change which stabilises an extended conformation. In this extended conformation, the ligand-binding site is exposed and exhibits high ligand affinity, permitting its association with extracellular ligand (Figure 1-10). Once integrins are activated and bound to ligand, they cluster at the plasma membrane (increased avidity) and are capable of transmitting signals from the outside to inside leading to recruitment of protein complexes (composed of scaffolding proteins, kinases, phosphatases and others) to the integrin cytoplasmic regions to control multiple cellular functions (‘’outside-in’’ signalling) (Figure 1-10). (Manakan Betsy Srichai, 2010; Askari et al., 2009; Legate et al., 2009; Bridgewater et al., 2012; Hohenester, 2014; Takagi et al., 2002; Moreno-Layseca et al., 2019; De Franceschi et al., 2015; Paul et al., 2015).

Another level of regulation of integrin function can be accomplished by their endocytic trafficking (Moreno-Layseca et al., 2019; De Franceschi et al., 2015; Paul et al., 2015). Different integrins follow different routes of internalisation, namely clathrin-mediated endocytosis, macropinocytosis, or different routes of clathrin-independent endocytosis. They are delivered to Rab-5 positive early endosomes, where they are sorted either for degradation in late endosomes/lysosomes or for recycling back to the plasma membrane. Recycling back to the plasma membrane occurs through either the Rab4-dependent short-loop pathway (fast recycling route) or the long-loop pathway (slow recycling route) where relocation of integrins to Rab11-positive perinuclear recycling compartments takes place before they are delivered back to the plasma membrane (Moreno-Layseca et al., 2019; De Franceschi et al., 2015; Paul et al., 2015). The majority of integrins is recycled, constantly supplying the cell with integrins to bind the ECM and form new adhesions (Moreno-Layseca et al., 2019; De Franceschi et al., 2015; Paul et al., 2015). The actin cytoskeletal machinery together with Rho GTPases, which regulate actin dynamics (Ridley, 2006), and members of Rab and Arf families of small GTPases with crucial roles in regulation of membrane trafficking, are critical for the regulation of integrin trafficking through the endocytic system (Moreno-Layseca et al., 2019; De Franceschi et al., 2015; Paul et al., 2015).

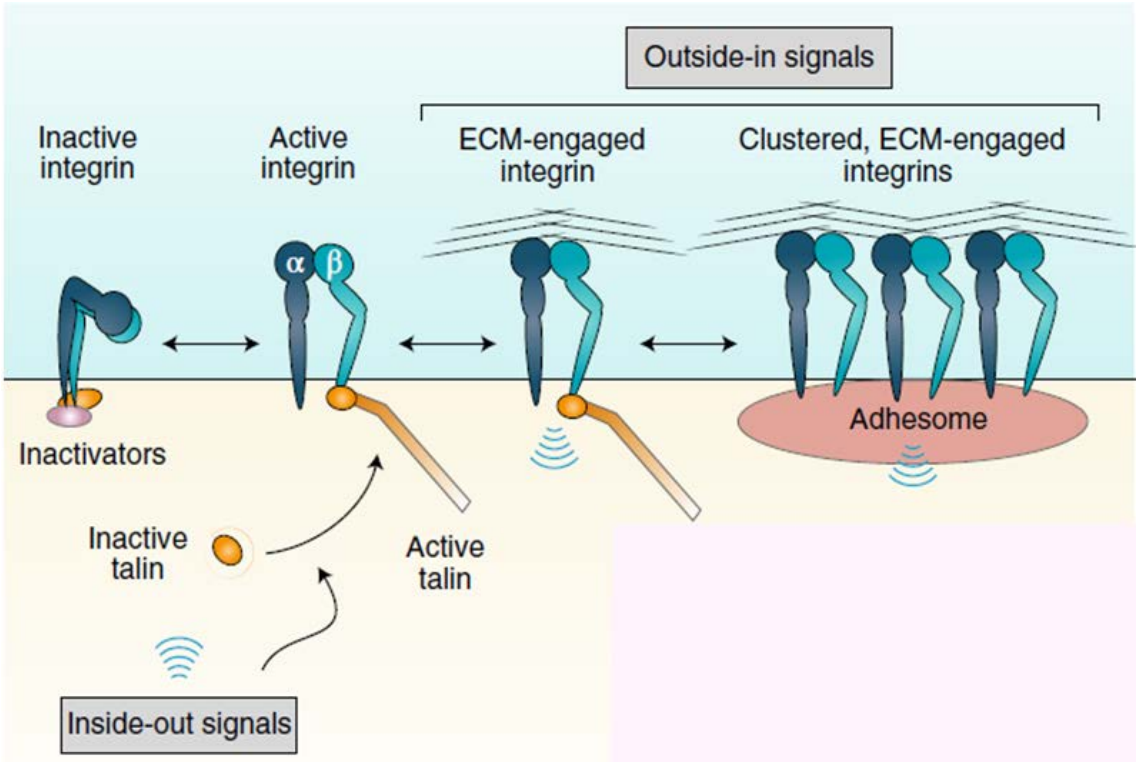


**Figure 1-10: Integrins signal bi-directionally**. In ''inside-out'' signalling, intracellular signals promote the association of talin with β integrin cytoplasmic tails, which in turn controls the integrin affinity for engagement to extracellular matrix components**.** Once integrins are activated and bound to ligand, they cluster at the plasma membrane leading to signal transmission from the outside to inside resulting in recruitment of protein complexes (composed of scaffolding proteins, kinases, phosphatases and others) to the integrin cytoplasmic regions to regulate multiple cellular functions (''outside-in'' signalling). [Adapted from (Moreno-Layseca et al., 2019). Copyright obtained by Springer Nature (Nature Cell Biology) and also by Professor Johanna Ivaska].

## 1.4.2 Adhesion structures, actin cytoskeleton dynamics and cell migration

*Adhesome*

The linkage between integrins and the actin cytoskeleton as well as downstream signal transduction cascades is mediated by a complex multiprotein network consisting of more than 200 molecules, collectively called ''adhesome''. The adhesome is responsible not only for the physical association between integrins and actin filaments, but also for the adhesion dependent signalling activity (Winograd-Katz et al., 2014; Zaidel-Bar et al., 2007; Parsons et al., 2010; Legate et al., 2009; Zaidel-Bar and Geiger, 2010). Considering the complexity of this network of protein interactions and its requirement to be very dynamic and robust at the same time, it is not surprising that these protein interactions can be turned ''on'' and ''off'' through multiple regulatory mechanisms (Zaidel-Bar and Geiger, 2010).

*Integrin-based cell-matrix adhesion components*

In general, the establishment and maintenance of the integrin-actin cytoskeleton link is mediated by integrin-based cell-matrix adhesion components. These include molecules which bind directly to both integrin cytoplasmic domains and

F-actin (like talin, α-actinin and filamin), proteins which bind directly to integrin cytoplasmic domains and indirectly to actin filaments (like paxillin, focal adhesion kinase (FAK), kindlins and integrin-linked kinase (ILK)), proteins that bind to actin filaments but not to integrins (like vinculin) and other proteins including adaptors (like zyxin) and enzymes (like class I PI3Ks, the tyrosine kinase Src and the protease calpain) (Manakan Betsy Srichai, 2010; Legate et al., 2009; Geiger et al., 2001).

*Types of integrin-based cell-matrix adhesion structures*

Several integrin-dependent cell-matrix adhesion structures have been described and their formation is considered to be a sequential procedure governed by the hierarchical recruitment of different adhesion components that mediate the ECM (extracellular matrix)-actin cytoskeleton linkage, thus these different adhesion structures are likely not representing separate classes (Parsons et al., 2010; Zaidel-Bar et al., 2004).

Nascent adhesions are the earliest observable small, highly dynamic adhesion structures, thus they are not easily detectable in all cell types. These adhesion structures can sequentially mature to relatively bigger dot-like and more stable focal complexes. Both these adhesion structures are found at the lamellipodium, with the former residing exactly behind the leading edge and the latter further back at the boundary between lamellipodium and lamella, a distinctive actin-rich region behind the lamellipodium (Parsons et al., 2010; Huttenlocher and Horwitz, 2011). Focal adhesions are considered as the ‘’classical’’ mature integrin-dependent cell-matrix adhesions and are more elongated and bigger structures compared to their precursors, the focal complexes. They usually anchor ends of stress fibres and can be found at both peripheral and central cell regions (Parsons et al., 2010; Huttenlocher and Horwitz, 2011; Geiger et al., 2001; Zaidel-Bar et al., 2004; Hotulainen and Lappalainen, 2006). Fibrillar adhesions reside more centrally in the cells and are more specialised, mature, rich in tensin and $\alpha_5\beta_1$ integrin, long-lived highly elongated streak-like structures. These adhesion structures are implicated in the assembly of fibronectin matrix and ECM remodelling (Zamir et al., 2000; Geiger et al., 2001; Parsons et al., 2010).

Podosomes and invadopodia are actin-enriched specialised types of integrin-based adhesions associated with a high migratory and invasive capability, respectively, and are distinctively present in some normal cells, like immune cells and osteoclasts (podosomes), as well as in tumour cells (invadopodia) (Parsons et al., 2010, Huttenlocher and Horwitz, 2011, Geiger et al., 2001). Both of them have the capability of ECM degradation by localised protease secretion (Parsons et al., 2010, Huttenlocher and Horwitz, 2011).

Different matrix-adhesion structures are required for different physiological processes. Generally, the size of adhesion structures is considered to inversely correlate with migration velocity, thus it is not surprising that cell migration is facilitated by highly dynamic short-lived adhesion structures, whereas tissue maintenance and organisation are enabled by stable, mature adhesion structures (Goult et al., 2018; Huttenlocher and Horwitz, 2011).

The generation of nascent adhesions is independent of myosin II, whereas myosin II-dependent tensile forces are critical for adhesion maturation (Parsons et al., 2010). Different components exhibit distinct sensitivity though, for example integrins and paxillin are incorporated independently of tensile forces, while zyxin and α-actinin depend on these (Parsons et al., 2010).

*Talin: a key component of adhesion structures*

During the process of adhesion maturation, new adhesion components appear and also the conformation of others can change, for example in response to tension.

Actin filament-bound talin is already detected at the stage of nascent adhesions and is a very important component of integrin-dependent cell-matrix adhesion structures (Legate et al., 2009; Parsons et al., 2010; Zaidel-Bar et al., 2004; Klapholz and Brown, 2017; Goult et al., 2018). Talin binds the cytoplasmic tails of β integrins and plays a crucial role in the bi-directional signalling of integrins. It possesses two integrin-binding sites and three actin-binding sites. It consists of a FERM domain-containing N-terminal head region, which associates with integrin cytoplasmic tails, and a tail rod region. This tail contains the second integrin-binding site and two actin-binding sites, as well as multiple vinculin binding sites whose exposure is mediated by mechanical force promoting adhesion maturation. Talin also plays a crucial role in outside-in integrin signalling by promoting integrin clustering at the plasma membrane and mediating the integrin linkage to the actin cytoskeleton leading in FA assembly together with other FA components. Considering the critical role of talin in integrin activation, it is not surprising that the activity of talin is strictly regulated and it is found in a closed, auto-inhibited conformation which is required to be relieved in order its binding sites to be exposed. $PI(4,5)P_2$ is a talin activator and the talin head is able to associate with PIPKIγ resulting in $PI(4,5)P_2$ production which reinforces integrin activation and focal adhesion formation (Manakan Betsy Srichai, 2010; Klapholz and Brown, 2017; Gough and Goult, 2018; Wang et al., 2018a).

Paxillin, a scaffolding protein which binds to integrin cytoplasmic domains, is also found at nascent adhesions. It has been proposed that focal adhesion kinase (FAK)-mediated phosphorylation of paxillin exposes its binding site for vinculin, which

in turn is ‘’delivered’’ to talin and actin, with $PI(4,5)P_2$ in the membrane further promoting vinculin’s activation (Pasapera et al., 2010; Atherton et al., 2016).

*Cell-matrix adhesion signalling*

Tyrosine phosphorylation plays a crucial role in cell-matrix adhesion signalling, with the non-receptor tyrosine kinases FAK and Src being two key regulators (Legate et al., 2009; Wozniak et al., 2004). Integrin ligand-binding and clustering leads to FAK activation by autophosphorylation at tyrosine 397 (Y397), to which Src is in turn recruited via its SH2 domain, resulting in stabilisation of the active state of Src (Legate et al., 2009; Wozniak et al., 2004). Sequentially, phosphorylation of additional tyrosines in FAK leads to complete activation of both enzymes. The newly phosphorylated residues function as docking sites for more adhesion components containing SH2 domains (Legate et al., 2009; Wozniak et al., 2004). One such example is the scaffold protein paxillin, which is tyrosine-phosphorylated by Src and FAK to generate docking sites for other proteins, thereby contributing to the formation of a large multiprotein complex (Legate et al., 2009; Kanteti et al., 2016).

*Physiological relevance of integrin-mediated cell adhesion*

Circulating platelets and leukocytes in the blood maintain their integrins in an inactive conformation until they face their ligands (Klapproth et al., 2015). Integrins represent the principal receptors of platelets that mediate both platelet adhesion and aggregation (Stefanini and Bergmeier, 2016). In intact vessels, platelets are sustained in a non-adhesive, quiescent mode (Stefanini and Bergmeier, 2016). The small GTPase Rap1 (Ras-related protein 1) has emerged to display a critical regulatory role in cell adhesion (Boettner and Van Aelst, 2009; Bos et al., 2001). Rap1, which exists in two isoforms-Rap1a and Rap1b-, has emerged to display a key role in theactivation of platelet integrins (Stefanini and Bergmeier, 2016; Chrzanowska-Wodnicka et al., 2005). Rap1b knockout mice are characterised by extended tail bleeding times and also protection against arterial thrombosis in vivo (Chrzanowska-Wodnicka et al., 2005). Additionally, T- and B- cells derived from Rap1a knockout mice display defective adhesion capability onto fibronectin or ICAM (intercellular adhesion molecule) (Duchniewicz et al., 2006). Furthermore, primary T-cells derived from transgenic mice expressing constitutively active Rap1a, V12Rap1a, under the control of a promoter which is specific for T-cells, show enhanced integrin-based adhesion onto fibronectin or ICAM-1 (Sebzda et al., 2002). As it has already been mentioned, talin represents a crucial component of adhesion structures with a key role in integrin activation both *in vitro* and *in vivo*in platelets and leukocytes (Klapholz and Brown, 2017; Nieswandt et al., 2007; Petrich et al., 2007). Interestingly, in leukocytes, RIAM (Rap1-GTP–

interacting adaptor molecule) which is a Rap1 effector, plays a key role in β2 integrin activation through its contribution to talin activation, while in platelets RIAM is not required (Klapproth et al., 2015; Klapholz and Brown, 2017). The activation status of Rap1 is regulated by GAPs and GEFs, with the Rap-GEF, CalDAG-GEFI, being reported as a crucial inducer of platelet activation and the the Rap-GAP, RASA3, being reported as a crucial inhibitor of platelet activation (Stefanini and Bergmeier, 2016).

A recent study focused on phenotypes related to not finely-regulated integrin-based cell-ECM adhesions used a mouse model in which talin auto-inhibition is impaired by an activating point mutation in talin (*Tln1*$^{E1770A}$) (Haage et al., 2018). MEFs derived from these mice are characterised by increased adhesion capability, deficient cell spreading and defective cell migration (Haage et al., 2018). Moreover, mice with defective talin auto-inhibition show impaired wound healing *in vivo,* as it was assessed by a biopsy punch wound healing assay (Haage et al., 2018).

### 1.4.3 Cell migration

Cell migration is a fundamental process involved in both physiological processes, such as embryogenesis, tissue repair and regeneration, and immune responses and pathological processes, such as cancer metastasis, atherosclerosis, arthritis, autoimmune diseases and chronic inflammation. It requires well-orchestrated coordination between constant FA assembly, maturation and disassembly and actin cytoskeleton reorganisation (Webb et al., 2002; Ridley et al., 2003; Lauffenburger and Horwitz, 1996; Ridley, 2015; Le Clainche and Carlier, 2008; Huttenlocher and Horwitz, 2011; Parsons et al., 2010).

*Rho GTPases*

Fundamentally, cell migration can be described as a cycle consisting of multiple steps. The Rho family of small GTPases are key components in the regulation of all the different types of cell migration with cell division control protein 42 (Cdc42), Rac, and Ras homologue gene family, member A (RhoA) being the most broadly studied (Ridley, 2015; Lawson and Ridley, 2018). These small GTPases cycle between an inactive GDP-bound and an active GTP-bound state. Key regulators in the shift between these two conformations are Rho-specific GEFs, which promote the exchange of GDP for GTP, and GAPs, which perform the catalysis of GTP hydrolysis to GDP (Ridley, 2015; Lawson and Ridley, 2018; Hodge and Ridley, 2016). Moreover, guanine nucleotide dissociation inhibitors (GDIs) associate with the GDP-bound conformation of Rho GTPases in the cytosol and prevent their recruitment to membranes or their activation by GEFs (Hodge and Ridley, 2016).

*Cell polarisation, membrane protrusions and adhesion structures assembly*

In lamellipodium-dependent migration, the initial step is cell polarisation and extension of actin-driven membrane protrusions, including lamellipodia and filopodia (Ridley, 2006; Ridley, 2015; Lawson and Ridley, 2018; Ridley et al., 2003; Parsons et al., 2010; Le Clainche and Carlier, 2008). The leading edge and the cell rear are characterised by distinct actin cytoskeleton organisation and adhesion structures (Ridley et al., 2003; Vicente-Manzanares et al., 2009). Cdc42, which determines cell polarity through the Par polarity complex and microtubules, and Rac are active at the cell front of migrating cells (Ridley, 2006; Ridley, 2015; Lawson and Ridley, 2018; Ridley et al., 2003; Parsons et al., 2010; Le Clainche and Carlier, 2008). Flat, broad plasma membrane extension in the lamellipodium is principally induced by Rac through activation of the WAVE complex, which in turn induces actin polymerisation through Arp2/3 complex activation (Figure 1-11) (Ridley, 2015). Filopodia are long, thin membrane protrusions whose formation is predominantly induced by Cdc42, which acts primarily through mDia formins (Ridley, 2015). Moreover, RhoA is also activated at the leading edge and it probably acts through formins (mDia1) to trigger actin polymerisation (Ridley, 2015; Parsons et al., 2010). These membrane projections are stabilised by the generation of integrin-based adhesions, which link the actin cytoskeleton to ECM. They also provide signals which stimulate Rac and Cdc42 activation, leading to amplified actin polymerisation at the cell front and generation of pushing forces that move the membrane forward (Figure 1-11) (Ridley et al., 2003; Parsons et al., 2010; Svitkina, 2018).

*Adhesion structures growth and maturation*

Concomitantly with the lamellipodium forward movement, nascent adhesions either dismantle or grow further and mature to focal complexes and focal adhesions at the transition zone between lamellipodium and lamella, with RhoA playing a key role in this process (Figure 1-11) (Parsons et al., 2010; Vicente-Manzanares et al., 2009). RhoA activates myosin II through its downstream effector Rho-associated protein kinase (ROCK) which is the major regulator of the activity of myosin II and either phosphorylates the regulatory light chains (RLCs) (direct myosin II activation) or inactivates the myosin phosphatase thereby resulting in increased levels of phosphorylated RLC (indirect myosin II activation) (Chengappa et al., 2018; Vicente-Manzanares et al., 2009; Newell-Litwa et al., 2015; Le Clainche and Carlier, 2008). Myosin II is composed of two heavy chains and four light chains, two regulatory (RLCs) and two essential (ELCs), and the globular head domain possesses binding sites for both actin and ATP (Vicente-Manzanares et al., 2009; Kassianidou and Kumar, 2015). Myosin II mediates adhesion maturation through actin filament cross-linking and

tension generation, which promotes conformational changes in adhesion components (Parsons et al., 2010). Exposure of cryptic protein-binding sites and/or phosphorylation sites occurs upon application of tensile forces. One well-characterised example is the actomysosin-induced exposure of talin's cryptic vinculin binding sites after sensing the force conveyed from the actin cytoskeleton to ECM, leading to talin-vinculin association and adhesion strengthening. Vinculin anchoring at cell-matrix adhesions is also tension-dependent (Parsons et al., 2010).

In mammals there are three myosin II isoforms (A, B and C) which are determined by the heavy chain (Vicente-Manzanares et al., 2009; Kassianidou and Kumar, 2015). Myosin IIA promotes adhesion maturation at the cell front, while myosin IIB's preferred localisation is at the cell rear in migrating cells (where myosin IIA can also be found), where adhesion dismantling and cell retraction occurs (Newell-Litwa et al., 2015; Parsons et al., 2010; Kassianidou and Kumar, 2015). Myosin IIC is the least investigated among them and has been implicated in neuronal cell adhesion and in neurite outgrowth (Newell-Litwa et al., 2015; Kassianidou and Kumar, 2015).

Following adhesion maturation, focal adhesions are anchored to stress fibres leading to the generation of the required contractile force to move the cell forward (Ridley et al., 2003; Le Clainche and Carlier, 2008; Kassianidou and Kumar, 2015; Newell-Litwa et al., 2015; Livne and Geiger, 2016).

*Stress fibres*

Contractile actomyosin bundles, composed of F-actin, myosin II, α-actinin and other cytoskeletal proteins, are ordinarily known as ''stress fibres''. In mammals, there are at least three different types of stress fibres depending on their association with focal adhesions, molecular composition, mechanisms of formation and dynamics and biological role. Transverse arcs are not directly anchored to focal adhesions, dorsal stress fibres are attached only at one end to a focal adhesion in close proximity to the cell front - with a seemingly minor role of myosin II in their formation - and the most regularly detectedmyosin II-enriched ventral stress fibres are associated at both their ends with focal adhesions (Livne and Geiger, 2016; Kassianidou and Kumar, 2015; Burridge and Guilluy, 2016; Burridge and Wittchen, 2013). Ventral stress fibres are long structures outspread from one side to the other side of the cell and can be formed by transverse arcs and dorsal stress fibres (Hotulainen and Lappalainen, 2006). There is an interconnection between ventral stress fibres and focal adhesions, thus disassembly of one leads to quick dismantling of the other (Livne and Geiger, 2016). In general, dorsal stress fibres and transverse arcs are mainly involved in cell spreading, while ventral stress fibres explore, interact with their substratum and produce strong

traction forces (Livne and Geiger, 2016; Kassianidou and Kumar, 2015). Actin cap stress fibres which wrap over the nucleus are a subcategory of ventral stress fibres (Burridge and Guilluy, 2016; Livne and Geiger, 2016).

*Adhesion structures dismantling*

In order for the migrating cell to continue its forward movement, adhesion structure dismantling occurs not only at the rear end, allowing tail detachment, but also at the leading edge, mainly at the transition zone between lamellipodium and lamella, enabling the generation of new protrusions and cell matrix-adhesions (Figure 1-11) (Parsons et al., 2010; Le Clainche and Carlier, 2008; Webb et al., 2002; McLean et al., 2005; Ridley et al., 2003; Huttenlocher and Horwitz, 2011).

Rac localised activation at the leading edge can reduce Rho activity via p190RhoGAP, leading to decreased myosin II-induced tension, thus permitting constant forward movement (Ridley et al., 2003; Parsons et al., 2010). On the other hand, Rho can inhibit Rac via a ROCK-involved pathway, probably inducing through tension a RacGAP, like ARHGAP22 (Parsons et al., 2010). Additionally, at the leading edge $PI(3,4,5)P_3$ (and $PI(3,4)P_2$) is generated by the localised activity of PI3K, while PTEN is restricted at the cell rear and sides (Ridley et al., 2003).

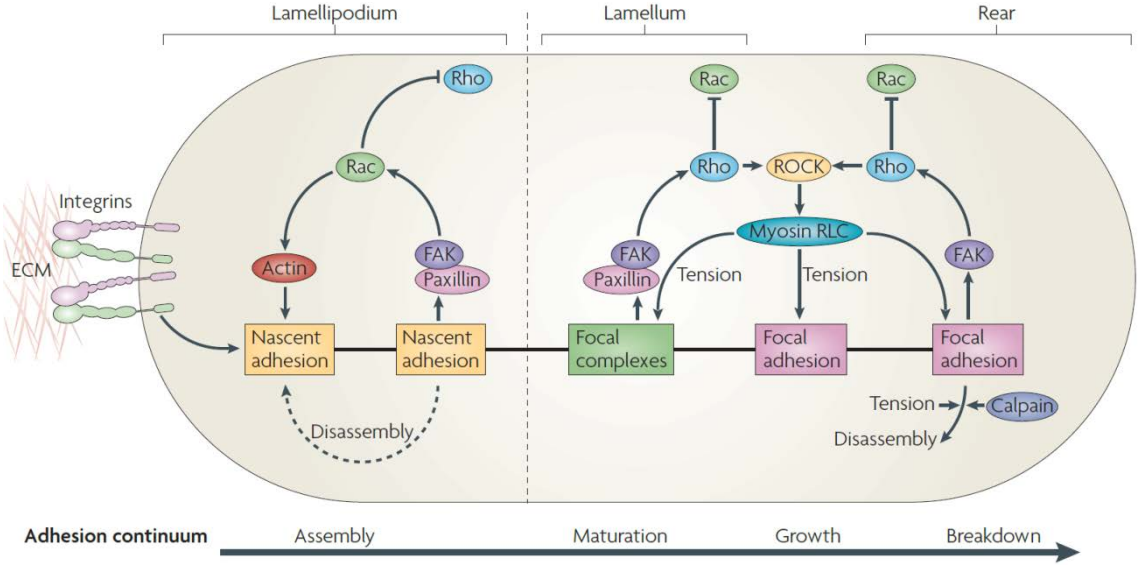


**Figure 1-11: Adhesion assembly, maturation and disassembly in coordination with regulation of Rho GTPase activation.** In lamellipodium-dependent migration, nascent adhesion assembly and dismantling, in the lamellipodium, is concomitant with the lamellipodium forward movement and is induced by Rac activation which in turn mediates paxillin and focal adhesion kinase (FAK) activation. Adhesion maintenance and maturation in the lamella is associated with Rho activation, possibly via FAK-mediated anchoring of RhoGEFs. RhoA activates myosin II through its downstream effector ROCK (Rho-associated protein kinase) which either phosphorylates myosin II regulatory light chains (RLCs) (direct myosin II activation) or inactivates the myosin phosphatase thus leading to elevated phosphorylated RLC levels (indirect myosin II activation). At the cell rear, adhesion dismantling occurs, with Rho GTPase, myosin and calpains being implicating in this process. [Adapted from (Parsons et al., 2010) Copyright obtained by Springer Nature (Nature Reviews Molecular Cell Biology) and also by Professor J. Thomas Parsons]**.**

### 1.4.4 Integrin-based cell-matrix structure turnover and disassembly

The understanding of the molecular mechanism of the process of focal adhesion disassembly (FA disassembly) is still limited. Nonetheless, it is accepted that it is not just a reverse process of adhesion complex assembly (Webb et al., 2002; Ezratty et al., 2005; Ezratty et al., 2009).

*Calpains*

Calpains, which are calcium-dependent cysteine proteases, have been implicated in the process of focal adhesion disassembly. These proteolytic enzymes have been reported to play a role in the process of adhesion disassembly in migrating fibroblasts (Huttenlocher and Horwitz, 2011; Dourdin et al., 2001). Furthermore, calpains have been reported to regulate adhesion disassembly by cleaving several cell-matrix adhesion components like integrins, talin, FAK and paxillin (Glading et al., 2002; Carragher et al., 1999; Chan et al., 2010; Cortesio et al., 2011; Flevaris et al., 2007; Franco and Huttenlocher, 2005; Franco et al., 2004) and it has also been reported that they can be activated downstream of ERK upon EGF stimulation to perform the abovementioned function (Glading et al., 2000). More specifically, it has been reported that calpain-mediated proteolysis of talin (Franco et al., 2004) as well as of FAK (Chan et al., 2010) can affect adhesion dynamics. Furthermore, calpain inhibition mediated by overexpression of its endogenous inhibitor, calpastatin, or cell permeable inhibitors leads to prevention of disassembly of adhesion complexes and it was also proposed that calpains act downstream of microtubules (Bhatt et al., 2002). A recent study claimed that Rab5 induces calpain 2 activation, which promotes in turn FA disassembly (Mendoza et al., 2018). On the contrary, another study reported that proteolytic cleavage of paxillin mediated by calpain leads to defective FA turnover (Cortesio et al., 2011). It seems that calpains are implicated in the regulation of various adhesion structures, since they have been reported to be involved in the dismantling of podosomes in dendritic cells and invadopodia in tumour cells (Huttenlocher and Horwitz, 2011). Overall, their exact mechanism of action in the regulations of FA dismantling remains still unclear.

*Microtubules*

Microtubules have been reported to play a crucial role in the process of FA disassembly. It has been reported that microtubules target adhesion structures and regulate their disassembly probably through delivery of relaxing signals (Kaverina et al., 1998; Kaverina et al., 1999) and can also mediate a localised ECM proteolysis through matrix metalloproteinases (MMPs) secretion (Stehbens and Wittmann, 2012; Kenific et al., 2016a). Microtubules have also been reported to promote FA

disassembly in a FAK- and dynamin-dependent manner but independently of Rho GTPases (Ezratty et al., 2005), although it has also been reported that microtubules can induce FA turnover through regulation of Rho GTPase signalling (Broussard et al., 2008; Huttenlocher and Horwitz, 2011). In a following study Ezratty et al. (Ezratty et al., 2009) reported that microtubule-triggered FA disassembly happens through integrin clathrin-dependent endocytosis with the clathrin adaptors autosomal recessive hypercholesteremia (ARH) and Disabled-2 (Dab2) being involved in that process. This pathway of disassembly seems to occur prominently at FAs found at central cell regions (cell midregion), in agreement with another study which reported that clathrin- and dynamin-dependent endocytosis of integrin β1 is required for FA disassembly (Chao and Kunz, 2009). In a following study, Chao et. al (Chao et al., 2010) reported that type I phosphatidylinositol phosphate kinase beta (PIPKIβ) through $PI(4,5)P_2$ production can regulate FA dismantling via controlling activated β1 integrin endocytosis. Collectively, internalisation of integrins induced by microtubules represents a pathway of disassembly at least of some FAs. However, the exact mechanism of how microtubules affect FA disassembly remains obscure.

*FAK and Src tyrosine kinases*

Several kinases and phosphatases, most of which are associated with FAK signalling pathways, are involved in the regulation of cell-matrix adhesion turnover (Broussard et al., 2008). It has been shown that fibroblasts derived from FAK knockout ($FAK^{-/-}$) mice are characterised by defective cell migration, an elevated number of enlarged peripheral adhesions and an altered morphology of stress fibres as a consequence of defective adhesion turnover (Ilic et al., 1995; Sieg et al., 1999), in agreement with a following study showing that FAK is required for adhesion disassembly (Webb et al., 2004). Interestingly, in cancer cells FAK has been reported to have a similar effect on FAs, but an opposite effect on invadopodia, i.e. increased invadopodium formation as a consequence of FAK depletion (Chan et al., 2009). Consistently, a later study reported that extended association of FAK at FAs as a consequence of locally increased $Ca^{2+}$ levels results in enhanced FA disassembly (Giannone et al., 2004). Autophosphorylation of FAK at residue Y397 results in Src recruitment via its SH2 domain upon ligand-binding and integrin clustering (Wozniak et al., 2004), thus it is not surprising that similarly to FAK, Src tyrosine kinases play a crucial role in regulation of adhesion turnover. Fibroblasts with loss of Src, Yes and Fyn or expression of kinase-inactive Src exhibit defective migration and decreased adhesion dismantling (Webb et al., 2004; Klinghoffer et al., 1999; Fincham and Frame, 1998), while enhancement of adhesion dismantling resulted from Src activation (Huttenlocher and Horwitz, 2011). Additionally, it has been suggested that FAK-Src

signalling through its downstream effectors extracellular signal-regulated kinase (ERK) and myosin light chain kinase (MLCK) regulates actomyosin contractility and in turn cell-matrix adhesion turnover (Webb et al., 2004). Interestingly, a more recent study suggested a model for FA reassembly following microtubule-mediated FA disassembly, in which recycled integrins maintain their active conformation through their association with FAK, talin and type I phosphatidylinositol phosphate kinase (PIPKIγ) as they transported via Rab5 and Rab11 endocytic compartments quickly to the cell surface to reconstitute new FAs due to their active state and interaction with FAK, talin and PIPKIγ. Collectively, these observations indicate that FAK probably plays distinct roles in these two processes (Nader et al., 2016).

*Rho GTPases*

FAK-Src signalling has also been reported to be upstream of Rho small GTPases, which in turn control actin and adhesion dynamics. It has been suggested that FAK phosphorylates Src and p190RhoGAP, which in turn inhibits Rho-triggered FA maintenance and stress fibre assembly and also stimulates anchoring and activation of the Rac/Cdc42 effector PAK (p21 activated kinase). PAK is in a complex with PAK interacting exchange factor (PIX) which is a Rac GEF, at FAs which in turn leads in myosin light chain kinase (MLCK) inhibition (Schober et al., 2007). A crucial role for the Rac/Cdc42 effector p21 activated kinase (PAK) family of serine/threonine kinases in integrin-dependent adhesion turnover has been reported (Ridley, 2015; Lawson and Ridley, 2018; Rane and Minden, 2014). Therefore, a shift from Rho-stimulated adhesion maintenance and stability to Rac-stimulated adhesion turnover is mediated by FAK. Collectively, these observations indicate a pivotal role for FAK in FA turnover regulation (Schober et al., 2007; Broussard et al., 2008; Huttenlocher and Horwitz, 2011). A less well investigated Rho GTPase, RhoJ (member of the Cdc42 subfamily) is also implicated in the regulation of endothelial FA disassembly through its association with the modulator of FA dismantling, the GIT (G protein coupled receptor kinase interacting target, which is a GAP for Arf GTPase)-PIX complex at FAs (Wilson et al., 2014; Lawson and Ridley, 2018; Ridley, 2015). Furthermore, paxillin, a crucial scaffolding protein of cell-matrix adhesions which lies downstream of FAK/Src signalling, appears early in their formation and has a key role in their turnover (Huttenlocher and Horwitz, 2011). It has been reported to get phosphorylated (at Ser 273) by PAK leading to GIT-PIX-PAK localisation at a subset of small and short-lived adhesions in close proximity to the leading edge, promoting adhesion turnover as a part of a positive-feedback loop (Nayal et al., 2006). Furthermore, PAK4 has been reported to promote in a kinase-independent manner RhoU stabilisation which enables paxillin phosphorylation at S272 which induces FA disassembly (Dart et al., 2015).

Additionally, a recent study showed that the small GTPase RhoG is implicated in the regulation of FA disassembly since depletion of it results in increased number and size of FA which are more stable and mature and exhibit modified location as well as altered stress fibre pattern and also delayed microtubule-triggered FA disassembly (Zinn et al., 2019). Therefore, it is apparent that the family of small Rho GTPases plays a critical role in dynamics of cell-matrix integrin-based adhesions and stress fibres as well as membrane protrusions and actomyosin contractility.

*Tyrosine phosphatases*

Apart from tyrosine kinases, tyrosine phosphatases are also involved in the regulation of adhesion turnover, indicating that both tyrosine phosphorylation and dephosphorylation are crucial for that process. Loss of the FA-localized tyrosine phosphatase PTP-PEST, which negatively controls FAK, p130Cas and paxillin tyrosine phosphorylation (Yu et al., 2010), results in an elevated number of FAs and defective cell migration (Angers-Loustau et al., 1999). An early study also reported that loss of the tyrosine phosphatase SHP-2 in fibroblasts results in an elevated number of FAs, altered actin stress fiber pattern and defective cellular migration, similarly to cells lacking FAK. This suggests that the roles of FAK and SHP-2 might be coordinated in the regulation of FAs dynamics (Yu et al., 1998).

*3-dimensional (3D) cell migration*

Cell motility on 2-dimensional (2D) extracellular matrix substrates *in vitro* has been the focus of many studies, but cell migration in not only 3-dimensional (3D) systems of ECM *in vitro* but also in animals *in vivo* have attracted the interest of recent research.

In 3D environments, cells are capable of using different types of cell migration, which depend on the robustness of cell-matrix adhesions, actomyosin contractility and RhoA/ROCK signalling, confinement and mechanical properties of microenvironment and also the availability of enzymes, like MMPs that degrade the surrounding pericellular environment (Ridley, 2015; Petrie and Yamada, 2016; Pankova et al., 2010; Petrie and Yamada, 2012; Friedl and Wolf, 2010). Cells are characterised by notable flexibility and can switch between distinct modes of 3D cell motility in response to intrinsic and extracellular signals, a process called migratory plasticity (Petrie and Yamada, 2016; Friedl and Wolf, 2010; Petrie and Yamada, 2012; Ridley, 2015; Pankova et al., 2010; Liu et al., 2015; DeSimone and Horwitz, 2014; Ruprecht et al., 2015). Therefore, both normal and cancer cells can switch between lamellipodium-dependent and bleb-dependent motility when a parameter that is determinant of either of these modes of cell migration is altered, demonstrating the capability of cells to

adapt to changes of their environment (Pankova et al., 2010; Petrie and Yamada, 2012; Friedl and Wolf, 2010; Ridley, 2015). In general, integrin-dependent cell-matrix adhesions are crucial for lamellipodium-dependent migration, parameter that is not necessary in bleb-dependent migration (Ridley, 2015). Primary human fibroblasts have the ability to display the whole range of the potential modes of cell migration (Petrie and Yamada, 2016). Primary human fibroblasts form rounded protrusions, namely lobopodia, in a cross-linked 3D-environment (Petrie et al., 2014). The formation and maintenance of these protrusions demand actomyosin contractility induced by Rho/ROCK activity to push the nucleus forward in a piston like manner (Petrie et al., 2014). In response to decreased actomyosin contractility, transition to lamellipodium-dependent motility occurs (Petrie and Yamada, 2016; Ridley, 2015).

Bleb-dependent migration occurs under both physiological, like in primordial germ cells (PGCs) in zebrafish and in *Drosophila melanogaster* embryos and also in *Dictyostelium discoideum* in response to a chemoattractant, and pathological conditions, like in cancer cells (Charras and Paluch, 2008; Ikenouchi and Aoki, 2017; Pankova et al., 2010; Petrie and Yamada, 2016). This type of migration is characterised by higher velocity than the one dependent on lamellipodia and filopodia (Ikenouchi and Aoki, 2017; Pankova et al., 2010) and is correlated with increased actomyosin contractility and RhoA activity, confined environments and decreased dependence on cell-matrix adhesions (Ridley, 2015; Friedl and Wolf, 2010; Petrie and Yamada, 2016; Ikenouchi and Aoki, 2017; Liu et al., 2015; Pankova et al., 2010; Petrie and Yamada, 2012).

Initiation/nucleation, expansion/growth and retraction are considered to be the three stages of a membrane bleb's life cycle (Charras and Paluch, 2008; Ikenouchi and Aoki, 2017; Paluch and Raz, 2013). RhoA is the principal Rho GTPase implicated in this mode of migration which leads to elevated levels of actomyosin contractility at the cell front and back compared to the sides (Ridley, 2015). The generation of a membrane bleb, which at its onset is free of F-actin filaments, initiates when local plasma membrane disengagement from F-actin filaments occurs driven by either a raise of intracellular pressure or local breakage of the actin cortex (Charras and Paluch, 2008; Ikenouchi and Aoki, 2017; Paluch and Raz, 2013; Ridley, 2015). Following the membrane bleb formation, the membrane bleb expansion takes places induced by intracellular pressure. Then, new actin filaments are reassembled covering and stabilising this membrane protrusion and eventually myosin accumulation to the reformed actin cortex and in turn actomyosin contractility leads to membrane bleb retraction (Charras and Paluch, 2008; Ikenouchi and Aoki, 2017; Paluch and Raz, 2013; Ridley, 2015).

## 1.5 Aims of this study

This study was focused on the class II PI3K isoform PI3K-C2β and principally aimed at improving the currently limited knowledge of biological processes in which this PI3K isoform is implicated and at elucidating its mechanisms of action. PI3K-C2β has repeatedly been shown to regulate cell migration (Blajecka et al., 2012; Maffucci et al., 2005; Domin et al., 2005; Katso et al., 2006). However, it has remained entirely unclear what aspect of the cell biology underlying migration is affected by PI3K-C2β. At the outset of this study, no molecular mechanism of action of PI3K-C2β had been described.

The hypothesis tested in the present study was that this PI3K isoform may regulate integrin-based cell-matrix adhesions and through this regulatory role orchestrate cell migration.

Two different strategies were employed to approach this aim:

i. Depletion of PI3K-C2β by RNA-interference in HeLa cells, a human cell line

ii. Catalytic inactivation of PI3K-C2β in immortalised mouse embryonic fibroblasts (MEFs) derived from WT or PI3K-C2β kinase-dead knock-in mice

Of note, no PI3K-C2β selective inhibitors are available to date. The PI3K-C2β kinase-dead knock-in (KI) mouse model has been generated by the host laboratory prior to this study. In this model, the kinase activity of PI3K-C2β is constitutively inactivated using a gene targeting approach that introduces a D1212A point mutation in the conserved DFG motif of the ATP binding site (Alliouachene et al., 2015) (see section 2.4.3). This strategy allows the assessment of kinase-dependent rather than possible scaffolding functions of the targeted PI3K isoform, thereby to some extent mimicking a pharmacological kinase inhibitor, without affecting the expression levels of the targeted or other non-targeted PI3K isoforms.

# 2. Material and Methods

## 2.1 Materials

### 2.1.1 Antibodies

All primary antibodies used in this study are summarised in Table 2-1. All fluorescent secondary antibodies were modified with Alexa Fluor dyes and were purchased from Invitrogen and were used at a dilution of 1:200. Alexa Fluor 647 Phalloidin (A22287) was purchased from Invitrogen and it was used at a dilution 1:500. For western blotting, horse radish peroxidase- (HRP) coupled secondary antibodies were purchased from GE Healthcare UK limited and were used at a dilution of 1:5,000.

**Table 2-1: Primary antibodies**. IF; immunofluorescence, IB; immunoblotting

| Antigen | Host | Catalogue Number | Manufacturer | Dilution IF | Dilution IB |
|---|---|---|---|---|---|
| APPL1 | rabbit | 3858 | Cell Signaling Technology | 1:200 | - |
| CD63 AF647 | mouse | 561983 | BD Biosciences | 1:100 | - |
| Clathrin Heavy Chain | rabbit | ab21679 | Abcam | 1:100-1:200 | - |
| DEPDC1B | rabbit | orb183064 | Biorbyt | - | 1:500 |
| DEPDC1B | rabbit | 8283 | ProSciΨ | - | 1:500 |
| EEA1 | rabbit | 3288 | Cell Signaling Technology | 1:400 | - |
| GFP | chicken | ab13970 | Abcam | 1:2,000 | - |
| GFP | mouse | 632380 | Clontech | - | 1:1,000 |
| GFP | rabbit | ab6556 | Abcam | - | 1;1,000 |
| GST | rabbit | ab9085 | Abcam | 1:100 | - |
| HA | rabbit | 162200 | Cayman | - | 1:400 |
| LAMP-1 (1D4B) | rat | sc-19992 | Santa Cruz Biotechnology | 1:100-1:200 | - |
| LAMP1 CD107a | mouse | 555798 | BD Pharmingen | 1:100-1:200 | - |
| LC3B | rabbit | 2775 | Cell Signaling Technology | - | 1:1,000 |
| Paxillin | mouse | 610051 | BD Bioscience | 1:400 | - |

| | | | | | |
|---|---|---|---|---|---|
| Phospho-4E-BP1 (Ser65) | rabbit | 9451S | Cell Signalling Technology | - | 1:500-1:1,000 |
| Phospho-S6 ribosomal protein (Ser240/244) | rabbit | 2215S | Cell Signalling Technology | - | 1:1,000 |
| PI(3,4)P2 | mouse | Z-P034b | Echelon Biosciences | 1:150 | - |
| PI3K-C2β | mouse | 611342 | BD Transduction Laboratories | - | 1:500 |
| P-Paxillin (Y31) (E228) | rabbit | ab32115 | Abcam | 1:100 | - |
| S6 ribosomal protein (54D2) | mouse | 2317 | Cell Signalling Technology | - | 1:1,000 |
| Talin | rabbit | Proteintech | 1468-1-AP | - | 1:500 |
| Talin | mouse | T3287 | Sigma | - | 1:500 |
| Total 4E-BP1 | rabbit | 9452S | Cell Signalling Technology | - | 1:1,000 |
| Tubulin | mouse | T6074 | Sigma | 1:400 | - |
| Vinculin | mouse | V9131 | Sigma | 1:400 | 1:10,000 |
| β-actin | mouse | A5441 | Sigma | - | 1:10,000 |

## 2.1.2 Buffers and other solutions

**Table 2-2: Buffers and other solutions**

| 10x Running buffer (in 1000 ml $H_20$) for Western blot analysis | |
|---|---|
| Glycine | 142 g |
| Tris-HCl | 30.2 g |
| SDS | 10 g |
| **10x Transfer buffer (in 1000 ml $H_2O$) for Western blot analysis** | |
| Glycine | 144 g |
| Tris-HCl | 30 g |
| **1x Transfer buffer for Western blot analysis** | |
| 10x stock | 100 ml |
| $H_20$ | 700 ml |

| | |
|---|---|
| Methanol | 200 ml |
| **Phospho-lysis buffer for western blot analysis** | |
| 50 mM Tris-HCl pH 7.4 | |
| 100 mM NaCl | |
| 50 mM NaF | |
| 5 mM EDTA | |
| 2 mM EGTA | |
| 1% Triton X-100 | |
| **4x sample buffer** | |
| 200 mM Tris-HCl pH 6.8 | |
| 400 mM DTT | |
| 8% SDS | |
| 40% glycerol | |
| Bromophenol blue to deep blue colour | |
| **1x TBS-T 0.1% (1 L)** | |
| 10x TBS | 100 ml |
| $H_2O$ | 900 ml |
| Tween20 | 1 ml |
| **TE buffer** | |
| 10 mM Tris | |
| 2 mM EDTA | |
| pH 8.0 | |
| **Lysis buffer LBA with Triton X-100 (for IPs)** | |
| 20 mM Hepes pH7.4 | |
| 100 mM KCl | |
| 2 mM $MgCl_2$ | |
| 1% Triton X-100 | |
| **Lysis buffer with saponin (for endogenous IP)** | |
| 20 mM Hepes pH7.4 | |
| 150 mM NaCl | |
| 0.05% | |
| **3% BSA in TBS-T (immunoblot antibody dilution solution)** | |
| BSA | 3 g |
| TBS-T | 100 ml |
| **3% BSA in PBS (IF blocking/antibody dilution solution)** | |
| BSA | 3 g |
| PBS | 100 ml |

| 5% milk in TBS-T (immunoblot blocking solution) | |
|---|---|
| milk (powder) | 5 g |
| TBS-T | 100 ml |

| Immunoblot stripping buffer |
|---|
| 62.5 mM Tris |
| 2% SDS (w/v) |
| pH 6.8 |
| To 10 ml buffer add 78 ul β-mercaptoethanol immediately before use |

| Live cell imaging solution |
|---|
| 10% FBS in DMEM/F-12 (1X) [Dulbecco's Modified Eagle Medium: Nutrient Mixture F-12 (DMEM/F-12)] |

| Pblec buffer (in PBS) |
|---|
| 1 mM $CaCl_2$ |
| 1 mM $MgCl_2$ |
| 1 mM $MnCl_2$ |
| 0.1% Tween-20 in PBS |

## 2.1.3 Other materials and reagents

**Table 2-3: Other materials and reagents**

| Reagent | Manufacturer | Catalogue Number |
|---|---|---|
| Bafilomycin A1 | Sigma | B1793 |
| Binding Control Magnetic Agarose Beads | ChromoTek | bmab-20 |
| Bio-Rad protein assay | BioRad | 500-0006 |
| Collagen I | BD Biosciences | 354236 |
| Crystal violet | Sigma | C0775 |
| DharmaFect 1 transfection reagent | Dharmacon | T-2001-03 |
| Digitonin | Sigma | D141 |
| DMSO | Sigma | D2650 |
| DNA Loading Dye solution | Fermentas | R0611 |
| dNTP Mix 10 mM | Thermo Scientific | R0192 |
| DPBS (Dulbecco's Phosphate Buffered Saline) | Sigma | D8537-500ML |
| DreamTaq Green PCR Master Mix (2X) | Thermo Scientific | K1081 |
| Dulbecco's Modified Eagle's Medium-high glucose (4500 mg/L glucose) (DMEM) | Sigma | D6429-500ML |

| | | |
|---|---|---|
| Dulbecco's Modified Eagle Medium: Nutrient Mixture F-12 (DMEM/F-12), no phenol red | Thermo Scientific | 21041-025 |
| Dynabeads Protein A for immunoprecipitation | Thermo Scientific | 10001D |
| Dynabeads Protein G for immunoprecipitation | Thermo Scientific | 10003D |
| ECL Western Blotting Substrate | Promega | W1001 |
| FBS, EU Professional from EU approved regions, filtered bovine serum | PAN-Biotech | P30-8500 |
| Fibronectin | BD Bioscience | 354008 |
| FuGene HD Transfection Reagent | Promega | E2311 |
| GFP-Trap Magnetic agarose | ChromoTek | gtma-10 |
| Gibco Hank's Balanced Salt Solution (HBSS) [+]$CaCl_2$ [+]$MgCl_2$ | Thermo Scientific | 14025-050 500ML |
| Immobilion-P membranes | Millipore | IPVH00010 |
| MassRuler DNA Ladder, High Range | Fermentas | SM0393 |
| MassRuler DNA Ladder, Low Range | Fermentas | SM0383 |
| Matrigel | Corning Life Sciences | 354248 |
| Mitomycin C | Sigma | M4287-2MG |
| Nocodazole | Sigma | M1404 |
| One Shot TOP10 Chemically Competent *E. coli* | Thermo Scientific | C404010 |
| Para-nitroblebbistatin | AXOL | Ax494693 |
| Penicillin-Streptomycin | PAA | P11-010 |
| Pierce Phosphatase Inhibitor Mini Tablet | Thermo Scientific | 88667 |
| Plasmid Maxi Kit | Qiagen | 12163 |
| Plasmid Midi Kit | Qiagen | 12143 |
| Plasmid Mini Kit | Qiagen | 12123 |
| Platinum-E Retroviral Packaging Cell Line | Cell Biolabs | RV-101 |
| Poly-L-lysine solution | Sigma | P4707-50ML |
| ProLong™ Gold Antifade Mountant with DAPI | Thermo Scientific | P10144 |
| Propidium iodide solution | Sigma | P4864 |
| Protease Inhibitor Cocktail | Sigma | P8340 |
| QiaQuick PCR purification Kit | Qiagen | 28104 |

| | | |
|---|---|---|
| Saponin | Sigma | 47036-250G-F |
| Trypsin-EDTA solution | Sigma | T4049 |

## 2.1.4 DNA oligonucleotides

Synthetic DNA oligonucleotides which were used as primers for polymerase chain reactions (PCRs) were purchased from Eurofins Genomics as a lyophilized powder and dissolved in TE buffer to a concentration of 100 µM. 10 µM working stocks in dd$H_2O$ were then prepared.

## 2.1.5 Small interfering RNA oligonucleotides

Synthetic RNA oligonucleotides for RNA interference were purchased from Eurofins Genomics as a lyophilized powder and dissolved to a concentration of 100 µM in RNAse-free siMAX buffer supplied by the manufacturer. All small interfering RNA (siRNA) sequences used in this study are listed in the Table 2-4. ON-TARGETplus Human DEPDC1B (55789) siRNA – SMARTpool, 5 nmol was obtained from Dharmacon. ON-TARGETplus TLN1 siRNA – SMARTpool, 5 nmol was obtained from Dharmacon.

**Table 2-4: Sequences of siRNAs used in this study**

| Targeted | siRNA | 5'-3' Sequence | Comment |
|---|---|---|---|
| none | Scrambled siRNA | GTAACTGTCGGCTCGTGGT | scrambled µ2 adaptin sequence, used only in the experiments with HeLa (PDC) cells |
| none | Scrambled siRNA | AUUGUUAACCGUAUUCUUA | |
| none | Control siRNA | Sequence not available from the provider | AllStars Neg. Control siRNA, # 1027281, QIAGEN |
| PI3K-C2β | PI3K-C2β#1 | GUUCGACACUUACCACAAU | |
| PI3K-C2β | PI3K-C2β#2 | GCUACCAGCUAUGAAGAUU | this siRNA used in the majority of experiments |
| DEPDC1B | DEPDC1B#1 of SMARTpool | GUACAAGCGUCACAGUAUU | ON-TARGETplus SMARTpool |
| DEPDC1B | DEPDC1B#2 of SMARTpool | CGAAGUUCAUCAUCCAUAA | ON-TARGETplus SMARTpool |
| DEPDC1B | DEPDC1B#3 of SMARTpool | GUACUGGGUUUGUUACAGA | ON-TARGETplus SMARTpool |

| | | | |
|---|---|---|---|
| DEPDC1B | DEPDC1B#4 of SMARTpool | GCGUGUGGCUCAUCUACGA | ON-TARGETplus SMARTpool |
| Talin 1 | SMARTpool: ON-TARGETplus TLN1 siRNA, L-012949-00-0005 Dharmacon | Sequence not available from the provider | SMARTpool: ON-TARGETplus TLN1 siRNA, Dharmacon |

## 2.1.6 Plasmids

The plasmids used in this study are listed in the Table 2-5.

The pceGFP-MK vector is a pcDNA3.1(+)-based vector with eGFP inserted between *Kpn*I and *BamH*I sites. The pcHA-MK vector is a pcDNA3.1(+)-based vector with HA inserted between *Kpn*I and *BamH*I sites. The pcmCherry-CAAX is a pcDNA3.1(+)-based vector with mCherry inserted between *Kpn*I and *BamH*I sites and a CAAX-box coding sequence (Malecz et al., 2000) inserted 3' of the *Not*I site.

**Table 2-5: Plasmid DNA constructs used in this study**

| Construct | Vector | REN sites | Bacterial resistance | Notes |
|---|---|---|---|---|
| pRetro-p53 shRNA | | | ampicillin | purchased from Cell Biolabs (RTV-40) |
| eGFP-mPI3K-C2β | pceGFP-MK | *EcoR*I - *Not*I | ampicillin | |
| 6x-Myc-mPI3K-C2β | pc6xMyc-MK | *EcoRI- KpnI* | ampicillin | |
| eGFP-hPI3K-C2β, siRNA resistance to siRNA#2 | pEGFP-C1 | | ampicillin | Provided by Prof. Volker Haucke, Berlin |
| eGFP-hPI3K-C2β kinase inactive, siRNA resistance to siRNA#2 | | | ampicillin | Provided by Prof. Volker Haucke, Berlin |
| HA-hPI3K-C2β | pcHA-MK | *EcoR*I - *XbaI* | ampicillin | Provided by Prof. Volker Haucke, |

| | | | | |
|---|---|---|---|---|
| | | | | Berlin |
| HA-hPI3K-C2β 456-1609 | pcDNA3.1 / pcHA-MK | *EcoR*I - *XbaI* | ampicillin | Provided by Prof. Volker Haucke, Berlin |
| HA-hPI3K-C2β 321-1609 | pcDNA3.1 / pcHA-MK | *EcoR*I - *XbaI* | ampicillin | Provided by Prof. Volker Haucke, Berlin |
| Vinculin-mCherry | | | kanamycin | Provided by Dr. Tanja Maritzen, Berlin |
| mCherry-INPP4B-CAAX | pcmCherry-CAAX | *EcoR*V - *Not*I | ampicillin | Provided by Dr. York Posor, UCL Cancer Insitute |
| mCherry-MTM1-CAAX | pcmCherry-CAAX | *EcoR*V - *Not*I | ampicillin | Provided by Dr. York Posor, UCL Cancer Institute |
| mCherry-INPP5E-CAAX | pcmCherry-CAAX | *EcoR*V - *Not*I | ampicillin | Provided by Dr. York Posor, UCL Cancer Institute |
| eGFGP-hDEPDC1B | pceGFP-MK | *BamHI* - *NotI* | ampicillin | |
| GST-2×FYVE$^{HRS}$ | | | | Provided by Harald Stenmark, Norway |
| pmaxGFP http://www.addgene.org/vector-database/3525/ | | | kanamycin | Amaxa kit from Lonza |

## 2.1.7 Eukaryotic cell lines

For all cell biological experiments, HeLa cells were used as a model system of mammalian cells that are easily transiently genetically manipulated. HeLa cells were derived from a cervix carcinoma in 1951. Two different HeLa cell lines were used, one was purchased from the American Type Culture Collection (ATCC) and the other one derived in the de Camilli laboratory (Yale University, USA), called HeLa (PDC) which was provided to us by Professor Volker Haucke, Berlin. For live cell imaging of FAs dynamics, a HeLa cell line stably expressing eGFP-human PI3K-C2β provided by Professor Volker Haucke, Berlin, was used.

For biochemical experiments, the human embryonic kidney cell line HEK293T and a HEK293T cell line stably expressing eGFP-PI3K-C2β provided by Professor Volker Haucke, Berlin, were used. HEK293T cells grow to high densities and therefore afford a high protein yield per growth area.

## 2.2 Cell biological methods

### 2.2.1 Cell culture

HeLa and HEK293T cells, including stable clones thereof, were cultured in a humidified incubator at 37˚C and 5% $CO_2$ in Dulbecco's Modified Eagle Medium (DMEM) – high glucose (4.5 mg/ml) containing 10% FBS and 1% penicillin-streptomycin (P/S). Cells were passaged every 3 to 4 days and plated into a new culture flask at a dilution of 1:5 to 1:20. For detaching, cells were washed with PBS and trypsinised with 1 volume of Trypsin-EDTA (1 ml in a 10 cm dish) for 5 min at 37˚C. Cells were resuspended in 10 volumes of culture medium containing FBS in order to inactivate trypsin.

Mouse embryonic fibroblasts (MEFs) were derived from wild-type (WT) and PI3K-C2β kinase-dead knock in (KI) mice and were immortalised by shRNA-mediated silencing of p53 tumour suppressor protein (see section 2.2.3). MEFs were cultured in a humidified incubator at 37˚C and 5% $CO_2$ and were maintained in Dulbecco's Modified Eagle Medium (DMEM) – high glucose (4.5 mg/ml) containing 10% FBS and 1% penicillin-streptomycin (P/S). Cells were passaged every 3 to 4 days and plated into a new culture flask at a dilution of 1:5 to 1:10. For detaching, cells were washed with PBS and trypsinised in 1 volume of Trypsin-EDTA (5 ml in 175 cm flask) for 5 min at 37˚C and were resuspended in 5 volumes of culture medium containing FBS in order to inactivate trypsin.

The MEFs used in this study were prepared by Dr Samira Alliouachene and Dr Michalina Jenkins prior to this study.

### 2.2.2 Transfection of plasmid DNA

HeLa cells and MEFs were seeded one day prior to transfection to achieve a confluency of about 75% on the day of transfection. Plasmid DNA was transfected using Fugene HD transfection reagent (Promega Corporation) according to the manufacturer's instructions. For a well in a 6-well culture plate, 3.3 µg plasmid DNA were used with 10 µl Fugene HD in a total volume of 155 µl OptiMEM. The experiment was performed between 20 to 26 h post-transfection. For microscopy, glass coverslips

were coated with matrigel (Corning Life Sciences) (500 µl matrigel per well in a 6-well culture plate) for around 1 hour at 37˚C prior to cell seeding in case of HeLa cells and with 1 µg/ml fibronectin (BD Bioscience) (500 µl of 1 µg/ml fibronectin per well in a 6-well culture plate) for around 1 hour at 37˚C prior to cell seeding in case of MEFs in the indicated experiments. Similarly, for live cell imaging, HeLa cells stably expressing eGFP-PI3K-C2β were plated onto matrigel-coated glass coverslips and were transfected with plasmid DNA one day prior to experiment using Fugene HD transfection reagent according to the manufacturer's instructions (see above).

For transfection of HEK293T cells with plasmid DNA, cells were seeded in a 10 cm culture dish prior to transfection to achieve a confluency of about 75% on the day of transfection. Plasmid DNA was transfected using Fugene HD transfection reagent (Promega Corporation) according to the manufacturer's instructions. For a 10 cm culture dish, 17 µg plasmid DNA with 51 µl Fugene HD in 750 µl OptiMEM were used. The experiment was performed between 20 to 26 hours post-transfection. Alternatively, transfection of HEK293T cells with plasmid DNA was carried out using TransIT-LT1 transfection reagent, for a 10 cm dish: 10 µg of DNA (in case of double transfections 10 µg of each plasmid) with 25 µl TransIT-LT1 transfection reagent in 1 ml P/S- and FBS-free DMEM were added to cells in 6 ml P/S-free DMEM supplemented with 10% FBS. The next day, 5 ml of culture medium (with P/S and 10% FBS) were added. The experiment was performed between 24 to 48 hours post-transfection.

### 2.2.3 Retroviral infection

Retroviruses are an efficient tool for gene delivery into dividing cells. Platinum-E (Plat-E) retroviral packaging cells efficiently express retroviral structural genes (gag, pol and env) (Morita et al., 2000) and were used for transduction of retroviral vectors. 8 µg of DNA (p53 shRNA construct) were combined with 18 µl Fugene HD in a total volume of 600 µl OptiMEM. This transfection mix was added to $5\times10^6$ of Plat-E cells in suspension (reverse transfection) in DMEM supplemented with 10% FBS. Cells were then plated on a 10 cm dish. The following day, early-passage (P2 to P5) MEFs were plated in 10 cm culture dishes in culture medium in order to reach 70%-80% confluency the next day. 48 hours after transfection, the supernatant from the packaging cell cultures was filtered and polybrene was added to a final concentration of 8 µg/ml. This viral transduction medium was then used to replace the growth medium on the MEFs. 6 hours and 24 hours after the first infection, the infection was repeated, using polybrene to a final concentration of only 4 µg/ml for the second infection. At least 6 hours after the third infection, selection was started. In case the cells were confluent, they were

split and the selection was only started the following day. MEFs stably expressing the pRetro-p53 shRNA construct were selected with 2 μg/ml puromycin for 10-14 days.

The MEFs used in this study were prepared by Dr Samira Alliouachene and Dr Michalina Jenkins prior to this study.

### 2.2.4 Scratch-wound assay

Immortalised WT and PI3K-C2β KI MEFs were plated onto 6-well culture plates and cultured in presence of serum until they formed a confluent monolayer. The scratch-wound assay was performed under serum starved conditions, in presence of serum or upon 50 ng/ml PDGF stimulation.

Cells were either serum starved overnight, a ‘’wound’’ was made the next day, followed by washing two times with PBS and the cells were either stimulated with 50 ng/ml PDGF or not, or a scratch was made in presence of serum, followed by washing two times with PBS and fresh culture medium containing 10% serum was added. The assay was performed in presence of 10 μg/ml mitomycin in order to inhibit cell proliferation, thereby allowing the assessment of clear cell migration. The percentage of wound closure was documented at 0, 8 and 24 hours by an EVOS differential interference contrast (DIC) microscope and Fiji-ImageJ software was used to calculate this percentage. More specifically, for every sample, images of the ‘’wound’’ (between 6 and 10 images that covered the whole wound area) were taken at 0, 8 and 24 hours and using the tool of ROI Manager of Fiji-ImageJ software the wound area (‘’free of cells’’) was selected at every time point. Then, the percentage of wound closure was calculated at 8 and 24 hours. Each experiment was repeated at least 3 independent times and bar graphs were used to present the data as mean values with error bars representing SEM (standard error of the mean). In case of experiments that were performed twice, dot plots were used to present the mean and the two values were presented as dots.

For HeLa cells, siRNA-treated cells were seeded and cultured in matrigel-coated 6-well culture plates until they formed a confluent monolayer. A ‘’wound’’ was made by scratching the monolayer using a 200 μl pipette tip, followed by washing two times with PBS. Fresh culture medium containing 10% serum and 1 μg/ml mitomycin was added. Images were taken using an EVOS DIC microscope and the percentage of wound closure was assessed at 0, 8 and 24 hours using Fiji-ImageJ software. The way of calculation of the percentage of wound closure was the same as the one described above for MEFs. A Nikon Biostation CT was also used for monitoring the movement of live cells during wound closure for 48 hours.

### 2.2.5 Nocodazole washout experiment – FA disassembly assay

Microtubules play an important role in the process of FA disassembly (see section 1.3.3). Nocodazole is a drug which induces microtubule depolymerisation thus nocodazole treatment represses FA disassembly. Nocodazole washout allows microtubule regrowth and FA disassembly. Therefore, the nocodazole washout experiment is a useful assay to study the process of FA disassembly (Ezratty et al., 2009; Ezratty et al., 2005; Chao and Kunz, 2009; Chao et al., 2010; Nagano et al., 2010; Feutlinske et al., 2015).

WT and PI3K-C2β KI MEFs (50,000 cells) were seeded onto glass coverslips (3 coverslips per well in a 6-well plate) and the following day were serum starved overnight. Next, cells were treated with 10 μM nocodazole for 2 hours to disrupt the microtubule network, which is necessary for FA dissociation. Then, nocodazole washout followed, during which nocodazole-containing medium was removed and cells were washed two times with PBS. After, serum starved medium was added for 10 minutes, allowing microtubule regrowth and FA dismantling. Cells were then fixed with 3.7 % formaldehyde in PBS for 15-20 minutes at room temperature, permeabilised for 10 minutes in 0.2 % Triton X-100 in PBS and blocked with 3 % BSA in PBS for 1 hour at room temperature. Cells were stained for Paxillin, a FAs marker, or α-tubulin, a microtubule subunit, in 3 % BSA in PBS for 2 hours at room temperature or overnight at 4˚C (see Table 2-1). After washing 3 times with PBS, secondary anti-mouse antibody coupled to Alexa Fluor 568 was applied at a dilution of 1:200 in 3 % BSA in PBS and incubated for 1 hour at room temperature. Cells were washed 3 times with PBS and coverslips were mounted using ProLong™ Gold Antifade Mountant (Invitrogen) containing the DNA-binding dye DAPI to counterstain nuclei.

### 2.2.6 Adhesion assay

The required number of wells of a 96-well plate were coated with 10 μg/ml fibronectin or collagen I for 1 hour in a humidified 5 % $CO_2$ incubator at 37°C and then blocked in 1 % BSA in serum starved medium for 1 hour at 37˚C. The last 10 minutes before seeding, the plates were chilled on ice. 50,000 WT and PI3K-C2β KI MEFs were seeded in 50 μl of culture medium per well, placed on ice and allowed to settle for around 10 min to collect cells at the bottom of each well. Cells were then left to adhere in a humidified 5 % $CO_2$ incubator at 37˚C for 30 minutes or 1 hour. Floating cells were removed by aspiration and one wash with PBS and adherent cells were fixed with 3.7 % formaldehyde in PBS for 15 to 20 minutes at room temperature. After 3 washes with PBS, the adherent cells were stained with 0.1% crystal violet for 10 to 20

minutes at room temperature, followed by 3 to 5 washes with PBS to remove unbound dye. Bound dye was solubilised in 1 % SDS and absorbance at 590 nm was quantified using a Tecan Sunrise microplate absorbance reader.

### 2.2.7 Small interfering RNA transfections and rescue experiments

Small interfering RNA (siRNA) is capable of regulating gene expression by targeting for degradation complementary mRNA molecules through RNA interference (RNAi) pathway. Firstly, double-stranded RNA (dsRNA) is cleaved into siRNAs by an RNase III-like activity. Subsequently, the siRNAs are integrated in an RNase complex, namely RNA-induced silencing complex (RISC), which mediates the degradation of the targeting mRNA through the action of Argonaut proteins (Ago2) which are the catalytic components of RISC (Agrawal et al., 2003; Dana et al., 2017).

Two different reagents for lipofection of small interfering RNAs were used, Dharmafect 1 (Dharmacon) and jetPRIME (Polyplus transfection). HeLa cells were plated onto matrigel-coated glass coverslips (3 glass coverslips per well in a 6-well culture plate) at a confluency of around 70 % in culture medium. The following day, cells were transfected with siRNAs using Dharmafect 1 (Dharmacon). For transfecting one 6-well using Dharmafect 1, 4 µl of 20 µM siRNA were combined with 4 µl Dharmafect 1 in a final volume of 400 µl OptiMEM, and after an incubation step of 20 minutes this was added to cells in 1.6 ml culture medium. 72 hours after transfection, cells were used for the experiment. Alternatively, for transfecting one 6-well using jetPRIME, 2 µl of 100 µM siRNA were combined with 4 µl jetPRIME in 200 µl jetPRIME buffer. After an incubation step of 10 to 15 minutes, this was added to cells which had just been plated onto matrigel-coated glass coverslips and were still in suspension (3 glass coverslips per well in a 6-well culture plate), using 2 ml culture medium per 6-well. The next day, cells were transfected for a second time. 72 hours after the first transfection, cells were used for the experiment.

For HEK293T cells in a 10 cm culture dish, 10 µl of 100 µM siRNA were combined with 20 µl jetPRIME transfection reagent in 500 µl jetPRIME buffer. After an incubation step of 10 to 15 minutes, this was added to cells which had just been plated onto a 10 cm culture dish and were still in suspension, using 9 ml of culture medium. The experiment was performed 72 hours after transfection.

For expression of recombinant proteins in siRNA-treated cells, plasmids were transfected around 24 hours prior to the experiment using either Fugene HD or jetPRIME according to the manufacturer's instructions. In brief, for a 6-well 3.3 µg plasmid DNA with 10 µl fugene HD in 155 µl OptiMEM total volume were used. When

using jetPRIME, for a 6-well 2 µg plasmid DNA were combined with 4 µl jetPRIME in 200 µl jetPRIME buffer.

For simultaneous depletion of two proteins in HeLa cells, termed a ‘’double knockdown’’, the jetPRIME protocol for a 6-well culture plate was modified as follows: 2 µl of a 100 µM stock of each siRNA were used with the same amount of jetPRIME transfection reagent. As described above, the first siRNA transfection was a reverse transfection followed by a second siRNA transfection the next day.

The efficiency of every single and all combinations of double knockdowns were validated by immunoblotting of cell extracts for every siRNA.

### 2.2.8 Immunofluorescence

HeLa cells were plated onto matrigel-coated glass coverslips and MEFs were plated onto uncoated coverslips or, where indicated, onto fibronectin-coated (1 µg/ml) glass coverslips. Cells were fixed with 3.7 % formaldehyde in PBS for 15 to 20 minutes at room temperature. Fixed cells were washed three times with PBS for 15 minutes at room temperature, permeabilised for 10 minutes in 0.2% Triton X-100 in PBS at room temperature for intracellular immunostainings and then blocked against unspecific binding with 3 % BSA in PBS for 1 hour at room temperature. Primary antibodies were diluted in 3% BSA in PBS (see Table 2-1) and were spotted onto parafilm in a humid chamber. Coverslips were put upside down on each drop of antibody dilution and were incubated either for 2 hours at room temperature or overnight at 4˚C. Coverslips were washed three times with PBS for 15 minutes at room temperature and then were incubated with secondary goat anti-mouse or anti-rabbit antibodies coupled to Alexa Fluor 488, 568 or 647 diluted to 1:200 in 3% BSA in PBS for 1 hour at room temperature as described above for the primary antibodies. At the same time with the incubation with the secondary antibodies, where indicated, coverslips were also incubated with phalloidin coupled to Alexa Fluor 647 diluted to 1:500. Coverslips were then washed three times with PBS for 15 minutes at room temperature and were mounted onto microscope slides using one drop per coverslip of proLong™ gold antifade mountant with DAPI (Invitrogen).

For labelling PI3P, the GST-2×FYVE$^{HRS}$ probe which binds specifically and with high affinity to PI3P (Gillooly et al., 2000) was used. This probe is composed of a tandem of FYVE domains of the hepatocyte growth factor-regulated tyrosine kinase substrate (Hrs) to increase the binding affinity for PI3P (Gillooly et al., 2000). Hrs is a protein which is implicated in vesicular trafficking via endosomes and specifically binds to PI(3)P (Komada and Soriano, 1999). MEFs were plated onto glass coverslips and

fixed with 3.7 % formaldehyde in PBS for 15 to 20 minutes at room temperature. After washing three times with 2 % BSA in PBS, two different ways of permeabilisation were used: fixed cells were either permeabilised with 20 µM digitonin in 2 % BSA in PBS for 5 minutes at room temperature or with 0.5 % saponin in 2 % BSA in PBS for 30 minutes at room temperature, followed by 3 washes with 2 % BSA in PBS for 15 minutes. Cells were blocked with 2% BSA in PBS for 30 minutes to 1 hour at room temperature. Coverslips were then incubated with the GST-2×FYVE$^{HRS}$ probe at 2 µg/ml for 45 minutes to 1 hour in 2 % BSA in PBS at room temperature, followed by 3 washes with 2 % BSA in PBS for 15 minutes. The probe was detected using an anti-GST antibody for 1 to 2 hours at room temperature, followed by incubation with the appropriate fluorescent secondary antibody for 1 hour at room temperature and 3 washes with PBS for 15 minutes, as described above. Similarly, for PI(3,4)$P_2$ antibody lipid staining, MEFs were fixed in 3.7 % formaldehyde in PBS for 15 to 20 minutes at room temperature, washed 3 times with 2 % BSA in PBS and permeabilised with 0.5 % saponin in 2 % BSA in PBS for 30 minutes at room temperature. Cells were blocked with 2 % BSA in PBS for 1 hour at room temperature, were labelled with the PI(3,4)$P_2$ lipid specific antibody and washed 3 times with 2 % BSA in PBS, incubated with the appropriate fluorescent secondary antibody for 1 hour at room temperature and washed 3 times with PBS for 15 minutes.

### 2.2.9 Confocal microscopy image acquisition and analysis

Fluorescence microscopy uses fluorescence to study the properties of biomolecules in fixed or living specimens. Fluorophores in a specimen are excited with light of a specific wavelength and in turn these fluorophores emit light of longer wavelength. In general, there are two different types of fluorophores; fluorescent moieties conjugated to antibodies which specifically label endogenous or overexpressed molecules and fluorescent proteins that are genetically encoded, permitting the observation of overexpressed proteins in fixed and also in living cells.

Confocal microscopy enhances the optical resolution of a light microscope image over and above the ability of widefield fluorescence microscopy via a spatial pinhole which prevents the out-of-focus light. However, the z resolution is still not as good as the xy resolution. In conventional widefield fluorescence microscopy the entire specimen is excited at the same time, while a confocal microscope is a scanning microscope and it uses point illumination, thus small regions of the specimen are excited one after another. 2D or 3D images are then generated by merging the data from a pile of images (Conchello and Lichtman, 2005; Combs and Shroff, 2017; Amos and White, 2003).

Images were acquired by confocal microscopy using LSM700, LSM780 or LSM880 microscopes and quantitative image analysis was performed using Fiji/ImageJ software. For these purposes, every cell was manually selected as a region of interest (ROI). Cell area was quantified using the tool Analyze → Measure in ImageJ. Fluorescence intensities and the number and size of individual objects were assessed by defining a fluorescence intensity threshold and the tool Analyze → Measure in ImageJ. More specifically, apart from the selection of every cell as a region of interest using the tool of ROI Manager of Fiji-ImageJ software that was done manually, the rest of image analysis process was automated. A Fiji-ImageJ macro was used in order the parameters of number, size and fluorescence intensity of individual objects as well as the cell area to be quantified. Each type of experiment was repeated at least 3 independent times and bar graphs were used to present the data as mean values with error bars representing SEM (standard error of the mean). In case of experiments that were performed twice, dot plots were used to present the mean and the two values were presented as dots.

### 2.2.10 Total internal reflection fluorescence microscopy (TIRFM)

TIRF microscopy was employed for visualisation of cell-matrix integrin-based adhesions, since this method is ideal for monitoring events that take place at the plasma membrane of adherent cells (Poulter et al., 2015). TIRFM provides images with a high axial resolution of up to 100 nm since this technique excites exclusively fluorophores that are found within around 100 nm of the phase boundary between glass coverslip and the aqueous sample, thus permitting the observation, with high signal-to-noise ratio, of fluorophores found in close proximity to the coverslip (Poulter et al., 2015). TIRF imaging was conducted using a Nikon Eclipse Ti, equipped with Andor sCMOS camera, Okolab incubator for live imaging, Nikon PerfectFocus autofocus system, 60x TIRF-objective, a custom-built solid state laser setup, operated by open source ImageJ-based Micromanager software in professor Volker Haucke's laboratory at the FMP, Berlin. For analysis of FAs dynamics, time lapse series of 2 to 4 hours were recorded with intervals of 5 minutes. For the analysis of eGFP-hPI3K-C2β recruitment to FAs, in a first set of experiments HeLa cells expressing both eGFP-hPI3K-C2β and vinculin-mCherry were used. In a second set of experiments, HeLa cells expressing endogenously eGFP-tagged hPI3K-C2β transfected with vinculin-mCherry were used. To trigger the process of FAs disassembly, cells were treated with 50 μM blebbistatin, an inhibitor of myosin II preventing FA maturation and resulting in an enrichment of smaller nascent adhesions. As an alternative stimulus to promote FA disassembly, cells were starved for 4 hours in Hank's Balanced Salt Solution (HBSS).

For the analysis of eGFP-hPI3K-C2β recruitment to FAs, both eGFP-hPI3K-C2β and vinculin-mCherry intensities were quantified over time using the Fiji/ImageJ software as described above. Fluorescence intensity was assessed by defining a fluorescence intensity threshold and the tool Analyze → Measure in ImageJ. More specifically, the selection of every cell as a region of interest was done manually using the tool of ROI Manager of Fiji-ImageJ software and then a Fiji-ImageJ macro was used in order the fluorescence intensity of individual objects to be quantified over time.

### 2.2.11 Measurement of cell size by flow cytometry

Flow cytometry is a frequently used laser-based cell biology technique of single-cell analysis which mediates the identification of a cell's physical and chemical characteristics. Cells are found in suspension in a saline solution and they pass through a laser light beam in a single cell manner. Key parameters that are determined by the flow cytometer are the forward scatter (FSC) which is relative to cell size and side scatter (SSC) which correlates with cell granularity.

Forward scatter was measured as an indication of cell size. Cells were plated in culture medium onto 60 mm culture dishes to reach confluency the next day. The following day, cells were trypsinised and counted. $1\times10^6$ cells were resuspended in 1 ml 2 % BSA in PBS containing 2 μg/ml propidium iodide (PI) and kept on ice. PI is a membrane-impermeable dye, which binds to double stranded DNA and it is generally used to stain dead cells with compromised membrane integrity, thereby assessing cell viability. For the PI-positive control sample, cells were incubated for 5 to 10 minutes at 65˚C shaking at 800 rpm followed by 5 to10 minutes on ice before staining with PI as described above. Data were acquired on a BD Fortessa X20 and 50,000 live single cells were measured per sample. FlowJo software was used to analyse the data, gating on single cells in the sideward scatter height over area plot and live cells as determined by PI staining.

## 2.3 Biochemical methods

### 2.3.1 Preparation of protein extracts from eukaryotic cells

Total protein extracts were prepared from MEFs, HeLa or HEK293T cells using lysis buffer (LB) containing the non-ionic detergent Triton X-100 at 1 %, which is generally used for membrane disruption and membrane protein solubilisation. Cells were grown on 10 cm culture dishes or 6-well culture plates, were placed on ice to minimise protease and phosphatase activity and washed with ice cold PBS to remove serum proteins. LB containing protease and phosphatase inhibitors was added and cells were harvested using a cell scraper. Cell lysates were incubated for around 20 minutes on ice to complete lysis. Cell lysates were then centrifuged at 15,000 rpm at 4˚C for 15 minutes to sediment insoluble material and the supernatant was transferred to fresh Eppendorf tubes. Protein concentrations were determined by Bradford protein assay.

**Table 2-6: Volume of lysis buffer (µl) used**

| Type of culture dish or plate | Volume of lysis buffer (µl) |
|---|---|
| 10 cm dish | 600 |
| 6-well plate | 150 |

### 2.3.2 Protein determination by Bradford protein assay

Protein concentration was determined by a colorimetric protein assay, where intensity of colour positively correlates with each sample's protein concentration, namely the Bradford assay. This assay is based on the dye Coomassie Brilliant Blue G-250. This dye in its anionic form binds via van der Waals forces and ionic interactions to the protein being determined and has an absorbance maximum at 595 nm. In an eppendorf tube, 2 µl of each sample were incubated with 1 ml of 1× Bradford reagent for around 5 minutes at room temperature. 300 µl of sample were transferred to a 96-well plate and the light absorbance of each sample at λ= 595 nm was measured by a Tecan Sunrise microplate reader. The absorbance values of each sample were used to determine its protein concentration based on a standard curve of bovine serum albumin protein concentration versus absorbance values.

### 2.3.3 Sodium dodecyl sulfate (SDS) polyacrylamide gel electrophoresis (SDS-PAGE)

SDS-PAGE is a method broadly used for separation of proteins based on their molecular weight. SDS is an ionic detergent which denatures proteins through

destabilisation of their secondary and tertiary structures via disruption of non-covalent interactions. SDS associates with and unfolds proteins into linear chains; thereby, polypeptides acquire a uniform negative charge along their length. In an electric field, they move towards the positively charged anode through the polyacrylamide gel. Thus, the separation of proteins depends only on their molecular weight, with smaller proteins migrating faster and larger proteins migrating slower through the mesh-like polyacrylamide gel. The resolution of the gel is defined by the acrylamide concentration, with higher acrylamide concentration providing better resolution of proteins with lower molecular weights, while lower acrylamide concentration leads in better resolution of proteins with higher molecular weights.

Sample buffer to a final concentration of 1× was added to cell lysates after determination of their protein concentration and samples were boiled at 95˚C for 5 minutes to achieve protein denaturation. 30 to 80 µg of protein were loaded per well to be analysed by SDS-PAGE. Gels were run at 15 mA per gel in presence of 1X running buffer (Table 2-7, Table 2-8).

**Table 2-7: Resolving gel**

| Separation gel (10 ml) | 8% (ml) | 10% (ml) | 15% (ml) |
|---|---|---|---|
| $H_20$ | 3.4 | 2.7 | 1.1 |
| Acrylamide mix | 2.7 | 3.3 | 5.0 |
| 1M Tris pH8.8 | 3.7 | 3.7 | 3.7 |
| 10% SDS | 0.10 | 0.10 | 0.10 |
| 10% APS | 0.10 | 0.10 | 0.10 |
| TEMED | 0.006 | 0.004 | 0.004 |

**Table 2-8: Stacking gel**

| Stacking gel | (10 ml) |
|---|---|
| $H_20$ | 6.82 |
| Acrylamide mix | 1.67 |
| 1M Tris pH8.8 | 1.30 |
| 10% SDS | 0.10 |
| 10% APS | 0.10 |
| TEMED | 0.01 |

## 2.3.4 Immunoblotting

After separation of proteins by SDS-PAGE, detection of proteins was carried out via immunoblotting or ‘’western blotting’’, which is a highly sensitive method using antibodies to recognize specific proteins. Proteins are transferred through a wet transfer procedure from the gel onto a PVDF or nitrocellulose membrane in an electrical field. This relies on the proteins still being associated with SDS and thereby

carrying a uniform negative charge. Wet transfer occurred for 1 hour and 30 minutes at 100 V at 4˚C. Membranes were washed once with TBS-T solution and then blocked against unspecific binding for 1 hour with 5 % milk powder in TBS-T at room temperature. After 3 washes with TBS-T, the proteins of interest were detected through overnight incubation at 4˚C with specific primary antibodies (Table 2-1) diluted in 3 % BSA in TBS-T. Primary antibodies were recycled and the membrane was washed three times with TBS-T every 10 to 15 minutes at room temperature, followed by 1 hour incubation at room temperature with horseradish peroxidase (HRP)-coupled secondary antibodies diluted at 1:5,000 in 3 % BSA in TBS-T, followed by three washes with TBS-T every 10 to 15 minutes at room temperature. HRP-linked secondary antibodies recognise specifically the constant region of immunoglobulins of the species the primary antibody was raised in, most commonly mouse or rabbit. Detection of target protein was mediated by chemiluminescence. Enhanced chemiluminescence reagent (ECL reagent) was added to the membrane as it functions as a substrate for HRP. HRP catalyses a luminescent reaction of luminol using hydrogen peroxide as the oxidizing agent. Signal intensity is proportional to the amount of HRP-linked secondary antibody. Detection and quantification of protein expression was carried out using an ImageQuant LAS 4000 camera system and control software.

### 2.3.5 Immunoprecipitations

In order to verify the potential interaction between PI3K-C2β and DEPDC1B or other FA components, immunoprecipitation assays were carried out. Immunoprecipitation is a very frequently used biochemical method which enables protein antigen detection, purification and isolation from a cell extract containing thousands of proteins. It makes use of an antibody which is coupled to beads and specifically recognises the protein of interest. Appropriate controls were included to check for unspecific binding to the stationary phase and for cross-reactivity of the antibodies used.

A first approach was to overexpress both eGFP-DEPDC1B and 6x-Myc-PI3K-C2β constructs in HEK293T cells and confirm the interaction by pulling-down from either the eGFP-DEPDC1B or the 6x-Myc-PI3K-C2β side. eGFP-DEPDC1B or 6x-Myc-PI3K-C2β single transfected HEK293T cells were used as controls. Cells were plated onto 10 cm culture dishes to reach 70 % confluency the next day, when they were either double transfected with both eGFP-DEPDC1B and 6x-Myc-PI3K-C2β or single transfected with either eGFP-DEPDC1B or 6x-Myc-PI3K-C2β (see section 2.2.2). Antibodies were coupled to magnetic beads conjugated to protein A or G (Dynabeads Protein A or G for immunoprecipitation, ThermoFisher Scientific) overnight at 4˚C

(Table 2-9). These proteins are derived from bacteria and specifically bind to immunoglobulin G (IgG) antibodies. They have a similar structure but they are characterised by different affinities for antibodies from different species. Generally, protein A has a greater affinity for rabbit IgG, while protein G for mouse and human IgG. 30 µl bead slurry were washed once with 0.1% Triton X-100 in PBS and incubated with 5 µg of each antibody in 500 µl of 0.1% Triton X-100 in PBS overnight rotating at 4˚C, followed by sedimentation using a magnetic rack and washing once with LBA (Table 2-9). The experiment was performed 48 hours after transfection. Confluent 10 cm cultures dishes of HEK293T cells transiently expressing both eGFP-DEPDC1B and 6x-Myc-PI3K-C2β, only eGFP-DEPDC1B or only 6x-Myc-PI3K-C2β were placed on ice, washed gently with cold PBS, harvested in 600 µl LBA buffer and incubated on ice for about 20 to 30 minutes. Debris was removed by centrifuging for 10 minutes at 13,000/15,000 rpm at 4˚C. Cleared lysates were incubated with the appropriate antibody coupled to magnetic beads rotating at 4˚C overnight (Table 2-9). Beads were washed 5 times with LBA and bound proteins were eluted at 95˚C for 5 minutes in 1X sample buffer. Samples were then resolved by SDS-PAGE and analysed by immunoblotting as described in sections 2.3.3 and 2.3.4.

**Table 2-9: Antibody coupling to magnetic beads conjugated to protein A or G.**

| Antibodies (Ab) | Type of bead slurry | µg of Ab used with 30 µl of bead slurry | Species |
|---|---|---|---|
| DEPDC1B | A | 5 | Rabbit |
| Myc | G | 5 | Mouse |
| Flag (used as control) | G | 5 | Mouse |
| Rabbit IgG (used as control) | A | 5 | Rabbit |

In a second approach, HEK293T cells expressing endogenous eGFP-tagged PI3K-C2β were used. This approach was applied in order to avoid possible artefacts associated with the use of overexpressed proteins, such as mislocalisation and protein aggregation (Ratz et al., 2015). Confluent 10 cm culture dishes of HEK293T cells expressing endogenous eGFP-PI3K-C2β were placed on ice, washed once gently with cold PBS, lysed in IP buffer (20 mM Hepes pH 7.4, 150 mM NaCl, 0.05% saponin, protease and phosphatase inhibitors) and centrifuged at 10,000 g for 10 minutes at 4˚C. The supernatant was then incubated with GFP-trap magnetic microparticles (GFP-Trap Magnetic agarose, ChromoTek) for 2 to 4 hours at 4˚C rotating. The GFP-Trap is composed of an anti-GFP nanobody/$V_HH$ (single variable domain) immobilised to (agarose or) magnetic agarose beads for capturing and immunoprecipitating GFP-

tagged proteins. Beads were washed 5 times with IP buffer and bound proteins were eluted at 95˚C for 5 minutes in 1X sample buffer. Samples were then resolved by SDS-PAGE and analysed by immunoblotting as described in sections 2.3.3 and 2.3.4.

## 2.4 Molecular Biology methods

### 2.4.1 Cloning strategies

Cloning strategies were designed using the program serial cloner. Primers were designed such that the salt-adjusted melting temperature was between 50˚C and 60˚C when calculated using the online tool: http://biotools.nubic.northwestern.edu/OligoCalc.html. Additionally, where possible sequences were chosen that the first and last two nucleotides had a G or C.*In silico* construction was carried out to exclude conceptual errors, like frame shifts or restriction site incompatibilities.

### 2.4.2 Polymerase chain reaction (PCR)

The polymerase chain reaction (PCR) is a very common technique in molecular biology, which permits the exponential amplification of a specific DNA sequence. It typically consists of repeated thermal cycles of template DNA denaturation, annealing of primers to each of the single-stranded DNA templates, and elongation of DNA strands. Multiple cycles of this process result in exponential DNA amplification.

PCRs were used to amplify protein coding sequences from cDNA or plasmid DNA for subsequent cloning into expression vectors. PCR reactions were set up and run as described in the following tables (Table 2-10, Table 2-11):

**Table 2-10: Master mix of RCR reaction reagents**

| Reagent | Volume (µl) |
|---|---|
| 5x HF (high fidelity)buffer | 10 |
| 2 mM dNTPs | 5 |
| 10 uM primers | 2.5 (of each primer) |
| 10 ng/ul DNA template | 1 |
| Phusion polymerase | 0.5 |
| $ddH_20$ | 28.5 |
| Total volume: 50 | |

**Table 2-11: PCR running program**

| Step | Temperature (˚C) and duration |
|---|---|
| Initial denaturation | 98˚C for 30 seconds |
| Denaturation | 98˚C for 5 seconds |
| Primmer annealing | 50-65˚C for 20 sec (depending on the salt-adjusted temperature of the primers) |
| Elongation | 72˚C for 20 seconds |
| Final elongation | 72˚C for 7 minutes |
| Steps 2 to 4: 30 cycles | |
| Store the reaction at 8˚C if needed | |

## 2.4.3 Generation of the PI3K-C2β kinase-dead knock-in mouse model

Prior to this study the PI3K-C2β kinase-dead KI mouse model was generated by the host laboratory (Alliouachene et al., 2015). In brief, a targeting vector composed of exons 21 to 25 of the *PIK3C2B* locus and a selection cassette containing a neomycin resistance gene flanked by FRT sites was employed to introduce a D1212A point mutation in exon 24 of the *PIK3C2B* gene, thereby converting the conserved DFG motif in the ATP-binding site to AFG (Figure 2-1). The selection cassette was deleted *in vivo* by breeding onto ACTB-Flp mice, which express Flp recombinase. The mice were backcrossed onto a C57BL/6 or BALB/c background for 6-10 generations. Taconic-Artemis (Cologne, Germany) created the gene targeting construct, established the embryonic stem (ES) cell lines and generated the mice (Alliouachene et al., 2015). PCR was used to confirm the presence of the D1212A allele and the left-over FRT site (Figure 2-1). A kinase assay was performed to assess the kinase activity of homozygous PI3K-C2β kinase-dead KI mutants, showing a complete loss of PI3K-C2β activity without affecting the expression levels of the targeted protein or of other non-targeted PI3K isoforms (Figure 2-1) (Alliouachene et al., 2015).

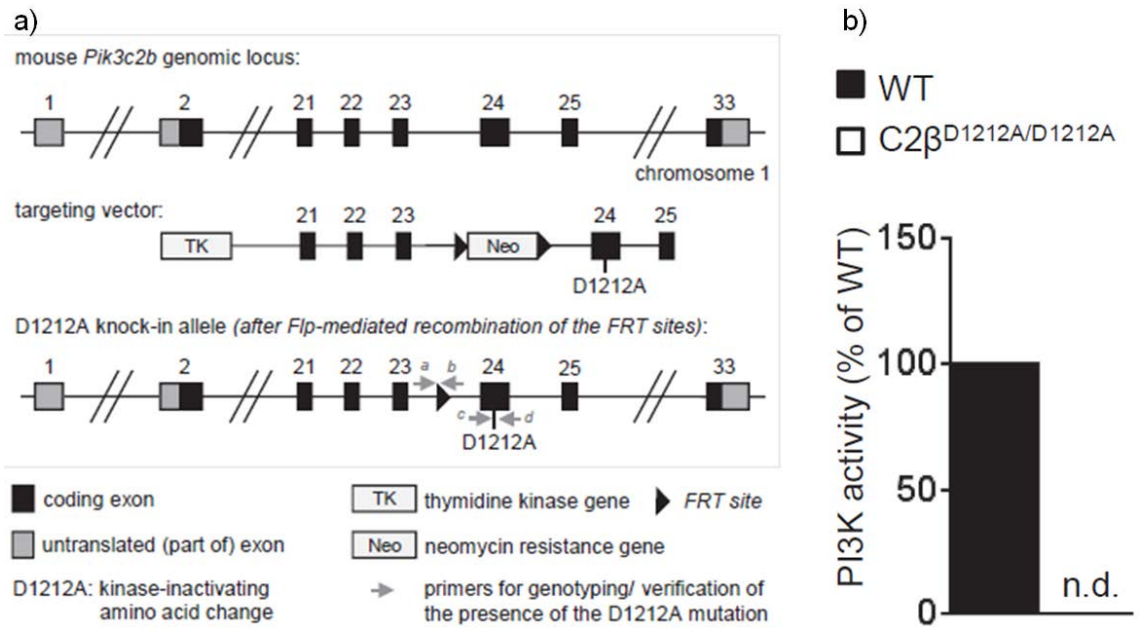


**Figure 2-1: Generation of PI3K-C2β kinase-dead knockin mouse model. a)** Schematic representation of the gene targeting strategy to create the constitutive D1212A knock-in point mutation in the PIK3C2B gene. **b)** Lipid kinase assay to assess the lipid kinase activity of WT and PI3K-C2β kinase-dead knockin mice using brain homogenates [adapted from (Alliouachene et al., 2015). This research was originally published in Elvesier (Cell Reports). Inactivation of the Class II PI3K-C2β Potentiates Insulin Signaling and Sensitivity. Vol: 13, Issue: 9, Samira Alliouachene, Benoit Bilanges, Gaëtan Chicanne, Karen E. Anderson, Wayne Pearce, Khaled Ali, Colin Valet, York Posor, Pei Ching Low, Claire Chaussade, Cheryl L. Scudamore, Rachel S. Salamon, Jonathan M. Backer, Len Stephens, Phill T. Hawkins, Payrastre, B., Vanhaesebroeck, B., Inactivation of the Class II PI3K-C2β Potentiates Insulin Signaling and Sensitivity, Pages: 1881-94, *Copyright © 2015, Elsevier* (open access article distributed under the terms of the Creative Commons CC-BY license)].

## 2.4.4 Genotyping

PCR was performed for genotyping of WT and PI3K-C2β kinase-dead KI mice or cells. DNA was isolated from mouse tail or ear biopsies or cell pellets. For digestion of tissue or cell pellets, 75 µl of alkaline lysis buffer (25 mM NaOH, 0.2 mM disodium EDTA) were added to each sample and samples were boiled at 95˚C for 1 hour, followed by addition of 75 µl neutralising buffer (40 mM Tris HCl, pH4.5). 2 µl of lysates were used for PCR reactions set up as detailed in Table 2-12.

**Table 2-12: Master mix of PCR reaction reagents**

| Reagent | Volume (µl) |
|---|---|
| DreamTaq Green PCR Master Mix | 12.5 |
| Primer mix (5 µM each) | 1.25 |
| $ddH_20$ | 9.25 |
| DNA | 2 |
| Total volume: 25 | |

The primers used for PI3K-C2β kinase-dead KI genotyping are: forward primer 5'-CACTGCAGGAAGTGTGAAGC and reverse primer 5'-GTGGACAGAAAGGCTGATGC. The following table (Table 2-13) shows the thermocycler program:

**Table 2-13: PCR program used for PI3K-C2β kinase-dead KI genotyping**

| Step | Temperature (˚C) and duration |
|---|---|
| Initial denaturation | 95˚C for 5 minutes |
| Denaturation | 95˚C for 30 seconds |
| Primmer annealing | 65˚C for 30 seconds |
| Elongation | 72˚C for 1 minutes |
| Final elongation | 72˚C for 2 minutes |
| Number of cycles: 35 | |

The expected amplificates are 235 bp for the WT allele and 398 bp for the PI3K-C2β kinase-dead KI allele. PCR products were analysed on 2 % agarose gels.

### 2.4.5 Agarose gel electrophoresis

Agarose powder was dissolved in 1X TAE buffer to a final concentration of 0.7 % to 2.0 % (w/v), depending on the size of DNA fragments which needed to be separated, by heating in the microwave until the agarose powder was fully dissolved. Ethidium bromide was added to a final concentration of 3 µg/ml and the solution was then poured into a gel tray where it solidified. The gel was submerged in 1X TAE buffer. DNA loading dye was added to samples at a final concentration of 1X and samples were loaded into gel wells and separated at a constant voltage of 100 V for 30 to 45 minutes. MassRuler DNA Ladder low, high or mix range was used to determine the size of DNA fragments and bands were visualised by exposure to UV light. In case DNA was intended to be used for further preparation, UV exposure was restricted to a minimum.

### 2.4.6 Purification of DNA from agarose gels

For purification of DNA from agarose gels, the band of interest was cut out from the gel under UV light, restricting UV exposure to a minimum, and DNA was purified using the QIAGEN Gel Extraction Kit according to the manufacturer's instructions. The gel band was dissolved completely in binding buffer at 55˚C, then bound to a silica membrane, washed with washing buffer containing ethanol and finally eluted in 30-40 µl of TE buffer.

### 2.4.7 Restriction digests

Restriction digests were carried out in a total volume of 20 µl to 50 µl using FastDigest enzymes (ThermoFisher). In case of restriction analyses 0.7 µg to 1 µg and in case of preparative restriction digests 3 µg of vector DNA were incubated with 0.5 µl of FastDigest enzyme per µg DNA at 37˚C for 30 minutes to 1 hour. In case of preparative restriction digests of vector DNA, DNA was separated on an agarose gel and purified using the QIAGEN Gel Extraction Kit following the manufacturer's instructions.

### 2.4.8 Dephosphorylation of vector DNA

In order to avoid vector self-ligation and eliminate the number of background-false positive colonies after transformation of ligation reactions, 1 µl of calf-intestinal alkaline phosphatase (CIP) was added to linearised vector DNA immediately after the completion of restriction digest reaction followed by incubation at 37˚C for 5 minutes. CIP catalyses the removal of 5'-phosphates from linear DNA molecules, thereby preventing recircularisation of linearised DNA vectors.

### 2.4.9 Ligation reaction

Ligation reactions with a vector to insert ratio of 1:3 were carried out in a total volume of 10 µl containing 1X ligase buffer and 1 µl of T4 DNA ligase. Ligation reactions were incubated overnight at 16˚C. The following day, 2 µl of a ligation reaction were transformed into chemically competent *E.coli* cells.

### 2.4.10 Transformation of chemically competent bacterial cells

One Shot TOP10 $CaCl_2$ chemically competent *E.coli* cells (50µl) were thawed on ice and mixed gently. DNA (2 µl of ligation reactions or 5 µl of 5 to 10 ng/µl plasmid DNA) was added to cells, mixed gently and the cells were incubated for 30 minutes on ice. Heat shock occurred by incubation of cells at 42˚C (water bath) for 40-50 seconds, followed by 2 minutes incubation on ice. 600 µl of LB medium free of antibiotics were added and the cells were incubated at 37˚C for 45 minutes shaking at 800 rpm before being plated on LB agar plates containing the appropriate antibiotic (either ampicillin or kanamycin). The LB agar plates were then incubated overnight at 37˚C.

### 2.4.11 Preparation of chemically competent *E.coli* cells

For preparation of chemically competent bacteria, a 50 ml LB culture of the *E. coli* strain of interest was started from a fresh plate or from a glycerol stock validated to

give highly competent bacteria. This culture was grown at 37°C and 250 rpm until the optical density at 600 nm (OD600) reached 0.4. Bacteria were harvested in sterile centrifuge tubes by centrifuging for 10 minutes at 4000 rpm and 4°C. The pellet was resuspended in 10 ml ice-cold and sterile 0.1 M $CaCl_2$ solution and incubated on ice for at least 15 to 30 minutes. Bacteria were then sedimented for 10 minutes at 4000 rpm and 4°C and the pellet was resuspended in 2 ml 0.1 M $CaCl_2$ solution. Glycerol was added to a final concentration of 10 % and 50 µl aliquots were prepared, snap-frozen in liquid nitrogen and stored at -80°C.This protocol was provided by Dr. York Posor.

### 2.4.12 Overnight cultures of *E. coli*

Colonies picked from LB agar plates containing the appropriate antibiotic after transformation of plasmid DNA or cells picked with a sterile pipette tip from a glycerol stock were inoculated in 5 ml (for a ‘’mini-prep’’) or 100-200 ml (for a ‘’maxi-prep’’) LB medium containing the appropriate antibiotic (either ampicillin or kanamycin) for overnight growth at 37˚C shaking at 230 rpm.

### 2.4.13 Plasmid DNA extraction and purification from *E. coli* cultures

Large scale plasmid preparations from 100-200 ml of *E. coli* overnight cultures (‘’maxi-prep’’) and small scale plasmid DNA preparations from 5 ml of *E. coli* overnight cultures (‘’mini-prep’’) were done using the QIAGEN Plasmid Maxi Kit and QIAGEN Plasmid Mini Kit according to the manufacturer’s instructions. In both cases, plasmid DNA was bound to a silica membrane, which in case of the QIAGEN Plasmid Maxi Kit is characterised by a higher DNA binding capacity. Additionally, for maxi-preps DNA eluted from the silica membrane was precipitated using isopropanol, followed by washing with ethanol and resuspension to the desired concentration in TE buffer.

### 2.4.14 Determination of DNA concentration

DNA concentration and quality were determined using a NanoDrop 2000 spectrophotometer (Thermo Scientific). 1-2 µl of DNA were analysed following the manufacturer’s instructions.

### 2.4.15 Sequencing

Sequencing of plasmid DNA was performed by Eurofins Genomics according to the Sanger sequencing method. Sequencing data were analysed by ‘’A plasmid Editor’’ (ApE) free software or serial cloner software.

## 2.5 Postnatal mouse retina isolation and immunostaining

P9 pups were sacrificed and two pieces from each mouse tail were kept for genotyping. After skin removal, eyeballs were isolated and fixed with 4% PFA in PBS for 1 hour and 15 minutes on ice, followed by two washes with cold PBS. Dissection of retinas was carried out under a binocular dissecting microscope. Briefly, after eyeball isolation and fixation specimen were placed in a 6 cm dish filled with PBS. Cornea was incised, cut and removed, then iris was also removed, followed by removal of the outer layer, sclera, pigmented layers, lens and vitrous humor and finally of the hyaloids vessels (Figure 2-2). Isolated retinas were then fixed with 4%PFA in PBS for 1 hour on ice, followed by two washes with cold PBS.

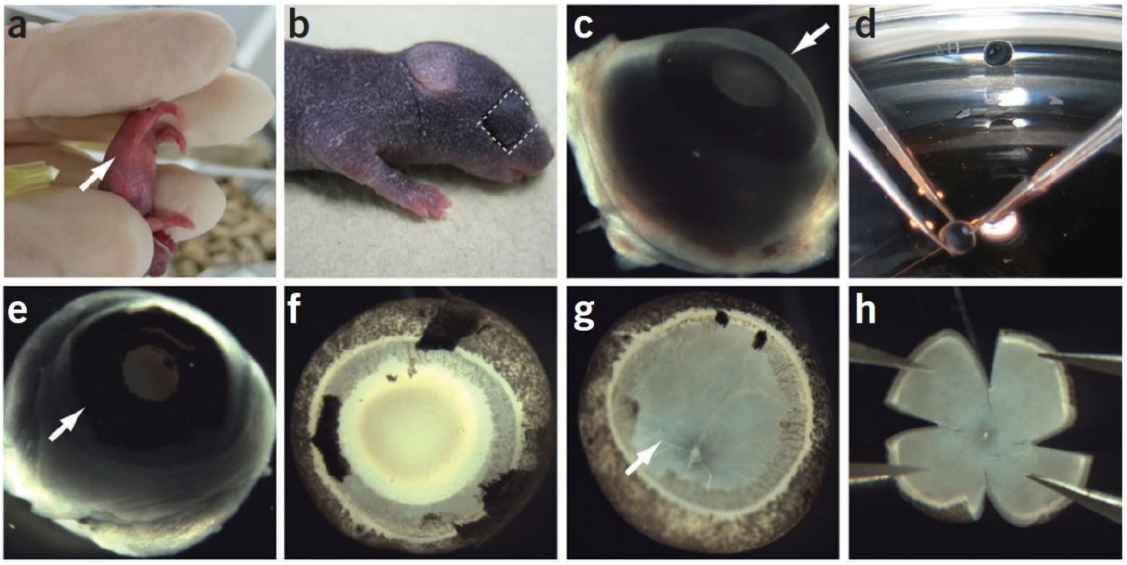


**Figure 2-2: Steps of eye isolation and retina dissection**. **b)** Depiction of where to make the four incisions around the eye of the pup. **c)** Isolated eyeball from a P6 pup. **d)** Overview of cornea isolation. **e)** Eyeball without cornea, isolated cornea indicated by arrow. **f)** Eye without sclera, choroid, cornea layers, pigmented layers and without iris. g) Eye without a lens. Hyaloid vessels indicated by arrow. h) Retina with four radial incisions [Adapted from (Pitulescu et al., 2010). Copyright obtained by Springer Nature (Nature Protocols) and also by Dr Mara Pitulescu].

Retinas were then blocked and permeabilised with permeabilisation/blocking buffer (1% bovine serum albumin (BSA), 0.3% Triton X-100 in PBS) overnight at 4˚C with gentle rocking. Retinas were incubated with the primary antibody anti-collagen IV, a marker of the endothelial basement membrane, at 1:100 dilution in permeabilisation/blocking solution overnight at 4˚C with gentle rocking, followed by three washes, 10 minutes each, with PBT buffer (0.1% Tween-20 in PBS) at room temperature. Subsequently, retinas were further incubated with Pblec buffer (1 mM $CaCl_2$, 1 mM $MgCl_2$, 1 mM $MnCl_2$ and 0.1% Tween-20 in PBS) for 30 minutes at room temperature and then with the secondary α-rabbit antibody coupled to Alexa Fluor 647 at a dilution of 1:300 and isolectin B4 conjugated to Alexa Fluor 488 at a dilution 1:300 in Pblec buffer either overnight at 4˚C or for 2 hours at room temperature. a-D-

galactosyl specific isolectin B4 is a glycoprotein of 114 kDa and a member of a family of five tetrameric type I isolectins ($IA_4$, $IA_3B$, $IA_2B_2$, $IAB_3$, and $IB_4$). It is derived from the tropical African medical plant *Griffonia simplicifolia* and it has been really useful for labelling endothelial cells in a number of species like mouse. Retinas were washed 3 times for 10 minutes each with PBT buffer at room temperature. Then, 4-5 incisions were made and retinas were flat-mounted on glass slides.

## 2.6 Statistical analysis

The majority of the experiments were repeated at least 3 independent times and bar graphs were used to present the data as mean values with error bars representing ±SEM (standard error of the mean). Data sets were compared for statistical significance using a two-tailed Student's t-test and statistical significance was indicated as $^{*}p < 0.05$, $^{**}p < 0.01$, $^{***}p < 0.001$. In case of experiments that were performed twice, dot plots were used to present the mean and the two values were presented as dots. Excel software was used for all the statistical analyses. In experiments where MEFs were used, in each experiment MEFs derived from 3 WT and 3 PI3K-C2β KI mice.

# 3. Results

Our understanding of the biological roles and the molecular mechanism of action of the class II PI3K isoform PI3K-C2β is still limited. Therefore, this project was focused on exploring further in which biological processes it is implicated and on uncovering its mechanism of action. Preliminary unpublished data from the host laboratory suggested that PI3K-C2β may play a role in integrin-based cell-matrix adhesions. Furthermore, PI3K-C2β has been reported to regulate cell migration but its precise role in this process is completely unclear (Blajecka et al., 2012; Maffucci et al., 2005; Domin et al., 2005; Katso et al., 2006). The hypothesis tested in this study was that PI3K-C2β may regulate adhesion dynamics and through this function orchestrate cell migration.

## 3.1 PI3K-C2β regulates cell-matrix adhesions and cell migration

Cells adhere to ECM through adhesion structures which mediate the connection between the extracellular environment and the actin cytoskeleton through integrins. In order the cells to migrate across the substratum, dynamic remodelling of those adhesion structures which is finely coordinated with actin cytoskeleton reorganisation is required (Webb et al., 2002; Ridley et al., 2003; Lauffenburger and Horwitz, 1996; Ridley, 2015; Le Clainche and Carlier, 2008; Huttenlocher and Horwitz, 2011; Parsons et al., 2010).

The appearance of focal adhesions (FAs) and stress fibres in siRNA-mediated PI3K-C2β-depleted HeLa cells was first characterised during this study.

### 3.1.1 PI3K-C2β depletion causes accumulation of focal adhesions (FAs) and stress fibres

*PI3K-C2β depletion leads to more focal adhesions*

In order to investigate the role of PI3K-C2β at focal adhesions (FAs), FAs were visualised by immunofluorescence staining for paxillin, which functions as a scaffold for binding of various signalling and structural molecules at focal adhesions (Turner, 2000). As a control, HeLa cells were mock-treated or transfected with a siRNA with scrambled sequence. For depletion of PI3K-C2β, two different siRNAs were used (Figure 3-1 ). FAs were also visualised by immunofluorescence staining for paxillin in a HeLa knock-in cell line expressing enhanced green fluorescent protein (eGFP)-tagged endogenous PI3K-C2β (kindly provided to us by Prof. Volker Haucke from Leibniz-Forschungsinstitut für Molekulare Pharmakologie (FMP), Berlin) (Figure 3-2), since the

efficiency of the PI3K-C2β knockdown could easily be assessed at single-cell level in these cells.

HeLa cells depleted of PI3K-C2β displayed an increased number of focal adhesions per cell and per cell area (Figure 3-1, Figure 3-2). Furthermore, PI3K-C2β depleted HeLa cells were characterised by an increased cell area (Figure 3-1, Figure 3-2). Of note, these findings were consistent across three different HeLa cell clones, obtained directly from the American Type Culture Collection (ATCC; Figure 3-1b,d), derived in the de Camilli laboratory, HeLa (PDC) (Yale University, USA; Figure 3-1c), or endogenously eGFP-PI3K-C2β-expressing HeLa cells (Figure 3-2).

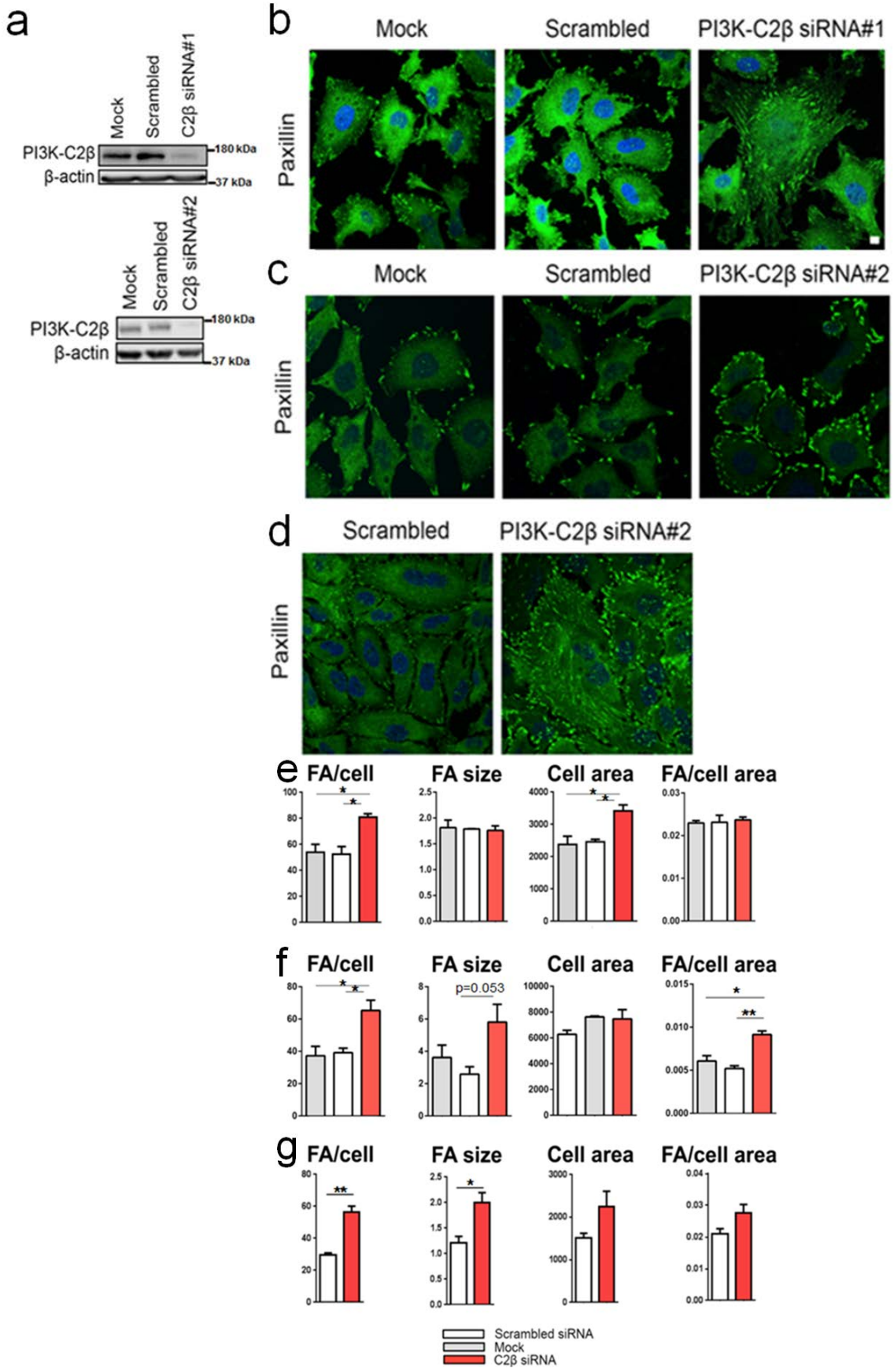


**Figure 3-1: PI3K-C2β-depleted HeLa cells display an increased number and size of FAs and also increased cell area. a)** Representative immunoblot of PI3K-C2β depleted HeLa cells. **b, c, d)** HeLa cells were plated onto matrigel-coated glass coverslips, cultured in presence of serum, fixed and stained for paxillin. HeLa cells obtained from ATCC were depleted of PI3K-C2β by **b)** siRNA#1 and the quantified data derived from them are presented in panel e or **d)** siRNA#2 and the quantified data derived from them are

presented in panel g. **c)** A different HeLa cell clone, HeLa (PDC), (provided by Professor Haucke, derived in the de Camilli laboratory, Yale University) was depleted of PI3K-C2β by siRNA#2 and the quantified data derived from them are presented in panel f. **e, f, g)** Quantifications were performed using Fiji-ImageJ software. Data represent mean ±SEM from n=3 independent experiments and at least 60 cells per condition were quantified per experiment. * p<0.05, **p<0.01, t-test. Scale bar: 10 μm.

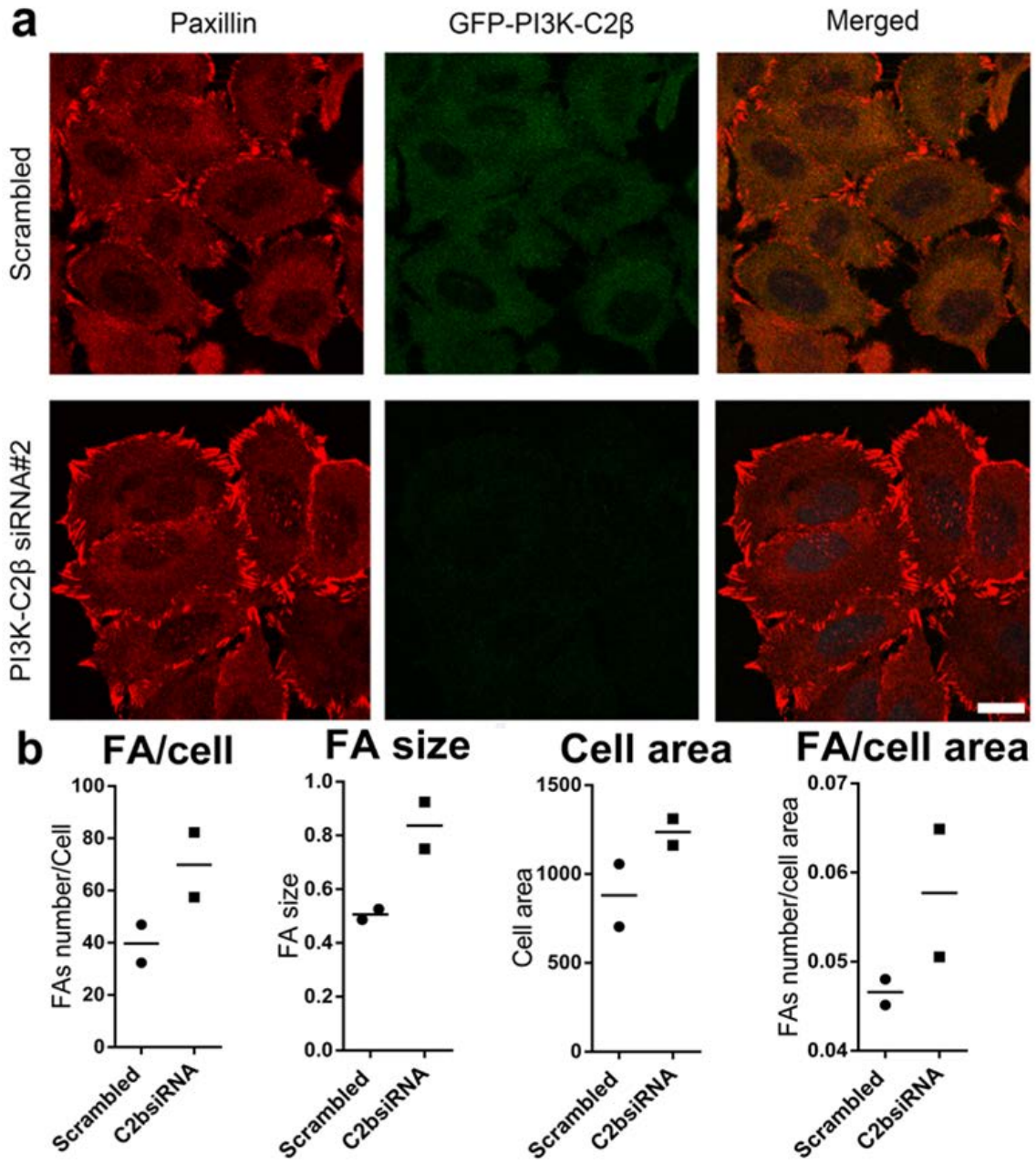


**Figure 3-2: Depletion of PI3K-C2β in HeLa cells expressing eGFP-tagged endogenous PI3K-C2β display an increased number and size of FAs and also increased cell area. a)** Control (scrambled siRNA) and PI3K-C2β-depleted HeLa cells expressing eGFP-tagged endogenous PI3K-C2β by siRNA#2 were plated onto matrigel-coated glass coverslips, cultured in presence of serum, fixed and stained for paxillin. **b)** Quantifications were performed using Fiji-ImageJ software and at least 60 cells per condition were quantified per experiment. Data represent mean from n=2 independent experiments. Scale bar: 20 μm.

*PI3K-C2β depletion leads to more stress fibres*

Integrin-based adhesions serve as anchoring points for actin stress fibres (F-actin) (Livne and Geiger, 2016). Therefore, control (scrambled siRNA) or PI3K-C2β-depleted HeLa cells were stained with phalloidin to visualise F-actin. Interestingly, the morphology of actin stress fibres was different in PI3K-C2β-depleted HeLa cells, which displayed increased and longer actin stress fibres (Figure 3-3).

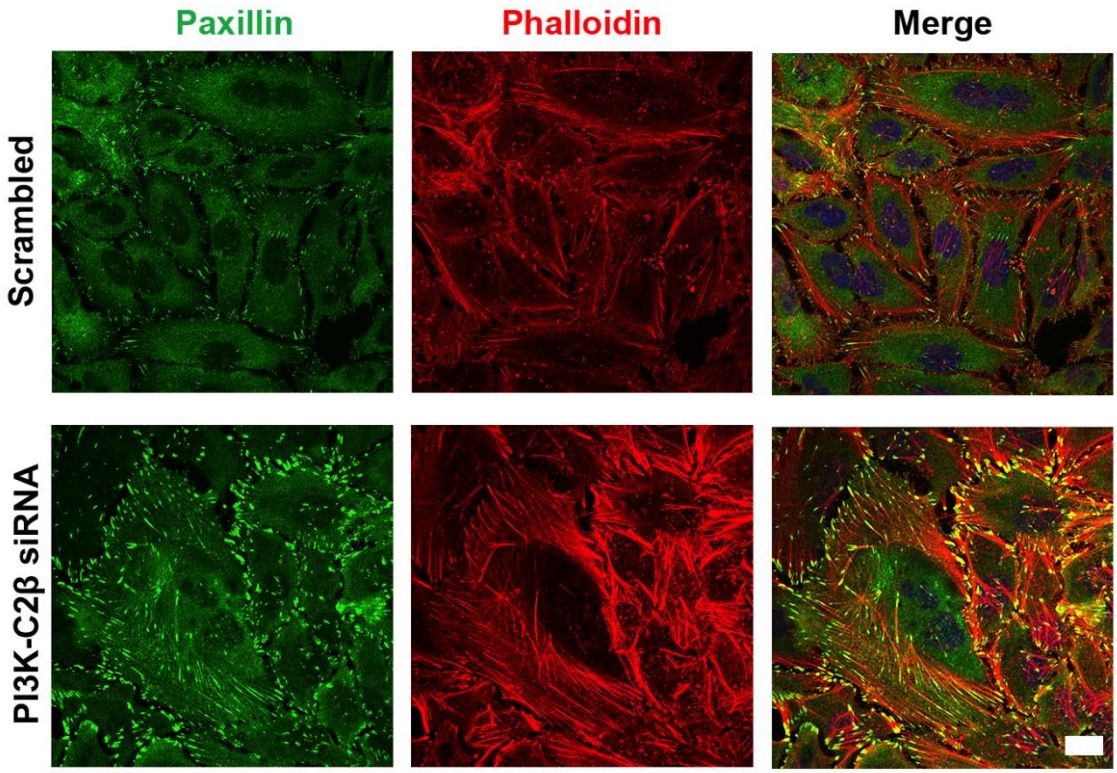


**Figure 3-3: PI3K-C2β-depleted HeLa cells display more and longer actin stress fibres.** Control (scrambled) or PI3K-C2β-depleted HeLa cells by siRNA#2 were plated onto matrigel-coated glass coverslips, cultured in presence of serum, fixed and stained for paxillin to visualise FAs and stained with Alexa Fluor 647-conjugated Phalloidin to visualise F-actin. The images presented are the same as the ones in figure 1d and are representative of n=3 independent experiments. Scale bar: 20 μm.

## 3.1.2 Loss of PI3K-C2β impairs cell migration

The essential multi-step process of cell migration is regulated by the dynamic assembly, maturation and disassembly of integrin-extracellular matrix adhesions in concert with reorganisation of the actin cytoskeleton (Parsons et al., 2010; Ridley et al., 2003; Huttenlocher and Horwitz, 2011). For cell migration to occur, cell polarisation is prerequisite, thus particular matrix-cell adhesion dynamics at the front, centre and rear of the cell are coordinated (Broussard et al., 2008).

Following the observation that PI3K-C2β depleted cells are characterised by an increased number and size of FAs, the impact of PI3K-C2β depletion on cell migration

was then investigated. The most common method used to assess cell migration, because it is cheap and easy to perform, is the scratch-wound assay (Cory, 2011) that measures the percentage of wound closure in a cell monolayer at different time points. For this purpose, the cells were plated onto 6 well-plates and when they formed a confluent monolayer, a scratch was made using a 200 µl pipette tip and the percentage of wound closure was documented at different time points by DIC microscopy in the presence of 10 % serum (Figure 3-4).

Considering that the *in vitro* scratch-wound assay mimics cell migration during wound healing *in vivo,* but does not allow determining whether wound closure is due to cell migration or cell proliferation, mitomycin C was also included in my protocol. Mitomycin C is a DNA replication inhibitor that works by covalently crosslinking complementary strands of DNA. Cells were treated with 1 µg/ml mitomycin during the whole duration of the assay and wound closure was measured at 8 and 24 hours (Figure 3-4). PI3K-C2β-depleted cells showed reduced capability of cell migration at both time points, in agreement with the published data (Katso et al., 2006; Blajecka et al., 2012; Maffucci et al., 2005; Domin et al., 2005). Additionally, under the same conditions, wound closure was monitored every hour for 48 hours using Nikon Biostation CT, further confirming that PI3K-C2β depletion leads to reduced cell movement (Figure 3-4).

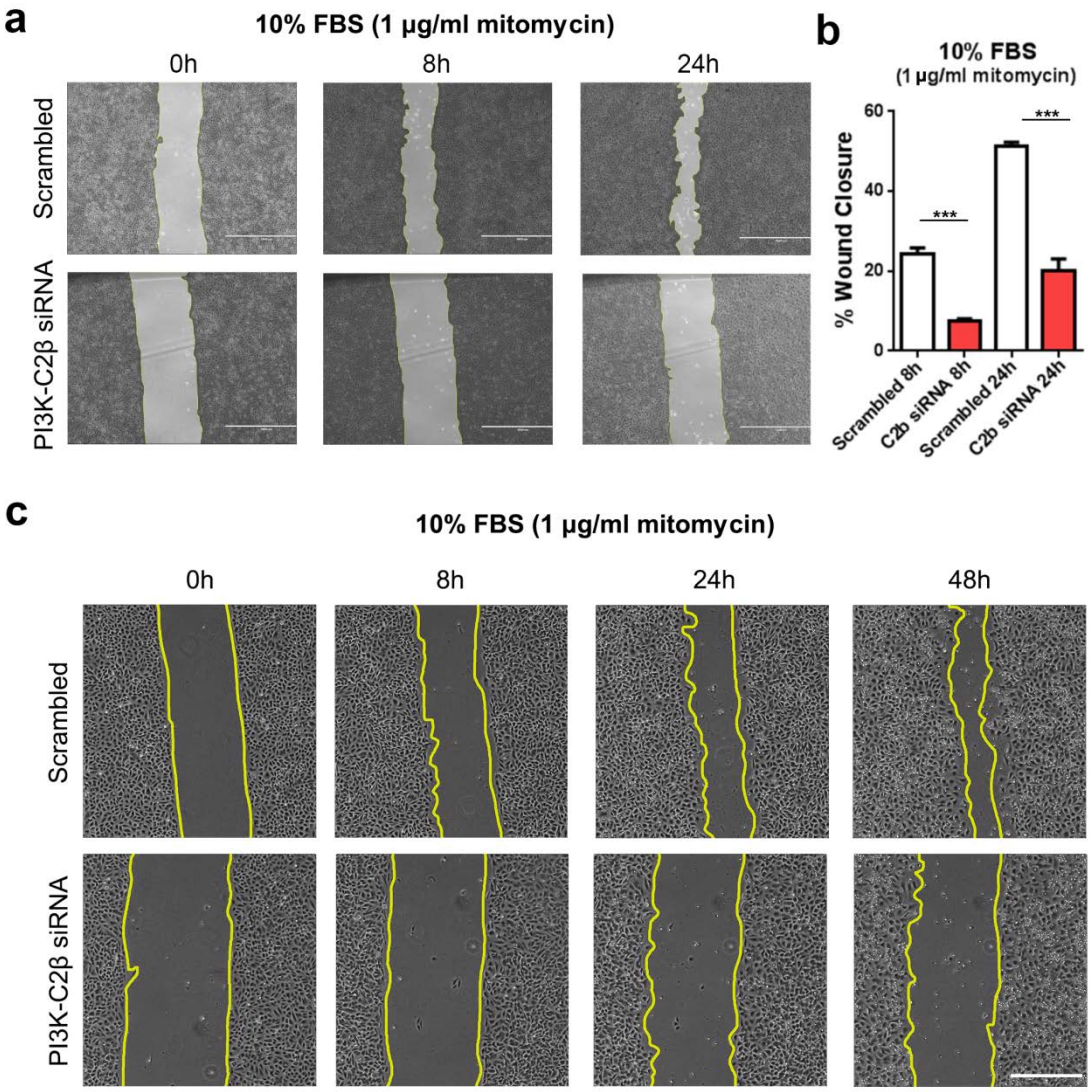


**Figure 3-4: PI3K-C2β-depleted HeLa cells display reduced cell migration.** Control (scrambled siRNA) and PI3K-C2β-depleted HeLa cells by siRNA#2 were plated onto 6-well plates and a ''wound'' was made by scratching the monolayer using a 200 µl pipette tip. The percentage of wound closure was documented at different time points by DIC microscopy in presence of serum and 1 µg/ml mitomycin. **a, b)** Fiji-ImageJ software was used to calculate the percentage of wound closure. Data are mean values with error bars representing ±SEM from n=3 independent experiments. **c)** The live movement of cells to close the wound was followed using Nikon Biostation CT for 48 hours. The images presented are representative of n=2 independent experiments. * p<0.05, **p<0.01, ***p<0.001, t-test. Scale bar: 1000 µm.

## 3.2 The role of PI3K-C2β in cell migration depends on its kinase activity

Enzymes have the capability of displaying apart from catalytic also catalytic-independent scaffold-dependent functions, as it is featured by the role of class II PI3K-C2α isoform in promoting the mitotic spindle stability during metaphase (Gulluni et al., 2017).

There are no selective PI3K-C2β inhibitors available to date and cell-based studies that have implicated this isoform in the regulation of cell migration and invasion (Katso et al., 2006; Blajecka et al., 2012; Maffucci et al., 2005; Domin et al., 2005) were performed using PI3K-C2β RNAi and overexpression approaches have not unequivocally implicated the kinase activity of this PI3K isoform in these phenomena. Therefore, I aimed to determine whether the role of PI3K-C2β in cell migration depends on its kinase activity and two different approaches were employed to this end.

### 3.2.1 Re-expression of wild-type but not kinase-dead PI3K-C2β rescues cell adhesion morphology

In order to address the question whether the role of PI3K-C2β at FAs is kinase dependent a first approach applied was the performance of rescue experiments. Thus, it was investigated whether the increased number and size of FAs in HeLa cells depleted of PI3K-C2β could be rescued by the re-expression of siRNA-resistant hPI3K-C2β. Interestingly, the overexpression of eGFP-hPI3K-C2β WT, but not of kinase-dead (KD) enzyme rescued the increased number of FAs, the elevated FA size and the cell area in HeLa cells depleted of endogenous PI3K-C2β (Figure 3-5). This indicates that the role of PI3K-C2β at FAs is kinase-dependent.

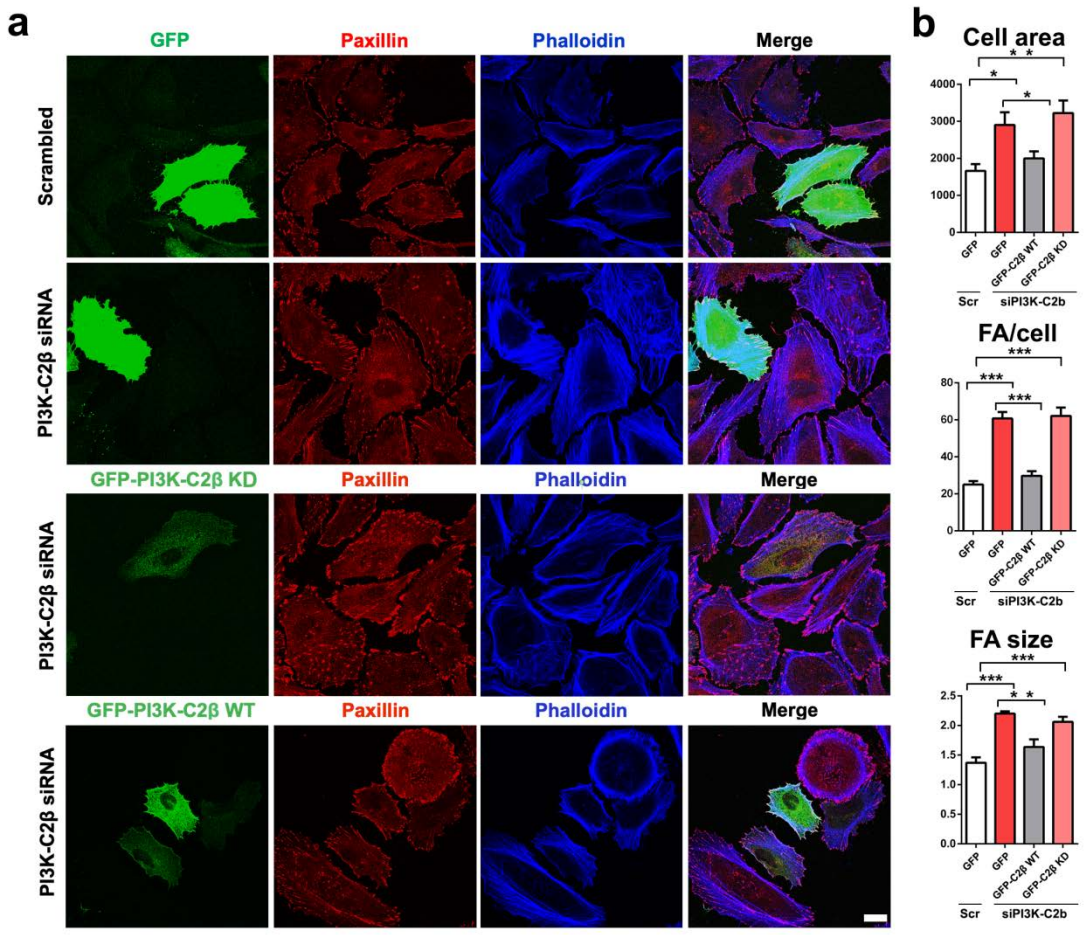


**Figure 3-5: The morphology of FAs in HeLa cells depleted of PI3K-C2β can be rescued by re-expression of hPI3K-C2β WT but not the kinase-dead protein**. **a, b)** Control (scrambled siRNA) and PI3K-C2β-depleted HeLa cells by siRNA#2 were plated onto matrigel-coated glass coverslips and cultured in presence of serum. One day prior to the end of the experiment, rescue transfections were performed. After fixation, the cells were stained for paxillin and with Alexa Fluor 647-conjugated phalloidin. **b)** Quantifications were performed using Fiji-ImageJ software. Data represent mean ±SEM from n=5 independent experiments, and at least 60 cells per condition were quantified per experiment.* p<0.05, **p<0.01, ***p<0.001, t-test. Scale bar: 20 µm.

## 3.2.2 Impaired migration in embryonic fibroblasts derived from PI3K-C2β$^{D1212A/D1212A}$ mice

*PI3K-C2β$^{D1212A/D121A2}$ kinase dead knock-in mice*

The host laboratory has generated the PI3K-C2β kinase dead knock-in (KI) mouse model in order to explore the physiological roles of the kinase activity of this PI3K isoform (Alliouachene et al., 2015). In this model, the endogenous PI3K-C2β has been catalytically inactivated by a gene targeting approach that introduces the point mutation D1212A in the ATP-binding site, converting the conserved DFG motif to AFG (Alliouachene et al., 2015). The expression levels of the targeted and non-targeted isoforms remain unaltered by this strategy, a problem observed in class I PI3K knockout mice (Vanhaesebroeck et al., 2005). Thereby, this strategy allows the

assessment of the kinase-dependent rather than possible scaffolding functions of the targeted PI3K isoform (Alliouachene et al., 2015).

*PI3K-C2β inactivation leads to more focal adhesions*

Since the rescue experiments that were performed in HeLa cells depleted of PI3K-C2β indicated that the role of this PI3K isoform at FAs is kinase-dependent, I was interested in confirming this observation using the PI3K-C2β KI mouse model that the host laboratory has generated (Alliouachene et al., 2015). For my studies, MEFs derived from WT and PI3K-C2β KI mice immortalised through stable shRNA-mediated knockdown of p53 were used.

In immortalised WT and PI3K-C2β KI MEFs, FAs were visualised by immunofluorescence staining for paxillin (Figure 3-6). PI3K-C2β KI MEFs were characterised by an increased number of FAs per cell compared to the WT cells which was statistically significant ($p=0.02$) similarly to HeLa cells depleted of PI3K-C2β. Moreover, they displayed a tendency for increased cell area which was not statistically significant though ($p=0.15$) due to the two SEM error bars which nearly overlapped (the repetition of the experiment could eliminate this). This further confirms that the role of PI3K-C2β at FAs is kinase dependent (Figure 3-6). Furthermore, in order to exclude the possibility that the effect of PI3K-C2β inactivation at FAs is paxillin-specific, immunofluorescence staining for vinculin, an actin-binding adaptor protein with a key role in the functional linkage between FAs/cytoplasmic domain of integrins and the actin cytoskeleton (Humphries et al., 2007; Bays and DeMali, 2017), was also used (Figure 3-6). Immunofluorescence staining for vinculin also revealed more FAs in PI3K-C2β KI MEFs, thus indicating that the elevated number of FAs upon PI3K-C2β inactivation is a general defect of FAs (Figure 3-6).

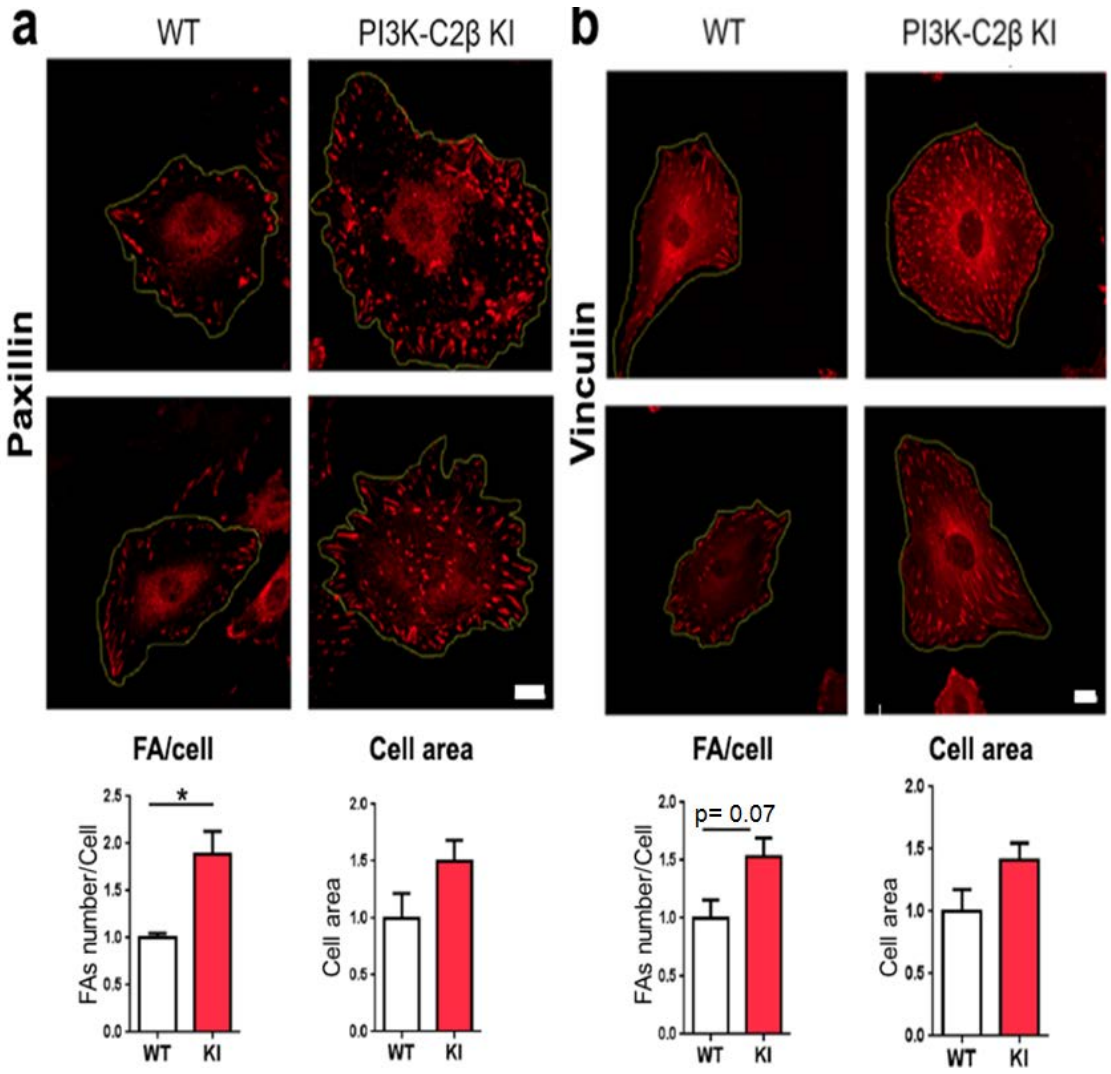


**Figure 3-6: PI3K-C2β KI MEFs display an increased number of FAs and increased cell area.** WT and PI3K-C2β KI MEFs were plated onto glass coverslips, cultured in the presence of serum, fixed and stained for **a)** paxillin or **b)** vinculin, two FA markers. Quantifications were performed using Fiji-ImageJ software. Data are mean values with error bars representing ±SEM from n=3 independent experiments and at least 40 cells per genotype were quantified per experiment. The MEFs used were derived from 3 WT (14-5, 14-6, 14-7) and 3 PI3K-C2β KI (13-3, 14-8, 14-9) mice. * p<0.05, t-test. Scale bar: 10 µm.

*PI3K-C2β inactivation leads to reduced cell migration*

As mentioned above, PI3K-C2β plays a role in the regulation of cell migration upon stimulation with EGF (Katso et al., 2006), PDGF (Blajecka et al., 2012) or LPA (Maffucci et al., 2005), but its mechanism of action is entirely unclear. These studies were performed using PI3K-C2β RNAi and overexpression approaches, and have not unequivocally implicated the kinase activity of this PI3K in these phenomena. Furthermore, the work presented here also showed that HeLa cells depleted of PI3K-C2β displayed a significant cell migration defect in presence of serum. Moreover, I observed that the role of this PI3K isoform at FAs is kinase-dependent. Based on these observations, whether immortalised PI3K-C2β KI MEFs were also characterised

by defective cell migration compared to WT MEFs was then investigated. For this purpose, the scratch-wound assay in WT and PI3K-C2β KI MEFs was performed in presence of 10 µg/ml mitomycin C to impair cell proliferation. The percentage of wound closure was documented at different time points by DIC microscopy and three sets of conditions were used: cells were either (1) serum-starved overnight; (2) serum-starved overnight and subsequently stimulated with PDGF, or (3) cultured in 10% serum (full medium) (Figure 3-7).

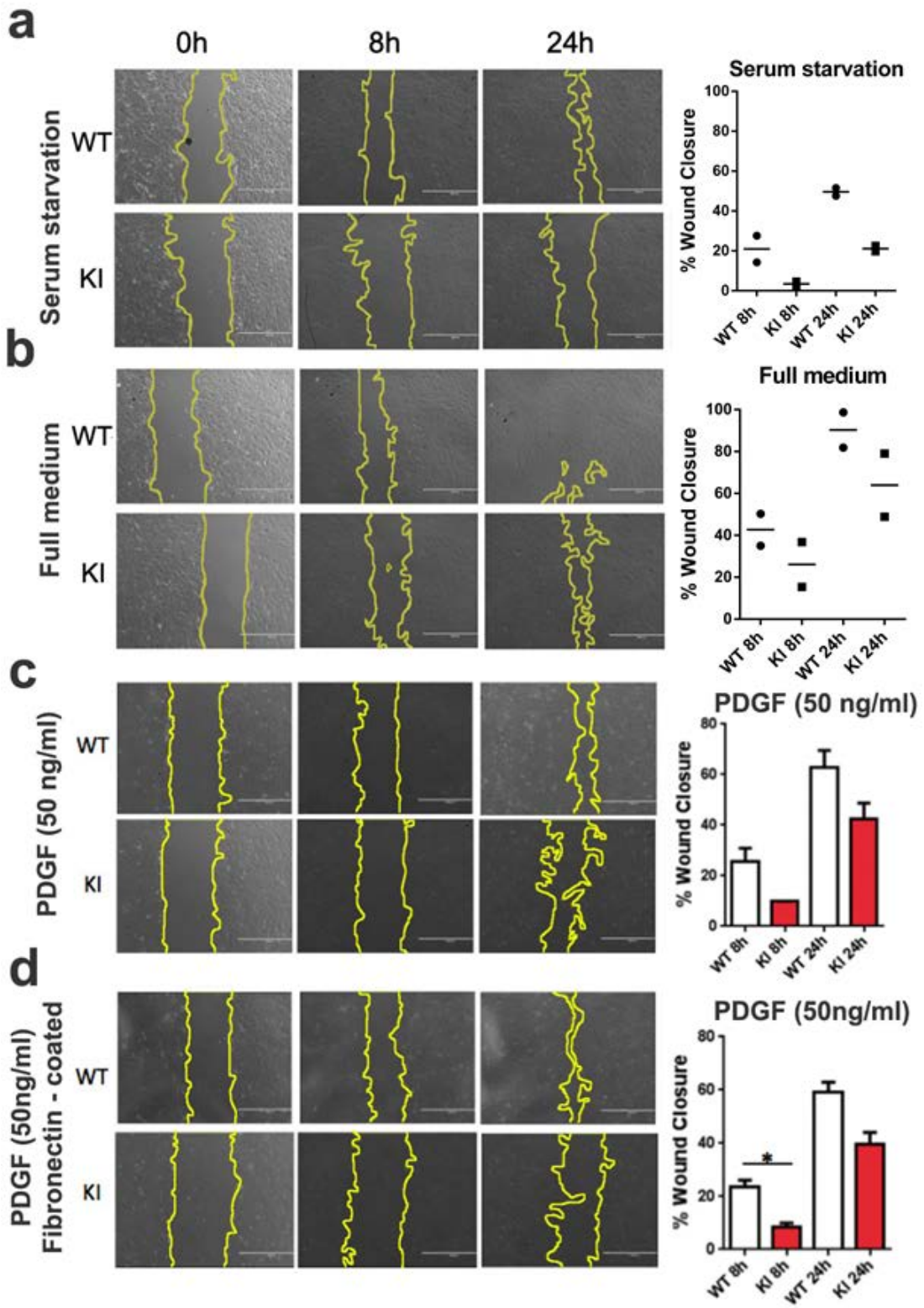


**Figure 3-7: Defective cell migration in PI3K-C2β KI MEFs**. WT and PI3K-C2β KI MEFs were seeded onto **a, b, c)** uncoated or **d)** fibronectin-coated glass bottom dishes and were **a, c, d)** serum starved overnight or **b)** cultured in full medium (presence of serum). A ''wound'' was made by scratching the monolayer using a 200 µl pipette tip and in presence of 10 µg/ml mitomycin to prevent proliferation, the assay was performed **a)** under serum starved conditions**, b)** in full medium (presence of serum) or **c, d)** upon PDGF stimulation (50 ng/ml). The percentage of wound closure was documented at different time points by DIC microscopy. Fiji-ImageJ software was used to calculate the percentage of wound closure. Data represent mean ±SEM from n=3 independent experiments in case of PDGF stimulation or mean from n=2 independent experiments in case of presence or absence of serum. The MEFs used were derived from 3 WT (14-5, 14-6, 14-7) and 3 PI3K-C2β KI (13-3, 14-8, 14-9) mice. *p<0.05, t-test. Scale bar: 1000 µm.

In all conditions tested, immortalised PI3K-C2β KI MEFs showed a decreased capability of cell migration with the most prominent effect observed upon PDGF stimulation. The abundance of migratory stimuli in presence of serum appears to weaken the effect, thus it seems that the cells need to ‘’be challenged’’ in order to display a more robust phenotype (Figure 3-7).

## 3.3 Cell spreading and cell size are increased upon inactivation of PI3K-C2β

Due to the increased cell area that was observed upon PI3K-C2β inactivation (Figure 3-6, Figure 3-8b) the cell size was then determined in the presence of serum by measuring the forward scatter by flow cytometry (Figure 3-8c). Interestingly, no effect on cell size upon PI3K-C2β inactivation in the presence of serum was noticed (Figure 3-8c). Additionally, total protein content per cell was measured as an indicator of cell size based on the hypothesis that if the cells were bigger, they would have an increased amount of protein per cell, but no difference was noticed (Figure 3-8e). Therefore, PI3K-C2β inactivation seemed to result in increased cell spreading that can be explained by the elevated number of FAs in PI3K-C2β KI MEFs. Interestingly, preliminary data suggested that upon HBSS starvation, PI3K-C2β KI MEFs are characterised by a mild increase in cell size determined by the forward scatter measurement in agreement with a recent study showing that PI3K-C2β KO HEK293T cells were larger compared to wild-type HEK293T cells (Marat et al., 2017) (Figure 3-8d). More experiments need to be performed to confirm this observation though.

Consistently, HeLa cells depleted of PI3K-C2β were also characterised by a mild but statistically significant increase in the cell size, assessed by the forward scatter measurement, under conditions of growth factor deprivation (HBSS starvation), whereas in presence of serum the cell size increase was milder and not statistically significant (Figure 3-8a).

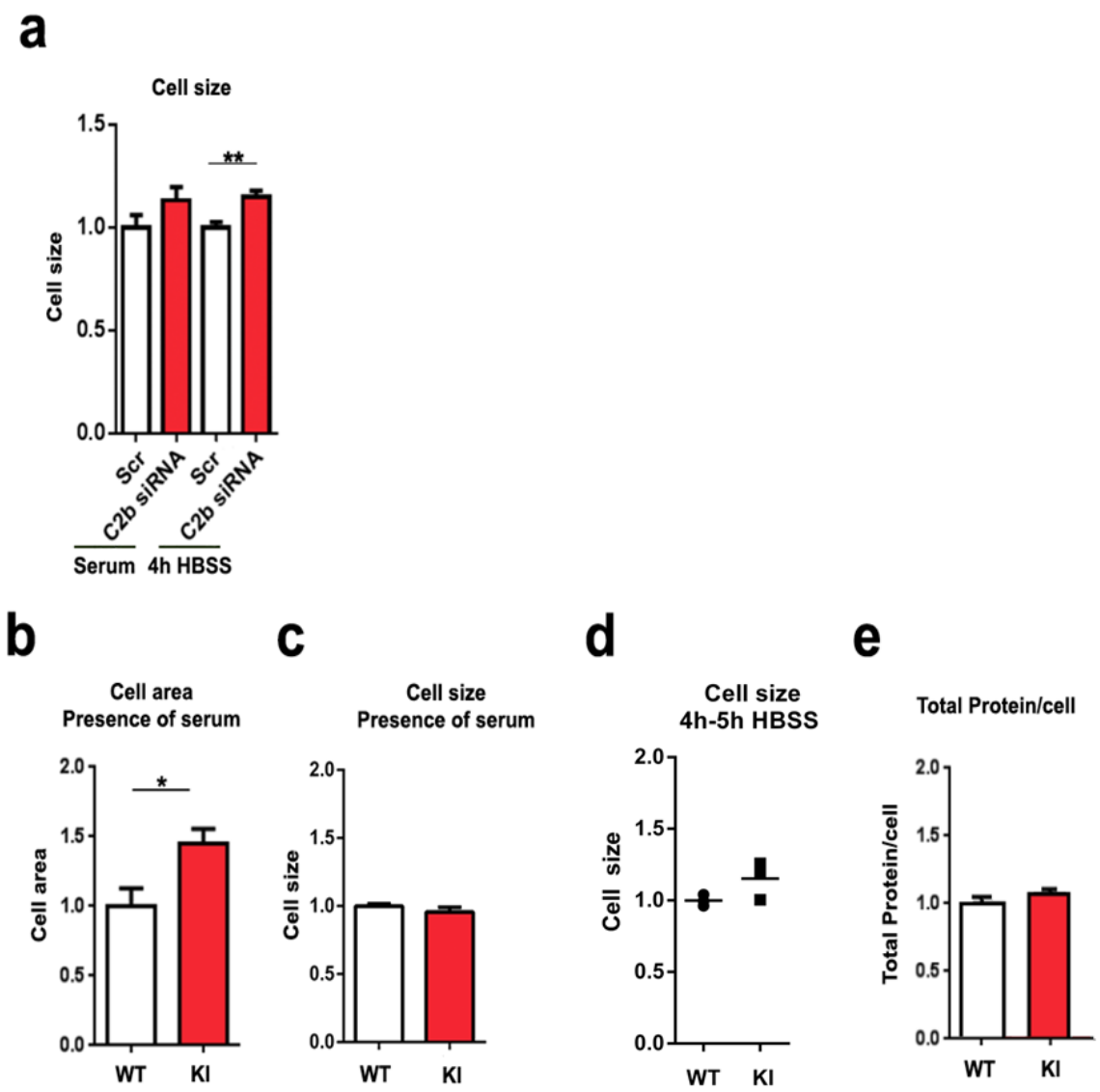


**Figure 3-8: PI3K-C2β-depleted HeLa cells and PI3K-C2β KI MEFs display increased spreading and cell size. a)** Determination of cell size by forward scatter signal in flow cytometry of control (scrambled siRNA) or PI3K-C2β-depleted HeLa cells by siRNA#2 in presence of serum or upon HBSS starvation for 4 hours. Data are mean values with error bars representing SEM from n=3 independent experiments. **b)** WT and PI3K-C2β KI MEFs were plated onto glass coverslips, cultured in presence of serum, fixed and stained for paxillin or vinculin. Average cell area was quantified using Fiji-ImageJ software. Data are mean values with error bars representing ±SEM from n=6 independent experiments and at least 50 cells per genotype were quantified per experiment. The MEFs used were derived from 3 WT and 3 PI3K-C2β KI mice. **c,d)** Determination of cell size of WT and PI3K-C2β KI MEFs by forward scatter signal in flow cytometry **c)** in presence of serum or **d)** upon HBSS starvation for 4 to 5 hours. **c)** Data are mean values with error bars representing ±SEM from n=3 independent experiments. **d)** Data are mean values from n=1 experiment and every dot in the graph represents a different mouse. **c,d)**The MEFs used were derived from 3 WT (14-5, 14-6, 14-7) and 3 PI3K-C2β KI (13-3, 14-8, 14-9) mice. **e)** Determination of total protein concentration per cell by Bradford protein assay. Data are mean values with error bars representing ±SEM from n=3 independent experiments. The MEFs used were derived from 3 WT and 3 PI3K-C2β KI mice. *p<0.05, **p<0.01, t-test.

## 3.4 Inactivation of PI3K-C2β impairs focal adhesion disassembly

Integrins are the major receptors for ECM components. Their presence at the cell surface is regulated by continuous cycles of internalisation and recycling back to the plasma membrane, thus controlling FA dynamics. Following their internalisation, integrins enter early endosomes, where they are sorted either for degradation in late endosomes/lysosomes or recycling back to the cell surface (De Franceschi et al., 2015).

*PI3K-C2β inactivation does not affect cell adhesion to ECM components*

The increased number of FAs observed upon depletion or inactivation of PI3K-C2β could be a consequence of changes in the processes of either FA assembly or FA disassembly, or both. Therefore, whether PI3K-C2β KI MEFs are characterised by an increased capability to adhere onto ECM components compared to WT was first investigated. For this purpose, the adhesion assay, in which cells are trypsinised and then are seeded to adhere onto the ECM substrates - fibronectin or collagen type I -, was performed. In this assay, formation of adhesions depends on the exocytosis of integrins as surface-exposed integrins are enzymatically cleaved during trypsinization. After allowing cells to adhere for 30 – 60 min, non-adherent cells were washed out and the adherent cells were quantified using crystal violet staining. No difference in the ability of PI3K-C2β KI MEFs to adhere onto ECM substrates compared to WT MEFs was observed. Therefore, these data suggest that the exocytosis of integrins from internal pools and the *de novo* formation of adhesions are not affected upon PI3K-C2β inactivation (Figure 3-9).

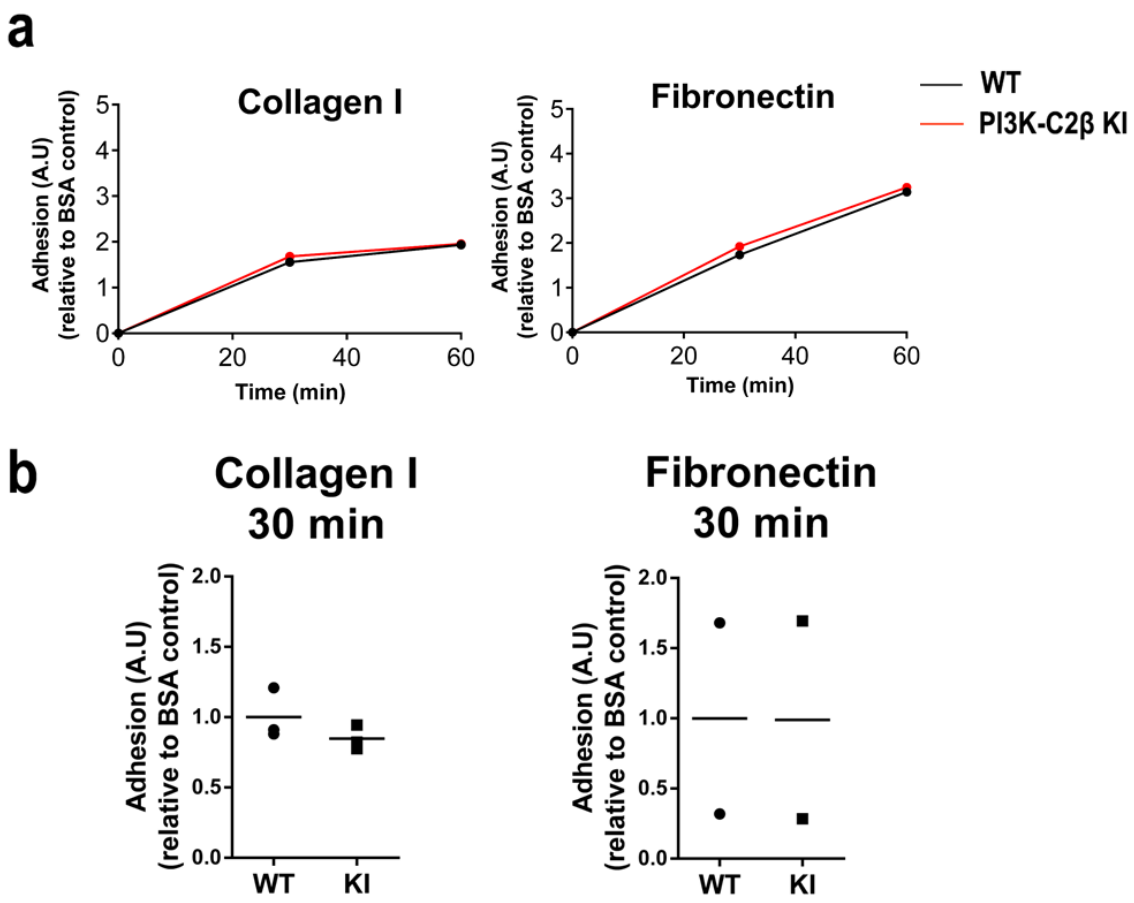


**Figure 3-9: No effect on cell adhesion onto ECM substrates upon PI3K-C2β inactivation**. WT and PI3K-C2β KI MEFs were seeded onto fibronectin- or collagen I-coated 96-well plates. Unbound cells were removed after **a, b)** 30 min or **a)** 1 h. Adherent cells were fixed with 3.7% formaldehyde, stained with 0.1% crystal violet and were detected by the absorbance at 600 nm. Data represent mean from **a)** n=1 experiment (each dot represent the average value of WT or KI mice from which the MEFs were derived) and **b)** n=2 independent experiments for fibronection (each dot represent the average of each experiment) and n=1 experiment for collagen I (each dot represent a mouse from which the MEFs were dereived). The MEFs used were derived from 3 WT (14-5, 14-6, 14-7) and 3 PI3K-C2β KI (13-3, 14-8, 14-9) mice in each independent experiment. These experiments were performed with the help of Dr Samira Alliouachene.

*PI3K-C2β inactivation delays FA disassembly*

The process of FA disassembly is less well-understood compared to the process of FA assembly. However, the microtubule network has been reported to play a crucial role in this process (Ezratty et al., 2009; Ezratty et al., 2005; Chao and Kunz, 2009; Chao et al., 2010; Nagano et al., 2010; Feutlinske et al., 2015).

Nocodazole is a drug that induces microtubule network disruption, thereby preventing the process of FA disassembly, and it has been proven to be a useful tool in FA disassembly studies (Ezratty et al., 2009; Ezratty et al., 2005; Chao and Kunz, 2009; Chao et al., 2010; Nagano et al., 2010; Feutlinske et al., 2015). In this experiment, nocodazole treatment results in microtubule depolymerisation, followed by nocodazole washout that allows microtubule regrowth and FA disassembly. Nocodazole washout has been used to study the molecular mechanism of FA disassembly and it has been reported that dynamin- and clathrin-dependent endocytosis is involved in this process (Ezratty et al., 2009; Ezratty et al., 2005; Chao

and Kunz, 2009; Chao et al., 2010). Based on nocodazole washout experiments, Dab2, a clathrin adaptor (Ezratty et al., 2009; Chao and Kunz, 2009), Stonin1, an endocytic adaptor (Feutlinske et al., 2015) and type I phosphatidylinositol phosphate kinase β (PIPKIβ) (Chao et al., 2010) have been implicated in the disassembly of FAs. Interestingly, the PI3K-C2β KI or knockdown phenotype may share some similarities with the Stonin 1 KO, the Dab2 knockdown or the PIPKIβ knockdown phenotype, since MEFs derived from Stonin1 KO mice displayed an elevated number of FAs (Feutlinske et al., 2015), PIPKIβ depleted human fibrosarcoma HT1080 cells were characterised by FA accumulation (Chao et al., 2010) and HT1080 cells depleted of Dab2 (Chao and Kunz, 2009) or NIH3T3 cells depleted of Dab2 (Ezratty et al., 2009) showed defective cell migration.

Consequently, whether PI3K-C2β was involved in the disassembly of FAs was then asked, based on the idea that alterations in the number of FAs may result from defective FA disassembly. Hence, I studied whether PI3K-C2β inactivation affects FA disassembly dynamics as assessed by the nocodazole washout experiment and visualization of adhesion structures by immunofluorescence staining for paxillin. As expected, the microtubule network was disrupted after nocodazole treatment and it regrew after nocodazole washout, as confirmed by staining for α-tubulin, a subunit of microtubules. Interestingly, 10 minutes after nocodazole washout, WT MEFs maintained 55% of their FAs relative to the nocodazole treated cells, while 84% of FAs remained in PI3K-C2β MEFs relative to nocodazole treated cells (Figure 3-10). These findings suggest that the kinase activity of PI3K-C2β is implicated in the process of FA disassembly.

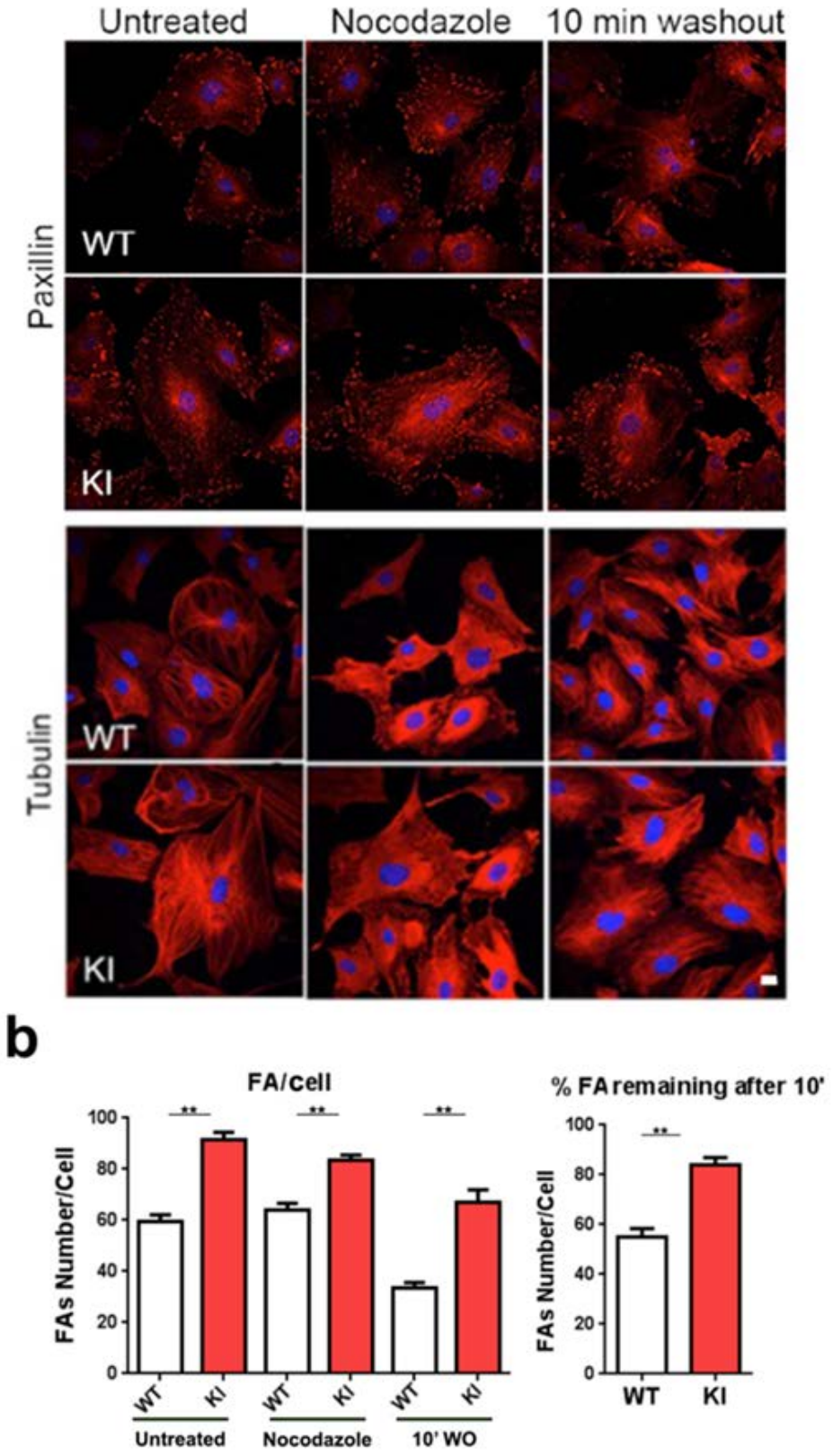


**Figure 3-10: PI3K-C2β inactivation delays FA disassembly. a)** Starved WT and PI3K-C2β KI MEFs were left untreated or were incubated with 10 μM nocodazole. After 2 hours, nocodazole was washed out to allow microtubule regrowth and FA disassembly. Cells were fixed and immunostained with antibodies against paxillin or tubulin. **b)** The percentage of FAs remaining after 10 minutes washout relative to nocodazole treated cells was quantified using Fiji-ImageJ software and at least 40 cells per genotype were quantified per experiment. Data are mean values with error bars representing ±SEM from n=3 independent experiments. The MEFs used were derived from 3 WT (14-5, 14-6, 14-7) and 3 PI3K-C2β KI (13-3, 14-8, 14-9) mice in 2 experiments and from 2 WT (14-5, 14-6) and PI3K-C2β (14-8, 14-9) KI mice in 1 experiment. * $p<0.05$, ** $p<0.01$, t-test. Scale bar: 20 μm

## 3.5 PI3K-C2β displays dynamic recruitment to focal adhesions

### 3.5.1 Characterisation of the subcellular localisation of PI3K-C2β

The visualisation of PI3K-C2β by immunofluorescence microscopy is not possible by commercially available antibodies. Therefore, in order to overcome this limitation, an eGFP-mPI3K-C2β expression plasmid was generated to overexpress mouse PI3K-C2β in MEFs. As expected, eGFP-mPI3K-C2β expressing cells showed elevated expression levels of PI3K-C2β and the indicative band for the eGFP-tagged mPI3K-C2β migrated at a higher apparent molecular weight than endogenous PI3K-C2β (PI3K-C2β: ~ 160-180 kDa, GFP: 27 kDa, eGFP-tagged PI3K-C2β: ~ 187-207 kDa) (Figure 3-11).

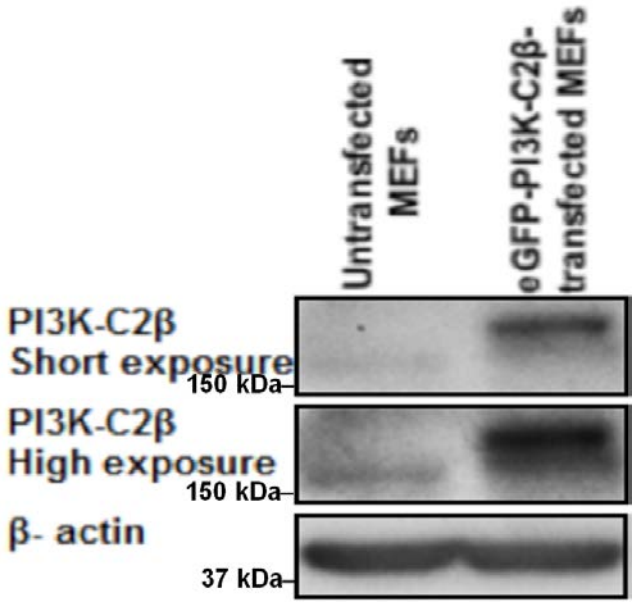


**Figure 3-11: Expression levels of PI3K-C2β in WT MEFs transiently transfected with eGFP-tagged recombinant full-length PI3K-C2β.** WT MEFs were transiently transfected for 24 hours with eGFP-tagged recombinant full-length PI3K-C2β and the expression levels of PI3K-C2β were determined by Western blot analysis.

Recent published data from the host laboratory (Alliouachene et al., 2015) showed that PI3K-C2β inactivation in hepatocytes leads to an increased number of APPL1-positive endosomes as well as enlarged EEA1-positive endosomes. Therefore, for a first characterisation of PI3K-C2β localisation, MEFs expressing eGFP-mPI3K-C2β were stained for APPL1 or EEA1 and images were acquired using confocal microscopy (Figure 3-12). Additionally, based on a recent study showing that under conditions of growth factor deprivation, PI3K-C2β is recruited to late endosomes/lysosomes and leads to mTORC1 suppression (Marat et al., 2017), MEFs expressing eGFP-mPI3K-C2β were also stained for LAMP-1 (Figure 3-12). Confocal images revealed eGFP-mPI3K-C2β to localise to punctate structures in the cytoplasm

without showing any significant co-localisation with EEA1, APPL1, or LAMP-1 (Figure 3-12).

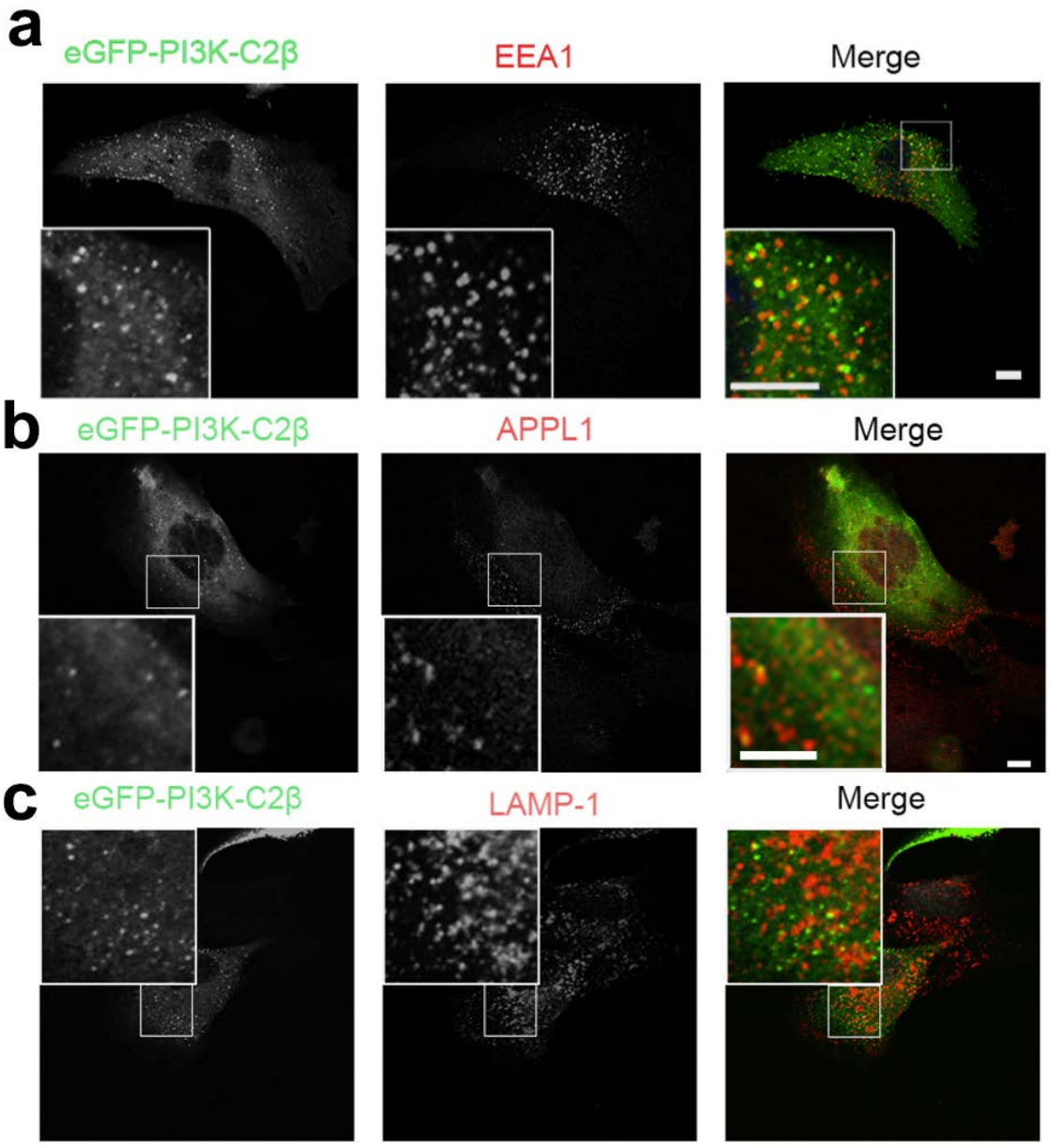


**Figure 3-12: MEFs transiently transfected with eGFP-mPI3K-C2β do not show any significant co-localisation with EEA1, APPL1 or LAMP-1.** Confocal images of WT MEFs expressing eGFP-mPI3K-C2β with EEA1, APPL1 or LAMP-1 co-staining. MEFs were plated onto glass coverslips, cultured in the presence of serum, transiently transfected for 24 hours with eGFP-mPI3K-C2β, fixed and stained for **b)** APPL1, **a)** EEA1 or **c)** LAMP-1. Scale bar: 10 µm**.**

Additionally, since according to my observations PI3K-C2β plays a role at FAs, I was interested in testing whether PI3K-C2β is localised at FAs. Therefore, as a pilot experiment, FAs were visualised by immunofluorescence staining for paxillin in MEFs expressing eGFP-mPI3K-C2β and images were acquired using confocal microscopy.

eGFP-PI3K-C2β tended to display partial co-localisation with paxillin mainly in the cell mid-region (Figure 3-13).

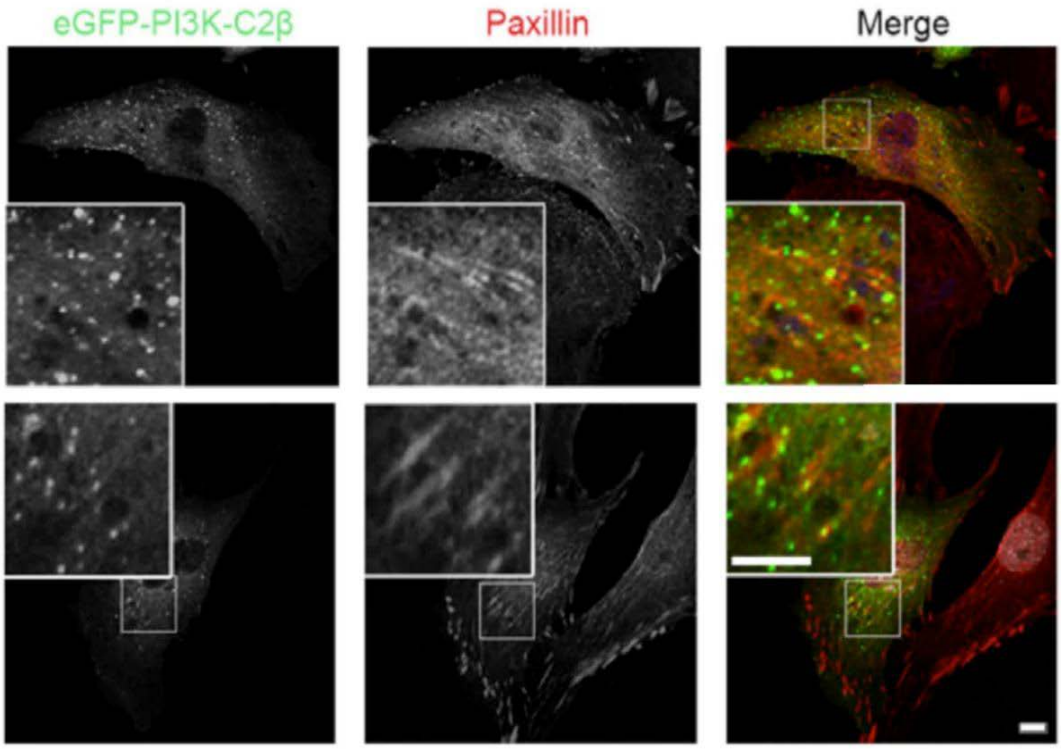


**Figure 3-13: eGFP-PI3K-C2β shows a tendency to partially co-localise with paxillin in the mid-region of the cell.** Confocal images of MEFs expressing eGFP-mPI3K-C2β with paxillin staining. MEFs were plated onto glass coverslips, cultured in the presence of serum, transiently transfected for 24 hours with eGFP-mPI3K-C2β, fixed and stained for paxillin. Scale bar: 10 μm.

However, because the thickness of the confocal image sections is approximately 1 μm, the partial co-localisation observed by confocal imaging is not certain that it is real and not an artefact of endosomal/cytoplasmic PI3K-C2β$^{+}$ structures overlapping with the paxillin staining in z. Therefore, verification of these results using total internal reflection fluorescence (TIRF) microscopy was required. This technique provides images with a high axial resolution of up to 100 nm and permits the observation, with high signal-to-noise ratio, of fluorophores found in close proximity to the coverslip. It is thus ideally suited for the study of endocytosis and FAs (Poulter et al., 2015). Interestingly, similar results were obtained that confirmed a partial co-localisation between PI3K-C2β and paxillin (Figure 3-14). However, because the transfection efficiency was low, it was difficult the results to be quantified. Therefore, a solution for this limitation could be the generation of eGFP-PI3K-C2β encoding lentiviral vectors that could possibly result in higher transduction efficiency, allowing for quantification of co-localization from a larger number of cells. Additionally, the use of

CRISPR engineering for tagging the endogenous protein could avoid possible artefacts resulting from overexpression of GFP-tagged protein.

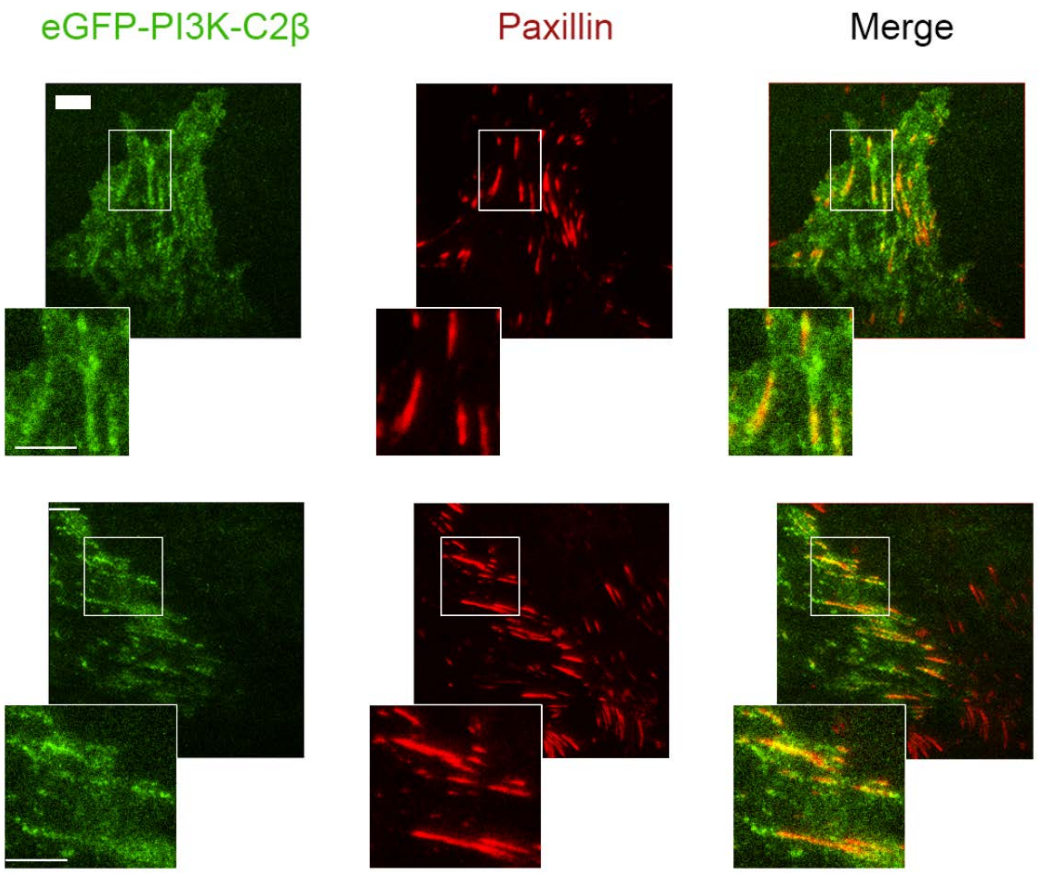


**Figure 3-14: eGFP-PI3K-C2β partially co-localises with paxillin.**TIRF microscopy of MEFs expressing eGFP-mPI3K-C2β with paxillin staining. MEFs were plated onto glass bottom dishes, cultured in the presence of serum, transiently transfected for 24 hours with eGFP-mPI3K-C2β, fixed and stained for paxillin. Scale bar: 10 µm Scale bar: 10 µm.

## 3.5.2 Focal adhesion disassembly triggers recruitment of PI3K-C2β to focal adhesions

*PI3K-C2β enrichment at FAs upon blebbistatin treatment*

Since the data acquired by this study indicate that PI3K-C2β is implicated in the process of FA disassembly it was crucial to test whether PI3K-C2β accumulates at FAs as FAs disassemble in live cells. For this purpose, total internal reflection fluorescence imaging of HeLa cells expressing both vinculin-mCherry and eGFP-tagged human PI3K-C2β (kindly provided by Prof. Volker Haucke, Berlin) was performed upon blebbistatin treatment.

Adhesion maturation and stability is dependent on myosin II-generated tension (Parsons et al., 2010; Feutlinske et al., 2015). Blebbistatin, which is an inhibitor of myosin II, causes prevention of FA maturation, triggers dismantling of mature FAs and leads to an accumulation of smaller nascent adhesions (Parsons et al., 2010;

Feutlinske et al., 2015). Therefore, blebbistatin treatment (50 μM for 2 hours) was used to trigger the process of FA disassembly (Feutlinske et al., 2015). Interestingly, in a pilot experiment using 27 minutes blebbistatin treatment, PI3K-C2β was strongly enriched at disassembling FAs (Figure 3-15).

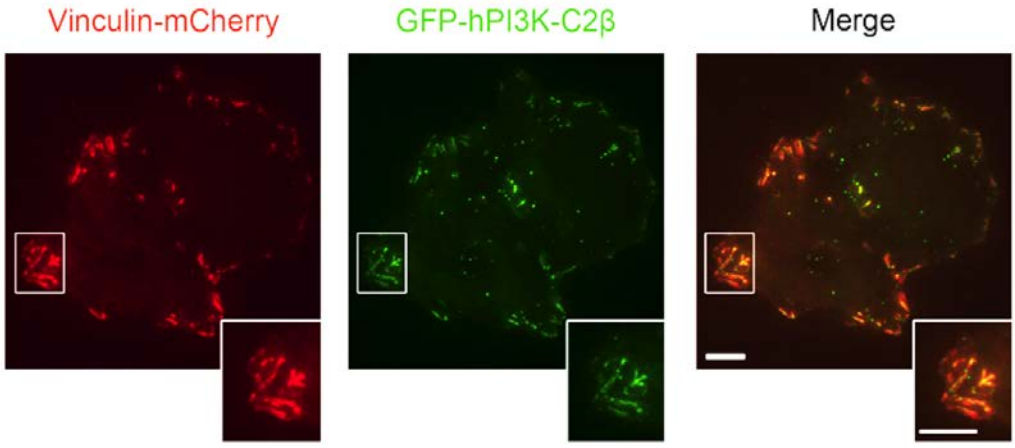


**Figure 3-15: Co-localisation between vinculin-mCherry and eGFP-hPI3K-C2β upon blebbistatin treatment**. Cells expressing both vinculin-mCherry and eGFP-tagged human PI3K-C2β were treated with 50 μM blebbistatin and imaged using TIRF microscopy after 27 minutes. Scale bar: 10 μm.

To expand on this observation, HeLa cells expressing both vinculin-mCherry and eGFP-hPI3K-C2β were treated with 50 μM blebbistatin and monitored using TIRF microscopy for 2 hours, with images being taken every 3 minutes. Preliminary data suggested that eGFP-hPI3K-C2β fluorescence accumulated when vinculin-mCherry fluorescence faded as FAs disassembled, indicating that PI3K-C2β is involved in the process of FA disassembly (Figure 3-16). Fluorescence intensity was assessed by defining a fluorescence intensity threshold and the tool Analyze → Measure in ImageJ. More specifically, the selection of every cell as a region of interest was done manually using the tool of ROI Manager of Fiji-ImageJ software and then a Fiji-ImageJ macro was used in order the fluorescence intensity of individual objects to be quantified over time.

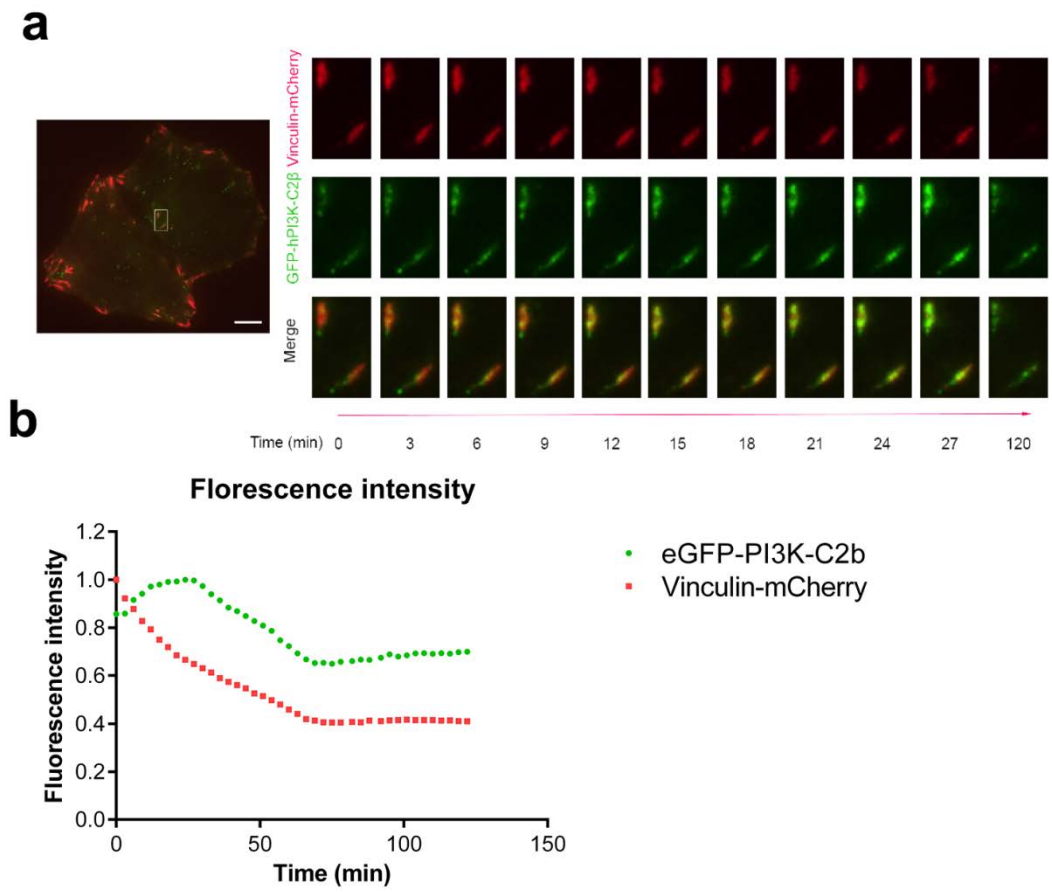


**Figure 3-16: PI3K-C2β accumulates at disassembling FAs. a)** TIRF microscopy of HeLa cells expressing both vinculin-mCherry and eGFP-hPI3K-C2β upon 50 µM blebbistatin treatment. The cells were monitored for 2 hours and images were taken every 3 minutes. PI3K-C2β fluorescence accumulated when vinculin fluorescence faded as FAs disassembled. **b)** Quantification of vinculin-mCherry and eGFP-PI3K-C2β fluorescence intensity over time from two representative cells expressing both vinculin-mCherry and eGFP-hPI3K-C2β using Fiji-ImageJ software. Scale bar: 10 µm.

After this observation and in order to avoid possible artefacts resulting from overexpression of eGFP-tagged protein, HeLa cells expressing endogenous eGFP-tagged PI3K-C2β were used (kindly provided by Prof. Haucke, Berlin). Therefore, HeLa cells expressing endogenous eGFP-tagged PI3K-C2β which were transiently transfected with vinculin-mCherry were monitored for 30 minutes without being treated with blebbistatin and then were treated with 50 µM blebbistatin and monitored for 4 hours using TIRF microscopy, with images being taken every 5 minutes. Interestingly, the same effect upon blebbistatin treatment was observed, i.e. an accumulation of PI3K-C2β at dismantling FAs while in absence of blebbistatin no further accumulation of PI3K-C2β at FAs was observed, further indicating that PI3K-C2β plays a role in FA disassembly (Figure 3-17). For the analysis of endogenous eGFP-tagged PI3K-C2β recruitment to FAs, both eGFP-hPI3K-C2β and vinculin-mCherry intensities were quantified over time using the Fiji/ImageJ software as described above.

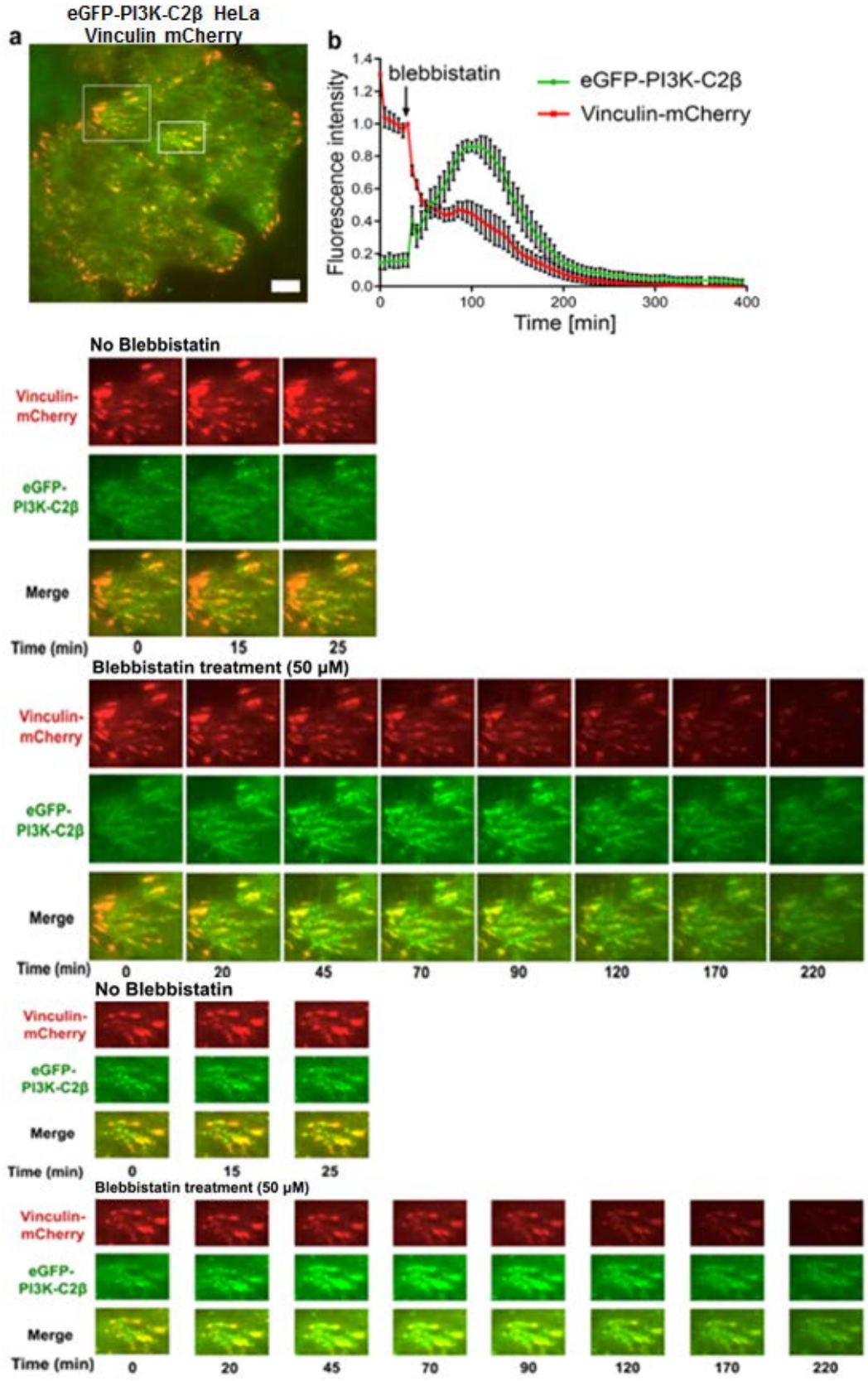


**Figure 3-17: Endogenous PI3K-C2β accumulates at disassembling FAs. a)** TIRF microscopy of HeLa cells expressing endogenous eGFP-tagged PI3K-C2β which were transiently transfected with vinculin-mCherry without or upon 50 µM blebbistatin treatment. The cells were monitored for 30 minutes without blebbistatin treatment and for 4 hours with blebbistatin treatment and images were taken every 5 minutes. PI3K-C2β fluorescence accumulated when vinculin fluorescence faded as FAs disassembled. **b)** Quantification of vinculin-mCherry and eGFP-PI3K-C2β fluorescence intensity over time without or with blebbistatin treatment in n= 8 videos containing 23 cells in total using Fiji-ImageJ software. Scale bar: 10 µm.

*PI3K-C2β enrichment at FAs under conditions of growth factor deprivation (HBSS starvation)*

A recently published study showed that under conditions of growth factor deprivation, PI3K-C2β is recruited at late endosomes/lysosomes and leads to mTORC1 suppression (Marat et al., 2017). An earlier study showed that serum starvation triggers the loss of stress fibres and FAs, while re-addition of serum or growth factors stimulates stress fibre and FA reassembly through RhoA activation (Ridley and Hall, 1992). Therefore, conditions of growth factor deprivation were used as a stimulus for FA disassembly to test whether PI3K-C2β is involved in that process under these conditions. This is connected to the question whether PI3K-C2β functions in absence of serum/growth factors as a major regulator of not only mTORC1 activity and lysosomal positioning, but also other cell biological effects of serum starvation, such as FA disassembly. The idea that late endosomes/lysosomes are implicated in the regulation of cell migration and FAs via delivery of cargoes to the cell surface is getting increasing attention (Paul et al., 2015; Marwaha et al., 2017). It has been reported that LAMTOR2/3 complex-positive late endosomes travel to the cell periphery and regulate FAs dynamics (Schiefermeier et al., 2014). Additionally, it has been reported that active α5β1 integrin is transported to lysosomes in a Rab25-dependent manner and is directed back to the plasma membrane while still in its active conformation by lysosomes (Dozynkiewicz et al., 2012).

Therefore, live HeLa cells expressing both vinculin-mCherry and eGFP-hPI3K-C2β were monitored for 1.5 hours using TIRF microscopy and images were taken every 3 minutes under conditions of growth factor deprivation, in presence of HBSS. Interestingly, preliminary data suggested an accumulation of eGFP-hPI3K-C2β fluorescence at FAs paralleling decreasing vinculin-mCherry fluorescence, in a similar way as when cells were treated with blebbistatin (Figure 3-18). More experiments need to be performed to corfirm this observation though. For the analysis of eGFP-hPI3K-C2β recruitment to FAs, both eGFP-hPI3K-C2β and vinculin-mCherry intensities were quantified over time using the Fiji/ImageJ software as described above (Figure 3-18).

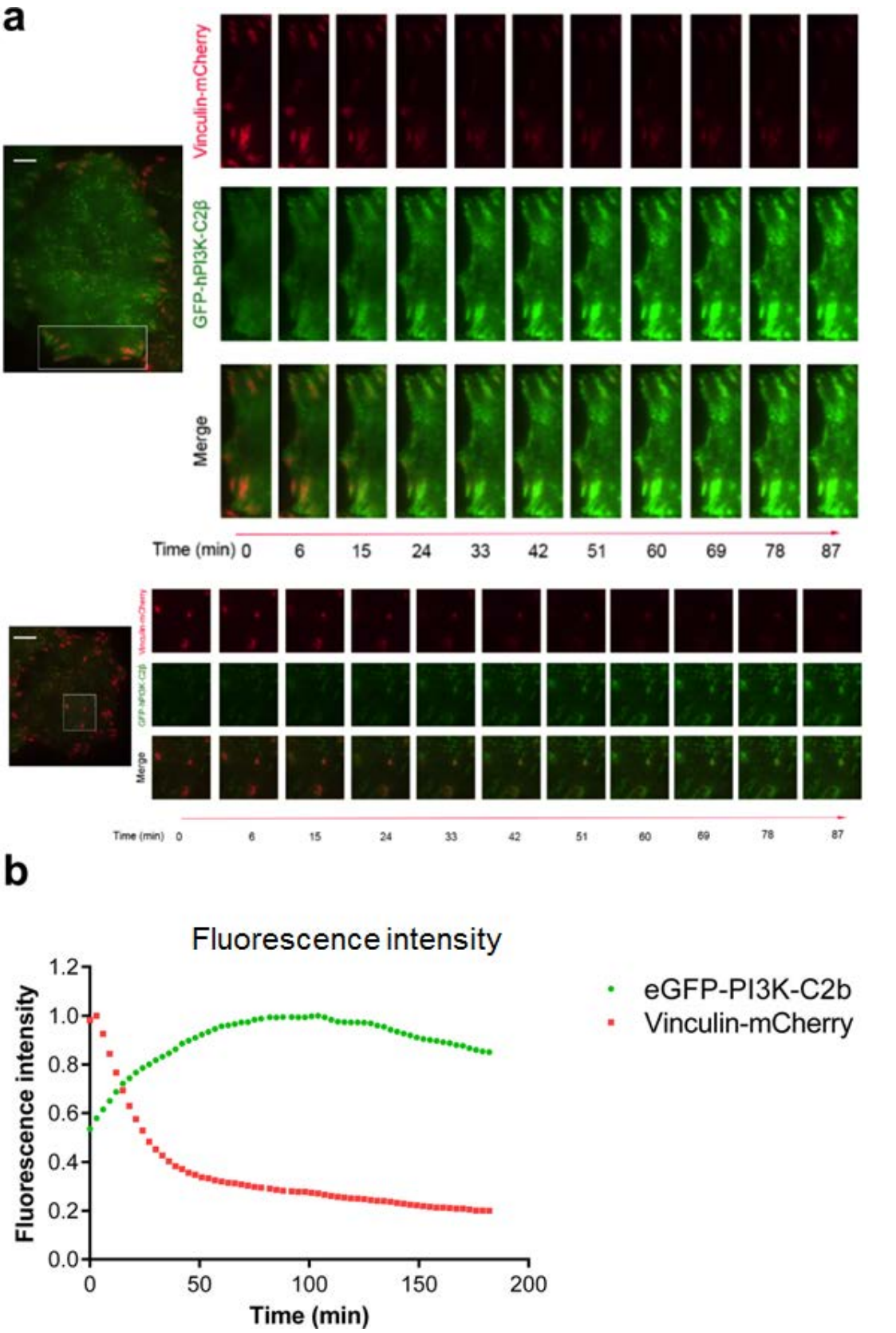


**Figure 3-18: PI3K-C2β accumulates at FAs upon HBSS starvation. a)** TIRF microscopy of HeLa cells expressing both vinculin-mCherry and eGFP-tagged human PI3K-C2β upon HBSS starvation. The full medium was removed, followed by two quick washes with HBSS and the specimen in presence of HBSS was placed immediately under the microscope. The cells were monitored for 1.5 hours and images were taken every 3 minutes. PI3K-C2β fluorescence accumulated when vinculin fluorescence faded as FAs disassembled. **b)** Quantification of vinculin-mCherry and eGFP-PI3K-C2β fluorescence intensity over time in four representative cells using Fiji-ImageJ software. Scale bar: 10 µm.

Subsequently, the experiment was repeated using the HeLa cell line expressing endogenous eGFP-tagged PI3K-C2β which was transiently transfected with vinculin-mCherry and a similar effect was observed, i.e. eGFP-PI3K-C2β accumulated at FAs upon HBSS starvation (Figure 3-19). The vinculin-mCherry signal did not present a significant decrease tough (Figure 3-19). Therefore, more experiments need to be performed in order to reach a safe conclusion.

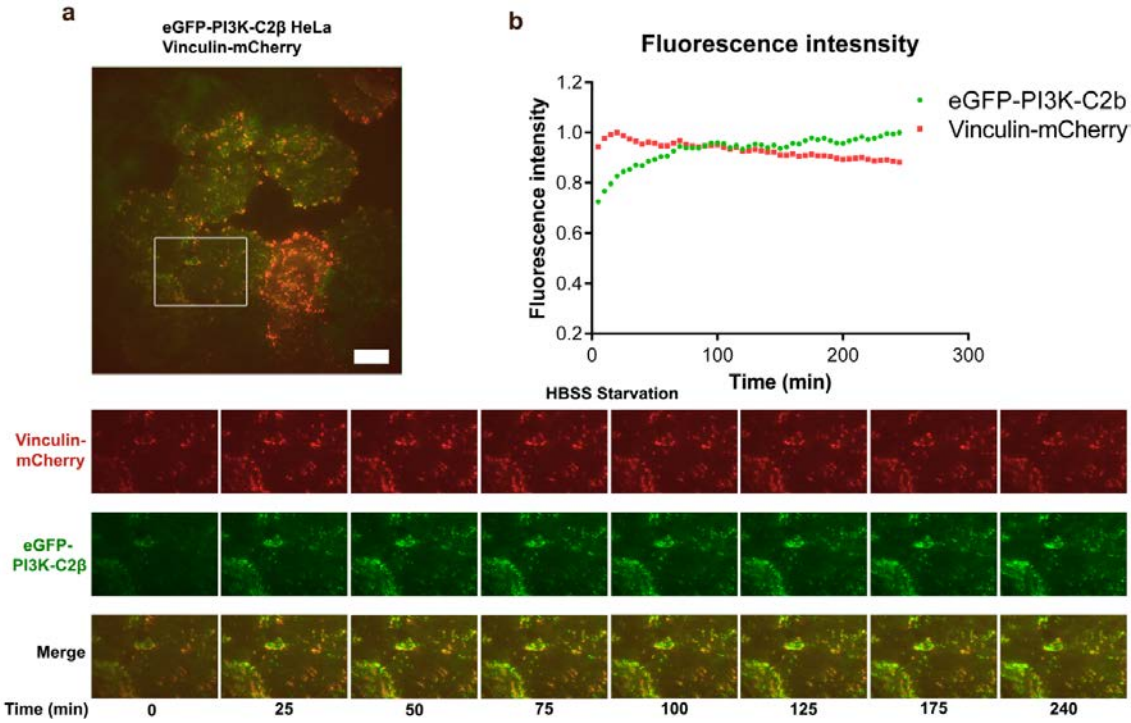


**Figure 3-19: PI3K-C2β accumulates at FAs upon HBSS starvation. a)** TIRF microscopy of HeLa cells expressing endogenous eGFP-tagged PI3K-C2β which were transiently transfected with vinculin-mCherry upon HBSS starvation. The specimen was placed under the microscope, the full medium was removed, followed by two quick washes with HBSS and then HBSS was added immediately. The cells were monitored for 4 hours and images were taken every 5 minutes. PI3K-C2β fluorescence accumulated when vinculin fluorescence faded as FAs disassembled. **b)** Quantification of vinculin- mCherry and eGFP-PI3K-C2β fluorescence intensity over time in four representative cells using Fiji-ImageJ software. Scale bar: 10 μm.

*The FA phenotype upon PI3K-C2β inactivation is more robust under serum-starved conditions*

The abundance of stimuli in presence of serum seemed to weaken the milder cell migration phenotype in PI3K-C2β KI MEFs. Additionally, absence of serum can promote FA disassembly (Ridley and Hall, 1992) and the study presented here also showed that PI3K-C2β accumulated at dismantling FAs under HBSS starvation. Therefore, an interesting question was whether the FA phenotype displayed by PI3K-C2β KI MEFs was even stronger under overnight serum-starved conditions and indeed, this was the case (Figure 3-20). Consistently, prelimary data suggested that HeLa cells depleted of PI3K-C2β also showed a strong FA and stress fibre phenotype under 2 or 4 hours HBSS starvation (Figure 3-21). On the contrary, as expected, control (scrambled

siRNA) cells showed less FAs and stress fibres under HBSS starvation, especially after 4 hours, compared to presence of serum conditions (Figure 3-21) .

Overall, PI3K-C2β-depleted HeLa cells or PI3K-C2β KI MEFs appeared to be resistant to stimuli promoting FA disassembly, further indicating that PI3K-C2β regulates FA dynamics.

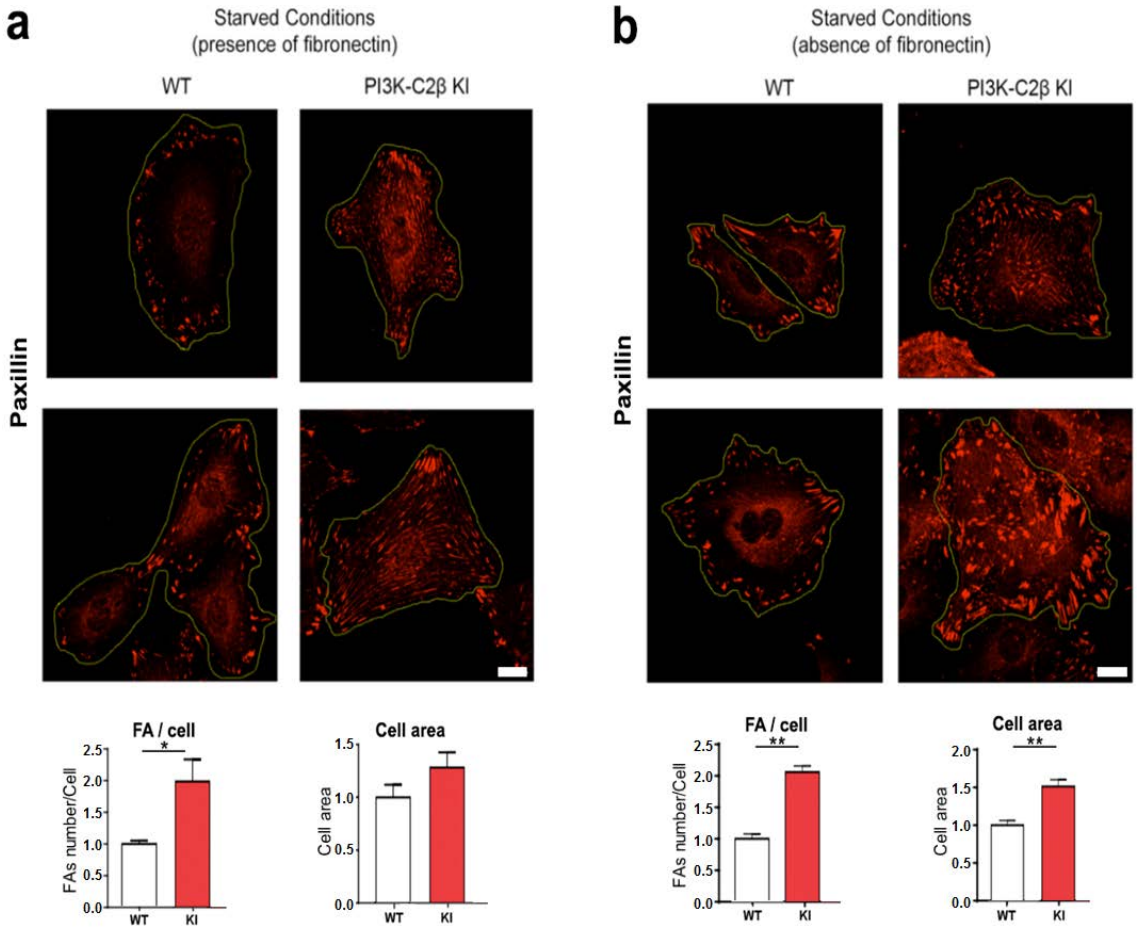


**Figure 3-20: PI3K-C2β KI MEFs display an increased number of FAs and increased cell area under serum starved conditions.** WT and PI3K-C2β KI MEFs were plated onto **a)** fibronectin-coated or **b)** uncoated glass coverslips, cultured in presence of serum, serum-starved overnight, fixed and stained for paxillin. Quantifications were performed using Fiji-ImageJ software, and at least 40 cells per genotype were quantified per experiment. Data are mean values with error bars representing ±SEM from n=3 independent experiments. The MEFs used were derived from 3 WT (14-5, 14-6, 14-7) and 3 PI3K-C2β KI (13-3, 14-8, 14-9) mice. * $p<0.05$, ** $p<0.01$, t-test. Scale bar: 20 μm.

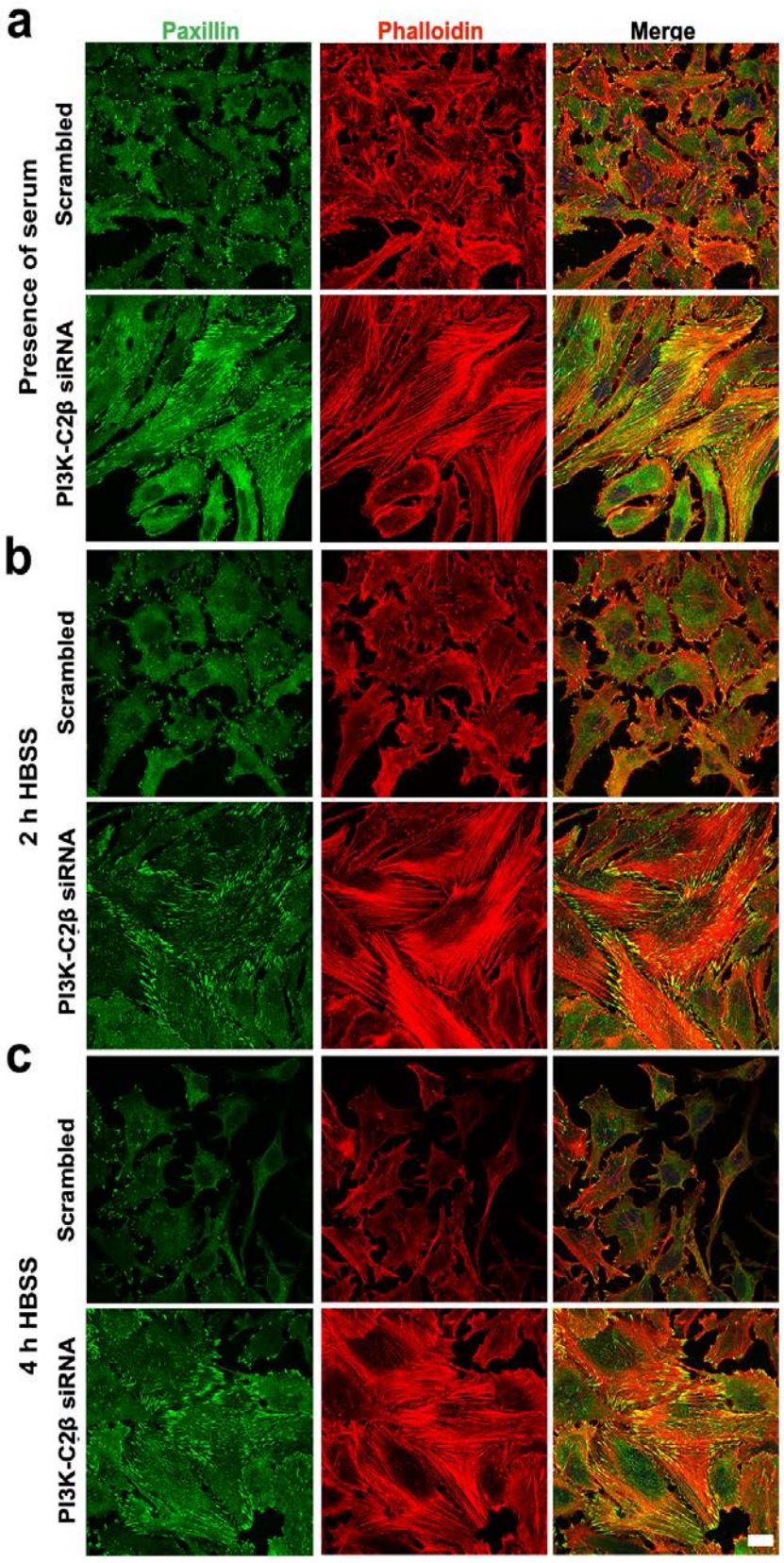


**Figure 3-21: PI3K-C2β-depleted HeLa cells display more FAs and stress fibres not only in presence of serum but also upon HBSS starvation.** Representative confocal images from n=2 independent experiments of control (scrambled siRNA) or PI3K-C2β-depleted HeLa cells using siRNA#1. Cells were plated onto matrigel-coated glass coverslips, cultured in presence of serum, and either **a)** fixed and stained for paxillin or followed by **b)** 2 hours or **c)** 4 hours HBSS starvation and then fixed and stained for paxillin. Scale bar: 20 µm.

### 3.5.3 The lipid product of PI3K-C2β at focal adhesions

It has now been accepted that class II PI3Ks are capable of producing both PI3P and PI(3,4)$P_2$ (Bilanges et al., 2019; Margaria et al., 2019). A question that the study presented here aimed to address was which lipid product is produced by PI3K-C2β to mediate its action at FAs.

The first approach applied was to estimate the PI(3)P levels in WT and PI3K-C2β kinase dead KI MEFs by immunofluorescence using the GST-2×FYVE$^{HRS}$ probe, which binds specifically and with high affinity to PI(3)P (Gillooly et al., 2000). This probe is composed of two FYVE finger domains of the hepatocyte growth factor-regulated tyrosine kinase substrate (Hrs) to achieve higher overall avidity for PI(3)P (Gillooly et al., 2000). Hrs is implicated in vesicular trafficking via endosomes and binds specifically to PI(3)P (Komada and Soriano, 1999). This method allows the visualisation of the localisation of the PI(3)P pools in the cell and this probe is supposed to be quantitative for relative comparisons. PFA-fixed WT and PI3K-C2β kinase dead KI MEFs were incubated with the GST-2×FYVE$^{HRS}$ probe, stained for GST and paxillin, and the PI(3)P intensity was quantified. Preliminary data suggested that PI3K-C2β inactivation led to a mild decrease of around ~ 22% of the PI3P level (Figure 3-22 a, b). Another interesting question was whether PI(3)P can be found at FAs, but no significant co-localisation between PI(3)P and paxillin in WT cells was observed. However, these preliminary data suggested that in some WT cells PI(3)P could be found at FAs in the cell mid region, whereas this was only rarely observed in PI3K-C2β KI MEFs (Figure 3-22). Further investigation needs to be performed in order to address this question and PI(3,4)$P_2$ levels and the potential role of this lipid at FAs should also be assessed.

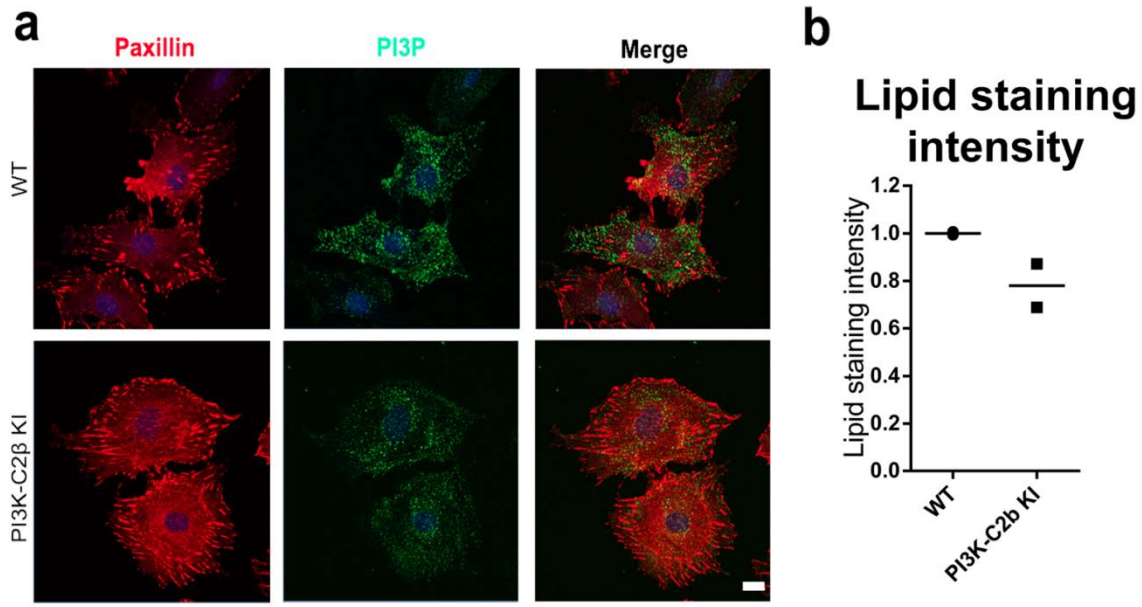


**Figure 3-22: PI3K-C2β KI MEFs display a mild decrease in PI3P levels in presence of serum. a)** WT and PI3K-C2β KI MEFs were cultured in presence of serum, fixed, permeabilised with either digitonin or saponin, incubated with GST-2xFYVE$^{HRS}$ probe and stained with anti-GST and anti-paxillin antibody. **b)** Quantifications were performed using Fiji-ImageJ software and at least 40 cells per genotype were quantified per experiment. Data represent mean from n=2 independent experiments. The MEFs used were derived from 3 WT (14-5, 14-6, 14-7) and PI3K-C2β KI (13-3, 14-8, 14-9) mice. Scale bar: 10 µm.

Another approach used to assess the lipid product of PI3K-C2β in the FA context was to deplete different PI species at the plasma membrane to test for a potential phenocopy of PI3K-C2β inactivation. To this end, the PI(3,4)$P_2$-specific 4-phosphatase INPP4B, the PI(3)P-specific phosphatase MTM1, or the catalytic domain of the PI(4,5)$P_2$-specific 5'-phosphatase INPP5E were expressed in MEFs. All three phosphatases are modified with a carboxy-terminal prenylation sequence derived from K-Ras (CAAX box) to anchor them to the plasma membrane [kindly provided by Dr. York Posor (Posor et al., 2013)]. Preliminary data suggested that cells expressing either mCherry-INPP4B-CAAX or mCherry-MTM1-CAAX had a tendency to show more FAs, mainly found in the cell mid-region, compared to untransfected cells, quantification needs to be done to confirm this preliminary observation though (Figure 3-23). This may suggest that the depletion of either PI(3)P or PI(3,4)$P_2$ perturbs FA dynamics. Therefore it was not possible to link only one of these lipids with the action of PI3K-C2β at FAs. Of note, depletion of PI(4,5)$P_2$ by the 5'-phosphatase mCherry-INPP5E-CAAX did not result in the same effect as the expression of mCherry-INPP4B-CAAX or mCherry-MTM1-CAAX. Cells undergoing PI(4,5)$P_2$ depletion were characterised by the complete absence of FAs in the cell mid-region and displayed only peripheral FAs (Figure 3-23). PI(4,5)$P_2$ is mainly found at the plasma membrane and is implicated in FA formation. It is involved in activation of several FA components including talin, vinculin and FAK but also in FA disassembly by promoting the activation of m-calpain (Atherton et al., 2016; Manakan Betsy Srichai, 2010; Klapholz and Brown,

2017; Gough and Goult, 2018; Wang et al., 2018a; Cai et al., 2008; Durand et al., 2016; Leloup et al., 2010). Nonetheless, for a conclusive analysis, the number of FAs would need to be quantified. Overall, more work needs to be performed to determine which PI3K-C2β lipid product is implicated in its action at FAs.

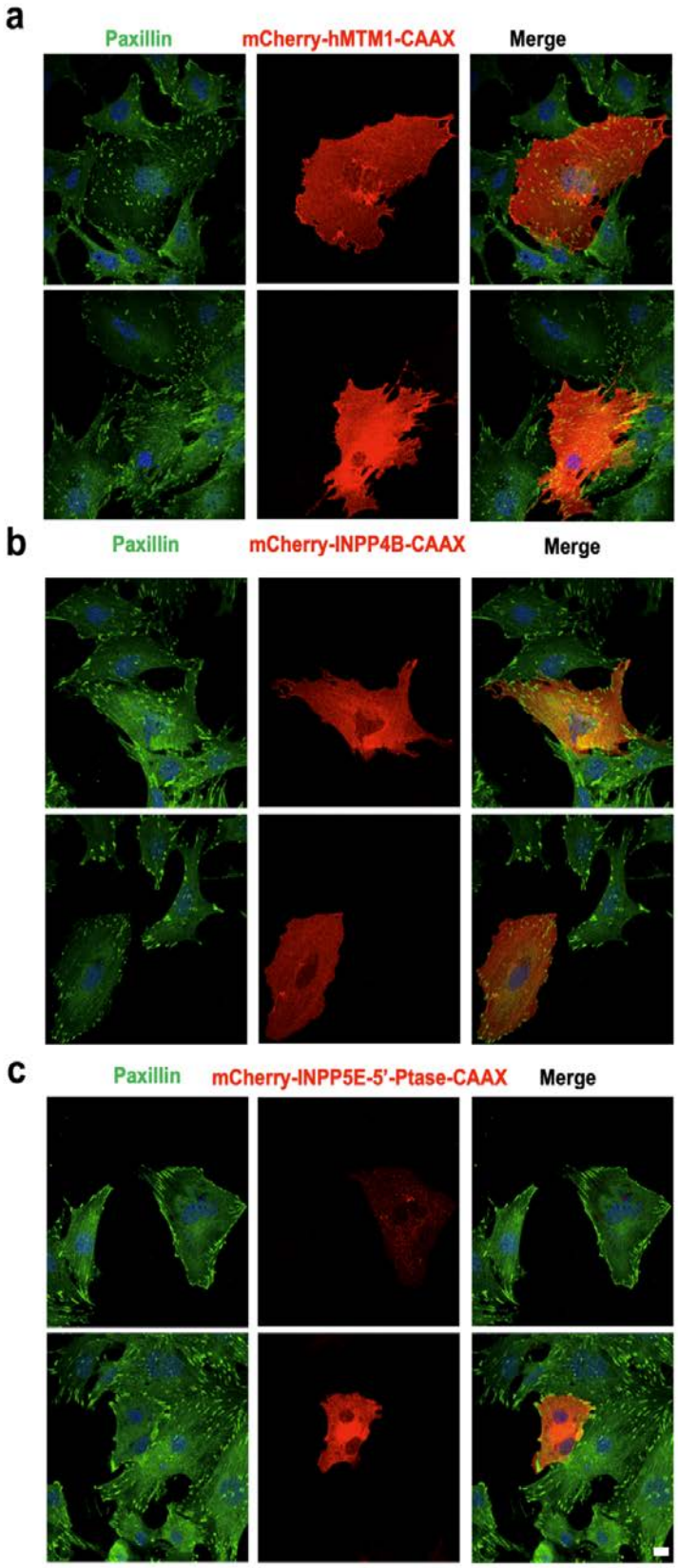


**Figure 3-23: MEFs undergoing depletion of PI(3)P or PI(3,4)$P_2$, but not PI(4,5)$P_2$, show a tendency to display more FAs.** Cells were transiently transfected with phosphatase-encoding constructs. Representative confocal images of FAs which were visualised by IF staining for paxillin from n=2 independent experiments in MEFs expressing **a)** mCherry-hMTM1-CAAX (PI(3)P depletion), or **b)** mCherry-INPP4B-CAAX (PI(3,4)$P_2$ depletion) or **c)**mCherry-INPP5E-CAAX (PI(4,5)$P_2$ depletion). Scale bar: 10 µm.

### 3.5.4 Clathrin structures at focal adhesions are not affected upon depletion of PI3K-C2β

As discussed above, clathrin-mediated endocytosis (CME) has been reported to play a crucial role in FA disassembly by promoting β1 integrin internalisation (Ezratty et al., 2009; Chao et al., 2010; Chao and Kunz, 2009; Maritzen et al., 2015). Moreover, using TIRF microscopy, clathrin localisation at large FAs in the cell mid-region during cell migration -when FAs disassemble- has been reported (Ezratty et al., 2009). Additionally, the N-terminal region of PI3K-C2β has been reported to be able to interact with clathrin (Wheeler and Domin, 2006) and intersectin (Das et al., 2007), whose role in CME is well-established (Hunter et al., 2013; Nakatsu et al., 2010; McMahon and Boucrot, 2011). PI3K-C2β and clathrin co-localisation at endocytic clathrin-coated pits has also been reported (Nakatsu et al., 2010). However, to date no role for this PI3K isoform in endocytosis has been identified. Furthermore, a local $PI(3,4)P_2$ pool produced by PI3K-C2α has been shown to be required for the maturation of clathrin-coated pits during the late stages of CME (Posor et al., 2013).

Based on the results presented above, PI3K-C2β seems to be involved in the process of FA disassembly. Therefore, whether PI3K-C2β plays a similar role to PI3K-C2α in CME specifically during FA disassembly was also tested. Control (scrambled siRNA) or PI3K-C2β-depleted HeLa cells were stained for clathrin heavy chain (CHC) and paxillin. However, no significant difference in the pattern of clathrin-coated structures or a reduced or increased co-localisation between clathrin and FAs in HeLa cells depleted of PI3K-C2β was observed (Figure 3-24). Thus, based on these very preliminary data, PI3K-C2β seems not to be implicated in the regulation of FA disassembly through CME. I therefore decided not to further investigate this hypothesis.

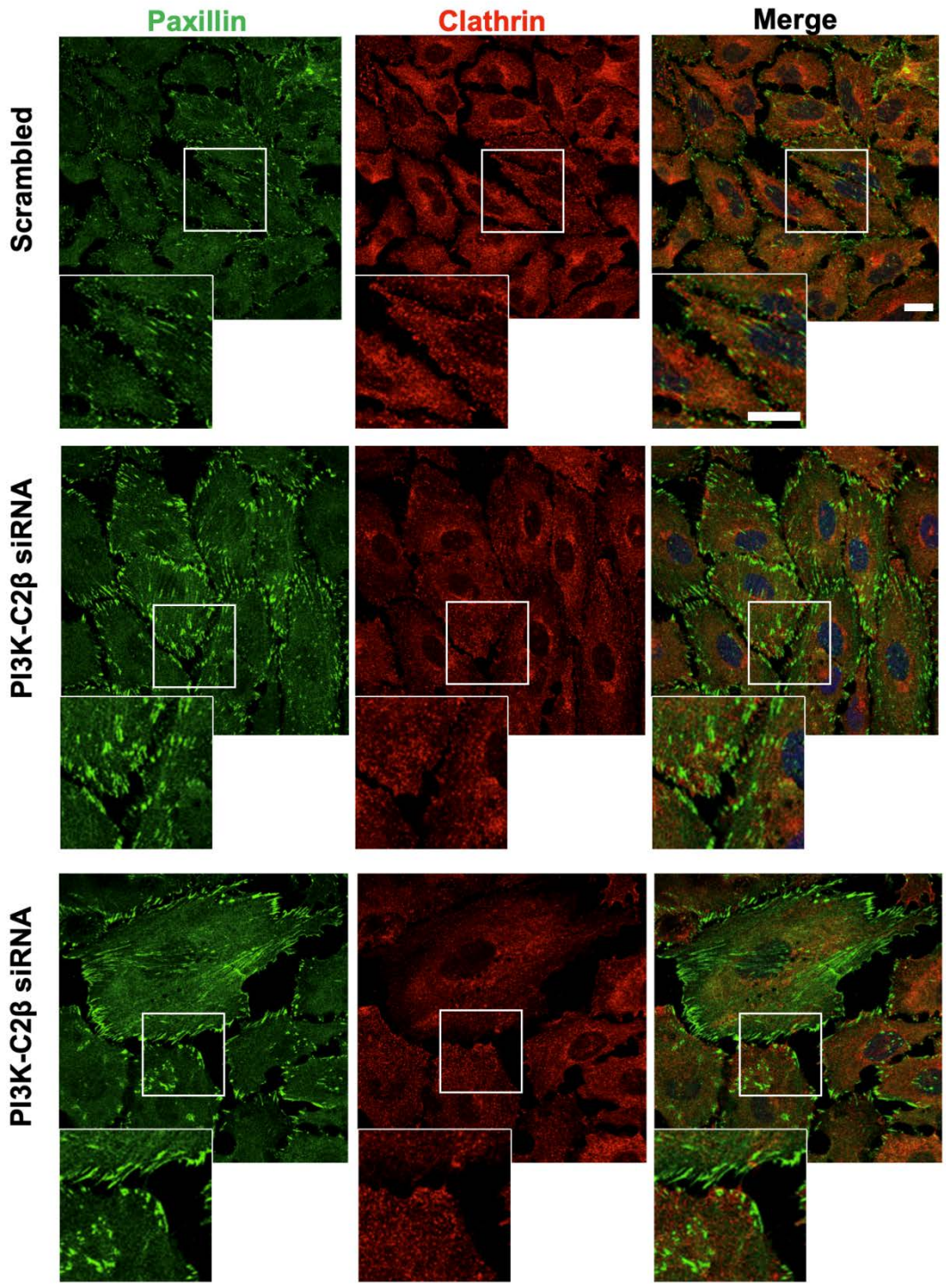


**Figure 3-24: PI3K-C2β-depleted HeLa cells do not display a different pattern of clathrin structures at FAs**. Representative confocal images of n=2 independent experiments of control (scrambled siRNA) and PI3K-C2β-depleted HeLa cells by siRNA#2 stained for clathrin heavy chain (CHC). Scale bar: 50 µm.

## 3.6 PI3K-C2β interacts with DEPDC1B, a focal adhesion disassembly factor

The host laboratory was interested in identifying potential interaction partners of PI3K-C2β and for this purpose a yeast-two-hybrid screen using amino acids 1 – 615 of PI3K-C2β as the bait fragment was performed. The yeast-two-hybrid screen was performed by the Hybrigenics Services. In this screen, DEPDC1B (amino acids 114-260) was identified as a potential interaction partner of PI3K-C2β (Figure 3-25).

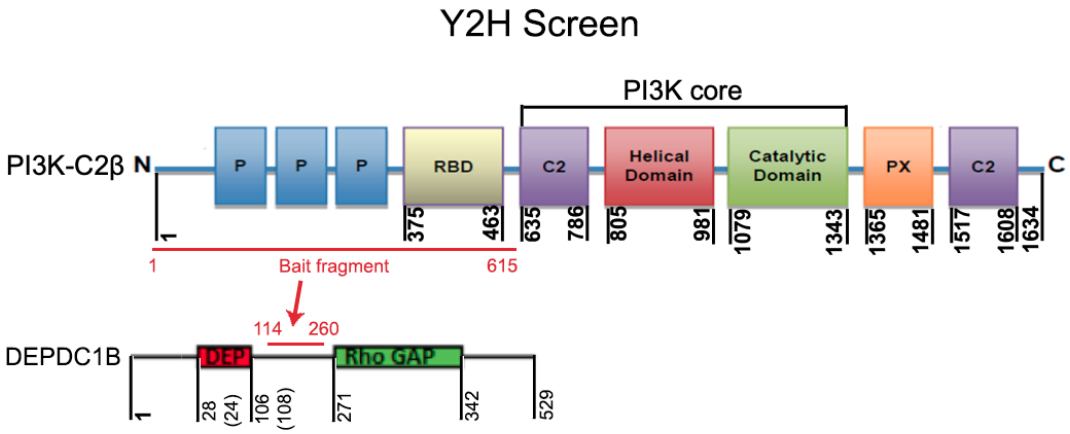


**Figure 3-25: A yeast two hybrid (Y2H) screening was employed to search for potential PI3K-C2β interactors and DEPDC1B was identified as one of them.** The yeast-two-hybrid screen used the amino acids 1 – 615 of PI3K-C2β as the bait fragment and DEPDC1B (amino acids 114-260) was identified as a potential interaction partner of PI3K-C2β. The yeast-two-hybrid screen was performed by the Hybrigenics Services.

This was of particular interest since DEPDC1B has been linked to FA disassembly. DEPDC1B was reported to accumulate during G2 phase and play a key role in FA disassembly, which is necessary for the morphological changes prior to mitotic entry (Marchesi et al., 2014; Garcia-Mata, 2014). More specifically, during G2 phase DEPDC1B accumulates and binds to the transmembrane protein tyrosine phosphatase, receptor type, F (PTPRF) which is found at FAs, resulting in RhoA displacement from this receptor and in turn adhesion disassembly and cell rounding. Mitotic entry is followed by DEPDC1B degradation (Figure 3-26) (Marchesi et al., 2014; Garcia-Mata, 2014). Cells depleted of DEPDC1B displayed larger FAs, increased actin stress fibres, elevated RhoA activity and phosphorylation levels of myosin light chain 2 (MLC2-Ser19) and delayed FA disassembly (Marchesi et al., 2014).

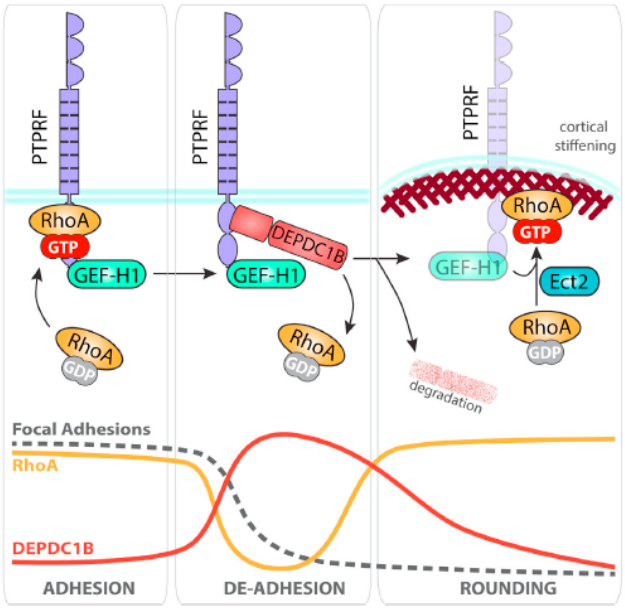


**Figure 3-26: Proposed model of DEPDC1B-mediated regulation of FA disassembly prior to mitotic entry.** RhoA, in its active GTP-bound state, is necessary for FA and stress fibre formation. GEF-H1 which is anchored at FAs by the transmembrane protein tyrosine phosphatase, receptor type, F (PTPRF) which is found at FAs, is involved in RhoA activation. During G2 phase, DEPDC1B accumulation occurs, leading to RhoA displacement from this receptor and in turn adhesion disassembly and cell rounding. RhoA activation in turn is mediated by Ect2, which is a RhoGEF, and induces actin filaments polymerisation which in turn mediates the mitotic spindle and cleavage furrow positioning. Mitotic entry is then followed by DEPDC1B proteasome-mediated degradation.
Ect2: epithelial cell transforming 2, GEF: guanine nucleotide exchange factor. [Adapted from (Garcia-Mata, 2014), Copyright obtained by Elsevier (Developmental Cell) and also by Professor Rafael Garcia Mata).

DEPDC1B consists of two conserved domains; a Dishevelled, EGL-10 and pleckstrin (DEP) domain whose predominant role is plasma membrane targeting (Consonni et al., 2014; Liao et al., 2016) and a RhoGAP domain (Bai et al., 2017; Marchesi et al., 2014; Wu et al., 2015a; Su et al., 2014). The published data regarding the activity of the GAP domain of DEPDC1B are contradictory. The absence of the critical arginine residue necessary for GAP activity indicates that DEPDC1B may not be an active GAP (Marchesi et al., 2014). Indeed, this study showed that the DEPDC1B GAP domain does not display any GAP activity towards RhoA (Marchesi et al., 2014). However, another study using an overexpression approach demonstrated that DEPDC1B supresses Rac1 activation and can associate with both GTP- and GDP-bound states of Rac1 (Wu et al., 2015a). Additionally, earlier studies reported that GAPs missing the critical arginine residue can still display GAP activity, suggesting that alternative mechanisms may occur in this circumstance (Seewald et al., 2002; Brinkmann et al., 2002; Faucherre et al., 2003; Scrima et al., 2008; Bos et al., 2007) and also that the arginine residue is not necessary for the association between Cdc42 and Cdc42-GAP (Leonard et al., 1998). Another study reported more conflicting data, suggesting that DEPDC1B associates with Rac1 to promote its activation (Su et al., 2014).

### 3.6.1 PI3K-C2β forms a complex with DEPDC1B and talin

*PI3K-C2β interacts with DEPDC1B*

Based on the published data regarding the biological function of DEPDC1B, a hypothesis tested by this study was that DEPDC1B may form a link between PI3K-C2β and FAs and the verification of the potential interaction between them by immunoprecipitation assays was aimed. For this purpose, 6x-Myc-PI3K-C2β and eGFP-DEPDC1B expressing HEK293T cells were first used. Lysates were incubated with antibodies to a) DEPDC1B or b) Myc and associated proteins were immunoprecipitated. This confirmed the interaction between PI3K-C2β and DEPDC1B from both sides (Figure 3-27a,b).

The verification of this interaction by endogenous co-IP was then attempted in order to avoid possible artefacts derived from overexpression approaches. For this purpose, endogenous eGFP-tagged PI3K-C2β expressing HEK293T cells were subjected to GFP nanobody immunoprecipitation (IP aGFP) and analysed by immunoblotting against DEPDC1B. This further confirmed formation of a complex between these two proteins (Figure 3-27c). Taken together, these results validated the interaction between PI3K-C2β and DEPDC1B.

*PI3K-C2β associates with talin*

Additionally, in order to investigate further the role of PI3K-C2β at FAs, this study aimed to investigate whether this PI3K isoform also interacts with other FA components. Interestingly, immunoprecipitation of endogenous GFP-tagged PI3K-C2β resulted in co-immunoprecipitation of talin, indicating that PI3K-C2β associates also with talin (Figure 3-27d).

Actin filament-associated talin, a large (~270 kDa) cytoplasmic adaptor protein, is a key component of integrin-dependent cell-matrix adhesion structures with a crucial role in integrin activation (Legate et al., 2009; Parsons et al., 2010; Zaidel-Bar et al., 2004; Klapholz and Brown, 2017; Goult et al., 2018; Atherton et al., 2016; Case et al., 2015). It is part of the central core of adhesion structures by mediating the integrin-actin cytoskeleton linkage via its association with integrin cytoplasmic tails (Legate et al., 2009; Parsons et al., 2010; Zaidel-Bar et al., 2004; Klapholz and Brown, 2017; Goult et al., 2018; Atherton et al., 2016; Case et al., 2015). It also possesses binding sites for recruiting more proteins, like vinculin, an adaptor protein which binds to actin and strengthens the integrin-actin cytoskeleton link, thereby promoting FA stability, growth and maturation (Legate et al., 2009; Parsons et al., 2010; Zaidel-Bar et al.,

2004; Klapholz and Brown, 2017; Goult et al., 2018; Atherton et al., 2016; Case et al., 2015). Therefore, a potential association between PI3K-C2β and talin also indicates that PI3K-C2β can be found at FAs and provides an another possible link between PI3K-C2β and FAs that needs to be investigated further in order to uncover the molecular mechanism of this PI3K isoform at FAs.

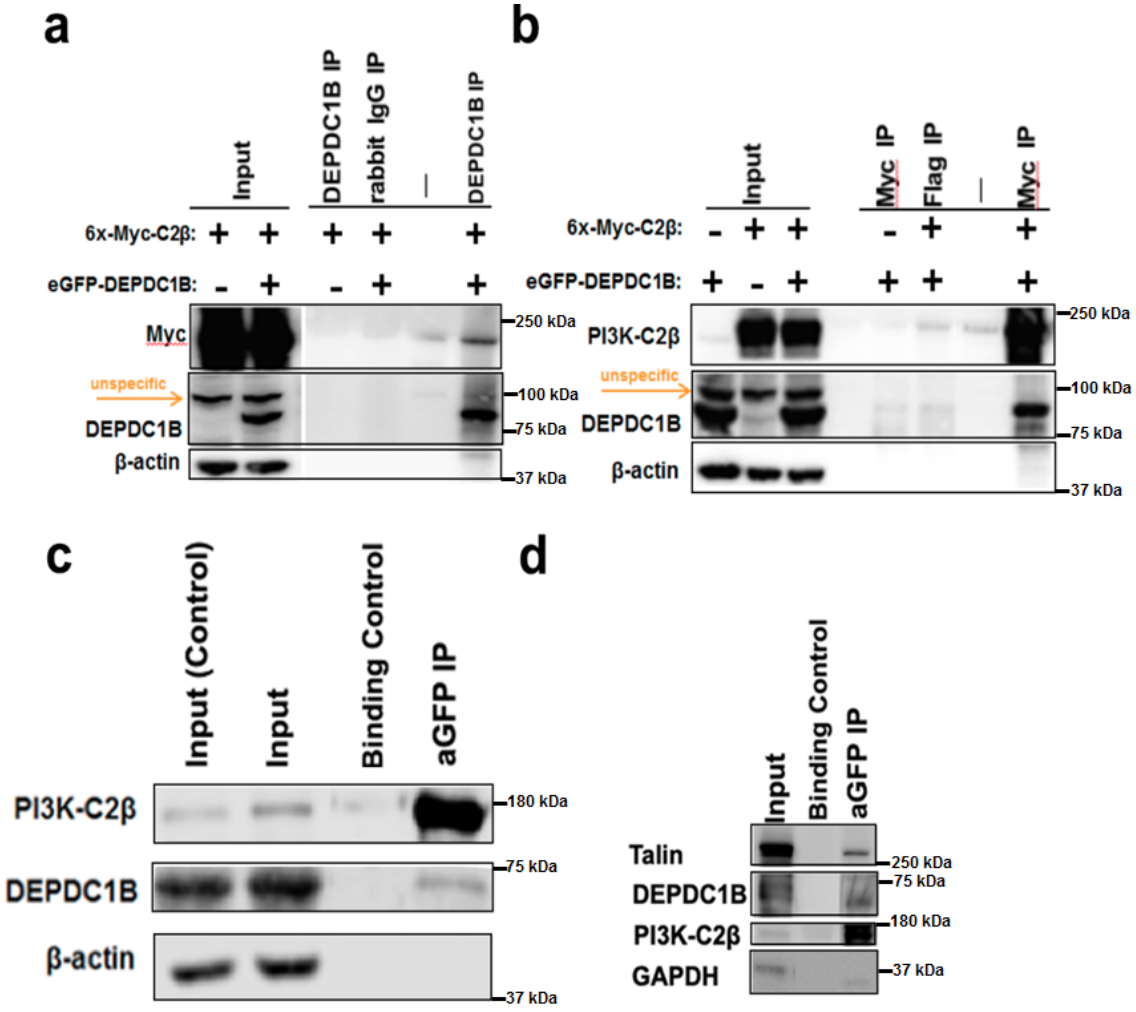


**Figure 3-27: PI3K-C2β associates with DEPDC1B and talin. a, b)** Co-immunoprecipitation assays were performed to detect the interaction of PI3K-C2β with DEPDC1B. 6x-Myc-PI3K-C2β and eGFP-DEPDC1B expressing HEK293T cell lysates were immunoprecipitated using antibodies to **a)** DEPDC1B, or **b)** Myc. **c)** Lysates from HEK293T cells expressing endogenous eGFP-tagged PI3K-C2β were subjected to GFP nanobody immunoprecipitation (IP aGFP) and analysed by immunoblotting to DEPDC1B. **d)** Lysates from HEK293T cells expressing endogenous eGFP-tagged PI3KC2β were subjected to aGFP IP and analysed by immunoblotting to talin or DEPDC1B. Blots shown are representative of n=3 independent experiments.

*First attempts to map the interaction between PI3K-C2β and DEPDC1B*

Additionally, further mapping of the the interaction between PI3K-C2β and DEPDC1B was also attempted. The data acquired from the yeast-two-hybrid screen strongly suggested that the interaction between these two proteins is mediated by the first 615 amino acids of PI3K-C2β. For this purpose, HA-tagged full length PI3K-C2β and HA-tagged truncated constructs of PI3K-C2β; HA-PI3K-C2β 456-1609 and HA-PI3K-C2β 321-1609 (these constructs were kindly provided by Prof. Haucke, Berlin) were used. HEK293T cells expressing eGFP-DEPDC1B and either of the HA-PI3K-

C2β full length or truncated constructs were subjected to GFP nanobody immunoprecipitation (IP aGFP) and analysed by immunoblotting against HA (Figure 3-28). Removal of neither the first 320 nor the first 455 amino acids of PI3K-C2β perturbed the interaction with DEPDC1B (Figure 3-28). Considering that the yeast two hybrid bait fragment encompassed amino acids 1 – 615 of PI3K-C2β, it appears likely that amino acids 456-615 of PI3K-C2β interact with DEPDC1B. Thus, the generation and test of the binding of HA-PI3K-C2β residues 456-615 to DEPDC1B, as well as other HA-tagged truncated PI3K-C2β constructs not including this region is required. This should allow the region of PI3K-C2β which interacts with DEPDC1B to be precisely identifying.

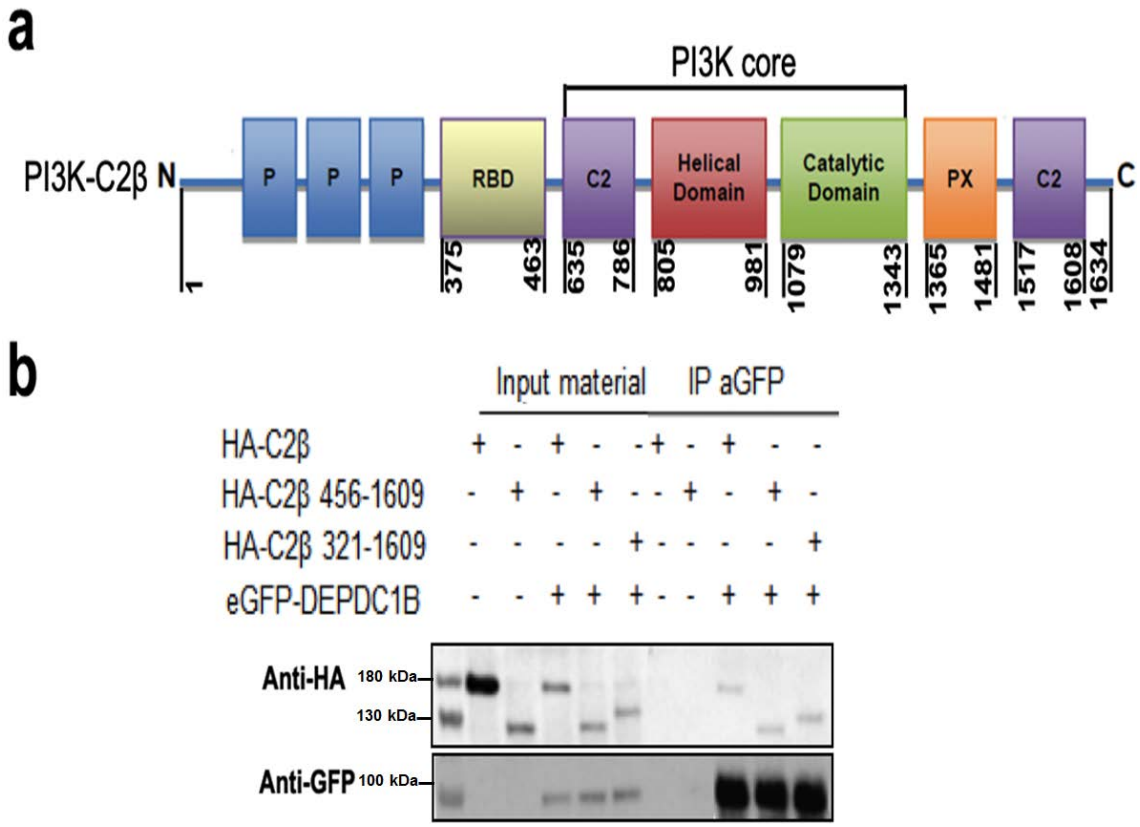


**Figure 3-28: Mapping of the interaction between PI3K-C2β and DEPDC1B**. **a)** Schematic representation of the domain structure of human PI3K-C2β. **b)** HEK293T cell lysates expressing eGFP-DEPDC1B and HA-PI3K-C2β full length or HA-PI3K-C2β 456-1609 or HA-PI3K-C2β 321-1609 constructs were subjected to GFP nanobody immunoprecipitation (IP aGFP) and analysed by immunoblotting against HA. Blot shown is representative of n=2 independent experiments.

*Indications that the PI3K-C2β-DEPDC1B interaction is enhanced during FA disassembly*

Subsequently, it was tested whether the association between PI3K-C2β and DEPDC1B or talin was enhanced during the process of FA disassembly. For this purpose, HEK293T cells expressing endogenous eGFP-tagged PI3K-C2β were treated with 100 µM blebbistatin for 10 minutes, 30 minutes and 1 hour in order to induce the dismantling of FAs. Then, endogenous eGFP-tagged PI3K-C2β expressing HEK293T cells were subjected to GFP nanobody immunoprecipitation (IP aGFP) and analysed

by immunoblotting against DEPDC1B or talin (Figure 3-29). Interestingly, preliminary data suggested that the interaction between PI3K-C2β and DEPDC1B was enhanced after 10 and 30 minutes of blebbistatin treatment, further indicating that this protein interaction is implicated in the process of FA disassembly (Figure 3-29). However, this was not applicable for the PI3K-C2β-talin association, since it seemed that this association was not affected by the blebbistatin treatment (Figure 3-29). However, the experiment needs to be repeated in order to confirm this observation.

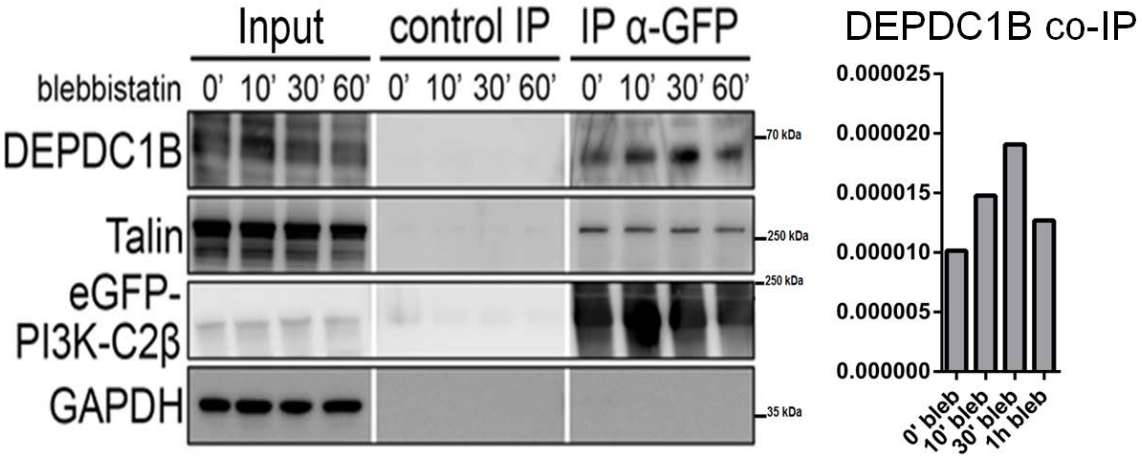


**Figure 3-29: Triggering FA disassembly tends to enhance the DEPDC1B-PI3K-C2β interaction**. Endogenous eGFP-tagged PI3K-C2β expressing HEK293T cell lysates treated with 100 µM blebbistatin for 10 minutes, 30 minutes and 1 hour were subjected to GFP nanobody immunoprecipitation (IP aGFP) and analysed by immunoblotting against DEPDC1B or talin. Blots shown are from a single membrane but intermittent lanes were spliced out. Data represent the quantification from this experiment. In order to quantify the amount of DEPDC1B that is co-immunoprecipited with eGFP-PI3K-C2β in the different time points of blebbistatin treatment, each DEPDC1B IP signal was normalised to both input material and eGFP-PI3K-C2β IP.

## 3.6.2 Depletion of DEPDC1B phenocopies loss of PI3K-C2β

*PI3K-C2β expression levels modulate DEPDC1B expression levels*

When routinely analysing protein levels in my overexpression and knockdown experiments, I noticed that eGFP-DEPDC1B expressing HeLa cells displayed increased PI3K-C2β levels. Interestingly, preliminary data suggested that HeLa cells depleted of PI3K-C2β were characterised by elevated DEPDC1B expression levels (Figure 3-30). These observations further confirm a functional interaction between these two proteins. In addition to interacting in a complex, one interaction partner modulates the expression and stability of the other. Furthermore, these observations may indicate that when FA disassembly is impaired as a consequence of PI3K-C2β depletion, other factors mediating this process may get upregulated, possibly explaining the elevated expression levels of DEPDC1B upon PI3K-C2β depletion. However, these experiments needs to be repeated in order these preliminary observations to be confirmed.

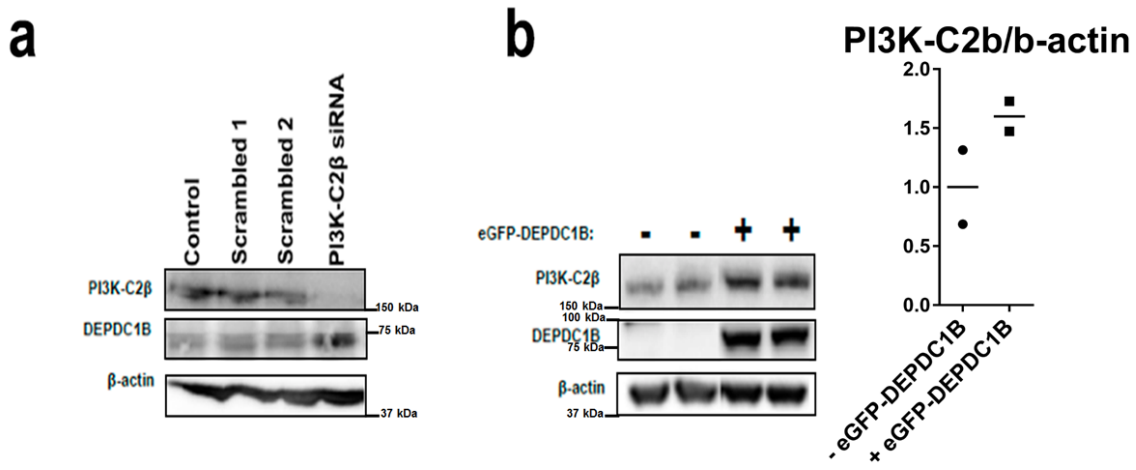


**Figure 3-30: PI3K-C2β expression levels tend to modulate DEPDC1B expression levels. a)** PI3K-C2β-depleted HeLa cells by siRNA#1 were characterised by increased DEPDC1B expression levels. The blot shown was derived from 1 experiment. **b)** eGFP-DEPDC1B expressing HeLa cells displayed increased PI3K-C2β levels. Blot shown is representative of n=2 independent experiments. Data represent mean from n=2 independent experiments.

*DEPDC1B depletion leads to more FAs and stress fibres*

The next question that was addressed was whether DEPDC1B operates in the same functional context as PI3K-C2β and was investigated whether HeLa cells depleted of DEPDC1B are also characterised by an increased number of FAs. The verification of the efficiency of siRNA-mediated DEPDC1B knockdown has been challenging, since it was difficult to find an antibody for specific detection of endogenous levels of DEPDC1B. As an alternative approach, overexpression of eGFP-DEPDC1B in parallel with siRNA-mediated DEPDC1B knockdown was employed and the expression levels of eGFP-DEPDC1B in control (scrambled siRNA) and in DEPDC1B-depleted cells were assessed (Figure 3-31a). Expression of eGFP-DEPDC1B was higher in control (mock, scrambled siRNA) compared to DEPDC1B-depleted cells (Figure 3-31a), indicating that the siRNA-mediated DEPDC1B knockdown was efficient.

Therefore, FAs were then visualised by immunofluorescence staining for paxillin in control (scrambled siRNA) and DEPDC1B-depleted HeLa cells. Preliminary data from two independent experiments suggested that DEPDC1B-depleted HeLa cells showed more FAs and an increased cell area, thus phenocopying PI3K-C2β-depleted HeLa cells (Figure 3-31b,c). Furthermore, these preliminary data also suggested that DEPDC1B-depleted HeLa cells displayed enlarged actin stress fibres, (Figure 3-31b) in agreement with a previous study (Marchesi et al., 2014) and similarly to PI3K-C2β-depleted HeLa cells, further indicating that DEPDC1B depletion phenocopies PI3K-C2β depletion. Thus, these observations indicate a possible functional interplay between PI3K-C2β and DEPDC1B in the process of FA disassembly. However, the experiment needs to be repeated in order to confirm these observations.

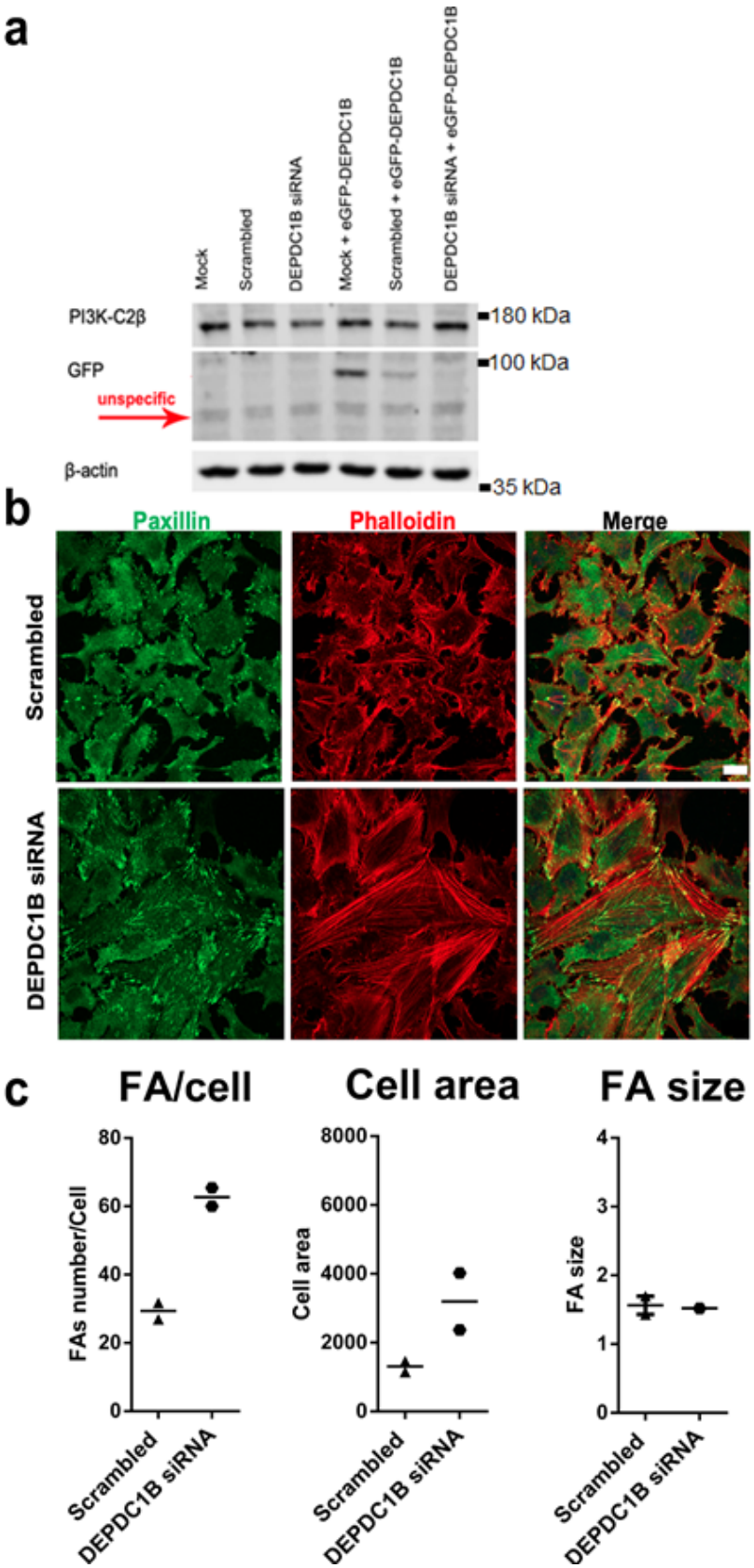


**Figure 3-31: DEPDC1B-depleted HeLa cells display more FAs and stress fibres and an increased cell area.** FAs were visualised by IF staining for paxillin in presence of serum in control (scrambled siRNA) or DEPDC1B-depleted HeLa cells by siRNA. **a)** Representative immunoblot of DEPDC1B depleted HeLa cells of n=2 independent experiments. **b)** Control (scrambled siRNA) or DEPDC1B-depleted by siRNA HeLa cells were plated onto matrigel- coated glass coverslips, cultured in presence of serum, fixed and stained for paxillin. **c)** Quantifications were performed using Fiji-ImageJ software and at least 60 cells per condition were quanitfied per experiment. Data represent mean from n=2 independent experiments. Scale bar: 20 µm.

*eGFP-DEPDC1B or eGFP-PI3K-C2β expression leads to cell rounding*

DEPDC1B has been reported to accumulate during G2 phase and to trigger FA disassembly and cell rounding (Marchesi et al., 2014). Therefore, this study aimed to reproduce induction of cell rounding by DEPDC1B overexpression and to test whether eGFP-PI3K-C2β expression in HeLa cells leads to the same phenotype. To this end, eGFP-, eGFP-DEPDC1B- or eGFP-PI3K-C2β-expressing HeLa cells were monitored for 12 hours after transfection using Nikon Biostation CT. Of note, with the Biostation only high expression levels are being picked up, while in the rest of the experiments we have been focused on low-level expressing cells.

Strikingly, both eGFP-DEPDC1B and eGFP-PI3K-C2β expression in HeLa cells resulted in cell rounding rapidly after transfection (10-12 hours post-transfection), while eGFP-expression did not have the same effect (Figure 3-32a). These data suggested that both DEPDC1B and PI3K-C2β regulate cell adhesion, and strengthened the notion of these two proteins operating in the same pathway.

Additionally, in order to exclude the possibility that eGFP-PI3K-C2β expression results in increased cell death and in turn in increased cell rounding, levels of cell death upon eGFP- or eGFP-PI3K-C2β overexpression were assessed. For this purpose, control (eGFP-expressing) or eGFP-PI3K-C2β-expressing HeLa cells were stained with propidium iodide (PI), a membrane-impermeable dye that is used to assess cell viability by flow cytometry. Expression of eGFP-PI3K-C2β did not cause any increase in the percentage of dead cells as compared to eGFP (Figure 3-32b) (data kindly provided by Dr. York Posor). Therefore, cell rounding in eGFP-PI3K-C2β expressing HeLa cells is not a consequence of cell death.

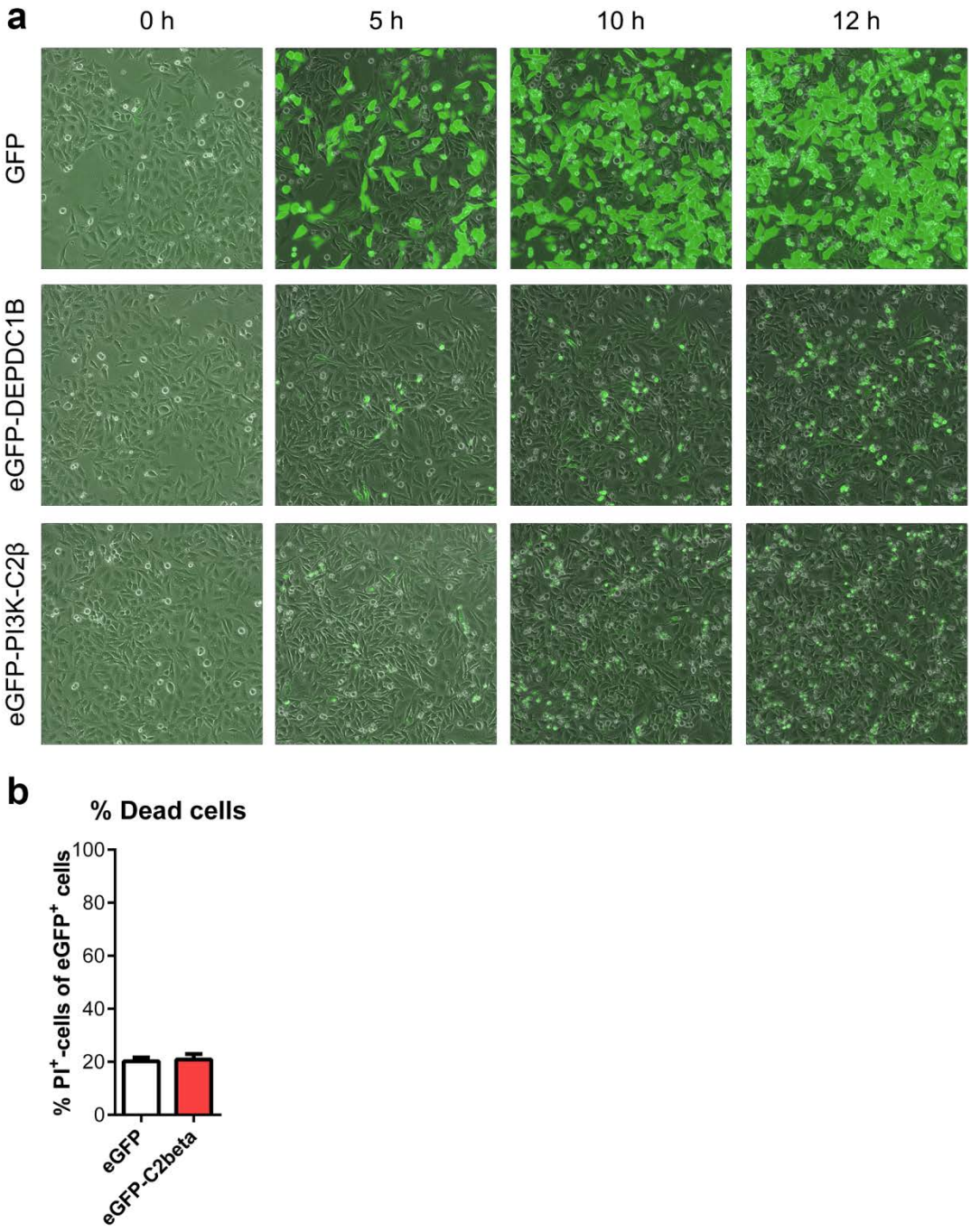


**Figure 3-32: Expression of either eGFP-DEPDC1B or eGFP-PI3K-C2β leads to rounded cell morphology**. **a)** eGFP-, eGFP-DEPDC1B- or eGFP-PI3K-C2β-expressing HeLa cells were monitored for 12 hours using Nikon Biostation CT. Images shown are representative of n=3 independent experiments. **b)** Assessment of cell death of eGFP- or eGFP-PI3K-C2β-expressing HeLa cells 48 hours post-transfection by flow cytometry. Data represent mean ±SEM from n=6 independent experiments (data kindly provided by Dr. York Posor).

### 3.6.3 Recruitment of PI3K-C2β to focal adhesions by DEPDC1B

DEPDC1B has been suggested to dynamically accumulate at disassembling FAs (Marchesi et al., 2014), similar to what I observed for PI3K-C2β. This raised the question whether DEPDC1B is directly responsible for recruiting PI3K-C2β to FAs, which was tested using two different approaches.

*TIRF imaging of PI3K-C2β recruitment to FAs in DEPDC1B-depleted HeLa cells*

First, TIRF imaging of DEPDC1B-depleted live HeLa cells expressing endogenous eGFP-tagged PI3K-C2β was performed. Cells were transiently transfected with vinculin-mCherry, and imaged using TIRF microscopy for 30 minutes without being treated with blebbistatin and then for 2.5 hours being treated with 50 μM blebbistatin with images being taken every 5 minutes to monitor the process of FA disassembly. The hypothesis tested was that if DEPDC1B is required for PI3K-C2β recruitment to FAs, then the accumulation of PI3K-C2β would be prevented by DEPDC1B depletion.

Strong recruitment of PI3K-C2β to FAs was observed in control (scrambled siRNA) cells (Figure 3-33a). Interestingly, some DEPDC1B-depleted cells displayed impaired accumulation of PI3K-C2β to FAs (Figure 3-33b), while in some others PI3K-C2β still accumulated to FAs, but the residual recruitment was in general not as strong as in the control cells (Figure 3-33b). It should be taken into account that it was not possible to be sure that all the cells monitored were depleted of DEPDC1B, thereby the effect observed may had been ‘‘weakened’’ by cells which still had functional DEPDC1B (Figure 3-33b). For the analysis of endogenous eGFP-tagged PI3K-C2β recruitment to FAs, both eGFP-hPI3K-C2β and vinculin-mCherry intensities were quantified over time using the Fiji/ImageJ software as described above. Therefore, more experiments need to be performed in order to uncover the functional interplay between PI3K-C2β and DEPDC1B in the process of FA disassembly.

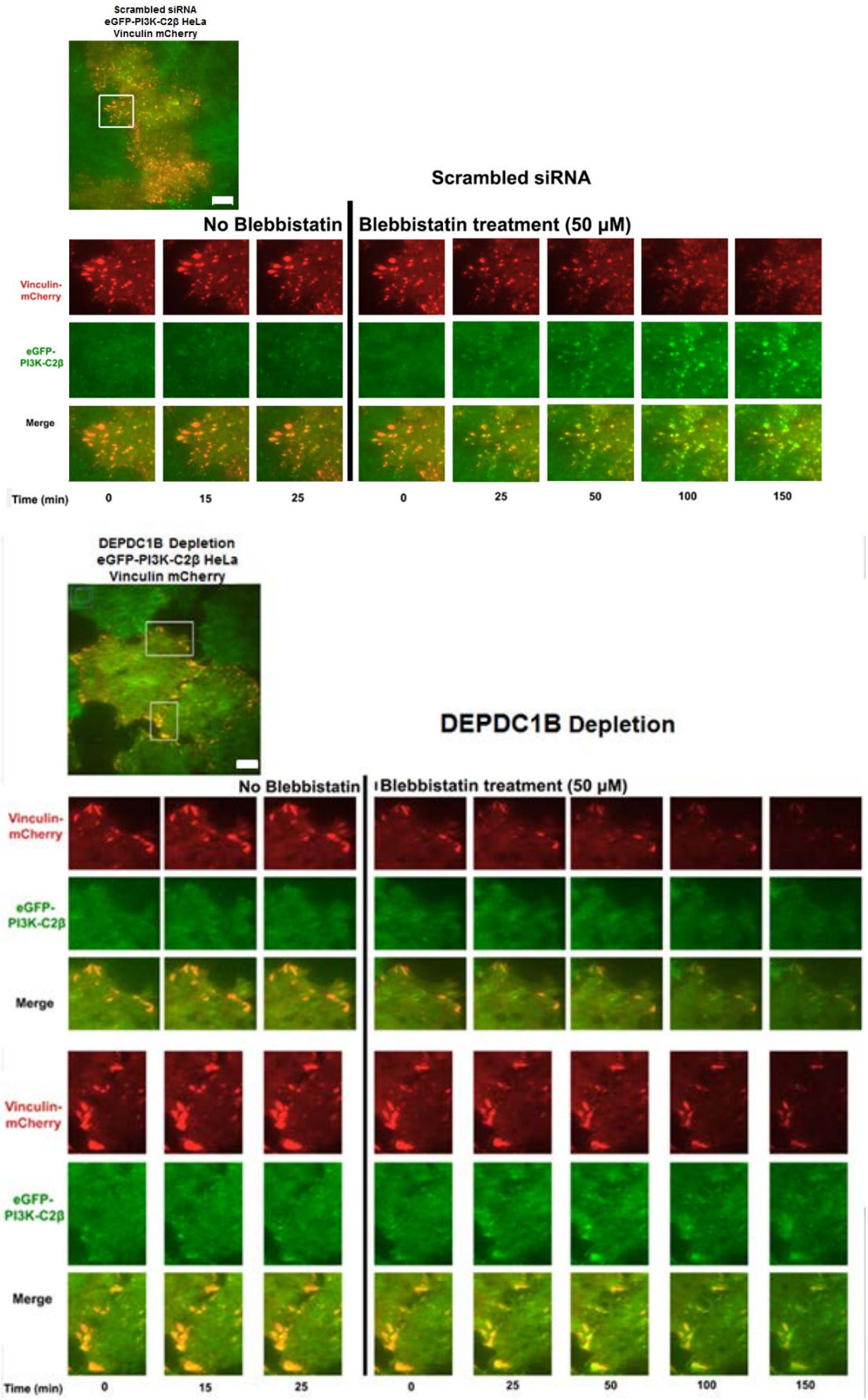


**Figure 3-33: DEPDC1B-depletion impairs accumulation of PI3K-C2β at disassembling FAs.** TIRF microscopy of **a)** control (scrambled) or **b)** DEPDC1B-depleted HeLa cells expressing endogenous eGFP-tagged PI3K-C2β which were transiently transfected with vinculin-mCherry before and after 50 µM

blebbistatin treatment. The cells were monitored for 30 minutes without blebbistatin treatment and for 2.5 hours after addition of blebbistatin and images were taken every 5 minutes. In case of **b)** DEPDC1B knockdown magnifications of two representative areas displaying different dynamics of PI3K-C2β accumulation to FAs are shown. In scrambled cells, PI3K-C2β fluorescence accumulated when vinculin fluorescence faded as FAs disassembled, an effect that seemed to be reduced upon DEPDC1B depletion. Representative images from one experiment. Scale bar: 10 μm.

*PI3K-C2β-talin association upon DEPDC1B depletion and PI3K-C2β-DEPDC1B interaction upon talin depletion*

A second approach was to investigate whether the association between talin and PI3K-C2β, as assessed by co-immunoprecipitation, was interrupted by DEPDC1B depletion. Based on the hypothesis that DEPDC1B is required for PI3K-C2β recruitment to FAs, the association between talin and PI3K-C2β should be lost or weakened in absence of DEPDC1B. Therefore, endogenous eGFP-PI3K-C2β expressing HEK293T cells were depleted of DEPDC1B and cell lysates were subjected to GFP nanobody immunoprecipitation (IP aGFP) and analysed by immunoblotting against talin and DEPDC1B. DEPDC1B consists of 590 amino acids so its expected molecular weight is around 64.9 kDa. In the experiment that I performed I was not able to confirm that the siRNA-mediated DEPDC1B knockdown was efficient, since the indicative band for its expected molecular weight appeared not only in control (scrambled siRNA) but also in DEPDC1B knockdown input material (Figure 3-34a). However, immunoprecipitation of endogenous eGFP-tagged PI3K-C2β resulted in the co-immunoprecipitation of DEPDC1B and talin (very faint upper band, around 270 kDa) in the control (scrambled siRNA) but not in the DEPDC1D knockdown (Figure 3-34a). The DEPDC proteins have seven members, DEPDC1-DEPDC7. Thus, the possibility that other DEPDC isoforms apart from DEPDC1B are recognised by the DEPDC1B antibody cannot be excluded. Therefore, more antibodies against this protein should be screened or a new homemade antibody should be generated.

Additionally, I also wanted to test if talin lies upstream of PI3K-C2β and recruits PI3K-C2β to FAs. For this purpose, endogenous eGFP-tagged PI3K-C2β expressing HEK293T cells were depleted of talin 1 (TLN1) and cell lysates were subjected to GFP nanobody immunoprecipitation (IP aGFP) and analysed by immunoblotting against talin and DEPDC1B (Figure 3-34b). The efficiency of talin knockdown was moderate but the interaction between PI3K-C2β and DEPDC1B was reduced, indicating that probably talin plays a crucial role for PI3K-C2β recruitment to FAs (Figure 3-34b). It has been reported that talin$^{-/-}$ undifferentiated embryonic stem cells are not able to form FAs and stress fibres (Priddle et al., 1998). Therefore it should be taken into account that talin depletion will possibly compromise FAs due to its key role in their formation, raising the possibility that loss of cellular adhesions as platforms for the interaction between PI3K-C2β and DEPDC1B is the underlying cause. Further investigation needs to occur in order to clarify this preliminary observation and further characterise how the actions of

PI3K-C2β, talin and DEPDC1B are coordinated to regulate the process of FA disassembly.

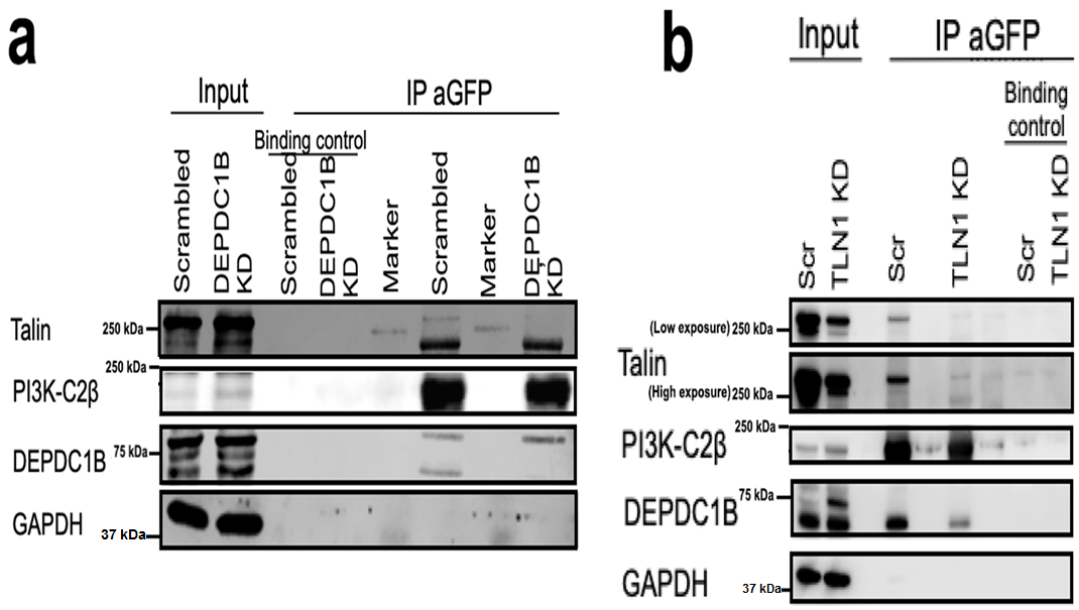


**Figure 3-34: PI3K-C2β-talin association upon DEPDC1B depletion and PI3K-C2β-DEPDC1B interaction upon talin depletion**. Cell lysates from endogenous eGFP-PI3K-C2β expressing HEK293T cells **a)** depleted of DEPDC1B or **b)** depleted of talin1 were subjected to GFP nanobody immunoprecipitation (IP aGFP) and analysed by immunoblotting against talin and DEPDC1B. Blots shown are derived from 1 experiment.

## 3.7 A possible link between the roles of PI3K-C2β at focal adhesions and in mTORC1 regulation

*Rapamycin treatment does not rescue the FA phenotype in HeLa cells depleted of PI3K-C2β*

The mechanistic target of rapamycin (mTOR) is a large serine threonine kinase which functions as the catalytic component of two distinct complexes, mTOR Complex 1 (mTORC1) and 2 (mTORC2) (Laplante and Sabatini, 2009; Saxton and Sabatini, 2017; Sabatini, 2017). mTORC1 has emerged as an important regulator of cell growth and metabolism by integrating multiple inputs, such as amino acids, growth factors, energy and oxygen status and DNA damage (Laplante and Sabatini, 2009; Saxton and Sabatini, 2017; Sabatini, 2017). The translocation of mTORC1 to lysosomes leads to its activation (Laplante and Sabatini, 2009; Saxton and Sabatini, 2017; Sabatini, 2017).

Interestingly, a recent study showed that PI3K-C2β is implicated in the regulation of mTORC1 signaling and lysosomal positioning. More specifically, in the absence of growth factors, PI3K-C2β interacts with the mTORC1 subunit Raptor at late endosomes/lysosomes and through a local production of $PI(3,4)P_2$, it represses mTORC1 activity (Marat et al., 2017).

Furthermore, mTORC1 has been implicated in the regulation of cell migration and adhesion, but data available to date are contradictory and the exact molecular mechanism is not yet known. Rapamycin has been reported to suppress insulin-like growth factor 1 (IGF-1)-triggered cell migration through mTORC1 inhibition (Liu et al., 2006) by inhibiting the actin cytoskeleton reorganization and phosphorylation of the FA components paxillin, FAK and $p130^{Cas}$ in a mTORC1-dependent manner (Liu et al., 2008). Additionally, rapamycin via mTORC1 inhibition has been reported to decrease the IGF-1-induced ability of multiple tumour cell lines to adhere onto ECM components (Chen et al., 2015). Nevertheless, a recent study using melanoma cancer cells stated that mTORC1/2 inhibition leads to reorganised FAs, elevated integrin α2 levels and increased cell migration and invasion (Yoon et al., 2017).

Therefore, considering that in the absence of growth factors PI3K-C2β depletion results in mTORC1 hyper-activation (Marat et al., 2017) and mTORC1 activity has been linked to the regulation of cell migration and invasion and cell adhesion, another hypothesis tested was whether overnight rapamycin treatment (100 nM) could rescue the elevated number and size of FAs and also the increased cell area in HeLa cells depleted of PI3K-C2β (Figure 3-35). For this purpose, control (scrambled siRNA) and PI3K-C2β-depleted HeLa cells with or without being treated with rapamycin were stained for paxillin (Figure 3-35). Only a mild decrease in the number of FAs but no difference in FA size or cell area was observed in two independent experiments, indicating that at least the duration and the concentration of rapamycin treatment that was used was not able to rescue the increased number and size of FAs and cell area in PI3K-C2β-depleted HeLa cells (Figure 3-35). However, it was not confirm that the selected rapamycin treatment was sufficient to switch off the mTORC1 activity. This can be done by checking the phosphorylation levels of the two key substrates of mTORC1 activity, 4EBP1 andS6K1, (Yoon et al., 2017; Ma and Blenis, 2009; Saxton and Sabatini, 2017). Nevertheless, overnight treatment with 100 nM of rapamycin should be enough to switch off the mTORC1 activity (Liu et al., 2006; Liu et al., 2008).

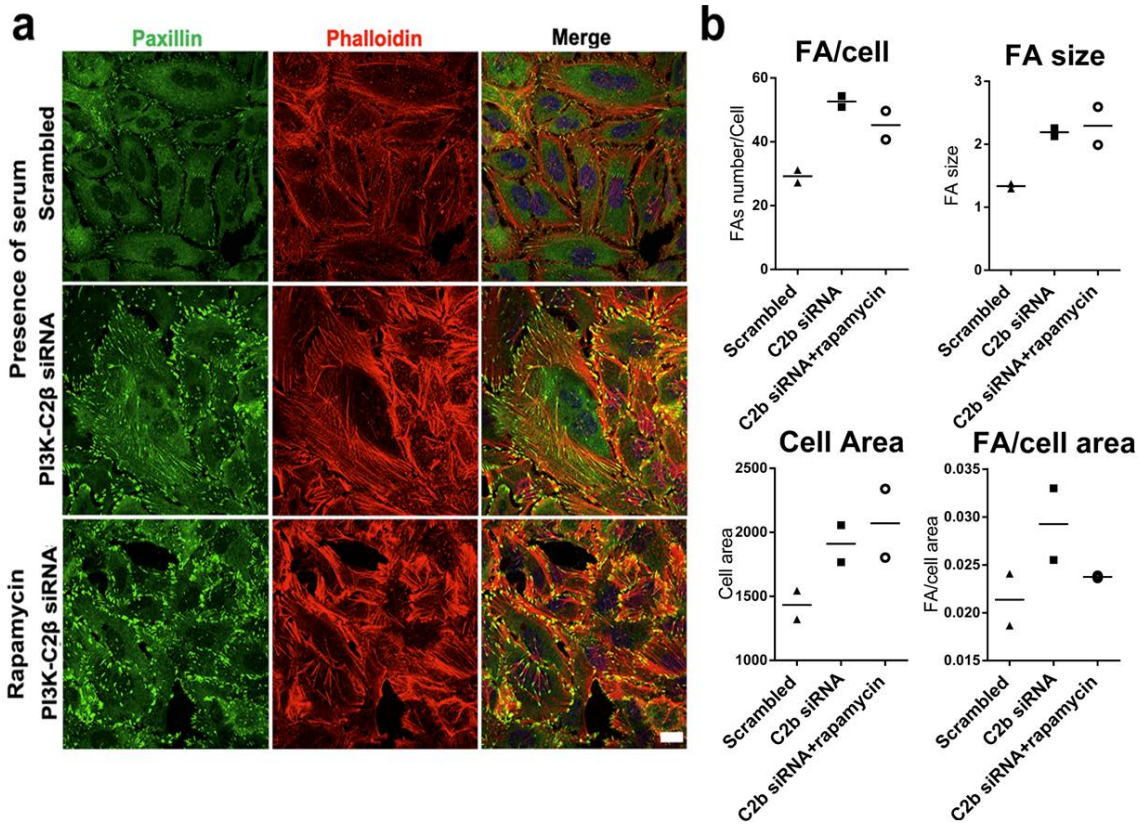


**Figure 3-35: The increased FA number, FA size and cell area observed in HeLa cells depleted of PI3K-C2β cannot be rescued by rapamycin treatment. a)** Control (scrambled siRNA) or PI3K-C2β-depleted ATCC HeLa cells by siRNA#2 were plated onto matrigel-coated glass coverslips, cultured in presence of serum, or overnight treated with rapamycin (100 nM) in case of PI3K-C2β-depletion, fixed and stained for paxillin. **b)** Quantifications were performed using Fiji-ImageJ softwareand at least 60 cells per condition were quantifiedin each experiment. Data represent mean from n=2 independent experiments. Scale bar: 20 µm.

*The function of PI3K-C2β at FAs seems to be independent of lysosomal positioning*

Moreover, considering that PI3K-C2β depletion results in peripheral lysosomal/late endosomal dispersion (Marat et al., 2017), another hypothesis tested was whether the role of PI3K-C2β at FAs is through its role in the regulation of lysosomal positioning. Two small GTPases, namely Rab7 and Arl8, have emerged as major regulators of late endosomal and lysosomal transportation and fusion with other compartments (Wallroth and Haucke, 2018; Marwaha et al., 2017). Rab7 is primarily found at perinuclear late endosomes/lysosomes, whereas Arl8b is mainly found at peripheral lysosomes (Marwaha et al., 2017; Wallroth and Haucke, 2018).

In presence of nutrients, the peripheral lysosomal dispersion is in correlation with the high activity of mTORC1, while in starved conditions lysosomes are clustered in the perinuclear region in correlation with suppressed mTORC1 activity (Korolchuk et al., 2011; Wallroth and Haucke, 2018). Arl8b depletion leads to lysosomal perinuclear

clustering and repression of mTORC1 activity (Korolchuk et al., 2011), in contrast to PI3K-C2β depletion (Marat et al., 2017). Furthermore, it has been reported that Arl8b-driven lysosomal positioning is implicated in the regulation of cell migration and FA dynamics (Schiefermeier et al., 2014). More specifically, LAMTOR2/3 carrying late endosomes are transported to the cell periphery in an Arl8b-dependent manner, where they regulate FA turnover. $p14^{-/-}$ knockout MEFs displayed defective cell migration, increased FA length and delayed FA turnover, phenotype that was not further affected after Arl8b depletion. Nonetheless, Arl8b-depleted $p14^{flox/-}$ MEFs also showed defective migration and increased FA length (Schiefermeier et al., 2014). Therefore, considering that depletion of Arl8b and PI3K-C2β seem to have opposite effects in lysosomal positioning and mTORC1 activation status, the effect of Arl8b siRNA treatment on FAs in PI3K-C2β-depleted HeLa (PDC) cells was tested. For this purpose FAs and late endosomes/lysosomes were visualised by immunofluorescence staining for Paxillin and CD63, which is late endosomal marker, in control (scrambled siRNA), PI3K-C2β-, or Arl8b-, or both PI3K-C2β- and Arl8b-depleted HeLa (PDC) cells (Figure 3-36). As expected, PI3K-C2β-depleted HeLa (PDC) cells displayed an increased number and size of FAs, a phenotype that appeared to be weaker and incompletely but substantially rescued upon Arl8b knockdown (Figure 3-36). However, the way the experiments were performed was not the most conclusive one, since the total amount of siRNA was not the same across all conditions, i.e. double knockdowns contained twice as much siRNA. Therefore, the effect observed in HeLa cells depleted of both PI3K-C2β and Arl8b may be due to a concomitant ‘’dilution’’ of PI3K-C2β siRNA, which leads to its reduced efficiency and in turn to a milder phenotype. However, western blot analysis showed that in double knockdowns the expression level of PI3K-C2β was comparable to the single knockdown. Therefore, in order to reach a clearer conclusion the experiment needs to be repeated in the proper way, i.e. the total amount of siRNA needs to be the same across all conditions.

Furthermore, under these conditions, i.e. in presence of serum, there was no significant difference in the lysosomal positioning between PI3K-C2β-depleted and control (scrambled siRNA) cells, as revealed by staining for the late endosomal marker, CD63. Of note, there is no antibody available to specifically recognise Arl8b from Arl8a which made it impossible to validate the Arl8b knockdown efficiency by western blot analysis. However, I did use the protocol for Arl8b siRNA transfection kindly provided by Prof. Haucke’s lab, whose efficiency was validated in HeLa knock-in cell line expressing enhanced green fluorescent protein (eGFP)-tagged endogenous Arl8b. Another quick method that could have been applied to validate the efficiency of the

Arl8b knockdown was qPCR to check whether the targeted mRNA was still present or not.

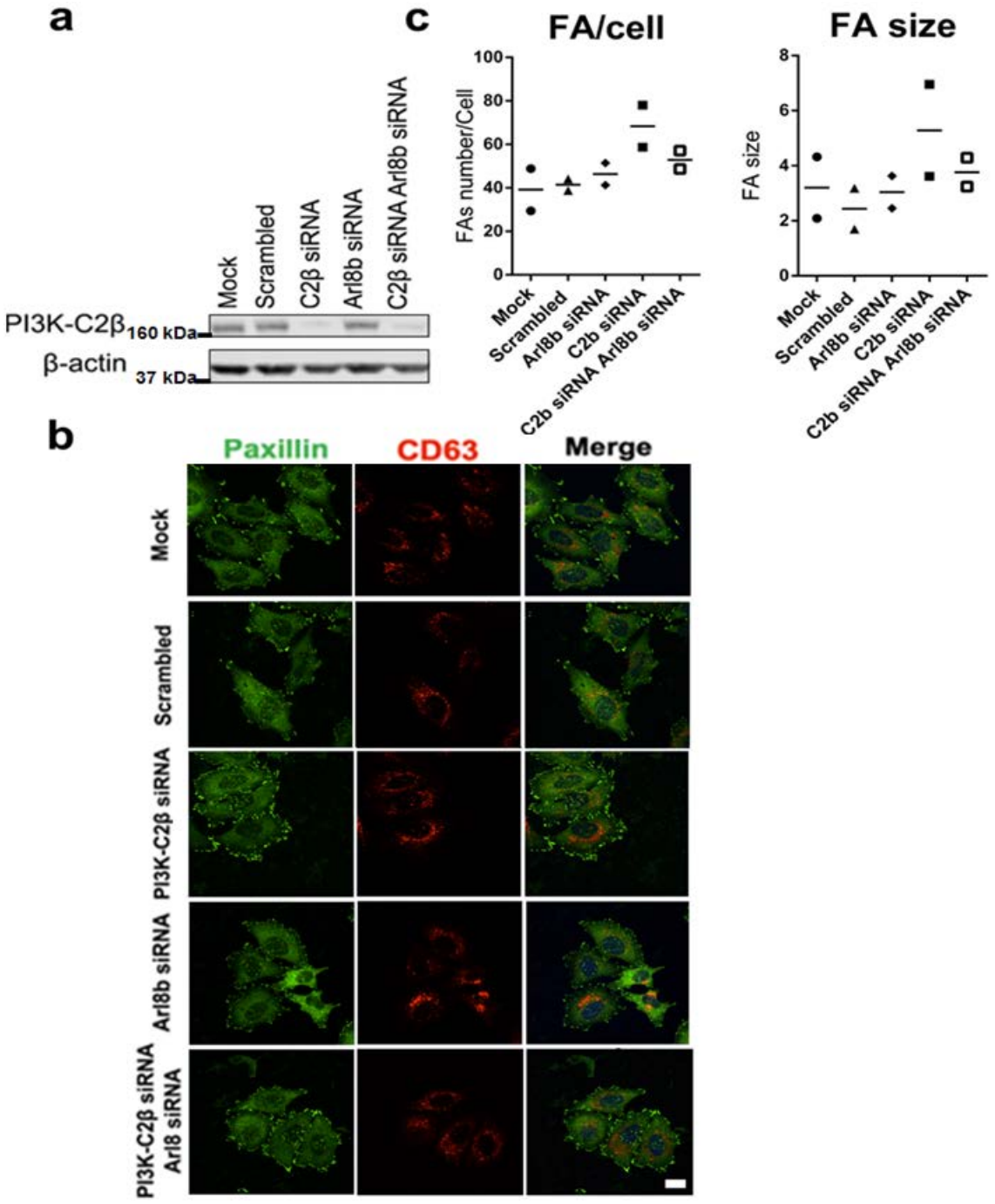


**Figure 3-36: Effect of Arl8b/PI3K-C2β double-knockdown on FAs.** FAs and late endosomes/lysosomes were visualised by IF staining for paxillin and CD63 in presence of serum in control (mock and scrambled siRNA), PI3K-C2β-, Arl8b- or PI3K-C2β- and Arl8b-depleted HeLa (PDC) cells by siRNAs. **a)** The immunoblot of PI3K-C2β depleted HeLa (PDC) cells shown is representativeof n=2 independent experiments. **b)** Control (mock, scrambled siRNA), PI3K-C2β-, Arl8b- or PI3K-C2β- and Arl8b-depleted HeLa (PDC) cells were plated onto matrigel coated glass coverslips, cultured in presence of serum, fixed and stained for paxillin and CD63. **c)** Quantifications were performed using Fiji-ImageJ software and at least 60 cells per condition were quantified in each experiment. Data represent mean from n=2 independent experiments. Scale bar: 20µm.

It was further investigated whether there was a difference in the lysosomal positioning revealed by immunofluorescence staining for lysosomal-associated membrane protein 1 (LAMP-1) between PI3K-C2β-depleted or control (scrambled siRNA) cells in the presence of serum or under 2 hours HBSS starvation (Figure 3-37). PI3K-C2β-depletion did not lead to significant lysosomal peripheral dispersion either in the presence of serum or under HBSS starvation. Additionally, no significant co-localisation between LAMP-1 and p-paxillin$^{Y31}$, a marker for FAs, was noticed, in all conditions tested (Figure 3-37). Overall, there was no significant difference between PI3K-C2β-depleted or control cells (scrambled siRNA) in lysosomal positioning (Figure 3-37). Therefore, I decided not to further pursue a potential functional link between regulation of FAs and of lysosomal positioning by PI3K-C2β.

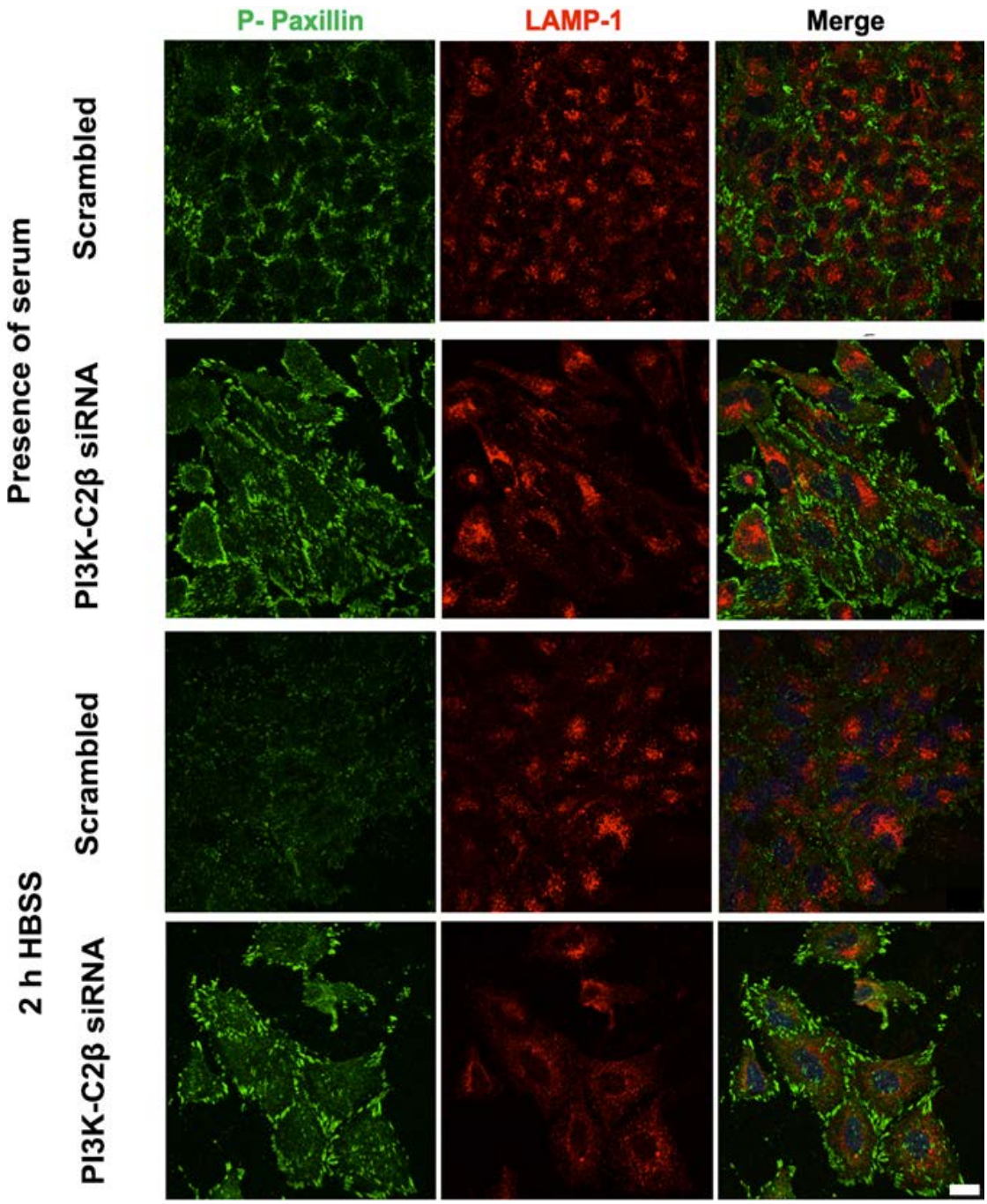


**Figure 3-37: PI3K-C2β depletion does not affect lysosomal positioning.** Control (scrambled siRNA) or PI3K-C2β-depleted ATCC HeLa cells by siRNA#2 were plated onto matrigel-coated glass coverslips, cultured in presence of serum or starved in HBSS for 2 hours, fixed and stained for LAMP-1 and p-paxillin$^{Y31}$. Images shown are representative of n=3 idependent experimets. Scale bar: 20 μm.

*Autophagy seems not to be affected upon PI3K-C2β inactivation*

During this study, whether autophagy was affected upon PI3K-C2β inactivation was also investigated considering that under serum-starved conditions PI3K-C2β KI MEFs are characterised by an elevated number of FAs and starved conditions can induce autophagy (Kaur and Debnath, 2015; Burman and Ktistakis, 2010; Ktistakis and Tooze, 2016a). Recent evidence suggests that autophagy is involved in the regulation of FA disassembly. For instance, it has been reported that NBR1, an autophagy cargo

receptor, triggers FA disassembly by associating with FAs, directing autophagosomes towards them and enhancing cell migration (Kenific et al., 2016b). Additionally, it has been reported that autophagy mediates degradation of paxillin and FA disassembly (Sharifi et al., 2016). Therefore, the expression levels of autophagic markers were assessed by western blot analysis: i.) the unconjugated cytosolic form of LC3 (LC3-I) and lipidated LC3 (LC3-II), which is found at autophagosomes and ii) p62, which is an autophagy cargo receptor mediating the degradation of ubiquitylated proteins that accumulates when autophagy is defective (Kaur and Debnath, 2015; Burman and Ktistakis, 2010; Ktistakis and Tooze, 2016a; Tanida and Waguri, 2010). In my experiments, bafilomycin A1 treatment was also included, which inhibits lysosomal acidification. It thereby inhibits the later stages of autophagy and allows the assessment of the autophagic flux of LC3-II. However, we should bear in mind that it can cause off-target effects since the V-ATPase is involved in the acidification of other cellular compartments, like endosomes and Golgi (Tanida and Waguri, 2010). A first set of two independent experiments was performed, focused only on conditions of overnight serum starvation or overnight serum starvation with bafilomycin treatment (100 nM, for the last 2 hours) (Figure 3-38). No significant difference was observed upon PI3K-C2β inactivation in the expression levels of the autophagy markers tested, so these preliminary data indicate that autophagy is not affected. This observation is consistent with a previous study from the host laboratory (Alliouachene et al., 2015), showing that PI3K-C2β is not involved in starvation-induced autophagy assessed by immunofluorescence staining for LC3. Therefore, it seems that PI3K-C2β does not regulate FA disassembly through regulation of autophagy.

Additionally, considering that PI3K-C2β has been recently reported to suppress mTORC1 activity in absence of growth factors (Marat et al., 2017), mTORC1 activity was also assessed. This was done by determining the phosphorylation levels of two well investigated substrates of mTORC1, i.e. p4EBP1$^{Ser65}$ and ribosomal protein pS6$^{Ser240/244}$, which is a substrate of S6K in a set of two independent experiments focused only on overnight serum starved conditions (Figure 3-38). Interestingly, according to these prelimany data, although no significant difference in the phosphorylation levels of pS6$^{Ser240/244}$ was observed in PI3K-C2β KI MEFs, p4EBP1$^{Ser65}$ levels were increased under overnight serum-starved conditions. Therefore, it seems that there may be a mild increase in mTORC1 activity upon PI3K-C2β inactivation, in agreement with the recent study showing that PI3K-C2β depletion leads to mTORC1 hyper-activation in absence of growth factors (Marat et al., 2017). However, the mild effect on mTORC1 activity observed in PI3K-C2β KI MEFs compared to the more robust published effects upon acute depletion of PI3K-C2β may be due to a possible

adaptation caused by long-term PI3K-C2β inactivation. Additionally, my experiment was focused on the effect of PI3K-C2β inactivation under serum-starved conditions since the FA phenotype of PI3K-C2β KI MEFs was observed under these conditions, which is a ''milder'' way of starvation compared to nutrient starvation in HBSS. Taken together with the observation of rapamycin treatment not rescuing the increased number of FAs in PI3K-C2β depleted HeLa cells, it seems that PI3K-C2β regulates FA dynamics independently from mTORC1 regulation.

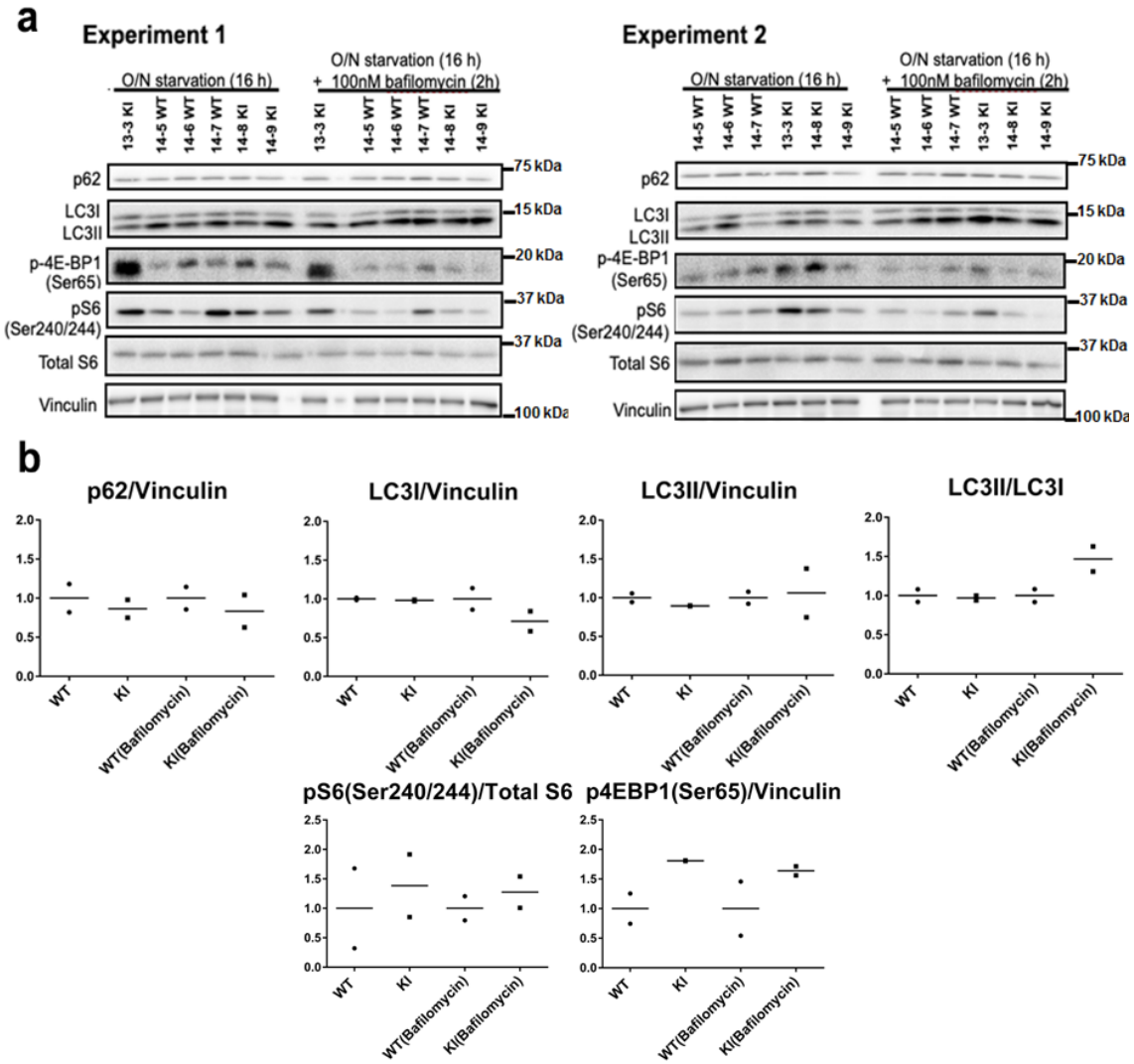


**Figure 3-38: PI3K-C2β inactivation does not seem to affect autophagy but seems to mildly enhance mTORC1 signalling**. **a)** WT and PI3K-C2β KI MEFs were serum-starved overnight treated the last 2 hours with vehicle or 100nM bafilomycin, followed by immunoblotting using antibodies to LC3, p62, S6, $pS6^{Ser240/244}$, $p4EBP1^{Ser65}$ or vinculin. **b)** Data represent mean values from n=2 independent experiments. The MEFs used were derived from 3 WT (14-5, 14-6, 14-7) and PI3K-C2β KI (13-3, 14-8, 14-9) mice.

## 3.8 Is PI3K-C2β implicated in vascular remodelling?

Another aim pursued in the present study was to link the *in vitro* phenotypes observed in HeLa cells depleted of PI3K-C2β or in MEFs with constitutively inactivated

PI3K-C2β, more specifically the increased number of FAs and the defective cell migration, with *in vivo* phenotypes in mice.

In vertebrates, blood vessel formation occurs through two distinct processes, namely vasculogenesis, which describes *de novo* blood vessel generation and angiogenesis, which describes vessel generation from pre-existing ones (Potente et al., 2011; Burri et al., 2004). Vasculogenic vessel formation combined with angiogenic sprouting creates a network which goes through extensive remodelling to turn into functional vasculature. Regression of redundant connections is a crucial element in this process (Franco et al., 2015). It has been reported that vessel regression in mouse developmental angiogenesis occurs through endothelial cell migration and to a great extent is independent of cell death in the retina (Franco et al., 2015). More specifically, it has been suggested that the first step is the selection of the regressing connection, followed by lumen stenosis, and endothelial cell retraction with the last step being their integration in neighbouring vessels (anastomosis in reverse) resulting in an empty basement membrane (Figure 3-39) (Franco et al., 2015). Therefore, the regression profiles are vessel sections which are characterised by the presence of collagen IV which is a marker of basement membrane and the absence of isolectin-B4, which is a marker of endothelial cells (Figure 3-39) (Franco et al., 2015).

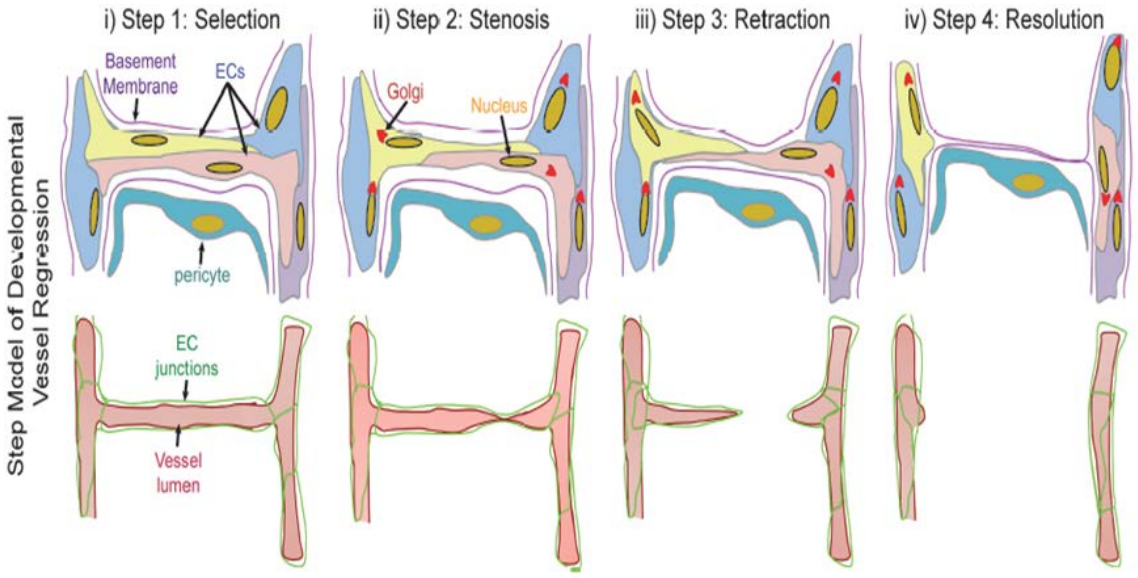


**Figure 3-39: Schematic representation of the proposed steps of developmental vessel regression.** During the first step, the selection of the regressing connection occurs followed by the lumen stenosis during the second stepand the endothelial cell migration towards the neighbouring vessels during the third step pf endothelial retraction. Endothelial integration in neighbouring vessels leading to an empty basement membrane takes plasce during the fourth and last step of the regressing vessel resolution.[Adapted by (Franco et al., 2015). Copyright: © 2015 Franco et al. This is an open access article. Franco CA, Jones ML, Bernabeu MO, Geudens I, Mathivet T, Rosa A, et al. (2015) Dynamic Endothelial Cell Rearrangements Drive Developmental Vessel Regression. PLoS Biol 13(4): e1002125**.**, Copyright also obtained by Professor Holger Gerhardt and Dr Claudio Areias Franco].

Considering that PI3K-C2β is implicated in the regulation of cell migration, a hypothesis tested was whether PI3K-C2β is implicated in vascular remodelling through

regulation of this process. For this purpose, the vessel retractions (ColIV$^{+}$IB-4$^{-}$ areas) were quantified, which are empty collagen IV ''sleeves'' indicating the regression of previous vessels in between two remaining vessels. WT and PI3K-C2β KI postnatal mouse retinas (P9) were stained for collagen IV, which is a marker of the basement membrane, and for isolectin-B4, which reveals endothelial cells (Figure 3-40). Unexpectedly, PI3K-C2β KI postnatal mouse retinas displayed a mild increase in the number of ColIV$^{+}$IB-4$^{-}$ areas (Figure 3-40), indicating that cell migration is mildly enhanced, an observation that is contradictory to the observations in PI3K-C2β KI MEFs and in PI3K-C2β-depleted HeLa cells. The way that these observations could be interpreted is that in different systems the same molecule, in this case PI3K-C2β, is able to regulate the same process in distinct ways leading to disparate outcomes. Interestingly, towards a similar direction it has been reported that cell adhesion molecules, like immunoglobulin-like cell adhesion molecule hepaCAM or the immunoglobulin superfamily carcinoembryonic antigen-related cell adhesion molecule 1 (CEACAM1), are able to repress cancer cell growth but at the same time promote cell migration and invasion (Moh and Shen, 2009). Further investigation needs to be performed to clarify whether PI3K-C2β is implicated in regulation of vessel regression in mouse developmental angiogenesis though regulation of cell migration.

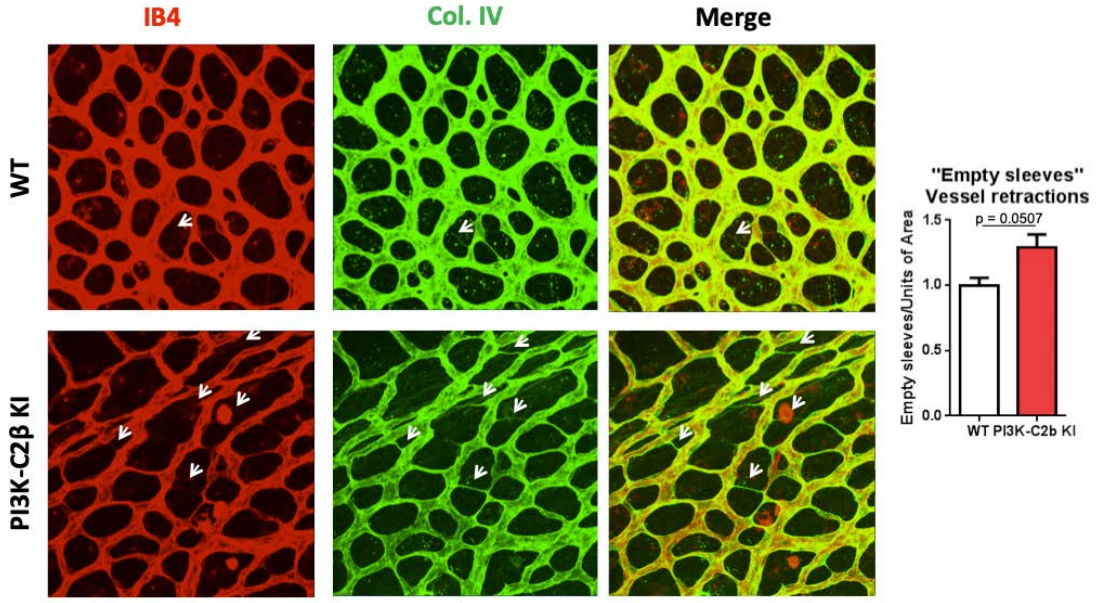


**Figure 3-40: Vessel retractions in littermate WT and PI3K-C2β KI mouse retinas. a)** Littermate WT and PI3K-C2β KI mouse retinas at P9 were stained for collagen IV (green, ECM marker) and isolectin-B4 (red, vasculature). **b)** Quantification of ColIV$^{+}$IB-4$^{-}$ areas (collagen IV empty ''sleeves''). Quantifications were performed using Fiji-ImageJ software. Data are mean values with error bars representing SEM from n=4 independent experiments. The retinas used were derived from 1 pair WT and PI3K-C2β KI littermate mice in each experiment.

# 4. Discussion

The aim of the present study was to improve the understanding of the biological functions and mechanisms of action of the class II PI3K isoform PI3K-C2β. To address this aim two approaches were applied: i) acute siRNA-mediated depletion of PI3K-C2β in HeLa cells and ii.) constitutive catalytic inactivation of PI3K-C2β in MEFs derived from a constitutive kinase-dead KI mouse model. These mice harbour a point mutation in the ATP-binding site of PI3K-C2β, allowing the assessment of the kinase-dependent functions of this enzyme (Alliouachene et al., 2015).

PI3K-C2β has previously been implicated in cell migration, yet its mechanism of action has remained elusive (Blajecka et al., 2012; Maffucci et al., 2005; Domin et al., 2005; Katso et al., 2006). In the present work, the previously reported positive regulatory role of PI3K-C2β in cell migration was confirmed and a molecular mechanism of action in the regulation of FA dynamics was uncovered. More specifically, PI3K-C2β inactivation results in an elevated number of FAs and delays FA disassembly, as assessed by the nocodazole washout experiment-FA disassembly assay. Using TIRF microscopy, dynamic recruitment of PI3K-C2β to disassembling FAs was also demonstrated. Moreover, DEPDC1B was identified as an interaction partner of PI3K-C2β. DEPDC1B is a factor triggering FA disassembly which is crucial for the morphological changes that occur prior to mitosis (Marchesi et al., 2014; Garcia-Mata, 2014). However, the characterisation of the interplay between PI3K-C2β and DEPDC1B in the regulation of FA disassembly needs further investigation. Furthermore, the present work provided evidence that PI3K-C2β also associates with talin, a well-characterised component of FAs, but the function of this association in the regulation of FA dynamics remains unclear.

## 4.1 PI3K-C2β regulates FA dynamics

*PI3K-C2β depletion or inactivation leads to an increased number of focal adhesions*

Both PI3K-C2β-depleted HeLa cells and immortalised PI3K-C2β KI MEFs displayed an increased number of FAs. Additionally, the elevated number of FAs in HeLa cells depleted of PI3K-C2β was rescued by the expression of a siRNA-resistant hPI3K-C2β WT but not the hPI3K-C2β kinase-dead (KD) construct, further indicating that the role of PI3K-C2β at FAs is kinase-dependent. However, the phenotype seemed to be even stronger upon acute PI3K-C2β depletion mediated by RNA-interference, indicating that long-term PI3K-C2β inactivation may lead to adaptation and

compensation. For this reason, early-passage primary MEFs should be used to repeat these experiments in order to reduce the likelihood of a possible compensatory mechanism developing over time.

*PI3K-C2β depletion and/or inactivation impairs focal adhesion disassembly*

Considering that the number of FAs is determined by the processes of FA assembly and FA disassembly, which of these parameters was affected upon perturbation of PI3K-C2β was tested. Since no difference in the capability of PI3K-C2β KI MEFs to adhere onto the ECM components fibronectin and collagen IV was observed, whether PI3K-C2β is implicated in the regulation of FA disassembly was then asked. For this purpose, a nocodazole washout experiment was performed, a commonly-used method to assess the process of FA disassembly. Interestingly, PI3K-C2β KI MEFs were characterised by delayed FA dismantling, indicating that the kinase activity of PI3K-C2β is required for this process.

*PI3K-C2β accumulates at dismantling focal adhesions*

Further confirmation of the implication of PI3K-C2β in the process of FA disassembly was provided by TIRF imaging in two sets of experiments. In the first one, HeLa cells were transiently co-transfected with vinculin-mCherry and eGFP-PI3K-C2β. In a second set of experiments, HeLa cells expressing endogenous eGFP-tagged PI3K-C2β (obtained from our collaborator Volker Haucke) which were transiently transfected with vinculin-mCherry were used. The advantage of using a cell line with endogenously eGFP-tagged PI3K-C2β is to exclude possible artefacts resulting from overexpression of eGFP-PI3K-C2β. In both experimental settings, blebbistatin treatment was used as a stimulus to trigger the FA disassembly process. Blebbistatin is a useful tool to study the process of FAs dismantling. It is an inhibitor of the myosin II motor protein, impedes FA maturation and triggers FA disassembly of mature FAs, resulting in an accumulation of smaller nascent adhesions. Under these experimental conditions which trigger FA dismantling, eGFP-hPI3K-C2β fluorescence drastically accumulated at FAs. Furthermore, the peak of eGFP-hPI3K-C2β recruitment corresponded to an acute vinculin-mCherry signal drop.This observation suggests that PI3K-C2β dynamically accumulates at FAs to promote FA disassembly. Interestingly, PI3K-C2β was found at a low level at some FAs at steady-state (before triggering the process of FA disassembly), with no difference in eGFP-hPI3K-C2β fluorescence observed over time. These observations indicate that PI3K-C2β is a constitutive component of FAs which is in an inactive state under normal conditions, requiring a stimulus to become activated and induce the process of FA dismantling. Furthermore,

the present work provided evidence that PI3K-C2β associates with talin, a key FA component, additionally indicating that PI3K-C2β is present at FAs at steady-state.

Another approach which could be used to further validate the regulatory role of PI3K-C2β in FA dynamics would be to test whether in vinculin-mCherry expressing HeLa cells PI3K-C2β-depletion affects FA dynamics.

As it will be discussed in the following sections, preliminary data of the present study suggest that DEPDC1B lies upstream of PI3K-C2β and it seems that it is required for PI3K-C2β recruitment to FAs, since partially depletion of DEPDC1B in HeLa cells mediated by siRNA led to decreased PI3K-C2β accumulation at FAs. However, further investigation should be done in order to confirm these preliminary observations and the generation of DEPDC1B KO cell lines using CRISPR/Cas9 gene targeting system could provide an unequivocal answer whether DEPDC1B lies upstream of DEPDC1B and regulates its role at FAs.

## 4.2 PI3K-C2β regulates cell migration

FA dynamics are directly linked with cell migration. Consistent with the already reported regulatory role of PI3K-C2β in cell migration (Blajecka et al., 2012; Maffucci et al., 2005; Domin et al., 2005; Katso et al., 2006), both PI3K-C2β-depleted HeLa cells and PI3K-C2β KI MEFs displayed reduced cell migration assessed by scratch-wound assay. The scratch-wound assay was performed in presence of mitomycin to inhibit cell proliferation, to exclude a possible contribution of this parameter during testing of PI3K-C2β inactivation in cell migration. In HeLa cells depleted of PI3K-C2β, cell migration was assessed in the presence of serum, while in MEFs it was determined in different conditions: i.) serum-starved overnight, ii.) serum-starved overnight followed by PDGF stimulation, or iii.) in the presence of serum. The observed inhibitory effect in cell migration was stronger in HeLa cells acutely depleted of PI3K-C2β by RNA-interference as compared to a milder effect in PI3K-C2β KI MEFs under all conditions tested. The more robust effect was observed when PI3K-C2β KI MEFs were serum starved overnight and stimulated with PDGF, indicating that abundance of migratory stimuli masks the milder defect seen in MEFs. These observations indicate again that adaptation to long-term PI3K-C2β inactivation may have occurred in the KI MEFs.

## 4.3 PI3K-C2β interacts with DEPDC1B, a FA disassembly factor and talin, a well-characterised FA component

*PI3K-C2β interacts with DEPDC1B*

A yeast-two-hybrid screen performed by Hybrigenics Services using amino acids 1–615 of PI3K-C2β as the bait fragment identified DEPDC1B (amino acids 114-260) as a potential interaction partner of PI3K-C2β, suggesting that the interaction between these two proteins is direct. This interaction was further confirmed by immunoprecipitation of endogenous proteins using endogenously eGFP-PI3K-C2β expressing HEK293T cells. DEPDC1B has been reported to act as a factor inducing FA disassembly, a requisite for the morphological alterations that occur prior to mitotic entry (Marchesi et al., 2014; Garcia-Mata, 2014). Thus, this study was focused on this interaction as it may be of particular importance for providing a mechanistic insight into the function of PI3K-C2β at FAs.

*DEPDC1B depletion phenocopies PI3K-C2β depletion*

Interestingly, siRNA-mediated acute DEPDC1B depletion in HeLa cells resulted in an elevated number of FAs, an altered pattern of stress fibres and an increased cell area, similarly to HeLa cells depleted of PI3K-C2β. Additionally, expression of eGFP-DEPDC1B or eGFP-PI3K-C2β in HeLa cells seemed to lead to cell rounding without causing any significant increase in cell death as compared to eGFP-expressing cells. This is consistent with the role of DEPDC1B in triggering cell rounding prior to entry of cells into mitosis (Marchesi et al., 2014; Garcia-Mata, 2014) and supports the concept of PI3K-C2β and DEPDC1B both promoting FA disassembly. Collectively, the present study provides evidence that PI3K-C2β and DEPDC1B interact and possibly work together in regulating FA disassembly.

*Recruitment of PI3K-C2β to focal adhesions by DEPDC1B*

Dynamic accumulation of DEPDC1B at disassembling FAs has been suggested to occur prior to mitotic entry (Marchesi et al., 2014; Garcia-Mata, 2014). Using TIRF microscopy, the study presented here showed that under experimental conditions which trigger FA disassembly, eGFP-hPI3K-C2β fluorescence drastically accumulated at FAs and the peak of this recruitment corresponded to an acute drop of the vinculin-mCherry signal. This observation suggests that PI3K-C2β dynamically accumulates at FAs to promote their disassembly. Therefore, the question that was raised was whether DEPDC1B is directly required for PI3K-C2β recruitment to FAs. If this hypothesis for the mechanism of PI3K-C2β recruitment to FAs is correct, siRNA-mediated depletion of DEPDC1B in HeLa cells should prevent PI3K-C2β accumulation at FAs during FA

dismantling. In order to test this hypothesis, TIRF imaging of DEPDC1B-depleted live HeLa cells expressing endogenous eGFP-tagged PI3K-C2β transiently transfected with vinculin-mCherry and treated with blebbistatin was performed and the process of FA disassembly was monitored. Interestingly, a higher percentage of cells in which PI3K-C2β was not accumulating at FAs was observed in DEPDC1B-depleted HeLa cells compared to control cells (scrambled siRNA). However, while the accumulation of PI3K-C2β to FA was overall not as robust as in control cells, a differential impact at the single cell level was observed, with impaired PI3K-C2β recruitment to FAs observed in some cells, while in others PI3K-C2β was still recruited to FAs. I believe that this is most likely due to incomplete knockdown of DEPDC1B in some cells. In general, difficulties were faced in verifying the efficiency of siRNA-mediated DEPDC1B knockdown, since it was difficult to source an antibody that specifically recognises DEPDC1B. As an alternative approach, I therefore decided to overexpress eGFP-DEPDC1B in parallel with siRNA-mediated DEPDC1B knockdown and to assess the expression levels of eGFP-DEPDC1B in control (mock, scrambled siRNA) and in DEPDC1B-depleted cells. The expression levels of eGFP-DEPDC1B were higher in control (mock, scrambled siRNA) compared to DEPDC1B-depleted cells, indicating that the acute depletion of DEPDC1B by RNA-interference was effective. Another method that I could also apply to assess whether depletion of endogenous DEPDC1B is efficient is to check by quantitative RT-PCR whether the targeted mRNA is still present or not. Therefore, more experiments need to be performed in order to confirm this observation.

Additionally, upon blebbistatin treatment, preliminary data suggested that immunoprecipitation of endogenous eGFP-tagged PI3K-C2β could result in enhanced co-immunoprecipitation of DEPDC1B, further indicating a potential functional interplay between these two proteins in promoting FA disassembly. However, more experiments need to be performed to confirm this observation.

Moreover, another experiment that needs to be performed in order to further support the functional interplay between DEPDC1B and PI3K-C2β at FAs is to check whether they co-localise at FAs. Ideally, this would be done as triple-colour live TIRF imaging using for example eGFP-PI3K-C2β, vinculin-mCherry and iRFP-DEPDC1B, a construct which would need to be generated.

Towards a more mechanistic understanding of the findings of this study, whether DEPDC1B lies upstream of DEPDC1B and is responsible for PI3K-C2β recruitment to FAs needs to be assessed. As it has already been mentioned, the yeast-two-hybrid screen revealed that a region found within 114-260 amino acids of DEPDC1B mediates the interaction with a region found within 1–615 amino acids of

PI3K-C2β. Therefore, whether GST-DEPDC1B$^{114-260}$ is capable of pulling down either full length or the region 1-615 amino acids of eGFP-PI3K-C2β transiently expressed in cells needs to be determined. If this is the case, *in vitro* lipid kinase assays will then be performed to define whether the kinase activity of PI3K-C2βwill be affected by DEPDC1B. As the achievement of an efficient DEPDC1B knockdown has been challenging, the generation of control and DEPDC1B KO HeLa and endogenously eGFP-PI3K-C2β expressing HEK293T cells using CRISPR/Cas9 gene targeting system, will be able to solve this problem. These DEPDC1B KO cell lines could then be used to: 1.) confirm the preliminary data obtained by this study that DEPDC1B depletion leads to a similar FA and F-actin stress fibres phenotype as PI3K-C2β depletion (phenocopy), 2.) using TIRF microscopy, study whether eGFP-PI3K-C2β accumulation at FAs will be prevented and 3.) assess whether the co-immunoprecipitation of talin with eGFP-PI3K-C2β will be prevented.

*PI3K-C2β associates with talin*

Talin is a large, cytoplasmic, actin-binding protein and a major component of integrin-based cell-matrix adhesions with a key role in bi-directional signalling of integrins (Manakan Betsy Srichai, 2010; Klapholz and Brown, 2017; Gough and Goult, 2018; Wang et al., 2018a).

This study provides evidence that PI3K-C2β associates with talin, since immunoprecipitation of endogenous eGFP-tagged PI3K-C2β resulted in co-immunoprecipitation of talin. Nonetheless, this interaction still needs to be verified by the converse approach, i.e. immunoprecipitation of talin. Interestingly, immunoprecipitation of endogenous eGFP-PI3K-C2β in talin-depleted HEK293T cells, in spite of poor knockdown efficiency, led to reduced co-immunoprecipitation of DEPDC1B, indicating that talin may play a critical role in the recruitment of PI3K-C2β to FAs. It has been reported though, that talin$^{-/-}$ embryonic stem cells are incapable of forming FAs and stress fibres (Priddle et al., 1998). Hence, it should be taken into account that siRNA-mediated depletion of talin will probably cause FA disappearance. It is therefore possible that the underlying reason for the decreased PI3K-C2β-DEPDC1B interaction is the loss of FAs as platforms for this interaction.

*PI3K-C2β-talin association upon DEPDC1B depletion*

Another approach that was used to investigate whether DEPDC1B is responsible for PI3K-C2β recruitment to FAs was to test whether immunoprecipitation of endogenous eGFP-tagged PI3K-C2β resulted in reduced co-immunoprecipitation of talin in DEPDC1B-depleted HEK293T cells. As discussed above, it was challenging to confirm by western blot analysis whether the DEPDC1B knockdown was successful

due to problems with antibody specificity. Of note, the DEPDC protein family contains several proteins closely related to DEPDC1B, raising the possibility of isoform cross-reactivity.

However, immunoprecipitation of endogenous eGFP-tagged PI3K-C2β did not result in co-immunoprecipitation of DEPDC1B and talin from DEPDC1B knockdown cells. Thus, in order to reach a conclusion, a specific antibody against DEPDC1B needs to be generated since it seems that the commercially available ones are not sufficiently specific. Alternatively, a HeLa knockout cell line for DEPDC1B could be generated.

Collectively, more investigation is needed to acquire a clear mechanistic insight into how the functions of PI3K-C2β, talin and DEPDC1B are coordinated to regulate the process of FA disassembly. This potential interplay between PI3K-C2β, DEPDC1B and talin based on my and the published observations summarized below:

i.) endogenous eGFP-tagged PI3K-C2β co-immunoprecipitates talin and DEPDC1B, and PI3K-C2β-DEPDC1B interaction seems to be enhanced following blebbistatin treatment
ii.) PI3K-C2β accumulates at dismantling FAs, but is also present at stable FAs at lower levels
iii.) talin-depletion appears to result in a decreased PI3K-C2β-DEPDC1B interaction
iv.) DEPDC1B depletion phenocopies PI3K-C2β depletion
v.) DEPDC1B depletion seems to lead to a reduced talin-PI3K-C2β interaction
vi.) DEPDC1B is recruited to disassembling FAs (Marchesi et al., 2014; Garcia-Mata, 2014)
vii.) DEPDC1B depletion impairs recruitment of PI3K-C2β to disassembling FAs

This process could work as follows: PI3K-C2β is present at FAs through its association with talin and is maintained inactive at steady-state and under FA disassembly-triggering conditions, PI3K-C2β-DEPDC1B interaction is enhanced and they function together to promote FA disassembly. It is still not clear how PI3K-C2β is recruited to FAs and triple-colour live TIRF imaging using for example eGFP-PI3K-C2β, vinculin-mCherry and iRFP-DEPDC1B should allow shedding light on this question.

## 4.4 Which phospholipid product of PI3K-C2β is functionally-relevant in regulating FA biology?

The ability of class II PI3Ks to generate both PI3P and $PI(3,4)P_2$ inositol lipids has now been established (Bilanges et al., 2019; Margaria et al., 2019).

It would be very useful to identify the lipid product of PI3K-C2β in the context of FAs, since it could provide a mechanistic understanding of this process and direct investigation into potential PI3K-C2β downstream effectors or other regulators, e.g. PI phosphatases. Additionally, it can add to the ongoing debate regarding the lipid products of class II PI3Ks and PI3K-C2β in particular. During this work, some very preliminary data related to the possible lipid product of PI3K-C2β in the FA context were acquired. However, more work is required to address this question.

Based on immunofluorescence-based estimation of PI3P levels using the GST-2×$FYVE^{HRS}$ PI-binding probe, PI3K-C2β KI MEFs were characterised by a small drop in PI3P levels. However, this small reduction in PI3P levels upon PI3K-C2β inactivation does not provide direct evidence of PI3K-C2β producing PI3P in the first place, since $PI(3,4)P_2$ can rapidly be metabolised into PI3P by the 4'-phosphatases INPP4A and INPP4B (Bilanges et al., 2019). I was also interested in testing whether in WT MEFs PI3P is found at FAs, but no significant co-localisation between PI3P and FAs was observed. Therefore, I did not manage to link the mild PI3P decrease with the increased number of FAs observed upon PI3K-C2β inactivation. The estimation of $PI(3,4)P_2$ levels by immunofluorescence staining has been more challenging in both MEFs and HeLa cells and a quantitative data set has not been obtained yet.

Another approach that was used to address this question was to test whether depletion of $PI(3,4)P_2$ or PI3P at the plasma membrane phenocopies PI3K-C2β inactivation. For this purpose, mCherry-INPP4B-CAAX (to deplete $PI(3,4)P_2$) or mCherry-MTM1-CAAX (to deplete PI3P) were transiently-transfected in WT MEFs. Interestingly, it appeared that in both cases, transfected cells exhibited more FAs, mostly found in the cell mid-region, compared to untransfected cells. This observation suggests that depletion of either $PI(3,4)P_2$ or PI3P impair FA dynamics. Therefore, it was not feasible to link the function of PI3K-C2β at FAs with only one of these lipids. Notably, 5'-phosphatase mCherry-INPP5E-CAAX-mediated depletion of $PI(4,5)P_2$ resulted in a complete absence of FAs in the cell mid-region and showed only peripheral FAs, a phenotype which was different from the one seen upon mCherry-INPP4B-CAAX or mCherry-MTM1-CAAX expression. However, the most appropriate control in this type of experiment would be to also express the kinase-inactive constructs to ensure the observed effects are indeed a consequence of specific lipid

depletion. Thus, these experiments need to be repeated including the appropriate controls in order to draw a firm conclusion.

Another approach that can be applied to investigate whether the increased number of FAs upon perturbation of PI3K-C2β is a consequence of defective PI(3)P or PI(3,4)$P_2$ formation is to use the cell-permeable PI-derivatives (Laketa et al., 2009; Subramanian et al., 2010), which permit the addition of exogenous PI3P or PI(3,4)$P_2$. In these compounds, acetoxymethylester (AM) groupsare used to mask the charged phosphate groups, thus these synthetic molecules are generally nonpolar and therefore membrane-permeable. Once inside the cell, the AM groups are cleaved off by endogenous esterases and lipases. However, it should be taken into account that the caveat of a short half-life of these molecules within the cells makes it difficult to rebalance a comparably slow process such as FA disassembly.

The activation loop in the kinase domain of PI3Ks greatly determines the substrate specificity of these enzymes. In the PI(3,4,5)$P_3$-synthesising class I PI3Ks, it contains two stretches of basic amino acids, which are absent from the PI3P-synthesing class III PI3K Vps34. In class II PI3Ks, this part of the kinase domain only contains the basic residues that coordinate the 4'-phosphatase group, indicating that PI4P is used by these enzymes to produce PI(3,4)$P_2$ (Bilanges et al., 2017; Posor et al., 2013; Bilanges et al., 2019). In order to discriminate between PI3K-C2α-dependent PI(3,4)$P_2$ and PI3P production, a recent study (Posor et al., 2013) engineered a construct in which the 4-phoshate-specific amino acid stretch was replaced with the equivalent sequence from Vps34. Therefore, another method that I could apply is the expression of a construct like this, that can produce PI3P but not PI(3,4)$P_2$ (Posor et al., 2013; Franco et al., 2014), in PI3K-C2β KI MEFs or PI3K-C2β-depleted HeLa cells and investigate whether the FA phenotype can be rescued.

The determination of the PI3K-C2β lipid product(s) in the FA context is required in order to identify which is/are its downstream effector(s) that mediate its regulatory role in FA dynamics. An interesting study described a siRNA-screen to identify genes which are involved in FA and cell shape control using YFP-paxillin expressing HeLa cells (Winograd-Katz et al., 2009). Therefore, this platform may represent a potential way to determine putative PI3K-C2β downstream effectors. Based on the idea that these should contain lipid binding domains which bind the PI3K-C2β lipid product(s), the potential candidates should contain either FYVE or PX lipid-binding domains in case PI3P is the lipid product, or additionally PH lipid-binding domains in case the lipid product is PI(3,4)$P_2$. A possible candidate may be the FYVE-containing protein ZF21 whose depletion leads to an elevated number of FAs, reduced cell migration and

delayed FA disassembly (Nagano et al., 2010), thus phenocopying PI3K-C2β depletion.

Interestingly, a recent study showed that $PI(3,4)P_2$ plays a regulatory role in FA dynamics in the MDA-MB-231 breast cancer cell line (Fukumoto et al., 2017). siRNA-mediated depletion of SHIP2, which produces $PI(3,4)P_2$ from $PI(3,4,5)P_3$, leads to an elevated number of FAs, increased cell area and decreased cell invasion, similarly to PI3K-C2β inactivation or depletion. On the contrary, PTEN depletion results in reduced cell area and increased cell invasion, phenotypes which are rescued by additional SHIP2 depletion (Fukumoto et al., 2017). Furthermore, siRNA-mediated depletion of lamellipodin, which contains a PH domain which specifically binds to $PI(3,4)P_2$ and has a regulatory role in lamellipodial dynamics (Krause et al., 2004), phenocopies SHIP2 knockdown (Fukumoto et al., 2017). Therefore, lamellipodin can also represent a possible downstream effector of PI3K-C2β. Last but not least, considering that the plasma membrane is characterised by high levels of PI4P and a low abundance of PI, my hypothesis is that PI3K-C2β produces $PI(3,4)P_2$ at FAs. Further investigation is definitely required to ascertain this hypothesis.

## 4.5 A hypothesis for the regulation of PI3K-C2β at FAs

A recent study reported a regulatory role for Protein Kinase D1 (PKD1) in FA dynamics (Durand et al., 2016). These authors showed that PKD1 localisation at FAs is induced downstream of a fibronectin-integrin-RhoA signalling pathway. PKD1 was found to reduce FA turnover and enhance FA maturation and stability through phosphorylation of PIP5Kγ (phosphatidylinositol-4-phosphate 5-kinase type-I gamma), leading to a decrease in its lipid kinase activity and association with talin (Durand et al., 2016). $PI(4,5)P_2$ is synthesised by the FA-located PIP5KIγ and has been reported to play a critical role in both FA assembly (by promoting the activation of various FA components like talin, FAK and vinculin) as well as FA dismantling (by triggering m-calpain activation) (Atherton et al., 2016; Manakan Betsy Srichai, 2010; Klapholz and Brown, 2017; Gough and Goult, 2018; Wang et al., 2018a; Cai et al., 2008; Durand et al., 2016; Leloup et al., 2010; Chinthalapudi et al., 2014). Therefore, disruption of the local balance of $PI(4,5)P_2$ can explain its ability to promote both FA assembly and disassembly, thereby playing a crucial role in FA dynamics regulation (Durand et al., 2016).

PKD1 activity promotes FA maturation and stability and delays FA turnover (Durand et al., 2016), similarly to depletion or kinase inactivation of PI3K-C2β, suggesting antagonistic roles of PKD1 and PI3K-C2β. PIP5Kγ was identified as a

phosphorylation target of PKD1 and its phosphorylation at serine residue 448 (S448) reduces its activity and its association with talin (Durand et al., 2016). Searching the sequence of human PI3K-C2β for sequences conforming to the PKD consensus phosphorylation motif revealed that PI3K-C2β has four potential PKD1 phosphorylation sites, S85, S277, S350 and S946, which are all conserved in the human, mouse and bovine PI3K-C2β proteins (Figure 4-1). Interestingly, a recent study showed that phosphorylation of PI3K-C2β at T279 mediated by PKN2 generates a docking site for 14-3-3 proteins that leads to PI3K-C2β cytoplasmic retention (Wallroth et al., 2019). Both PKN1 and PKN2 isoforms positively regulate cell migration (Lachmann et al., 2011) though, so it is doubtful that these protein kinases mediate negative regulation of PI3K-C2β recruitment to FAs. Intriguingly, this phosphorylation site also conforms to the PKD consensus phosphorylation motif. Therefore, a hypothesis that needs to be tested is whether PI3K-C2β phosphorylation by PKD1 leads to PI3K-C2β inhibition and in turn to delayed FA disassembly. More specifically, when RhoA is active, promoting F-actin filaments and FA stabilisation and integrity, PI3K-C2β phosphorylation at T279 mediated by PKD would sequester PI3K-C2β in the cytoplasm through generation of 14-3-3 docking site in PI3K-C2β. However, when RhoA activity is decreased, PI3K-C2β could be capable of associating with FAs and induce their dismantling. In order this hypothesis to be tested, a pan-PKD inhibitor (CRT0066101) or PKD depletion mediated by siRNAs could be used. Furthermore, phosphorylation of PI3K-C2β by PKD may affect both recruitment of this PI3K to FAs and its kinase activity, or only one of these functions. In order to assess these possibilities, two different PI3K-C2β mutants could be tested; i.) non-phosphorylatable PI3K-C2β mutant, in which threonine (or serine in case the other phosphorylation sites need to also be tested) is mutated to alanine and ii.) phospho-mimetic mutant, in which serine is mutated to aspartic acid. I have shown that upon blebbistatin treatment, which triggers FA disassembly, PI3K-C2β is recruited to dismantling FAs. Therefore, if PI3K-C2β phosphorylation perturbs recruitment, the phospho-mimetic PI3K-C2β mutant may display less recruitment to FAs upon blebbistatin treatment, thus impaired FA disassembly, whereas the non-phospho PI3K-C2β mutant may display the same or even stronger recruitment to FAs compared to WT. Additionally, I have demonstrated that the role of PI3K-C2β at FAs is kinase-dependent. Therefore, if phosphorylation inhibits kinase activity, the phospho-mimetic mutant may not rescue the FA phenotype observed in HeLa cells depleted of PI3K-C2β, while the non-phospho PI3K-C2β mutant should rescue the FA phenotype and result in a decreased number of FAs. Furthermore, if phosphorylation inhibits either recruitment to FAs or the kinase activity of PI3K-C2β or both of these functions, then the non-phospho mutant should be hyper-active, thus overexpression should lead to less FAs, and perhaps even cell rounding at lower expression levels.

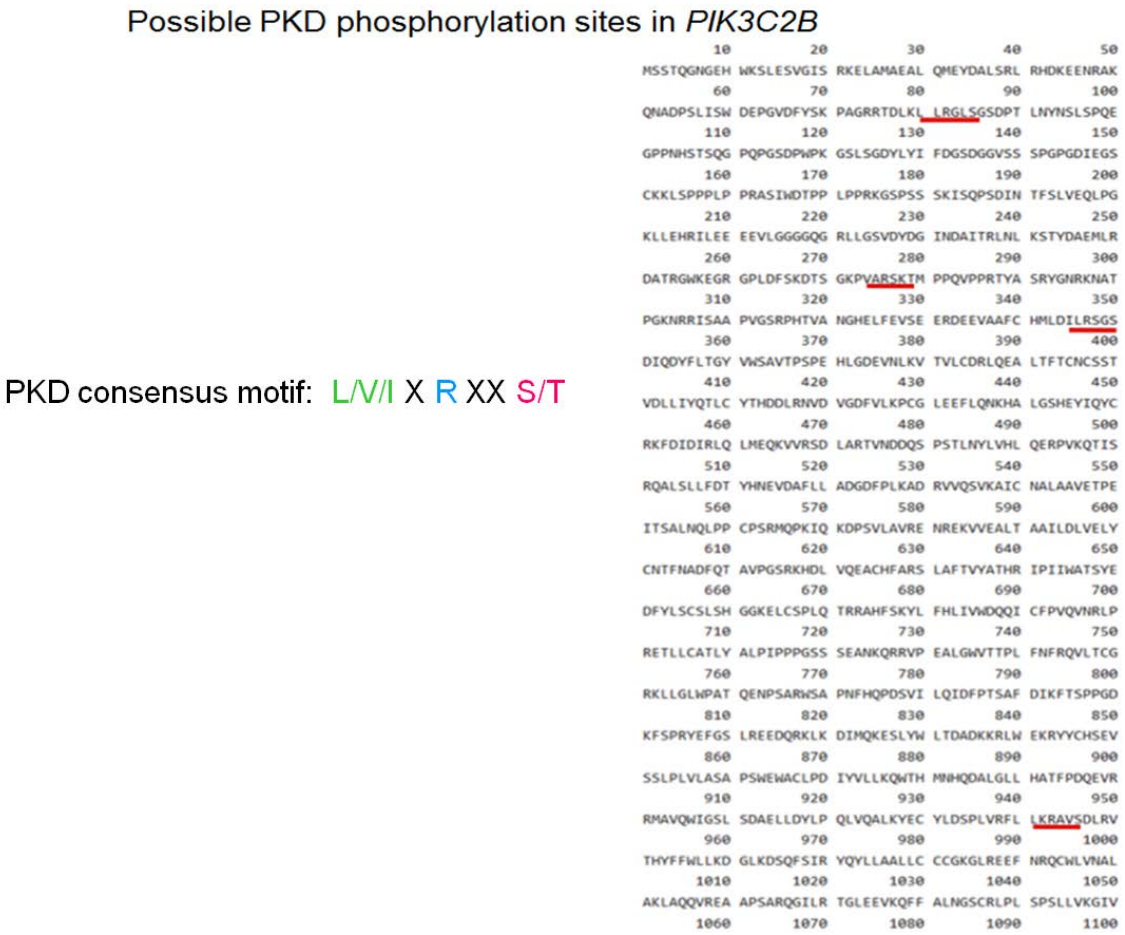


**Figure 4-1: Potential PKD1 phosphorylation sites in *PIK3C2B*.** Sequence of human PI3K-C2 β was searched for sequences conforming to the PKD consensus phosphorylation motif and potential PKD1 phosphorylation sites were identified (underlined). T279 phosphorylation site also conforms to the PKD consensus phosphorylation motif (underlined). [Adapted from (Durand et al., 2016)]

## 4.6 How can integrin-based cell-matrix adhesion dynamics and wound healing be assessed *in vivo*?

An outstanding question is what the functional relevance of the role of PI3K-C2β in FA dynamics is at the organismal level. For this purpose, an experimental paradigm that can assess integrin-based cell-matrix adhesion dynamics and wound healing *in vivo* needs to be determined.

A recent study investigating phenotypes related to deregulated integrin-based cell-ECM adhesions used a mouse model in which talin auto-inhibition is disrupted by an activating point mutation in talin (*Tln1*$^{E1770A}$). This study applied both *in vitro* and *in vivo* approaches to show that talin auto-inhibition regulates integrin-based cell-matrix adhesions, cell migration and wound healing *in vivo*. More specifically, a biopsy punch wound healing assay in mice was used to assess the effects of this activating point mutation in talin in wound healing *in vivo.* In brief, after anaesthesia, mice were shaved and cleaned on the dorsal side, a single wound was made and healing was monitored

daily for 2 weeks (Haage et al., 2018). This approach could represent an easily-applicable assay to assess the role of PI3K-C2β in wound healing *in vivo*.

Another approach that could be applied is intravital microscopy which allows dynamic visualisation of biological processes in live animals (Weigert et al., 2010). For instance, a study focused on the role of ARAP3, an Arf6- and RhoA-GAP, in murine neutrophils studied the impact of ARAP3 loss on adhesions *in vivo* by assessing intravascular adhesion using intravital microscopy in the cremaster muscle (Gambardella et al., 2011; Rius and Sanz, 2015). Thus, the same method could be used to evaluate the adhesion capability of PI3K-C2β KI neutrophils compared to WT. However, performing intravital microscopy would only be possible as part of a collaboration given that the expertise for this is not present in our laboratory.

# 5. Bibliography

AGRAWAL, N., DASARADHI, P. V., MOHMMED, A., MALHOTRA, P., BHATNAGAR, R. K. & MUKHERJEE, S. K. 2003. RNA interference: biology, mechanism, and applications. *Microbiol Mol Biol Rev,* 67, 657-685.

AKI, S., YOSHIOKA, K., OKAMOTO, Y., TAKUWA, N. & TAKUWA, Y. 2015. Phosphatidylinositol 3-kinase class II alpha-isoform PI3K-C2alpha is required for transforming growth factor beta-induced Smad signaling in endothelial cells. *J Biol Chem,* 290, 6086-6105.

ALLIOUACHENE, S., BILANGES, B., CHAUSSADE, C., PEARCE, W., FOUKAS, L. C., SCUDAMORE, C. L., MONIZ, L. S. & VANHAESEBROECK, B. 2016. Inactivation of class II PI3K-C2alpha induces leptin resistance, age-dependent insulin resistance and obesity in male mice. *Diabetologia,* 59, 1503-1512.

ALLIOUACHENE, S., BILANGES, B., CHICANNE, G., ANDERSON, K. E., PEARCE, W., ALI, K., VALET, C., POSOR, Y., LOW, P. C., CHAUSSADE, C., SCUDAMORE, C. L., SALAMON, R. S., BACKER, J. M., STEPHENS, L., HAWKINS, P. T., PAYRASTRE, B. & VANHAESEBROECK, B. 2015. Inactivation of the Class II PI3K-C2beta Potentiates Insulin Signaling and Sensitivity. *Cell Rep,* 13, 1881-1894.

AMOS, W. B. & WHITE, J. G. 2003. How the confocal laser scanning microscope entered biological research. *Biol Cell,* 95, 335-342.

ANGERS-LOUSTAU, A., COTE, J. F., CHAREST, A., DOWBENKO, D., SPENCER, S., LASKY, L. A. & TREMBLAY, M. L. 1999. Protein tyrosine phosphatase-PEST regulates focal adhesion disassembly, migration, and cytokinesis in fibroblasts. *J Cell Biol,* 144, 1019-1031.

ARCARO, A., KHANZADA, U. K., VANHAESEBROECK, B., TETLEY, T. D., WATERFIELD, M. D. & SECKL, M. J. 2002. Two distinct phosphoinositide 3-kinases mediate polypeptide growth factor-stimulated PKB activation. *EMBO J,* 21, 5097-5108.

ARCARO, A., VOLINIA, S., ZVELEBIL, M. J., STEIN, R., WATTON, S. J., LAYTON, M. J., GOUT, I., AHMADI, K., DOWNWARD, J. & WATERFIELD, M. D. 1998. Human phosphoinositide 3-kinase C2beta, the role of calcium and the C2 domain in enzyme activity. *J Biol Chem,* 273, 33082-33090.

ARCARO, A., ZVELEBIL, M. J., WALLASCH, C., ULLRICH, A., WATERFIELD, M. D. & DOMIN, J. 2000. Class II phosphoinositide 3-kinases are downstream targets of activated polypeptide growth factor receptors. *Mol Cell Biol,* 20, 3817-3830.

ASATI, V., MAHAPATRA, D. K. & BHARTI, S. K. 2016. PI3K/Akt/mTOR and Ras/Raf/MEK/ERK signaling pathways inhibitors as anticancer agents: Structural and pharmacological perspectives. *Eur J Med Chem,* 109, 314-341.

ASKARI, J. A., BUCKLEY, P. A., MOULD, A. P. & HUMPHRIES, M. J. 2009. Linking integrin conformation to function. *J Cell Sci,* 122, 165-170.

ASSOIAN, R. K. & KLEIN, E. A. 2008. Growth control by intracellular tension and extracellular stiffness. *Trends Cell Biol,* 18, 347-352.

ATHERTON, P., STUTCHBURY, B., JETHWA, D. & BALLESTREM, C. 2016. Mechanosensitive components of integrin adhesions: Role of vinculin. *Exp Cell Res,* 343, 21-27.

BACKER, J. M. 2016. The intricate regulation and complex functions of the Class III phosphoinositide 3-kinase Vps34. *Biochem J,* 473, 2251-2271.

BAI, S., CHEN, T., DU, T., CHEN, X., LAI, Y., MA, X., WU, W., LIN, C., LIU, L. & HUANG, H. 2017. High levels of DEPDC1B predict shorter biochemical recurrence-free survival of patients with prostate cancer. *Oncol Lett,* 14, 6801-6808.

BALLA, T. 2013. Phosphoinositides: tiny lipids with giant impact on cell regulation. *Physiol Rev,* 93, 1019-1137.

BANFIC, H., VISNJIC, D., MISE, N., BALAKRISHNAN, S., DEPLANO, S., KORCHEV, Y. E. & DOMIN, J. 2009. Epidermal growth factor stimulates translocation of the class II phosphoinositide 3-kinase PI3K-C2beta to the nucleus. *Biochem J,* 422, 53-60.

BARONE, V. & HEISENBERG, C. P. 2012. Cell adhesion in embryo morphogenesis. *Curr Opin Cell Biol,* 24, 148-153.

BAYS, J. L. & DEMALI, K. A. 2017. Vinculin in cell-cell and cell-matrix adhesions. *Cell Mol Life Sci,* 74, 2999-3009.

BEHNIA, R. & MUNRO, S. 2005. Organelle identity and the signposts for membrane traffic. *Nature,* 438, 597-604.

BERGMEIER, W. & HYNES, R. O. 2012. Extracellular matrix proteins in hemostasis and thrombosis. *Cold Spring Harb Perspect Biol,* 4.

BHATT, A., KAVERINA, I., OTEY, C. & HUTTENLOCHER, A. 2002. Regulation of focal complex composition and disassembly by the calcium-dependent protease calpain. *J Cell Sci,* 115, 3415-3425.

BILANGES, B., ALLIOUACHENE, S., PEARCE, W., MORELLI, D., SZABADKAI, G., CHUNG, Y. L., CHICANNE, G., VALET, C., HILL, J. M., VOSHOL, P. J., COLLINSON, L., PEDDIE, C., ALI, K., GHAZALY, E., RAJEEVE, V., TRICHAS, G., SRINIVAS, S., CHAUSSADE, C., SALAMON, R. S., BACKER, J. M., SCUDAMORE, C. L., WHITEHEAD, M. A., KEANEY, E. P., MURPHY, L. O., SEMPLE, R. K., PAYRASTRE, B., TOOZE, S. A. & VANHAESEBROECK, B. 2017. Vps34 PI 3-kinase inactivation

enhances insulin sensitivity through reprogramming of mitochondrial metabolism. *Nat Commun,* 8, 1804.

BILANGES, B., POSOR, Y. & VANHAESEBROECK, B. 2019. PI3K isoforms in cell signalling and vesicle trafficking. *Nat Rev Mol Cell Biol,* 20(9):515-534.

BISWAS, K., YOSHIOKA, K., ASANUMA, K., OKAMOTO, Y., TAKUWA, N., SASAKI, T. & TAKUWA, Y. 2013. Essential role of class II phosphatidylinositol-3-kinase-C2alpha in sphingosine 1-phosphate receptor-1-mediated signaling and migration in endothelial cells. *J Biol Chem,* 288, 2325-2339.

BLAJECKA, K., MARINOV, M., LEITNER, L., UTH, K., POSERN, G. & ARCARO, A. 2012. Phosphoinositide 3-kinase C2beta regulates RhoA and the actin cytoskeleton through an interaction with Dbl. *PLoS One,* 7, e44945.

BOLLER, D., DOEPFNER, K. T., DE LAURENTIIS, A., GUERREIRO, A. S., MARINOV, M., SHALABY, T., DEPLEDGE, P., ROBSON, A., SAGHIR, N., HAYAKAWA, M., KAIZAWA, H., KOIZUMI, T., OHISHI, T., FATTET, S., DELATTRE, O., SCHWERI-OLAC, A., HOLAND, K., GROTZER, M. A., FREI, K., SPERTINI, O., WATERFIELD, M. D. & ARCARO, A. 2012. Targeting PI3KC2beta impairs proliferation and survival in acute leukemia, brain tumours and neuroendocrine tumours. *Anticancer Res,* 32, 3015-3027.

BOS, J. L., REHMANN, H. & WITTINGHOFER, A. 2007. GEFs and GAPs: critical elements in the control of small G proteins. *Cell,* 129, 865-877.

BRACCINI, L., CIRAOLO, E., CAMPA, C. C., PERINO, A., LONGO, D. L., TIBOLLA, G., PREGNOLATO, M., CAO, Y., TASSONE, B., DAMILANO, F., LAFFARGUE, M., CALAUTTI, E., FALASCA, M., NORATA, G. D., BACKER, J. M. & HIRSCH, E. 2015. PI3K-C2gamma is a Rab5 effector selectively controlling endosomal Akt2 activation downstream of insulin signalling. *Nat Commun,* 6, 7400.

BRIDGEWATER, R. E., NORMAN, J. C. & CASWELL, P. T. 2012. Integrin trafficking at a glance. *J Cell Sci,* 125, 3695-3701.

BRINKMANN, T., DAUMKE, O., HERBRAND, U., KUHLMANN, D., STEGE, P., AHMADIAN, M. R. & WITTINGHOFER, A. 2002. Rap-specific GTPase activating protein follows an alternative mechanism. *J Biol Chem,* 277, 12525-12531.

BROUSSARD, J. A., WEBB, D. J. & KAVERINA, I. 2008. Asymmetric focal adhesion disassembly in motile cells. *Curr Opin Cell Biol,* 20, 85-90.

BROWN, N. H., GREGORY, S. L. & MARTIN-BERMUDO, M. D. 2000. Integrins as mediators of morphogenesis in Drosophila. *Dev Biol,* 223, 1-16.

BROWN, R. A., HO, L. K., WEBER-HALL, S. J., SHIPLEY, J. M. & FRY, M. J. 1997. Identification and cDNA cloning of a novel mammalian C2 domain-containing phosphoinositide 3-kinase, HsC2-PI3K. *Biochem Biophys Res Commun,* 233, 537-544.

BURKE, J. E. 2018. Structural Basis for Regulation of Phosphoinositide Kinases and Their Involvement in Human Disease. *Mol Cell,* 71, 653-673.

BURMAN, C. & KTISTAKIS, N. T. 2010. Regulation of autophagy by phosphatidylinositol 3-phosphate. *FEBS Lett,* 584, 1302-1312.

BURRI, P. H., HLUSHCHUK, R. & DJONOV, V. 2004. Intussusceptive angiogenesis: its emergence, its characteristics, and its significance. *Dev Dyn,* 231, 474-488.

BURRIDGE, K. & GUILLUY, C. 2016. Focal adhesions, stress fibers and mechanical tension. *Exp Cell Res,* 343, 14-20.

BURRIDGE, K. & WITTCHEN, E. S. 2013. The tension mounts: stress fibers as force-generating mechanotransducers. *J Cell Biol,* 200, 9-19.

CAI, X., LIETHA, D., CECCARELLI, D. F., KARGINOV, A. V., RAJFUR, Z., JACOBSON, K., HAHN, K. M., ECK, M. J. & SCHALLER, M. D. 2008. Spatial and temporal regulation of focal adhesion kinase activity in living cells. *Mol Cell Biol,* 28, 201-214.

CAI, X., SRIVASTAVA, S., SUN, Y., LI, Z., WU, H., ZUVELA-JELASKA, L., LI, J., SALAMON, R. S., BACKER, J. M. & SKOLNIK, E. Y. 2011. Tripartite motif containing protein 27 negatively regulates CD4 T cells by ubiquitinating and inhibiting the class II PI3K-C2beta. *Proc Natl Acad Sci U S A,* 108, 20072-20077.

CAMPA, C. C., MARGARIA, J. P., DERLE, A., DEL GIUDICE, M., DE SANTIS, M. C., GOZZELINO, L., COPPERI, F., BOSIA, C. & HIRSCH, E. 2018. Rab11 activity and PtdIns(3)P turnover removes recycling cargo from endosomes. *Nat Chem Biol,* 14, 801-810.

CARRAGHER, N. O., LEVKAU, B., ROSS, R. & RAINES, E. W. 1999. Degraded collagen fragments promote rapid disassembly of smooth muscle focal adhesions that correlates with cleavage of pp125(FAK), paxillin, and talin. *J Cell Biol,* 147, 619-630.

CASARES, D., ESCRIBA, P. V. & ROSSELLO, C. A. 2019. Membrane Lipid Composition: Effect on Membrane and Organelle Structure, Function and Compartmentalization and Therapeutic Avenues. *Int J Mol Sci,* 20, 2167

CASE, L. B., BAIRD, M. A., SHTENGEL, G., CAMPBELL, S. L., HESS, H. F., DAVIDSON, M. W. & WATERMAN, C. M. 2015. Molecular mechanism of vinculin activation and nanoscale spatial organization in focal adhesions. *Nat Cell Biol,* 17, 880-892.

CHAN, K. T., BENNIN, D. A. & HUTTENLOCHER, A. 2010. Regulation of adhesion dynamics by calpain-mediated proteolysis of focal adhesion kinase (FAK). *J Biol Chem,* 285, 11418-11426.

CHAN, K. T., CORTESIO, C. L. & HUTTENLOCHER, A. 2009. FAK alters invadopodia and focal adhesion composition and dynamics to regulate breast cancer invasion. *J Cell Biol,* 185, 357-370.

CHAO, W. T., ASHCROFT, F., DAQUINAG, A. C., VADAKKAN, T., WEI, Z., ZHANG, P., DICKINSON, M. E. & KUNZ, J. 2010. Type I phosphatidylinositol phosphate kinase beta regulates focal adhesion disassembly by promoting beta1 integrin endocytosis. *Mol Cell Biol,* 30, 4463-4479.

CHAO, W. T. & KUNZ, J. 2009. Focal adhesion disassembly requires clathrin-dependent endocytosis of integrins. *FEBS Lett,* 583, 1337-1343.

CHEN, L., XU, B., LIU, L., LIU, C., LUO, Y., CHEN, X., BARZEGAR, M., CHUNG, J. & HUANG, S. 2015. Both mTORC1 and mTORC2 are involved in the regulation of cell adhesion. *Oncotarget,* 6, 7136-7150.

CHENGAPPA, P., SAO, K., JONES, T. M. & PETRIE, R. J. 2018. Intracellular Pressure: A Driver of Cell Morphology and Movement. *Int Rev Cell Mol Biol,* 337, 185-211.

CHIKH, A., FERRO, R., ABBOTT, J. J., PINEIRO, R., BUUS, R., IEZZI, M., RICCI, F., BERGAMASCHI, D., OSTANO, P., CHIORINO, G., LATTANZIO, R., BROGGINI, M., PIANTELLI, M., MAFFUCCI, T. & FALASCA, M. 2016. Class II phosphoinositide 3-kinase C2beta regulates a novel signaling pathway involved in breast cancer progression. *Oncotarget,* 7(14):18325-45.

CHINTHALAPUDI, K., RANGARAJAN, E. S., PATIL, D. N., GEORGE, E. M., BROWN, D. T. & IZARD, T. 2014. Lipid binding promotes oligomerization and focal adhesion activity of vinculin. *J Cell Biol,* 207, 643-656.

CIRAOLO, E., MORELLO, F. & HIRSCH, E. 2011. Present and future of PI3K pathway inhibition in cancer: perspectives and limitations. *Curr Med Chem,* 18, 2674-2685.

COMBS, C. A. & SHROFF, H. 2017. Fluorescence Microscopy: A Concise Guide to Current Imaging Methods. *Curr Protoc Neurosci,* 79, 2 1 1-2 1 25.

CONCHELLO, J. A. & LICHTMAN, J. W. 2005. Optical sectioning microscopy. *Nat Methods,* 2, 920-931.

CONSONNI, S. V., MAURICE, M. M. & BOS, J. L. 2014. DEP domains: structurally similar but functionally different. *Nat Rev Mol Cell Biol,* 15, 357-362.

CORTESIO, C. L., BOATENG, L. R., PIAZZA, T. M., BENNIN, D. A. & HUTTENLOCHER, A. 2011. Calpain-mediated proteolysis of paxillin negatively regulates focal adhesion dynamics and cell migration. *J Biol Chem,* 286, 9998-10006.

CORY, G. 2011. Scratch-wound assay. *Methods Mol Biol,* 769, 25-30.

COURTNEY, K. D., CORCORAN, R. B. & ENGELMAN, J. A. 2010. The PI3K pathway as drug target in human cancer. *J Clin Oncol,* 28, 1075-1083.

CRLJEN, V., VOLINIA, S. & BANFIC, H. 2002. Hepatocyte growth factor activates phosphoinositide 3-kinase C2 beta in renal brush-border plasma membranes. *Biochem J,* 365, 791-799.

CROSS, D. A., ALESSI, D. R., COHEN, P., ANDJELKOVICH, M. & HEMMINGS, B. A. 1995. Inhibition of glycogen synthase kinase-3 by insulin mediated by protein kinase B. *Nature,* 378, 785-789.

DANA, H., CHALBATANI, G. M., MAHMOODZADEH, H., KARIMLOO, R., REZAIEAN, O., MORADZADEH, A., MEHMANDOOST, N., MOAZZEN, F., MAZRAEH, A., MARMARI, V., EBRAHIMI, M., RASHNO, M. M., ABADI, S. J. & GHARAGOUZLO, E. 2017. Molecular Mechanisms and Biological Functions of siRNA. *Int J Biomed Sci,* 13, 48-57.

DAS, M., SCAPPINI, E., MARTIN, N. P., WONG, K. A., DUNN, S., CHEN, Y. J., MILLER, S. L., DOMIN, J. & O'BRYAN, J. P. 2007. Regulation of neuron survival through an intersectin-phosphoinositide 3'-kinase C2beta-AKT pathway. *Mol Cell Biol,* 27, 7906-7917.

DE CRAENE, J. O., BERTAZZI, D. L., BAR, S. & FRIANT, S. 2017. Phosphoinositides, Major Actors in Membrane Trafficking and Lipid Signaling Pathways. *Int J Mol Sci,* 18 634,

DE FRANCESCHI, N., HAMIDI, H., ALANKO, J., SAHGAL, P. & IVASKA, J. 2015. Integrin traffic - the update. *J Cell Sci,* 128, 839-852.

DE MATTEIS, M. A. & GODI, A. 2004. PI-loting membrane traffic. *Nat Cell Biol,* 6, 487-492.

DENLEY, A., KANG, S., KARST, U. & VOGT, P. K. 2008. Oncogenic signaling of class I PI3K isoforms. *Oncogene,* 27, 2561-2574.

DI PAOLO, G. & DE CAMILLI, P. 2006. Phosphoinositides in cell regulation and membrane dynamics. *Nature,* 443, 651-657.

DIOUF, B., CHENG, Q., KRYNETSKAIA, N. F., YANG, W., CHEOK, M., PEI, D., FAN, Y., CHENG, C., KRYNETSKIY, E. Y., GENG, H., CHEN, S., THIERFELDER, W. E., MULLIGHAN, C. G., DOWNING, J. R., HSIEH, P., PUI, C. H., RELLING, M. V. &

EVANS, W. E. 2011. Somatic deletions of genes regulating MSH2 protein stability cause DNA mismatch repair deficiency and drug resistance in human leukemia cells. *Nat Med,* 17, 1298-1303.

DOMIN, J., GAIDAROV, I., SMITH, M. E., KEEN, J. H. & WATERFIELD, M. D. 2000. The class II phosphoinositide 3-kinase PI3K-C2alpha is concentrated in the trans-Golgi network and present in clathrin-coated vesicles. *J Biol Chem,* 275, 11943-11950.

DOMIN, J., HARPER, L., AUBYN, D., WHEELER, M., FLOREY, O., HASKARD, D., YUAN, M. & ZICHA, D. 2005. The class II phosphoinositide 3-kinase PI3K-C2beta regulates cell migration by a PtdIns3P dependent mechanism. *J Cell Physiol,* 205, 452-462.

DOMIN, J., PAGES, F., VOLINIA, S., RITTENHOUSE, S. E., ZVELEBIL, M. J., STEIN, R. C. & WATERFIELD, M. D. 1997. Cloning of a human phosphoinositide 3-kinase with a C2 domain that displays reduced sensitivity to the inhibitor wortmannin. *Biochem J,* 326 ( Pt 1), 139-147.

DORNAN, G. L. & BURKE, J. E. 2018. Molecular Mechanisms of Human Disease Mediated by Oncogenic and Primary Immunodeficiency Mutations in Class IA Phosphoinositide 3-Kinases. *Front Immunol,* 9, 575.

DOURDIN, N., BHATT, A. K., DUTT, P., GREER, P. A., ARTHUR, J. S., ELCE, J. S. & HUTTENLOCHER, A. 2001. Reduced cell migration and disruption of the actin cytoskeleton in calpain-deficient embryonic fibroblasts. *J Biol Chem,* 276, 48382-48388.

DOZYNKIEWICZ, M. A., JAMIESON, N. B., MACPHERSON, I., GRINDLAY, J., VAN DEN BERGHE, P. V., VON THUN, A., MORTON, J. P., GOURLEY, C., TIMPSON, P., NIXON, C., MCKAY, C. J., CARTER, R., STRACHAN, D., ANDERSON, K., SANSOM, O. J., CASWELL, P. T. & NORMAN, J. C. 2012. Rab25 and CLIC3 collaborate to promote integrin recycling from late endosomes/lysosomes and drive cancer progression. *Dev Cell,* 22, 131-145.

DURAND, N., BASTEA, L. I., LONG, J., DOPPLER, H., LING, K. & STORZ, P. 2016. Protein Kinase D1 regulates focal adhesion dynamics and cell adhesion through Phosphatidylinositol-4-phosphate 5-kinase type-I gamma. *Sci Rep,* 6, 35963.

EZRATTY, E. J., BERTAUX, C., MARCANTONIO, E. E. & GUNDERSEN, G. G. 2009. Clathrin mediates integrin endocytosis for focal adhesion disassembly in migrating cells. *J Cell Biol,* 187, 733-747.

EZRATTY, E. J., PARTRIDGE, M. A. & GUNDERSEN, G. G. 2005. Microtubule-induced focal adhesion disassembly is mediated by dynamin and focal adhesion kinase. *Nat Cell Biol,* 7, 581-590.

FALASCA, M., HAMILTON, J. R., SELVADURAI, M., SUNDARAM, K., ADAMSKA, A. & THOMPSON, P. E. 2017. Class II Phosphoinositide 3-Kinases as Novel Drug Targets. *J Med Chem,* 60, 47-65.

FALASCA, M. & MAFFUCCI, T. 2012. Regulation and cellular functions of class II phosphoinositide 3-kinases. *Biochem J,* 443, 587-601.

FAUCHERRE, A., DESBOIS, P., SATRE, V., LUNARDI, J., DORSEUIL, O. & GACON, G. 2003. Lowe syndrome protein OCRL1 interacts with Rac GTPase in the trans-Golgi network. *Hum Mol Genet,* 12, 2449-2456.

FEUTLINSKE, F., BROWARSKI, M., KU, M. C., TRNKA, P., WAICZIES, S., NIENDORF, T., STALLCUP, W. B., GLASS, R., KRAUSE, E. & MARITZEN, T. 2015. Stonin1 mediates endocytosis of the proteoglycan NG2 and regulates focal adhesion dynamics and cell motility. *Nat Commun,* 6, 8535.

FINCHAM, V. J. & FRAME, M. C. 1998. The catalytic activity of Src is dispensable for translocation to focal adhesions but controls the turnover of these structures during cell motility. *EMBO J,* 17, 81-92.

FLEVARIS, P., STOJANOVIC, A., GONG, H., CHISHTI, A., WELCH, E. & DU, X. 2007. A molecular switch that controls cell spreading and retraction. *J Cell Biol,* 179, 553-565.

FRANCO, C. A., JONES, M. L., BERNABEU, M. O., GEUDENS, I., MATHIVET, T., ROSA, A., LOPES, F. M., LIMA, A. P., RAGAB, A., COLLINS, R. T., PHNG, L. K., COVENEY, P. V. & GERHARDT, H. 2015. Dynamic endothelial cell rearrangements drive developmental vessel regression. *PLoS Biol,* 13, e1002125.

FRANCO, I., GULLUNI, F., CAMPA, C. C., COSTA, C., MARGARIA, J. P., CIRAOLO, E., MARTINI, M., MONTEYNE, D., DE LUCA, E., GERMENA, G., POSOR, Y., MAFFUCCI, T., MARENGO, S., HAUCKE, V., FALASCA, M., PEREZ-MORGA, D., BOLETTA, A., MERLO, G. R. & HIRSCH, E. 2014. PI3K class II alpha controls spatially restricted endosomal PtdIns3P and Rab11 activation to promote primary cilium function. *Dev Cell,* 28, 647-658.

FRANCO, I., MARGARIA, J. P., DE SANTIS, M. C., RANGHINO, A., MONTEYNE, D., CHIARAVALLI, M., PEMA, M., CAMPA, C. C., RATTO, E., GULLUNI, F., PEREZ-MORGA, D., SOMLO, S., MERLO, G. R., BOLETTA, A. & HIRSCH, E. 2016. Phosphoinositide 3-Kinase-C2alpha Regulates Polycystin-2 Ciliary Entry and Protects against Kidney Cyst Formation. *J Am Soc Nephrol,* 27, 1135-1144.

FRANCO, S. J. & HUTTENLOCHER, A. 2005. Regulating cell migration: calpains make the cut. *J Cell Sci,* 118, 3829-3838.

FRANCO, S. J., RODGERS, M. A., PERRIN, B. J., HAN, J., BENNIN, D. A., CRITCHLEY, D. R. & HUTTENLOCHER, A. 2004. Calpain-mediated proteolysis of talin regulates adhesion dynamics. *Nat Cell Biol,* 6, 977-983.

FRUMAN, D. A., CHIU, H., HOPKINS, B. D., BAGRODIA, S., CANTLEY, L. C. & ABRAHAM, R. T. 2017. The PI3K Pathway in Human Disease. *Cell,* 170, 605-635.

FRUMAN, D. A. & ROMMEL, C. 2014. PI3K and cancer: lessons, challenges and opportunities. *Nat Rev Drug Discov,* 13, 140-156.

FUKUMOTO, M., IJUIN, T. & TAKENAWA, T. 2017. PI(3,4)P2 plays critical roles in the regulation of focal adhesion dynamics of MDA-MB-231 breast cancer cells. *Cancer Sci,* 108, 941-951.

GAIDAROV, I., SMITH, M. E., DOMIN, J. & KEEN, J. H. 2001. The class II phosphoinositide 3-kinase C2alpha is activated by clathrin and regulates clathrin-mediated membrane trafficking. *Mol Cell,* 7, 443-449.

GAMBARDELLA, L., ANDERSON, K. E., NUSSBAUM, C., SEGONDS-PICHON, A., MARGARIDO, T., NORTON, L., LUDWIG, T., SPERANDIO, M., HAWKINS, P. T., STEPHENS, L. & VERMEREN, S. 2011. The GTPase-activating protein ARAP3 regulates chemotaxis and adhesion-dependent processes in neutrophils. *Blood,* 118, 1087-1098.

GARCIA-MATA, R. 2014. Arrested detachment: a DEPDC1B-mediated de-adhesion mitotic checkpoint. *Dev Cell,* 31, 387-389.

GEIGER, B., BERSHADSKY, A., PANKOV, R. & YAMADA, K. M. 2001. Transmembrane crosstalk between the extracellular matrix--cytoskeleton crosstalk. *Nat Rev Mol Cell Biol,* 2, 793-805.

GIANNONE, G., RONDE, P., GAIRE, M., BEAUDOUIN, J., HAIECH, J., ELLENBERG, J. & TAKEDA, K. 2004. Calcium rises locally trigger focal adhesion disassembly and enhance residency of focal adhesion kinase at focal adhesions. *J Biol Chem,* 279, 28715-28723.

GILLOOLY, D. J., MORROW, I. C., LINDSAY, M., GOULD, R., BRYANT, N. J., GAULLIER, J. M., PARTON, R. G. & STENMARK, H. 2000. Localization of phosphatidylinositol 3-phosphate in yeast and mammalian cells. *EMBO J,* 19, 4577-4588.

GLADING, A., CHANG, P., LAUFFENBURGER, D. A. & WELLS, A. 2000. Epidermal growth factor receptor activation of calpain is required for fibroblast motility and occurs via an ERK/MAP kinase signaling pathway. *J Biol Chem,* 275, 2390-2398.

GLADING, A., LAUFFENBURGER, D. A. & WELLS, A. 2002. Cutting to the chase: calpain proteases in cell motility.*Trends Cell Biol,* 12, 46-54.

GOUGH, R. E. & GOULT, B. T. 2018. The tale of two talins - two isoforms to fine-tune integrin signalling. *FEBS Lett,* 592, 2108-2125.

GOULT, B. T., YAN, J. & SCHWARTZ, M. A. 2018. Talin as a mechanosensitive signaling hub. *J Cell Biol,* 217, 3776-3784.

GULLUNI, F., DE SANTIS, M. C., MARGARIA, J. P., MARTINI, M. & HIRSCH, E. 2019. Class II PI3K Functions in Cell Biology and Disease. *Trends Cell Biol,* 29, 339-359.

GULLUNI, F., MARTINI, M., DE SANTIS, M. C., CAMPA, C. C., GHIGO, A., MARGARIA, J. P., CIRAOLO, E., FRANCO, I., ALA, U., ANNARATONE, L., DISALVATORE, D., BERTALOT, G., VIALE, G., NOATYNSKA, A., COMPAGNO, M., SIGISMUND, S., MONTEMURRO, F., THELEN, M., FAN, F., MERALDI, P., MARCHIO, C., PECE, S., SAPINO, A., CHIARLE, R., DI FIORE, P. P. & HIRSCH, E. 2017. Mitotic Spindle Assembly and Genomic Stability in Breast Cancer Require PI3K-C2alpha Scaffolding Function. *Cancer Cell,* 32, 444-459 e447.

GWINN, D. M., SHACKELFORD, D. B., EGAN, D. F., MIHAYLOVA, M. M., MERY, A., VASQUEZ, D. S., TURK, B. E. & SHAW, R. J. 2008. AMPK phosphorylation of raptor mediates a metabolic checkpoint. *Mol Cell,* 30, 214-226.

HAAGE, A., GOODWIN, K., WHITEWOOD, A., CAMP, D., BOGUTZ, A., TURNER, C. T., GRANVILLE, D. J., LEFEBVRE, L., PLOTNIKOV, S., GOULT, B. T. & TANENTZAPF, G. 2018. Talin Autoinhibition Regulates Cell-ECM Adhesion Dynamics and Wound Healing In Vivo. *Cell Rep,* 25, 2401-2416 e2405.

HARADA, K., TRUONG, A. B., CAI, T. & KHAVARI, P. A. 2005. The class II phosphoinositide 3-kinase C2beta is not essential for epidermal differentiation. *Mol Cell Biol,* 25, 11122-11130.

HAWKINS, P. T. & STEPHENS, L. R. 2016. Emerging evidence of signalling roles for PI(3,4)P2 in Class I and II PI3K-regulated pathways. *Biochem Soc Trans,* 44, 307-314.

HEMMINGS, B. A. & RESTUCCIA, D. F. 2012. PI3K-PKB/Akt pathway.*Cold Spring Harb Perspect Biol,* 4, a011189.

HO, L. K., LIU, D., ROZYCKA, M., BROWN, R. A. & FRY, M. J. 1997. Identification of four novel human phosphoinositide 3-kinases defines a multi-isoform subfamily. *Biochem Biophys Res Commun,* 235, 130-137.

HODGE, R. G. & RIDLEY, A. J. 2016. Regulating Rho GTPases and their regulators.*Nat Rev Mol Cell Biol,* 17, 496-510.

HOHENESTER, E. 2014. Signalling complexes at the cell-matrix interface. *Curr Opin Struct Biol,* 29, 10-16.

HOTULAINEN, P. & LAPPALAINEN, P. 2006. Stress fibers are generated by two distinct actin assembly mechanisms in motile cells. *J Cell Biol,* 173, 383-394.

HUMPHRIES, J. D., WANG, P., STREULI, C., GEIGER, B., HUMPHRIES, M. J. & BALLESTREM, C. 2007. Vinculin controls focal adhesion formation by direct interactions with talin and actin. *J Cell Biol,* 179, 1043-1057.

HUNTER, M. P., RUSSO, A. & O'BRYAN, J. P. 2013. Emerging roles for intersectin (ITSN) in regulating signaling and disease pathways. *Int J Mol Sci,* 14, 7829-7852.

HUTTENLOCHER, A. & HORWITZ, A. R. 2011. Integrins in cell migration. *Cold Spring Harb Perspect Biol,* 3, a005074.

ILIC, D., FURUTA, Y., KANAZAWA, S., TAKEDA, N., SOBUE, K., NAKATSUJI, N., NOMURA, S., FUJIMOTO, J., OKADA, M. & YAMAMOTO, T. 1995. Reduced cell motility and enhanced focal adhesion contact formation in cells from FAK-deficient mice. *Nature,* 377, 539-544.

JANKU, F., YAP, T. A. & MERIC-BERNSTAM, F. 2018. Targeting the PI3K pathway in cancer: are we making headway? *Nat Rev Clin Oncol,* 15, 273-291.

KANCHANAWONG, P., SHTENGEL, G., PASAPERA, A. M., RAMKO, E. B., DAVIDSON, M. W., HESS, H. F. & WATERMAN, C. M. 2010. Nanoscale architecture of integrin-based cell adhesions. *Nature,* 468, 580-584.

KANTETI, R., BATRA, S. K., LENNON, F. E. & SALGIA, R. 2016. FAK and paxillin, two potential targets in pancreatic cancer.*Oncotarget,* 7, 31586-31601.

KASSIANIDOU, E. & KUMAR, S. 2015. A biomechanical perspective on stress fiber structure and function.*Biochim Biophys Acta,* 1853, 3065-3074.

KATSO, R. M., PARDO, O. E., PALAMIDESSI, A., FRANZ, C. M., MARINOV, M., DE LAURENTIIS, A., DOWNWARD, J., SCITA, G., RIDLEY, A. J., WATERFIELD, M. D. & ARCARO, A. 2006. Phosphoinositide 3-Kinase C2beta regulates cytoskeletal organization and cell migration via Rac-dependent mechanisms. *Mol Biol Cell,* 17, 3729-3744.

KAUR, J. & DEBNATH, J. 2015. Autophagy at the crossroads of catabolism and anabolism. *Nat Rev Mol Cell Biol,* 16, 461-472.

KAVERINA, I., KRYLYSHKINA, O. & SMALL, J. V. 1999. Microtubule targeting of substrate contacts promotes their relaxation and dissociation. *J Cell Biol,* 146, 1033-1044.

KAVERINA, I., ROTTNER, K. & SMALL, J. V. 1998. Targeting, capture, and stabilization of microtubules at early focal adhesions. *J Cell Biol,* 142, 181-190.

KENIFIC, C. M., STEHBENS, S. J., GOLDSMITH, J., LEIDAL, A. M., FAURE, N., YE, J., WITTMANN, T. & DEBNATH, J. 2016a. NBR1 enables autophagy-dependent focal adhesion turnover. *J Cell Biol,* 212, 577-590.

KENIFIC, C. M., WITTMANN, T. & DEBNATH, J. 2016b. Autophagy in adhesion and migration. *J Cell Sci,* 129, 3685-3693.

KITATANI, K., USUI, T., SRIRAMAN, S. K., TOYOSHIMA, M., ISHIBASHI, M., SHIGETA, S., NAGASE, S., SAKAMOTO, M., OGISO, H., OKAZAKI, T., HANNUN, Y. A., TORCHILIN, V. P. & YAEGASHI, N. 2015. Ceramide limits phosphatidylinositol-3-kinase C2beta-controlled cell motility in ovarian cancer: potential of ceramide as a metastasis-suppressor lipid. *Oncogene,* 35(21):2801-12.

KLAPHOLZ, B. & BROWN, N. H. 2017. Talin - the master of integrin adhesions. *J Cell Sci,* 130, 2435-2446.

KLINGHOFFER, R. A., SACHSENMAIER, C., COOPER, J. A. & SORIANO, P. 1999. Src family kinases are required for integrin but not PDGFR signal transduction. *EMBO J,* 18, 2459-2471.

KNOBBE, C. B. & REIFENBERGER, G. 2003. Genetic alterations and aberrant expression of genes related to the phosphatidyl-inositol-3'-kinase/protein kinase B (Akt) signal transduction pathway in glioblastomas. *Brain Pathol,* 13, 507-518.

KOMADA, M. & SORIANO, P. 1999. Hrs, a FYVE finger protein localized to early endosomes, is implicated in vesicular traffic and required for ventral folding morphogenesis. *Genes Dev,* 13, 1475-1485.

KOROLCHUK, V. I., SAIKI, S., LICHTENBERG, M., SIDDIQI, F. H., ROBERTS, E. A., IMARISIO, S., JAHREISS, L., SARKAR, S., FUTTER, M., MENZIES, F. M., O'KANE, C. J., DERETIC, V. & RUBINSZTEIN, D. C. 2011. Lysosomal positioning coordinates cellular nutrient responses. *Nat Cell Biol,* 13, 453-460.

KOUTROS, S., SCHUMACHER, F. R., HAYES, R. B., MA, J., HUANG, W. Y., ALBANES, D., CANZIAN, F., CHANOCK, S. J., CRAWFORD, E. D., DIVER, W. R., FEIGELSON, H. S., GIOVANUCCI, E., HAIMAN, C. A., HENDERSON, B. E., HUNTER, D. J., KAAKS, R., KOLONEL, L. N., KRAFT, P., LE MARCHAND, L., RIBOLI, E., SIDDIQ, A., STAMPFER, M. J., STRAM, D. O., THOMAS, G., TRAVIS, R. C., THUN, M. J., YEAGER, M. & BERNDT, S. I. 2010. Pooled analysis of phosphatidylinositol 3-kinase pathway variants and risk of prostate cancer. *Cancer Res,* 70, 2389-2396.

KRAUSE, M., LESLIE, J. D., STEWART, M., LAFUENTE, E. M., VALDERRAMA, F., JAGANNATHAN, R., STRASSER, G. A., RUBINSON, D. A., LIU, H., WAY, M., YAFFE, M. B., BOUSSIOTIS, V. A. & GERTLER, F. B. 2004. Lamellipodin, an Ena/VASP ligand, is implicated in the regulation of lamellipodial dynamics. *Dev Cell,* 7, 571-583.

KRAUSS, M. & HAUCKE, V. 2007. Phosphoinositide-metabolizing enzymes at the interface between membrane traffic and cell signalling. *EMBO Rep,* 8, 241-246.

KTISTAKIS, N. T. & TOOZE, S. A. 2016a. Digesting the Expanding Mechanisms of Autophagy.*Trends Cell Biol*.

KTISTAKIS, N. T. & TOOZE, S. A. 2016b. Digesting the Expanding Mechanisms of Autophagy.*Trends Cell Biol,* 26, 624-635.

LAKETA, V., ZARBAKHSH, S., MORBIER, E., SUBRAMANIAN, D., DINKEL, C., BRUMBAUGH, J., ZIMMERMANN, P., PEPPERKOK, R. & SCHULTZ, C. 2009. Membrane-permeant phosphoinositide derivatives as modulators of growth factor signaling and neurite outgrowth. *Chem Biol,* 16, 1190-1196.

LAPLANTE, M. & SABATINI, D. M. 2009. mTOR signaling at a glance. *J Cell Sci,* 122, 3589-3594.

LAUFFENBURGER, D. A. & HORWITZ, A. F. 1996. Cell migration: a physically integrated molecular process. *Cell,* 84, 359-369.

LAWSON, C. D. & RIDLEY, A. J. 2018. Rho GTPase signaling complexes in cell migration and invasion. *J Cell Biol,* 217, 447-457.

LE CLAINCHE, C. & CARLIER, M. F. 2008. Regulation of actin assembly associated with protrusion and adhesion in cell migration. *Physiol Rev,* 88, 489-513.

LEE, Y. R., CHEN, M. & PANDOLFI, P. P. 2018. The functions and regulation of the PTEN tumour suppressor: new modes and prospects. *Nat Rev Mol Cell Biol,* 19, 547-562.

LEGATE, K. R., WICKSTROM, S. A. & FASSLER, R. 2009. Genetic and cell biological analysis of integrin outside-in signaling. *Genes Dev,* 23, 397-418.

LELOUP, L., SHAO, H., BAE, Y. H., DEASY, B., STOLZ, D., ROY, P. & WELLS, A. 2010. m-Calpain activation is regulated by its membrane localization and by its binding to phosphatidylinositol 4,5-bisphosphate. *J Biol Chem,* 285, 33549-33566.

LEMMON, M. A. 2008. Membrane recognition by phospholipid-binding domains. *Nat Rev Mol Cell Biol,* 9, 99-111.

LEONARD, D. A., LIN, R., CERIONE, R. A. & MANOR, D. 1998. Biochemical studies of the mechanism of action of the Cdc42-GTPase-activating protein. *J Biol Chem,* 273, 16210-16215.

LIANG, J., ZUBOVITZ, J., PETROCELLI, T., KOTCHETKOV, R., CONNOR, M. K., HAN, K., LEE, J. H., CIARALLO, S., CATZAVELOS, C., BENISTON, R., FRANSSEN, E. & SLINGERLAND, J. M. 2002. PKB/Akt phosphorylates p27, impairs nuclear import of p27 and opposes p27-mediated G1 arrest. *Nat Med,* 8, 1153-1160.

LIAO, Z., WANG, X., ZENG, Y. & ZOU, Q. 2016. Identification of DEP domain-containing proteins by a machine learning method and experimental analysis of their expression in human HCC tissues. *Sci Rep,* 6, 39655.

LIU, L., CHEN, L., CHUNG, J. & HUANG, S. 2008. Rapamycin inhibits F-actin reorganization and phosphorylation of focal adhesion proteins. *Oncogene,* 27, 4998-5010.

LIU, L., LI, F., CARDELLI, J. A., MARTIN, K. A., BLENIS, J. & HUANG, S. 2006. Rapamycin inhibits cell motility by suppression of mTOR-mediated S6K1 and 4E-BP1 pathways. *Oncogene,* 25, 7029-7040.

LIU, P., CHENG, H., ROBERTS, T. M. & ZHAO, J. J. 2009. Targeting the phosphoinositide 3-kinase pathway in cancer. *Nat Rev Drug Discov,* 8, 627-644.

LIU, P., MORRISON, C., WANG, L., XIONG, D., VEDELL, P., CUI, P., HUA, X., DING, F., LU, Y., JAMES, M., EBBEN, J. D., XU, H., ADJEI, A. A., HEAD, K., ANDRAE, J. W., TSCHANNEN, M. R., JACOB, H., PAN, J., ZHANG, Q., VAN DEN BERGH, F., XIAO, H., LO, K. C., PATEL, J., RICHMOND, T., WATT, M. A., ALBERT, T., SELZER, R., ANDERSON, M., WANG, J., WANG, Y., STARNES, S., YANG, P. & YOU, M. 2012. Identification of somatic mutations in non-small cell lung carcinomas using whole-exome sequencing. *Carcinogenesis,* 33, 1270-1276.

LIU, Z., SUN, C., ZHANG, Y., JI, Z. & YANG, G. 2011. Phosphatidylinositol 3-kinase-C2beta inhibits cisplatin-mediated apoptosis via the Akt pathway in oesophageal squamous cell carcinoma. *J Int Med Res,* 39, 1319-1332.

LIVNE, A. & GEIGER, B. 2016. The inner workings of stress fibers - from contractile machinery to focal adhesions and back. *J Cell Sci,* 129, 1293-1304.

LOW, S., VOUGIOUKAS, V. I., HIELSCHER, T., SCHMIDT, U., UNTERBERG, A. & HALATSCH, M. E. 2008. Pathogenetic pathways leading to glioblastoma multiforme: association between gene expressions and resistance to erlotinib. *Anticancer Res,* 28, 3729-3732.

LU, N., SHEN, Q., MAHONEY, T. R., NEUKOMM, L. J., WANG, Y. & ZHOU, Z. 2012. Two PI 3-kinases and one PI 3-phosphatase together establish the cyclic waves of phagosomal PtdIns(3)P critical for the degradation of apoptotic cells. *PLoS Biol,* 10, e1001245.

LUO, B. H., CARMAN, C. V. & SPRINGER, T. A. 2007. Structural basis of integrin regulation and signaling. *Annu Rev Immunol,* 25, 619-647.

MA, X. M. & BLENIS, J. 2009. Molecular mechanisms of mTOR-mediated translational control. *Nat Rev Mol Cell Biol,* 10, 307-318.

MACDOUGALL, L. K., DOMIN, J. & WATERFIELD, M. D. 1995. A family of phosphoinositide 3-kinases in Drosophila identifies a new mediator of signal transduction. *Curr Biol,* 5, 1404-1415.

MAFFUCCI, T., COOKE, F. T., FOSTER, F. M., TRAER, C. J., FRY, M. J. & FALASCA, M. 2005. Class II phosphoinositide 3-kinase defines a novel signaling pathway in cell migration. *J Cell Biol,* 169, 789-799.

MAFFUCCI, T. & FALASCA, M. 2014. New insight into the intracellular roles of class II phosphoinositide 3-kinases. *Biochem Soc Trans,* 42, 1378-1382.

MALECZ, N., MCCABE, P. C., SPAARGAREN, C., QIU, R., CHUANG, Y. & SYMONS, M. 2000. Synaptojanin 2, a novel Rac1 effector that regulates clathrin-mediated endocytosis. *Curr Biol,* 10, 1383-1386.

MALEK, M., KIELKOWSKA, A., CHESSA, T., ANDERSON, K. E., BARNEDA, D., PIR, P., NAKANISHI, H., EGUCHI, S., KOIZUMI, A., SASAKI, J., JUVIN, V., KISELEV, V. Y., NIEWCZAS, I., GRAY, A., VALAYER, A., SPENSBERGER, D., IMBERT, M., FELISBINO, S., HABUCHI, T., BEINKE, S., COSULICH, S., LE NOVERE, N., SASAKI, T., CLARK, J., HAWKINS, P. T. & STEPHENS, L. R. 2017. PTEN Regulates PI(3,4)P2 Signaling Downstream of Class I PI3K. *Mol Cell,* 68, 566-580 e510.

MANAKAN BETSY SRICHAI, R. Z., AMBRA POZZI 2010. *Cell-Extracellular Matrix Interactions in Cancer, Chapter 2: Integrin Structure and Function,* New York, Springer New York.

MARAT, A. L. & HAUCKE, V. 2016. Phosphatidylinositol 3-phosphates-at the interface between cell signalling and membrane traffic. *EMBO J,* 35, 561-579.

MARAT, A. L., WALLROTH, A., LO, W. T., MULLER, R., NORATA, G. D., FALASCA, M., SCHULTZ, C. & HAUCKE, V. 2017. mTORC1 activity repression by late endosomal phosphatidylinositol 3,4-bisphosphate. *Science,* 356, 968-972.

MARCHESI, S., MONTANI, F., DEFLORIAN, G., D'ANTUONO, R., CUOMO, A., BOLOGNA, S., MAZZOCCOLI, C., BONALDI, T., DI FIORE, P. P. & NICASSIO, F. 2014. DEPDC1B coordinates de-adhesion events and cell-cycle progression at mitosis. *Dev Cell,* 31, 420-433.

MARGARIA, J. P., RATTO, E., GOZZELINO, L., LI, H. & HIRSCH, E. 2019. Class II PI3Ks at the Intersection between Signal Transduction and Membrane Trafficking. *Biomolecules,* 9, 104.

MARITZEN, T., SCHACHTNER, H. & LEGLER, D. F. 2015. On the move: endocytic trafficking in cell migration. *Cell Mol Life Sci,* 72, 2119-2134.

MARWAHA, R., ARYA, S. B., JAGGA, D., KAUR, H., TULI, A. & SHARMA, M. 2017. The Rab7 effector PLEKHM1 binds Arl8b to promote cargo traffic to lysosomes. *J Cell Biol,* 216, 1051-1070.

MAVROMMATI, I., CISSE, O., FALASCA, M. & MAFFUCCI, T. 2016. Novel roles for class II Phosphoinositide 3-Kinase C2beta in signalling pathways involved in prostate cancer cell invasion. *Sci Rep,* 6, 23277.

MCLEAN, G. W., CARRAGHER, N. O., AVIZIENYTE, E., EVANS, J., BRUNTON, V. G. & FRAME, M. C. 2005. The role of focal-adhesion kinase in cancer - a new therapeutic opportunity. *Nat Rev Cancer,* 5, 505-515.

MCMAHON, H. T. & BOUCROT, E. 2011. Molecular mechanism and physiological functions of clathrin-mediated endocytosis. *Nat Rev Mol Cell Biol,* 12, 517-533.

MENDOZA, P. A., SILVA, P., DIAZ, J., ARRIAGADA, C., CANALES, J., CERDA, O. & TORRES, V. A. 2018. Calpain2 mediates Rab5-driven focal adhesion disassembly and cell migration. *Cell Adh Migr,* 12, 185-194.

MISAWA, H., OHTSUBO, M., COPELAND, N. G., GILBERT, D. J., JENKINS, N. A. & YOSHIMURA, A. 1998. Cloning and characterization of a novel class II phosphoinositide 3-kinase containing C2 domain. *Biochem Biophys Res Commun,* 244, 531-539.

MOH, M. C. & SHEN, S. 2009. The roles of cell adhesion molecules in tumor suppression and cell migration: a new paradox. *Cell Adh Migr,* 3, 334-336.

MORENO-LAYSECA, P., ICHA, J., HAMIDI, H. & IVASKA, J. 2019. Integrin trafficking in cells and tissues. *Nat Cell Biol,* 21, 122-132.

MORITA, S., KOJIMA, T. & KITAMURA, T. 2000. Plat-E: an efficient and stable system for transient packaging of retroviruses. *Gene Ther,* 7, 1063-1066.

MOUNTFORD, J. K., PETITJEAN, C., PUTRA, H. W., MCCAFFERTY, J. A., SETIABAKTI, N. M., LEE, H., TONNESEN, L. L., MCFADYEN, J. D., SCHOENWAELDER, S. M., ECKLY, A., GACHET, C., ELLIS, S., VOSS, A. K., DICKINS, R. A., HAMILTON, J. R. & JACKSON, S. P. 2015. The class II PI 3-kinase, PI3KC2alpha, links platelet internal membrane structure to shear-dependent adhesive function. *Nat Commun,* 6, 6535.

NADER, G. P., EZRATTY, E. J. & GUNDERSEN, G. G. 2016. FAK, talin and PIPKIgamma regulate endocytosed integrin activation to polarize focal adhesion assembly. *Nat Cell Biol,* 18, 491-503.

NAGANO, M., HOSHINO, D., SAKAMOTO, T., KAWASAKI, N., KOSHIKAWA, N. & SEIKI, M. 2010. ZF21 protein regulates cell adhesion and motility. *J Biol Chem,* 285, 21013-21022.

NAKATSU, F., PERERA, R. M., LUCAST, L., ZONCU, R., DOMIN, J., GERTLER, F. B., TOOMRE, D. & DE CAMILLI, P. 2010. The inositol 5-phosphatase SHIP2 regulates endocytic clathrin-coated pit dynamics. *J Cell Biol,* 190, 307-315.

NAYAL, A., WEBB, D. J., BROWN, C. M., SCHAEFER, E. M., VICENTE-MANZANARES, M. & HORWITZ, A. R. 2006. Paxillin phosphorylation at Ser273 localizes a GIT1-PIX-PAK complex and regulates adhesion and protrusion dynamics. *J Cell Biol,* 173, 587-589.

NEWELL-LITWA, K. A., HORWITZ, R. & LAMERS, M. L. 2015. Non-muscle myosin II in disease: mechanisms and therapeutic opportunities. *Dis Model Mech,* 8, 1495-1515.

NOBUSAWA, S., LACHUER, J., WIERINCKX, A., KIM, Y. H., HUANG, J., LEGRAS, C., KLEIHUES, P. & OHGAKI, H. 2010. Intratumoral patterns of genomic imbalance in glioblastomas. *Brain Pathol,* 20, 936-944.

PARSONS, J. T., HORWITZ, A. R. & SCHWARTZ, M. A. 2010. Cell adhesion: integrating cytoskeletal dynamics and cellular tension. *Nat Rev Mol Cell Biol,* 11, 633-643.

PASAPERA, A. M., SCHNEIDER, I. C., RERICHA, E., SCHLAEPFER, D. D. & WATERMAN, C. M. 2010. Myosin II activity regulates vinculin recruitment to focal adhesions through FAK-mediated paxillin phosphorylation. *J Cell Biol,* 188, 877-890.

PAUL, N. R., JACQUEMET, G. & CASWELL, P. T. 2015 .Endocytic Trafficking of Integrins in Cell Migration. *Curr Biol,* 25, R1092-1105.

PITULESCU, M. E., SCHMIDT, I., BENEDITO, R. & ADAMS, R. H. 2010. Inducible gene targeting in the neonatal vasculature and analysis of retinal angiogenesis in mice. *Nat Protoc,* 5, 1518-1534.

PLAYFORD, M. P. & SCHALLER, M. D. 2004. The interplay between Src and integrins in normal and tumor biology. *Oncogene,* 23, 7928-7946.

POSOR, Y., EICHHORN-GRUENIG, M., PUCHKOV, D., SCHONEBERG, J., ULLRICH, A., LAMPE, A., MULLER, R., ZARBAKHSH, S., GULLUNI, F., HIRSCH, E., KRAUSS, M., SCHULTZ, C., SCHMORANZER, J., NOE, F. & HAUCKE, V. 2013. Spatiotemporal control of endocytosis by phosphatidylinositol-3,4-bisphosphate. *Nature,* 499, 233-237.

POSOR, Y., EICHHORN-GRUNIG, M. & HAUCKE, V. 2015. Phosphoinositides in endocytosis. *Biochim Biophys Acta,* 1851, 794-804.

POTENTE, M., GERHARDT, H. & CARMELIET, P. 2011. Basic and therapeutic aspects of angiogenesis. *Cell,* 146, 873-887.

POULTER, N. S., PITKEATHLY, W. T., SMITH, P. J. & RAPPOPORT, J. Z. 2015. The physical basis of total internal reflection fluorescence (TIRF) microscopy and its cellular applications. *Methods Mol Biol,* 1251, 1-23.

PRIDDLE, H., HEMMINGS, L., MONKLEY, S., WOODS, A., PATEL, B., SUTTON, D., DUNN, G. A., ZICHA, D. & CRITCHLEY, D. R. 1998. Disruption of the talin gene compromises focal adhesion assembly in undifferentiated but not differentiated embryonic stem cells. *J Cell Biol,* 142, 1121-1133.

PRIOR, I. A. & CLAGUE, M. J. 1999. Localization of a class II phosphatidylinositol 3-kinase, PI3KC2alpha, to clathrin-coated vesicles. *Mol Cell Biol Res Commun,* 1, 162-166.

RANE, C. K. & MINDEN, A. 2014. P21 activated kinases: structure, regulation, and functions. *Small GTPases,* 5: e28003.

RAO, S. K., EDWARDS, J., JOSHI, A. D., SIU, I. M. & RIGGINS, G. J. 2010. A survey of glioblastoma genomic amplifications and deletions. *J Neurooncol,* 96, 169-179.

RATZ, M., TESTA, I., HELL, S. W. & JAKOBS, S. 2015. CRISPR/Cas9-mediated endogenous protein tagging for RESOLFT super-resolution microscopy of living human cells. *Sci Rep,* 5, 9592.

RIDLEY, A. J. 2006. Rho GTPases and actin dynamics in membrane protrusions and vesicle trafficking. *Trends Cell Biol,* 16, 522-529.

RIDLEY, A. J. 2015. Rho GTPase signalling in cell migration. *Curr Opin Cell Biol,* 36, 103-112.

RIDLEY, A. J. & HALL, A. 1992. The small GTP-binding protein rho regulates the assembly of focal adhesions and actin stress fibers in response to growth factors. *Cell,* 70, 389-399.

RIDLEY, A. J., SCHWARTZ, M. A., BURRIDGE, K., FIRTEL, R. A., GINSBERG, M. H., BORISY, G., PARSONS, J. T. & HORWITZ, A. R. 2003. Cell migration: integrating signals from front to back. *Science,* 302, 1704-1709.

RIEMENSCHNEIDER, M. J., KNOBBE, C. B. & REIFENBERGER, G. 2003. Refined mapping of 1q32 amplicons in malignant gliomas confirms MDM4 as the main amplification target. *Int J Cancer,* 104, 752-757.

RIUS, C. & SANZ, M. J. 2015. Intravital Microscopy in the Cremaster Muscle Microcirculation for Endothelial Dysfunction Studies. *Methods Mol Biol,* 1339, 357-366.

RUSSO, A. & O'BRYAN, J. P. 2012. Intersectin 1 is required for neuroblastoma tumorigenesis. *Oncogene,* 31, 4828-4834.

RUSSO, A., OKUR, M. N., BOSLAND, M. & O'BRYAN, J. P. 2015. Phosphatidylinositol 3-kinase, class 2 beta (PI3KC2beta) isoform contributes to neuroblastoma tumorigenesis. *Cancer Lett,* 359, 262-268.

SABATINI, D. M. 2017. Twenty-five years of mTOR: Uncovering the link from nutrients to growth. *Proc Natl Acad Sci U S A,* 114, 11818-11825.

SABHA, N., VOLPATTI, J. R., GONORAZKY, H., REIFLER, A., DAVIDSON, A. E., LI, X., ELTAYEB, N. M., DALL'ARMI, C., DI PAOLO, G., BROOKS, S. V., BUJ-BELLO, A., FELDMAN, E. L. & DOWLING, J. J. 2016. PIK3C2B inhibition improves function and prolongs survival in myotubular myopathy animal models. *J Clin Invest,* 126, 3613-3625.

SATO, N., FUKUSHIMA, N., MAITRA, A., IACOBUZIO-DONAHUE, C. A., VAN HEEK, N. T., CAMERON, J. L., YEO, C. J., HRUBAN, R. H. & GOGGINS, M. 2004. Gene expression profiling identifies genes associated with invasive intraductal papillary mucinous neoplasms of the pancreas. *Am J Pathol,* 164, 903-914.

SAXTON, R. A. & SABATINI, D. M. 2017. mTOR Signaling in Growth, Metabolism, and Disease. *Cell,* 169, 361-371.

SCHIEFERMEIER, N., SCHEFFLER, J. M., DE ARAUJO, M. E., STASYK, T., YORDANOV, T., EBNER, H. L., OFFTERDINGER, M., MUNCK, S., HESS, M. W., WICKSTROM, S. A., LANGE, A., WUNDERLICH, W., FASSLER, R., TEIS, D. & HUBER, L. A. 2014. The late endosomal p14-MP1 (LAMTOR2/3) complex regulates focal adhesion dynamics during cell migration. *J Cell Biol,* 205, 525-540.

SCHINK, K. O., TAN, K. W. & STENMARK, H. 2016. Phosphoinositides in Control of Membrane Dynamics. *Annu Rev Cell Dev Biol,* 32, 143-171.

SCHOBER, M., RAGHAVAN, S., NIKOLOVA, M., POLAK, L., PASOLLI, H. A., BEGGS, H. E., REICHARDT, L. F. & FUCHS, E. 2007. Focal adhesion kinase modulates tension signaling to control actin and focal adhesion dynamics. *J Cell Biol,* 176, 667-680.

SCHONEBERG, J., LEHMANN, M., ULLRICH, A., POSOR, Y., LO, W. T., LICHTNER, G., SCHMORANZER, J., HAUCKE, V. & NOE, F. 2017. Lipid-mediated PX-BAR domain recruitment couples local membrane constriction to endocytic vesicle fission. *Nat Commun,* 8, 15873.

SCHWARTZ, M. A. & ASSOIAN, R. K. 2001. Integrins and cell proliferation: regulation of cyclin-dependent kinases via cytoplasmic signaling pathways. *J Cell Sci,* 114, 2553-2560.

SCITA, G., NORDSTROM, J., CARBONE, R., TENCA, P., GIARDINA, G., GUTKIND, S., BJARNEGARD, M., BETSHOLTZ, C. & DI FIORE, P. P. 1999. EPS8 and E3B1 transduce signals from Ras to Rac. *Nature,* 401, 290-293.

SCRIMA, A., THOMAS, C., DEACONESCU, D. & WITTINGHOFER, A. 2008. The Rap-RapGAP complex: GTP hydrolysis without catalytic glutamine and arginine residues. *EMBO J,* 27, 1145-1153.

SEEWALD, M. J., KORNER, C., WITTINGHOFER, A. & VETTER, I. R. 2002. RanGAP mediates GTP hydrolysis without an arginine finger. *Nature,* 415, 662-666.

SHARIFI, M. N., MOWERS, E. E., DRAKE, L. E., COLLIER, C., CHEN, H., ZAMORA, M., MUI, S. & MACLEOD, K. F. 2016. Autophagy Promotes Focal Adhesion Disassembly and Cell Motility of Metastatic Tumor Cells through the Direct Interaction of Paxillin with LC3. *Cell Rep,* 15, 1660-1672.

SHIN, I., YAKES, F. M., ROJO, F., SHIN, N. Y., BAKIN, A. V., BASELGA, J. & ARTEAGA, C. L. 2002. PKB/Akt mediates cell-cycle progression by phosphorylation of p27(Kip1) at threonine 157 and modulation of its cellular localization. *Nat Med,* 8, 1145-1152.

SIEG, D. J., HAUCK, C. R. & SCHLAEPFER, D. D. 1999. Required role of focal adhesion kinase (FAK) for integrin-stimulated cell migration. *J Cell Sci,* 112 ( Pt 16), 2677-2691.

SINDIC, A., ALEKSANDROVA, A., FIELDS, A. P., VOLINIA, S. & BANFIC, H. 2001. Presence and activation of nuclear phosphoinositide 3-kinase C2beta during compensatory liver growth. *J Biol Chem,* 276, 17754-17761.

SINDIC, A., CRLJEN, V., MATKOVIC, K., LUKINOVIC-SKUDAR, V., VISNJIC, D. & BANFIC, H. 2006. Activation of phosphoinositide 3-kinase C2 beta in the nuclear matrix during compensatory liver growth. *Adv Enzyme Regul,* 46, 280-287.

SPANO, D., HECK, C., DE ANTONELLIS, P., CHRISTOFORI, G. & ZOLLO, M. 2012. Molecular networks that regulate cancer metastasis. *Semin Cancer Biol,* 22, 234-249.

SRIVASTAVA, S., CAI, X., LI, Z., SUN, Y. & SKOLNIK, E. Y. 2012. Phosphatidylinositol-3-kinase C2beta and TRIM27 function to positively and negatively regulate IgE receptor activation of mast cells. *Mol Cell Biol,* 32, 3132-3139.

SRIVASTAVA, S., DI, L., ZHDANOVA, O., LI, Z., VARDHANA, S., WAN, Q., YAN, Y., VARMA, R., BACKER, J., WULFF, H., DUSTIN, M. L. & SKOLNIK, E. Y. 2009. The class II phosphatidylinositol 3 kinase C2beta is required for the activation of the K+ channel KCa3.1 and CD4 T-cells. *Mol Biol Cell,* 20, 3783-3791.

SRIVASTAVA, S., LI, Z. & SKOLNIK, E. Y. 2017. Phosphatidlyinositol-3-kinase C2 beta (PI3KC2beta) is a potential new target to treat IgE mediated disease. *PLoS One,* 12, e0183474.

STEHBENS, S. & WITTMANN, T. 2012. Targeting and transport: how microtubules control focal adhesion dynamics. *J Cell Biol,* 198, 481-489.

STJEPANOVIC, G., BASKARAN, S., LIN, M. G. & HURLEY, J. H. 2017. Unveiling the role of VPS34 kinase domain dynamics in regulation of the autophagic PI3K complex. *Mol Cell Oncol,* 4, e1367873.

SU, Y. F., LIANG, C. Y., HUANG, C. Y., PENG, C. Y., CHEN, C. C., LIN, M. C., LIN, R. K., LIN, W. W., CHOU, M. Y., LIAO, P. H. & YANG, J. J. 2014. A putative novel protein, DEPDC1B, is overexpressed in oral cancer patients, and enhanced anchorage-independent growth in oral cancer cells that is mediated by Rac1 and ERK. *J Biomed Sci,* 21, 67.

SUBRAMANIAN, D., LAKETA, V., MULLER, R., TISCHER, C., ZARBAKHSH, S., PEPPERKOK, R. & SCHULTZ, C. 2010. Activation of membrane-permeant caged PtdIns(3)P induces endosomal fusion in cells. *Nat Chem Biol,* 6, 324-326.

SULZMAIER, F. J., JEAN, C. & SCHLAEPFER, D. D. 2014. FAK in cancer: mechanistic findings and clinical applications. *Nat Rev Cancer,* 14, 598-610.

SVITKINA, T. M. 2018. Ultrastructure of the actin cytoskeleton. *Curr Opin Cell Biol,* 54, 1-8.

TAKAGI, J., PETRE, B. M., WALZ, T. & SPRINGER, T. A. 2002. Global conformational rearrangements in integrin extracellular domains in outside-in and inside-out signaling. *Cell,* 110, 599-511.

TANIDA, I. & WAGURI, S. 2010. Measurement of autophagy in cells and tissues. *Methods Mol Biol,* 648, 193-214.

THORPE, L. M., YUZUGULLU, H. & ZHAO, J. J. 2015. PI3K in cancer: divergent roles of isoforms, modes of activation and therapeutic targeting. *Nat Rev Cancer,* 15, 7-24.

TIBOLLA, G., PINEIRO, R., CHIOZZOTTO, D., MAVROMMATI, I., WHEELER, A. P., NORATA, G. D., CATAPANO, A. L., MAFFUCCI, T. & FALASCA, M. 2013. Class II phosphoinositide 3-kinases contribute to endothelial cells morphogenesis. *PLoS One,* 8, e53808.

TIOSANO, D., BARIS, H. N., CHEN, A., HITZERT, M. M., SCHUELER, M., GULLUNI, F., WIESENER, A., BERGUA, A., MORY, A., COPELAND, B., GLEESON, J. G., RUMP, P., VAN MEER, H., SIVAL, D. A., HAUCKE, V., KRIWINSKY, J., KNAUP, K. X., REIS, A., HAUER, N. N., HIRSCH, E., ROEPMAN, R., PFUNDT, R., THIEL, C. T., WIESENER, M. S., ASLANYAN, M. G. & BUCHNER, D. A. 2019. Mutations in PIK3C2A cause syndromic short stature, skeletal abnormalities, and cataracts associated with ciliary dysfunction. *PLoS Genet,* 15, e1008088.

TURNER, C. E. 2000. Paxillin and focal adhesion signalling. *Nat Cell Biol,* 2, E231-236.

VALDEMBRI, D. & SERINI, G. 2012. Regulation of adhesion site dynamics by integrin traffic. *Curr Opin Cell Biol,* 24, 582-591.

VALET, C., CHICANNE, G., SEVERAC, C., CHAUSSADE, C., WHITEHEAD, M. A., CABOU, C., GRATACAP, M. P., GAITS-IACOVONI, F., VANHAESEBROECK, B., PAYRASTRE, B. & SEVERIN, S. 2015. Essential role of class II PI3K-C2alpha in platelet membrane morphology. *Blood,* 126, 1128-1137.

VAN MEER, G., VOELKER, D. R. & FEIGENSON, G. W. 2008. Membrane lipids: where they are and how they behave. *Nat Rev Mol Cell Biol,* 9, 112-124.

VANHAESEBROECK, B., ALI, K., BILANCIO, A., GEERING, B. & FOUKAS, L. C. 2005. Signalling by PI3K isoforms: insights from gene-targeted mice. *Trends Biochem Sci,* 30, 194-204.

VANHAESEBROECK, B., GUILLERMET-GUIBERT, J., GRAUPERA, M. & BILANGES, B. 2010. The emerging mechanisms of isoform-specific PI3K signalling. *Nat Rev Mol Cell Biol,* 11, 329-341.

VANHAESEBROECK, B., STEPHENS, L. & HAWKINS, P. 2012. PI3K signalling: the path to discovery and understanding. *Nat Rev Mol Cell Biol,* 13, 195-203.

VANHAESEBROECK, B., WHITEHEAD, M. A. & PINEIRO, R. 2016. Molecules in medicine mini-review: isoforms of PI3K in biology and disease. *J Mol Med (Berl),* 94, 5-11.

VICENTE-MANZANARES, M., MA, X., ADELSTEIN, R. S. & HORWITZ, A. R. 2009. Non-muscle myosin II takes centre stage in cell adhesion and migration. *Nat Rev Mol Cell Biol,* 10, 778-790.

VIGLIETTO, G., MOTTI, M. L., BRUNI, P., MELILLO, R. M., D'ALESSIO, A., CALIFANO, D., VINCI, F., CHIAPPETTA, G., TSICHLIS, P., BELLACOSA, A., FUSCO, A. & SANTORO, M. 2002. Cytoplasmic relocalization and inhibition of the cyclin-dependent kinase inhibitor p27(Kip1) by PKB/Akt-mediated phosphorylation in breast cancer. *Nat Med,* 8, 1136-1144.

VISNJIC, D., CRLJEN, V., CURIC, J., BATINIC, D., VOLINIA, S. & BANFIC, H. 2002. The activation of nuclear phosphoinositide 3-kinase C2beta in all-trans-retinoic acid-differentiated HL-60 cells. *FEBS Lett,* 529, 268-274.

VISNJIC, D., CURIC, J., CRLJEN, V., BATINIC, D., VOLINIA, S. & BANFIC, H. 2003. Nuclear phosphoinositide 3-kinase C2beta activation during G2/M phase of the cell cycle in HL-60 cells. *Biochim Biophys Acta,* 1631, 61-71.

WALKER, J. L. & ASSOIAN, R. K. 2005. Integrin-dependent signal transduction regulating cyclin D1 expression and G1 phase cell cycle progression. *Cancer Metastasis Rev,* 24, 383-393.

WALLROTH, A. & HAUCKE, V. 2018. Phosphoinositide conversion in endocytosis and the endolysosomal system. *J Biol Chem,* 293, 1526-1535.

WANG, D., GUO, Q., WEI, A. & LI, A. 2018a. Differential Binding of Active and Inactive Integrin to Talin. *Protein J,* 37, 280-289.

WANG, H., LO, W. T., VUJICIC ZAGAR, A., GULLUNI, F., LEHMANN, M., SCAPOZZA, L., HAUCKE, V. & VADAS, O. 2018b. Autoregulation of Class II Alpha PI3K Activity by Its Lipid-Binding PX-C2 Domain Module. *Mol Cell,* 71, 343-351 e344.

WEBB, D. J., DONAIS, K., WHITMORE, L. A., THOMAS, S. M., TURNER, C. E., PARSONS, J. T. & HORWITZ, A. F. 2004. FAK-Src signalling through paxillin, ERK and MLCK regulates adhesion disassembly. *Nat Cell Biol,* 6, 154-161.

WEBB, D. J., PARSONS, J. T. & HORWITZ, A. F. 2002. Adhesion assembly, disassembly and turnover in migrating cells -- over and over and over again. *Nat Cell Biol,* 4, E97-100.

WEIGERT, R., SRAMKOVA, M., PARENTE, L., AMORNPHIMOLTHAM, P. & MASEDUNSKAS, A. 2010. Intravital microscopy: a novel tool to study cell biology in living animals. *Histochem Cell Biol,* 133, 481-491.

WHEELER, M. & DOMIN, J. 2001. Recruitment of the class II phosphoinositide 3-kinase C2beta to the epidermal growth factor receptor: role of Grb2. *Mol Cell Biol,* 21, 6660-6667.

WHEELER, M. & DOMIN, J. 2006. The N-terminus of phosphoinositide 3-kinase-C2beta regulates lipid kinase activity and binding to clathrin. *J Cell Physiol,* 206, 586-593.

WILSON, E., LESZCZYNSKA, K., POULTER, N. S., EDELMANN, F., SALISBURY, V. A., NOY, P. J., BACON, A., RAPPOPORT, J. Z., HEATH, J. K., BICKNELL, R. & HEATH, V. L. 2014. RhoJ interacts with the GIT-PIX complex and regulates focal adhesion disassembly. *J Cell Sci,* 127, 3039-3051.

WINOGRAD-KATZ, S. E., FASSLER, R., GEIGER, B. & LEGATE, K. R. 2014. The integrin adhesome: from genes and proteins to human disease. *Nat Rev Mol Cell Biol,* 15, 273-288.

WINOGRAD-KATZ, S. E., ITZKOVITZ, S., KAM, Z. & GEIGER, B. 2009. Multiparametric analysis of focal adhesion formation by RNAi-mediated gene knockdown. *J Cell Biol,* 186, 423-436.

WONG, K. A., RUSSO, A., WANG, X., CHEN, Y. J., LAVIE, A. & O'BRYAN, J. P. 2012. A new dimension to Ras function: a novel role for nucleotide-free Ras in Class II phosphatidylinositol 3-kinase beta (PI3KC2beta) regulation. *PLoS One,* 7, e45360.

WOZNIAK, M. A., MODZELEWSKA, K., KWONG, L. & KEELY, P. J. 2004. Focal adhesion regulation of cell behavior. *Biochim Biophys Acta,* 1692, 103-119.

WU, D., ZHU, X., JIMENEZ-COWELL, K., MOLD, A. J., SOLLECITO, C. C., LOMBANA, N., JIAO, M. & WEI, Q. 2015a. Identification of the GTPase-activating protein DEP domain containing 1B (DEPDC1B) as a transcriptional target of Pitx2. *Exp Cell Res,* 333, 80-92.

WU, K., YANG, L., CHEN, J., ZHAO, H., WANG, J., XU, S. & HUANG, Z. 2015b. miR-362-5p inhibits proliferation and migration of neuroblastoma cells by targeting phosphatidylinositol 3-kinase-C2beta. *FEBS Lett,* 589, 1911-1919.

YOON, S. O., SHIN, S., KARRETH, F. A., BUEL, G. R., JEDRYCHOWSKI, M. P., PLAS, D. R., DEDHAR, S., GYGI, S. P., ROUX, P. P., DEPHOURE, N. & BLENIS, J. 2017. Focal Adhesion- and IGF1R-Dependent Survival and Migratory Pathways Mediate Tumor Resistance to mTORC1/2 Inhibition. *Mol Cell,* 67, 512-527 e514.

YOSHIOKA, K., YOSHIDA, K., CUI, H., WAKAYAMA, T., TAKUWA, N., OKAMOTO, Y., DU, W., QI, X., ASANUMA, K., SUGIHARA, K., AKI, S., MIYAZAWA, H., BISWAS, K., NAGAKURA, C., UENO, M., ISEKI, S., SCHWARTZ, R. J., OKAMOTO, H., SASAKI, T., MATSUI, O., ASANO, M., ADAMS, R. H., TAKAKURA, N. & TAKUWA, Y. 2012. Endothelial PI3K-C2alpha, a class II PI3K, has an essential role in angiogenesis and vascular barrier function. *Nat Med,* 18, 1560-1569.

YU, D. H., QU, C. K., HENEGARIU, O., LU, X. & FENG, G. S. 1998. Protein-tyrosine phosphatase Shp-2 regulates cell spreading, migration, and focal adhesion. *J Biol Chem,* 273, 21125-21131.

YU, J. A., DEAKIN, N. O. & TURNER, C. E. 2010. Emerging role of paxillin-PKL in regulation of cell adhesion, polarity and migration. *Cell Adh Migr,* 4, 342-347.

ZAIDEL-BAR, R., COHEN, M., ADDADI, L. & GEIGER, B. 2004. Hierarchical assembly of cell-matrix adhesion complexes. *Biochem Soc Trans,* 32, 416-420.

ZAIDEL-BAR, R. & GEIGER, B. 2010. The switchable integrin adhesome. *J Cell Sci,* 123, 1385-1388.

ZAIDEL-BAR, R., ITZKOVITZ, S., MA'AYAN, A., IYENGAR, R. & GEIGER, B. 2007. Functional atlas of the integrin adhesome. *Nat Cell Biol,* 9, 858-867.

ZAMIR, E., KATZ, M., POSEN, Y., EREZ, N., YAMADA, K. M., KATZ, B. Z., LIN, S., LIN, D. C., BERSHADSKY, A., KAM, Z. & GEIGER, B. 2000. Dynamics and segregation of cell-matrix adhesions in cultured fibroblasts. *Nat Cell Biol,* 2, 191-196.

ZHANG, J., BANFIC, H., STRAFORINI, F., TOSI, L., VOLINIA, S. & RITTENHOUSE, S. E. 1998. A type II phosphoinositide 3-kinase is stimulated via activated integrin in platelets. A source of phosphatidylinositol 3-phosphate. *J Biol Chem,* 273, 14081-14084.

ZHANG, L., HUANG, J., YANG, N., GRESHOCK, J., LIANG, S., HASEGAWA, K., GIANNAKAKIS, A., POULOS, N., O'BRIEN-JENKINS, A., KATSAROS, D., BUTZOW, R., WEBER, B. L. & COUKOS, G. 2007. Integrative genomic analysis of phosphatidylinositol 3'-kinase family identifies PIK3R3 as a potential therapeutic target in epithelial ovarian cancer. *Clin Cancer Res,* 13, 5314-5321.

ZHOU, B. P., LIAO, Y., XIA, W., SPOHN, B., LEE, M. H. & HUNG, M. C. 2001. Cytoplasmic localization of p21Cip1/WAF1 by Akt-induced phosphorylation in HER-2/neu-overexpressing cells. *Nat Cell Biol,* 3, 245-252.

ZHOU, X., TAKATOH, J. & WANG, F. 2011. The mammalian class 3 PI3K (PIK3C3) is required for early embryogenesis and cell proliferation. *PLoS One,* 6, e16358.

ZINN, A., GOICOECHEA, S. M., KREIDER-LETTERMAN, G., MAITY, D., AWADIA, S., CEDENO-ROSARIO, L., CHEN, Y. & GARCIA-MATA, R. 2019. The small GTPase RhoG regulates microtubule-mediated focal adhesion disassembly. *Sci Rep,* 9, 5163.

ZONCU, R., PERERA, R. M., BALKIN, D. M., PIRRUCCELLO, M., TOOMRE, D. & DE CAMILLI, P. 2009. A phosphoinositide switch controls the maturation and signaling properties of APPL endosomes. *Cell,* 136, 1110-1121.

BOETTNER, B. & VAN AELST, L. 2009. Control of cell adhesion dynamics by Rap1 signaling. *Curr Opin Cell Biol,* 21**,** 684-693.

BOS, J. L., DE ROOIJ, J. & REEDQUIST, K. A. 2001. Rap1 signalling: adhering to new models. *Nat Rev Mol Cell Biol,* 2**,** 369-377.

CHARRAS, G. & PALUCH, E. 2008. Blebs lead the way: how to migrate without lamellipodia. *Nat Rev Mol Cell Biol,* 9**,** 730-736.

CHRZANOWSKA-WODNICKA, M., SMYTH, S. S., SCHOENWAELDER, S. M., FISCHER, T. H. & WHITE, G. C., 2ND 2005. Rap1b is required for normal platelet function and hemostasis in mice. *J Clin Invest,* 115**,** 680-687.

DART, A. E., BOX, G. M., COURT, W., GALE, M. E., BROWN, J. P., PINDER, S. E., ECCLES, S. A. & WELLS, C. M. 2015. PAK4 promotes kinase-independent stabilization of RhoU to modulate cell adhesion. *J Cell Biol,* 211**,** 863-879.

DESIMONE, D. W. & HORWITZ, A. R. 2014. Cell Biology. Many modes of motility. *Science,* 345**,** 1002-1003.

DI PAOLO, G. & DE CAMILLI, P. 2006. Phosphoinositides in cell regulation and membrane dynamics. *Nature,* 443**,** 651-657.

DUCHNIEWICZ, M., ZEMOJTEL, T., KOLANCZYK, M., GROSSMANN, S., SCHEELE, J. S. & ZWARTKRUIS, F. J. 2006. Rap1A-deficient T and B cells show impaired integrin-mediated cell adhesion. *Mol Cell Biol,* 26**,** 643-653.

DURAND, N., BASTEA, L. I., LONG, J., DOPPLER, H., LING, K. & STORZ, P. 2016. Protein Kinase D1 regulates focal adhesion dynamics and cell adhesion through Phosphatidylinositol-4-phosphate 5-kinase type-l gamma. *Sci Rep,* 6**,** 35963.

FRANCO, I., GULLUNI, F., CAMPA, C. C., COSTA, C., MARGARIA, J. P., CIRAOLO, E., MARTINI, M., MONTEYNE, D., DE LUCA, E., GERMENA, G., POSOR, Y., MAFFUCCI, T., MARENGO, S., HAUCKE, V., FALASCA, M., PEREZ-MORGA, D., BOLETTA, A., MERLO, G. R. & HIRSCH, E. 2014. PI3K class II alpha controls spatially restricted endosomal PtdIns3P and Rab11 activation to promote primary cilium function. *Dev Cell,* 28**,** 647-658.

FRIEDL, P. & WOLF, K. 2010. Plasticity of cell migration: a multiscale tuning model. *J Cell Biol,* 188**,** 11-19.

GARCIA-MATA, R. 2014. Arrested detachment: a DEPDC1B-mediated de-adhesion mitotic checkpoint. *Dev Cell,* 31**,** 387-389.

HAAGE, A., GOODWIN, K., WHITEWOOD, A., CAMP, D., BOGUTZ, A., TURNER, C. T., GRANVILLE, D. J., LEFEBVRE, L., PLOTNIKOV, S., GOULT, B. T. & TANENTZAPF, G. 2018. Talin Autoinhibition Regulates Cell-ECM Adhesion Dynamics and Wound Healing In Vivo. *Cell Rep,* 25**,** 2401-2416 e2405.

IKENOUCHI, J. & AOKI, K. 2017. Membrane bleb: A seesaw game of two small GTPases. *Small GTPases,* 8**,** 85-89.

KLAPHOLZ, B. & BROWN, N. H. 2017. Talin - the master of integrin adhesions. *J Cell Sci,* 130**,** 2435-2446.

KLAPPROTH, S., SPERANDIO, M., PINHEIRO, E. M., PRUNSTER, M., SOEHNLEIN, O., GERTLER, F. B., FASSLER, R. & MOSER, M. 2015. Loss of the Rap1 effector RIAM results in leukocyte adhesion deficiency due to impaired beta2 integrin function in mice. *Blood,* 126**,** 2704-2712.

LACHMANN, S., JEVONS, A., DE RYCKER, M., CASAMASSIMA, A., RADTKE, S., COLLAZOS, A. & PARKER, P. J. 2011. Regulatory domain selectivity in the cell-type specific PKN-dependence of cell migration. *PLoS One,* 6**,** 6.

LIU, P., MORRISON, C., WANG, L., XIONG, D., VEDELL, P., CUI, P., HUA, X., DING, F., LU, Y., JAMES, M., EBBEN, J. D., XU, H., ADJEI, A. A., HEAD, K., ANDRAE, J. W., TSCHANNEN, M. R., JACOB, H., PAN, J., ZHANG, Q., VAN DEN BERGH, F., XIAO, H., LO, K. C., PATEL, J., RICHMOND, T., WATT, M. A., ALBERT, T., SELZER, R., ANDERSON, M., WANG, J., WANG, Y., STARNES, S., YANG, P. & YOU, M. 2012. Identification of somatic mutations in non-small cell lung carcinomas using whole-exome sequencing. *Carcinogenesis,* 33**,** 1270-1276.

LIU, Y. J., LE BERRE, M., LAUTENSCHLAEGER, F., MAIURI, P., CALLAN-JONES, A., HEUZE, M., TAKAKI, T., VOITURIEZ, R. & PIEL, M. 2015. Confinement and low

adhesion induce fast amoeboid migration of slow mesenchymal cells. *Cell,* 160**,** 659-672.

MARAT, A. L. & HAUCKE, V. 2016. Phosphatidylinositol 3-phosphates-at the interface between cell signalling and membrane traffic. *EMBO J,* 35**,** 561-579.

MARCHESI, S., MONTANI, F., DEFLORIAN, G., D'ANTUONO, R., CUOMO, A., BOLOGNA, S., MAZZOCCOLI, C., BONALDI, T., DI FIORE, P. P. & NICASSIO, F. 2014. DEPDC1B coordinates de-adhesion events and cell-cycle progression at mitosis. *Dev Cell,* 31**,** 420-433.

NIESWANDT, B., MOSER, M., PLEINES, I., VARGA-SZABO, D., MONKLEY, S., CRITCHLEY, D. & FASSLER, R. 2007. Loss of talin1 in platelets abrogates integrin activation, platelet aggregation, and thrombus formation in vitro and in vivo. *J Exp Med,* 204**,** 3113-3118.

PALUCH, E. K. & RAZ, E. 2013. The role and regulation of blebs in cell migration. *Curr Opin Cell Biol,* 25**,** 582-590.

PANKOVA, K., ROSEL, D., NOVOTNY, M. & BRABEK, J. 2010. The molecular mechanisms of transition between mesenchymal and amoeboid invasiveness in tumor cells. *Cell Mol Life Sci,* 67**,** 63-71.

PARSONS, J. T., HORWITZ, A. R. & SCHWARTZ, M. A. 2010. Cell adhesion: integrating cytoskeletal dynamics and cellular tension. *Nat Rev Mol Cell Biol,* 11**,** 633-643.

PETRICH, B. G., MARCHESE, P., RUGGERI, Z. M., SPIESS, S., WEICHERT, R. A., YE, F., TIEDT, R., SKODA, R. C., MONKLEY, S. J., CRITCHLEY, D. R. & GINSBERG, M. H. 2007. Talin is required for integrin-mediated platelet function in hemostasis and thrombosis. *J Exp Med,* 204**,** 3103-3111.

PETRIE, R. J., KOO, H. & YAMADA, K. M. 2014. Generation of compartmentalized pressure by a nuclear piston governs cell motility in a 3D matrix. *Science,* 345**,** 1062-1065.

PETRIE, R. J. & YAMADA, K. M. 2012. At the leading edge of three-dimensional cell migration. *J Cell Sci,* 125**,** 5917-5926.

PETRIE, R. J. & YAMADA, K. M. 2016. Multiple mechanisms of 3D migration: the origins of plasticity. *Curr Opin Cell Biol,* 42**,** 7-12.

POSOR, Y., EICHHORN-GRUENIG, M., PUCHKOV, D., SCHONEBERG, J., ULLRICH, A., LAMPE, A., MULLER, R., ZARBAKHSH, S., GULLUNI, F., HIRSCH, E., KRAUSS, M., SCHULTZ, C., SCHMORANZER, J., NOE, F. & HAUCKE, V. 2013. Spatiotemporal control of endocytosis by phosphatidylinositol-3,4-bisphosphate. *Nature,* 499**,** 233-237.

RIDLEY, A. J. 2015. Rho GTPase signalling in cell migration. *Curr Opin Cell Biol,* 36**,** 103-112.

RUPRECHT, V., WIESER, S., CALLAN-JONES, A., SMUTNY, M., MORITA, H., SAKO, K., BARONE, V., RITSCH-MARTE, M., SIXT, M., VOITURIEZ, R. & HEISENBERG, C. P. 2015. Cortical contractility triggers a stochastic switch to fast amoeboid cell motility. *Cell,* 160**,** 673-685.

SEBZDA, E., BRACKE, M., TUGAL, T., HOGG, N. & CANTRELL, D. A. 2002. Rap1A positively regulates T cells via integrin activation rather than inhibiting lymphocyte signaling. *Nat Immunol,* 3**,** 251-258.

STEFANINI, L. & BERGMEIER, W. 2016. RAP1-GTPase signaling and platelet function. *J Mol Med,* 94**,** 13-19.

VANHAESEBROECK, B., GUILLERMET-GUIBERT, J., GRAUPERA, M. & BILANGES, B. 2010. The emerging mechanisms of isoform-specific PI3K signalling. *Nat Rev Mol Cell Biol,* 11**,** 329-341.

WALLROTH, A., KOCH, P. A., MARAT, A. L., KRAUSE, E. & HAUCKE, V. 2019. Protein kinase N controls a lysosomal lipid switch to facilitate nutrient signalling via mTORC1. *Nat Cell Biol,* 21**,** 1093-1101.

WONG, K. A., RUSSO, A., WANG, X., CHEN, Y. J., LAVIE, A. & O'BRYAN, J. P. 2012. A new dimension to Ras function: a novel role for nucleotide-free Ras in Class II phosphatidylinositol 3-kinase beta (PI3KC2beta) regulation. *PLoS One,* 7**,** e45360.

YOSHIOKA, K., YOSHIDA, K., CUI, H., WAKAYAMA, T., TAKUWA, N., OKAMOTO, Y., DU, W., QI, X., ASANUMA, K., SUGIHARA, K., AKI, S., MIYAZAWA, H., BISWAS, K., NAGAKURA, C., UENO, M., ISEKI, S., SCHWARTZ, R. J., OKAMOTO, H., SASAKI, T., MATSUI, O., ASANO, M., ADAMS, R. H., TAKAKURA, N. & TAKUWA, Y. 2012. Endothelial PI3K-C2alpha, a class II PI3K, has an essential role in angiogenesis and vascular barrier function. *Nat Med,* 18**,** 1560-1569.